

Numerical analysis of the influence of end restraints on the fire resistance of continuous concrete beams and slabs

Numerieke analyse van de invloed op de brandweerstand van vervormingsverhindering aan de steunpunten van doorgaande balken en platen in gewapend beton

Limin LU

Promotoren: prof. dr. ir. Luc Taerwe, prof. dr. ir. Robby Caspeele, prof. dr. ir. Yong Yuan
Proefschrift ingediend tot het behalen van de graad van
Doctor in de Ingenieurswetenschappen: Bouwkunde

Vakgroep Bouwkundige Constructies
Voorzitter: prof. dr. ir. Luc Taerwe
Faculteit Ingenieurswetenschappen en Architectuur
Academiejaar: 2014-2015



Acknowledgement

It is a great pleasure to thank everyone who helped with the completion of my thesis. This research finishes in Gent University and under the financial support of CSC (China Scholarship Council) and the BOF scholarship of Gent University, so here the CSC and Gent University are to be acknowledged.

First of all, I would like to express my gratitude to my promoters: Professor Luc Taerwe and Professor Yong Yuan. Thanks professor Taerwe give me the chance to study in Magnel lab and supervise me patiently for these years. Your professional supervision give me a great help on the research. Thanks to my Chinese supervise Professor Yong Yuan, who is always smiling and talk like a friend but push a lot on my work. Your continuous encouragement and precious advices helped me to get through all the difficulties during the research. Thank you very much!

I also want to thanks to Prof. Geert De Schutter, Prof. Stijn Matthys, Prof. Guang Ye and Prof. Nele De Belie. Thanks for all your help in the lab. Special thanks to the help from Prof. Emmanuel Annerel and Prof. Robby Caspeele, thanks for your help on the guidance of my research and supervise of my papers. It's your suggestions that make me moving on when I was stocked.

Thanks to my dear officemate: Mieke De Schepper, Nicolas Robeyst, Didier Snoeck and Eleni Arvaniti,, you give me a lot of friendly companion and help. I am really happy to be with you, wish you all good luck.

Thanks to all my colleagues in Magnel lab for all the helps both in research and life in Belgium. Special thanks to Brenda Debbaut, Peter De Pauw, Philip Van den Heede, Ruben Van Coile, Peter Van Den Bussche, Nicolas Coppieters, Stephan De Bock, I am really lucky to have you as my Belgium friends. Thanks to my Chinese friends: Liu Zanjun, Tan zhijun, Gao yun, Mu Song, Wang Jianyun, Jiang Wei, Wu Kai, Wang Lijie, Zheng Kunpeng, Lv Yang, Xiao Wenhao, Liu Jisheng, Ye Danqing. Also thanks to my foreigner friends: Dorleta ertzibengoa, Aniba Maury Ramirez, Hugo Eguez Alava and Crina Sosdean and so on. Thanks for your companion here. It is because of you, I've never had homesick. You will be forever my best friends in my heart. Best wishes for you all.

Thanks to the support of my parents and my dear sister. Thanks for your endless love and all the encouragement during the 30 years on my way of moving forward. In the end, I would like to express my great love to my husband Bairen Lu. I am really lucky to fall in love with

Acknowledgement

you and to have you as my family. It is your love and smile that always make me alright when I am feeling blue. And Annie, my baby, you are forever my sweat!

Limin Lu

1st Feb, 2015

Table of Contents

Acknowledgement	
Samenvatting	I
Summary.....	V
Glossary	VIII
Chapter 1	
General introduction.....	- 1 -
1.1 Problem statement	- 1 -
1.2 Objective and scope	- 4 -
1.3 Outline of the thesis.....	- 5 -
Chapter 2	
Review of Fire Resistance Research	- 7 -
2.1 Design codes on fire resistance	- 7 -
2.1.1 Design methods in EC 2.....	- 9 -
2.1.2 Design approaches in fib bulletins	- 10 -
2.1.3 ACI Method.....	- 11 -
2.1.4 Limitations of current design methods.....	- 12 -
2.2 Progress on fire-resistance research	- 13 -
2.2.1 Thermal analysis	- 13 -
2.2.2 Sectional analysis	- 14 -
2.2.3 Structural analysis on restraints.....	- 16 -
2.2.4 Experiments	- 17 -
2.3 Main Research.....	- 18 -

Chapter 3

Material properties at elevated temperatures	- 20 -
3.1 Thermal properties of concrete under elevated temperatures.....	- 20 -
3.1.1 Thermal conductivity of concrete.....	- 20 -
3.1.2 Specific heat.....	- 22 -
3.1.3 Density of concrete	- 24 -
3.2 Mechanical properties of concrete under elevated temperatures	- 24 -
3.2.1 The compressive strength of concrete.....	- 25 -
3.2.2 The tensile strength of concrete.....	- 27 -
3.2.3 The elastic modulus of concrete.....	- 28 -
3.2.4 Thermal strains of concrete	- 29 -
3.2.5 Spalling of concrete.....	- 36 -
3.3 Thermal properties of steel bars	- 39 -
3.3.1 Thermal conductivity of steel bars	- 39 -
3.3.2 Specific heat of steel bars.....	- 40 -
3.3.3 Density of steel bars	- 40 -
3.4 Mechanical properties of steel bars at elevated temperatures	- 40 -
3.4.1 The strength of steel at high temperatures.....	- 41 -
3.4.2 The elastic modulus of steel at high temperatures.....	- 42 -
3.4.3 Thermal strains of steel	- 43 -
3.5 Bond strength between steel bars and concrete.....	- 45 -
3.6 Summary	- 46 -

Chapter 4

Simplified multi-iteration method for fire resistance calculation of RC elements	- 47 -
4.1 General Introduction	- 47 -
4.2 Temperature field calculation	- 49 -

4.2.1 General introduction	- 50 -
4.2.2 Fire curves	- 50 -
4.2.3 Temperature field of members under various fire curves	- 53 -
4.3 Analysis of sectional equilibrium	- 59 -
4.3.1 Assumptions	- 59 -
4.3.2 Strains of concrete and steel at elevated temperatures	- 60 -
4.3.3 Equilibrium state of a cross-section	- 62 -
4.3.4 Multi- iteration method	- 64 -
4.3.5 An example of the cross-sectional analysis	- 68 -
4.4 Structural analysis	- 69 -
4.4.1 The equilibrium state of the member	- 70 -
4.4.2 Computation of deformations.....	- 74 -
4.5 Verification by fire tests from literature	- 75 -
4.5.1 Set-up for simply supported slab tests.....	- 75 -
4.5.2 Results and conclusions for the simply supported slab tests	- 77 -
4.5.3 Test set-up for rotationally restrained slabs.....	- 81 -
4.5.4 Results and conclusions for the restrained slab tests.....	- 84 -
4.6 Conclusions	- 87 -

Chapter 5

Parametric study of the fire performance of RC beams with implicit and explicit transient creep strain models	- 89 -
5.1 General Introduction	- 90 -
5.2 Analytical procedure and test validation	- 92 -
5.2.1 General introduction of the simulation process.....	- 92 -
5.2.2 Differences between the fire behaviour of members with transient creep strain considered implicitly and explicitly	- 93 -
5.2.3 Differences between the fire behaviour of restrained members with transient creep strain considered implicitly and explicitly	- 96 -

5.3 Influence of heating curves on the fire behaviour of RC beams simulated with the two material models	- 98 -
5.3.1 Heating curves.....	- 98 -
5.3.2 Characteristics of the simulated beams	- 99 -
5.3.3 Simulation results and conclusions	- 101 -
5.4 Influence of the reinforcement ratio on the fire behaviour	- 107 -
5.4.1 Characteristics of the simulated beams	- 107 -
5.4.2 Simulation results and conclusions	- 108 -
5.5 Influence of the size of the cross-section on the fire behaviour.....	- 109 -
5.5.1 Characteristics of the simulated beams	- 110 -
5.5.2 Simulation results for beams with the same width.....	- 112 -
5.5.3 Simulation results for beams with the same height.....	- 113 -
5.5.4 Simulation results for beams with the same reinforcement ratio	- 116 -
5.6 Conclusions	- 117 -
 Chapter 6	
Influence of restraints on fire behaviour of RC elements	- 119 -
6.1 General Introduction	- 119 -
6.1.1 Influence of axial restraints	- 120 -
6.1.2 Influence of rotational restraints	- 123 -
6.1.3 Objective of the research.....	- 125 -
6.2 The beam model as part of a frame and the corresponding restraints....	- 126 -
6.2.1 Axial restraint stiffness for beams in a multi-layered frame	- 128 -
6.2.2 Rotational restraint stiffness for beams in a multi-storey frame	- 132 -
6.2.3 Characteristics of the beam model	- 133 -
6.3 Fire behaviour of beams with various axial restraints.....	- 135 -
6.3.1 Survey of the simulations.....	- 135 -
6.3.2 Rotationally free beams with varying axial restraints	- 136 -

Table of contents

6.3.3 Rotationally restrained beams with varying axial restraint	- 145 -
6.3.4 Summary	- 156 -
6.4 Fire behaviour of beams with various rotational restraints	- 157 -
6.4.1 Survey of the simulations.....	- 157 -
6.4.2 Axially free but rotationally restrained slabs.....	- 157 -
6.4.3 Axially free but rotationally restrained beams	- 160 -
6.4.4 Axially restrained beams with various rotational restraints	- 163 -
6.4.5 Summary	- 172 -
6.5 General Conclusions	- 172 -
Chapter 7	
Conclusions and suggestions.....	- 175 -
7.1 Summary of the research project and conclusions	- 175 -
7.2 Suggestions for future research	- 177 -
References	- 178 -
Curriculum vitae.....	- 190 -

Samenvatting

Onderzoek naar het brandgedrag van bovengrondse en ondergrondse betonconstructies toont dat in deze laatste categorie steeds zwaardere rampen voorkomen met grotere consequenties. Branden in ondergrondse constructies gaan ook meestal gepaard met hogere temperaturen die langer op een hoog niveau blijven. Vanuit structureel oogpunt is het grootste verschil tussen bovengrondse en ondergrondse constructies het feit dat in het laatste geval steeds een belangrijke vervormingsverhinderende aan de uiteinden van de elementen optreedt. De verhinderingskrachten die bij ondergrondse constructies optreden, hebben in eerste instantie te maken met grond-structuur interactie.

Alhoewel de invloed van hoge temperaturen op de respons van betonbalken en -platen de voorbije decennia uitgebreid bestudeerd werd, blijkt uit een literatuurstudie dat het zwaartepunt van dit onderzoek betrekking heeft op het gedrag bij brand van afzonderlijke elementen. Dit geldt des te meer voor het experimenteel onderzoek waarbij, door de beperkingen eigen aan de beschikbare beproevingsfaciliteiten, slechts een zeer beperkt aantal brandproeven uitgevoerd werd met vervormingsverhinderende. Nochtans hebben vervormingsverhinderende meestal een significante invloed op het gedrag bij buiging van gewapende betonelementen onderworpen aan hoge temperaturen. In het beschikbaar onderzoek op het vlak van vervormingsverhinderende wordt er nagenoeg steeds van uitgegaan dat het verhinderingsmoment of de verhinderingskracht constant blijft gedurende de volledige brand, hetgeen niet met de realiteit overeenstemt. Ten gevolge van de geleidelijke afname van de buigstijfheid van een element onderworpen aan brand, zal de relatieve verhinderingsstijfheid toenemen met de brandduur. Dit zal aanleiding geven tot een toename van de verhinderingskrachten en een herverdeling van de buigende momenten langsheen het element. Bijgevolg moet de invloed van vervormingsverhinderende onderzocht worden door expliciet het tijdsafhankelijk aspect van de verhinderingsstijfheden in rekening te brengen.

Wegens het complexe karakter van de simulatie bij brand van elementen met vervormingsverhinderende dient men in principe gebruik te maken van Eindige Elementen software. Toepassing van EE methoden vraagt echter meestal veel rekentijd terwijl het rekenproces als dusdanig niet steeds overzichtelijk is, aangezien het zich afspeelt in een "black box". Bovendien zijn vele EE programma's niet zeer gebruiksvriendelijk en laten ze bijvoorbeeld niet toe om zelf materiaalmodellen te definiëren. Teneinde over een gebruiksvriendelijke onderzoekstool te kunnen beschikken die zowel op boven- als

ondergrondse structuren van toepassing is, werd een nieuw vereenvoudigd numeriek model ontwikkeld, om het gedrag bij brand van elementen die hoofdzakelijk aan buiging onderworpen zijn te simuleren. Met dit numeriek model werden parameterstudies uitgevoerd waarbij de invloed van impliciete en expliciete transiënte kruipmodellen en de invloed van vervormingsverhinderingen op het brandgedrag bestudeerd werden.

Het numeriek model is gebaseerd op het temperatuurveld in een dwarsdoorsnede en de mechanische eigenschappen van beton en wapeningsstaal bij hoge temperaturen. Via een multi-iteratief proces wordt het krachtsevenwicht uitgedrukt en tevens wordt een equivalente buigstijfheid afgeleid voor de structurele analyse. Vervolgens wordt een moment-krommingsdiagram (M-k) gegenereerd voor een gegeven dwarsdoorsnede onderworpen aan een bepaalde langskracht. De kromming ten gevolge van de thermische vervormingen en het bezwijkmoment bij hoge temperaturen, kunnen afgeleid worden uit het berekende M-k diagram. Er wordt voorgesteld gebruik te maken van een effectieve stijfheid die uit het M-k diagram berekend wordt. De doorbuiging van een element evenals de verhoinderingskrachten worden bekomen als finaal resultaat van een iteratie op de effectieve stijfheid van ieder segment in het structureel rekenproces. De beschreven vereenvoudigde multi-iteratieve rekenmethode is zeer gebruiksvriendelijk en laat de invoer toe van zelf gedefiniëerde materiaalmodellen, brandcurven en verhoinderingsstijfheden. Het ontwikkeld rekenmodel werd gevalideerd aan de hand van de resultaten van brandproeven uitgevoerd aan de UGent volgens de ISO-834 brandcurve op vrij opgelegde betonplaten en op platen met rotatieverhoindering. De ontwikkelde methode voor brandsimulaties blijkt voldoende nauwkeurig, praktisch toepasbaar en zeer efficiënt te zijn naar rekentijd toe.

De meeste simulaties van het gedrag bij brand die in de literatuur teruggevonden worden, maken gebruik van het impliciet materiaalmodel voor beton, zoals opgenomen in EN 1992-1-2 (EC 2). Dit model is bijzonder handig voor courante nazichtsberekeningen, maar is uiteraard niet van toepassing wanneer het juist de bedoeling is om de effecten van transiënte kruip in detail te onderzoeken. Hiertoe is het noodzakelijk om het verschil in brandgedrag te vergelijken zoals bekomen met het expliciet en het impliciet model. Verschillende invloedsparameters werden onderzocht om inzicht te krijgen in het verschil tussen de twee modellen. De parameterstudie werd voornamelijk uitgevoerd op enkelvoudig opgelegde balken. Analyse van de resultaten toont aan dat de berekeningen in beperkte mate nauwkeuriger worden wanneer transiënte kruip expliciet in rekening gebracht wordt.

Doorbuigingen van balken en platen dragend in één richting worden lichtjes overschat gedurende brand bij toepassing van het impliciete materiaalmodel uit EC2. Uit deze studie kan besloten worden dat de invloed van verschillende modellen voor transiënte kruip praktisch gezien verwaarloosd kan worden voor elementen die hoofdzakelijk aan buiging onderworpen worden. Als parameters werden verschillende brandkrommen, wapeningsverhoudingen en afmetingen van de dwarsdoorsnede in beschouwing genomen. De resultaten tonen aan dat het verschil tussen de simulaties bekomen met de twee materiaalmodellen: 1) toeneemt met de blootstellingstijd aan brand; 2) afneemt naarmate de wapeningsverhouding toeneemt; en 3) niet beïnvloed wordt door de afmetingen van de dwarsdoorsnede.

Teneinde een duidelijk idee te bekomen omtrent het brandgedrag van gewapende betonelementen met realistische inklemmingsomstandigheden, m.a.w. rekening houdend met de vervormingsverhinderingsomstandigheden ten gevolge van de er mee verbonden naburige elementen, en ten einde een dieper inzicht te bekomen in de invloed van deze vervormingsverhinderingsomstandigheden op het brandgedrag van het beschouwde element, werden verscheidene reeksen balken met verschillende verhinderingsvoorwaarden gesimuleerd en geanalyseerd. Eerst werden de verhinderingsvoorwaarden voor balken in een meerlagig raamwerk berekend en werden vereenvoudigde vergelijkingen afgeleid voor het geval van hoge temperaturen. Vervolgens werden de axiale en de rotationele verhinderingsomstandigheden vertaald naar translatie- en rotatieverhinderingsomstandigheden die aan de uiteinden van de beschouwde balk aangebracht worden. De analyse van balken met verschillende waarden voor de axiale verhinderingsomstandigheden toont aan dat een sterke axiale verhinderingsomstandigheden de brandweerstandsduur van gewapende betonelementen significant kan verminderen. Uit de resultaten bekomen op balken met zowel axiale als rotationele verhinderingsomstandigheden volgt dat de rotationele verhinderingsomstandigheden de invloed van de axiale verhinderingsomstandigheden kan verminderen. Uit de analyse van balken met rotationele verhinderingsomstandigheden volgt dat deze gunstig is voor het brandgedrag van elementen onderworpen aan buiging. Het gunstig effect van de rotationele verhinderingsomstandigheden op het brandgedrag kan afnemen ten gevolge van de axiale verhinderingsomstandigheden. Bij elementen met sterke rotationele verhinderingsomstandigheden bereiken de momenten gegenereerd ter plaatse van de steunpunten vlugger hun maximum wegens de bijdrage van de thermische momenten en kan het element aldus bezwijken. Ter plaatse van de steunpunten van elementen met rotationele verhinderingsomstandigheden moet aldus extra wapening voorzien worden om de negatieve steunpuntsmomenten op te vangen.

Tot slot worden een aantal suggesties geformuleerd met betrekking tot het performantie-gebaseerd ontwerp van gewapende betonelementen rekening houdend met vervormingsverhindering aan de steunpunten.

Summary

Fire resistance research of underground structures and structures above ground shows that the underground structures are always subjected to more severe fire disasters. Fire accidents in underground structures experience higher and longer temperature histories. From the structural side of view, the most obvious difference between the underground ones and the ones above ground is the restraint system at the boundaries. Underground structures are subjected to restraint forces which primarily result from the interaction with the surrounding soil.

Although the effects of high temperature on the response of concrete beams and slabs have been widely studied in recent years, a literature review indicates that the fire behaviour of single members has been the main focus of most of the research projects. Especially from the experimental side, due to the limitations of the commonly available fire test set-ups, very few fire tests include restrained beams and slabs. However, restraints may have a significant influence on the flexural behaviour of reinforced concrete (RC) members at elevated temperatures. The existing research on the effect of restraints is always assuming a constant restraint moment or an axial force during the whole fire exposure process which is not in agreement with the real conditions. Due to the decrease of the member's stiffness while exposed to fire, the restraint stiffness will increase with heating time. This will lead to an increase in restraint forces and a redistribution of the bending moment along the member. Hence, the investigation of the effect of restraints based on temperature-dependent restraint stiffness needs further attention.

Since the fire simulation of restrained members is always very complex, finite element packages have to be applied. However, finite element methods are always time consuming, and the process is not clear since all the computing is performed by the computer "in a black box". Moreover, some of the programs are not so user friendly and do not allow to define material models freely. In order to dispose of a user friendly research method for both structures above ground and underground structures, a new simplified numerical model was developed to simulate the fire performance of reinforced RC members related to bending. Parametric studies including the influence of implicit and explicit transient creep strain models and the influence of restraints on fire performance of RC members have been carried out with the proposed method.

The numerical model is based on the temperature field of the cross-section and the mechanical properties of concrete and reinforcing steel at elevated temperatures. A multi-iteration process is carried out in order to obtain force equilibrium, and an equivalent bending stiffness is defined for the structural analysis. A moment-curvature (M-k) relationship can be generated in the sectional analysis process for a given axial force. The curvature caused by thermal deformations as well as the ultimate moment of the RC member at elevated temperatures can be calculated according to the M-k relationship. The concept of effective stiffness is proposed based on the M-k relationship. The deflection of the member and the restraint forces can be calculated by iterating the effective stiffness of each segment of the member in the structural computing process. The simplified multi-iteration method is user friendly and allows inputting user defined material models, fire curves, and restraint stiffness. The proposed method was validated by fire tests executed at Ghent University on simply supported slabs and rotationally restrained slabs exposed to the ISO-834 standard fire. It appears to be sufficiently accurate, practical and time-effective for fire performance simulations.

Most of the fire-performance simulations found in literature use the implicit material model of concrete, as presented by EN 1992-1-2 (EC 2), which is a viable tool in current design practice, but cannot be used when transient creep effects have to be studied in detail. Therefore, it is necessary to compare the difference in fire performance of RC beams with implicit and explicit models and to study the influencing parameters to evaluate the difference between the two models. The parametric study of the fire performance of RC members with an implicit and an explicit transient creep strain model is carried out on simply supported beam models. The analysis shows that the calculations become slightly more accurate when transient creep strain is considered explicitly. The deflections for RC elements during fire related to bending like beams and one-way slabs will be slightly overestimated with the material model in EC 2. From this it can be concluded that the influence of different transient creep strain models can be neglected in most of the cases for beams and slabs subjected to bending. Parameters including the different fire curves, the reinforcement ratio and size of the cross-section which may influence the fire performances are also studied. The results show that the difference between the simulation results of the two models: 1) increases with heating time; 2) is reduced by increasing the reinforcement area; and 3) is not sensitive to the size of the cross-section.

In order to have a clear idea of the fire performance of RC beams in real conditions, i.e. considering various restraints from surrounding members, and to get a deeper insight on the influence of these restraints on the fire behaviour of RC members, several series of beams with different restraint conditions were simulated and analyzed. The restraint conditions of beams in a multi-layered frame are firstly studied and simplified equations under elevated temperatures are elaborated. Then, the axial and rotational restraints are simplified into axial and rotational springs applied at the end of the beam models. The analysis of beams with various axial restraints shows that a strong axial restraint can severely decrease the fire-resistance time of RC members. The results of beams with both axial and rotational restraints show that the rotational restraints can decrease the influence of axial restraints. The analysis of beams with rotational restraints shows that the rotational restraints are beneficial for the fire-resistance behaviour of RC members subjected to bending. The beneficial effect of rotational restraint on the fire resistance of RC members can be reduced by the axial restraints. For the members with stronger rotational restraints, the restraint moments at the supports reach their maximum earlier due to the thermal moments and may cause the failure of the member. So for the supporting ends of the rotationally restrained members, additional reinforcement should be provided for resisting the negative moment.

Finally, suggestions on performance-based fire resistance design of restrained RC members are formulated.

Glossary

t	Time
θ	Temperature
λ_c	Thermal conductivity of concrete
c_c	Specific heat of concrete
ρ_c	Density of concrete;
f_c	Compressive strength of concrete
$f_{ck,t}$	Tensile strength of concrete
E_c	Elastic modulus of concrete
$\varepsilon_{c,\sigma}$	Stress dependent strain of concrete
$\varepsilon_{c,th}$	Thermal elongation of concrete
$\varepsilon_{c,cr}$	Creep strain of concrete
$\varepsilon_{c,tr}$	Transient strain of concrete
σ_c	Stress of concrete
λ_s	Thermal conductivity of steel bar
c_s	Specific heat of steel bar
ρ_s	Density of steel bar;
f_y	Yield strength of steel bar
f_u	Ultimate strength of steel bar

Glossary

E_s	Young's modulus of steel bar
$\epsilon_{s,\sigma}$	Stress dependent strain of steel bar
$\epsilon_{s,th}$	Thermal elongation of steel bar
$\epsilon_{s,cr}$	Creep strain of steel bar
L	Length of the RC member;
b	Width of the cross-section of the RC member;
h	Height of the cross-section of the RC member;
N	Axial force
M	Moment
k	Curvature of a flexural member
k_t	Thermal induced curvature of a flexural member
q	Applied distributed load
C	Total axial force of concrete;
S_1	Total force of steel bars in tension
S_2	Total force of steel bars in compression
d_1	Axial distance of steel bars in tension to concrete surface
d_2	Axial distance of steel bars in compression to concrete surface
$[K_g]$	Global stiffness matrix
$[U]$	Nodal displacement matrix
$[P]$	Matrix of the nodal load vectors
γ_{axi}	Axial restraint ratio

γ_{rot} Rotational restraint ratio

Chapter 1

General introduction

Compared to structures above ground, underground structures are always submitted to more severe fire disasters and different loading and restraint conditions. There has been a limited research and fire test on reinforced concrete members considering the effect of various support conditions on the behaviour of reinforced concrete beams.

1.1 Problem statement

Underground structures are widely related to tunnels, underground garages, subway stations, storage and underground passage. Along with the development of big cities, underground space was extensively exploited and became an important solution for the lack of space. At the same time, the safety problems related to these underground structures become a big issue. Recent accidents in tunnels and subway stations have resulted in severe destruction of underground structures in consequence of fire loading or earthquakes. According to a systematic survey of a research group in Japan (Chinese Academy of Engineering, 2001), between 1970~1990, fire accidents take 1/3 of all the serious disasters that happened in underground structures worldwide. Fire becomes a disaster that has the largest frequency and losses in underground structures (Beard, A. et al. 2005). Information about recent fires in underground structures (Zhou Y. et al. 2004) is given in Table 1.01. Fire resistance research of underground structures becomes a more and more important and urgent item today (International Tunnelling Association, 2004).

Table 1.01 Recent fire disasters in underground subway stations

Time	Cases	# Injured	# Dead	Cause of fire
1983.08.06	Nagoya subway station, Japan	3	3	Electricity

Chapter 1

1987.11.08	London King's subway station, U.K	32	100	Electricity
1991.04.16	Zurich subway station, Switzerland	58	None	Electricity
1991.08.28	New York subway, U.S.A	155	5	Vehicle fire
1995.04.28	Taegu subway station, Korea	230	103	Construction
1995.10.28	BAK subway station, Azerbaijan	269	558	Vehicle fire
2003.02.18	NO.1 Taegu subway station, Korea	148	192	Manmade fire
2005.07.07	London subway station, U.K.	> 1000	45	Manmade fire
2008	English-France Channel Tunnel	14	None	

Regarding tunnel engineering, for which the fire resistance and design has already been paid attention to, many important programs about tunnels were carried out, like EUREKA.EU.499, DARTS, FIT, UPTUN, Safe Tunnel, SIRTAKI, Virtual Fires, Safe-T, L-SURF, SOLIT and other programs. These research programs contain both fire science and structural design. However, most of these programs are focused on tunnels, like the test for the fire spread in the Channel Tunnel (Kirkland, C.J. 2002), the escape and rescue test for the fire safety of the repaired Mont Blanc Tunnel in the year 2002, and so on. For related codes, the International Tunnel Administration WG6 (ITA) elaborated Guidelines for Structural Fire Resistance for Road Tunnels 05.05.B in 1999, PIARC Proposal on the Design Criteria for Resistance to Fire for Road Tunnel Structures in 2002, Systems and Equipment for Fire and Smoke Control in Road Tunnels in 2004. There are also national standards in Germany, France, America, Japan, and other countries, but all of them are focused on tunnels and say nothing on other types of underground structures.

Besides tunnels, subway stations, underground garages, some commercial and cultural buildings are also a great part of underground structures. They are made up with frames and beam-plate members, which are different from linings as they are more complicated and varying. For these structures, fire-resistance research is limited. EC 2 (EN 1992-1-2, 2004), ACI 216.1 (2007), and fib bulletins (fib bulletin 3, 1999; fib bulletin 38, 2007) supplied general requirements for fire resistance design of single members and frames, but do not

clearly distinguish members from structures above ground or underground. The Code for metro design (GB50157-2003) and the Code for fire protection design of civil air defense works (GB50098-1998) separately give some requirements on fire-proofing and evacuation for metros and garages. However, they only set fire resistance time like the requirements for buildings above ground.

There are many differences between fire conditions of underground structures and buildings above ground.

(1) As underground structures are in a more closed space compared to the structures above ground, they always experience higher and longer temperature histories. This can be concluded from the information on fire accidents in recent years (Ron, A. 2008; NFPA 502, 2001) (Table 1.02). These characteristic temperature curves will lead to a larger risk of spalling and failure of concrete elements, which make the fire accidents in underground structures more dangerous.

Table 1.02 Information on recent fire disasters in tunnels

Fire	year	Duration	Highest temperature
English-France Channel Tunnel	2008	2 hrs-20 hrs.	1000°C
St. Gotthard Tunnel, Switzerland	2001	24 hrs.	1200°C
Gleinalm Tunnel, Austria	2001	37 min	1000°C
Mont Blanc Tunnel, France	1999	53 hrs.	1000°C
Tauern Tunnel, Austria	1999	14 hrs.	1200°C
English-France Channel Tunnel	1996	10hrs	1100°C

(2) The construction of underground projects always needs concrete with high strength and good workability. Therefore, self-compacting concrete (SCC) and other high performance concretes with good flow-ability and self-compacting ability are easily to be accepted by designers. However, different concrete materials and relative members may have different fire performances. Take SCC for example: SCC has a larger conductivity than normal concrete, which make the inner temperature gradient a little smaller than that of normal concrete, but it has a larger possibility of spalling.

(3) From the structural point of view, one of the most obvious differences between the

underground ones and the ones above ground is the restraint system at the boundaries. Underground structures, whether flexural or compressive, are subjected to restraints and forces from the interaction with the surrounding soil. The end restraints can be rotational, axial or both. Rotational restraints are expected to have a positive effect on the fire resistance of RC beams, while in the axially restrained beams a compressive axial force is induced owing to the inhibited expansion. The axial force combined with the deflection developed under fire conditions, will induce second-order effects that might be significant and could initiate member failure (Selvaggio S.L. et al. 1963). This makes the fire resistance analysis more complicated.

There are many well-known researches available on fire performance of steel and concrete materials, and there are also many calculations and tests on fire performance of reinforced concrete structures (GB T9978-1999). However, most of them are simplified methods with a constant load on a single unrestrained element. There is limited research available about the influence of varying support conditions on fire-resistance of concrete structures. There are still many problems both in the theoretical and the experimental fields that need further research as e.g.:

(1) The assumptions for the fire behaviour of normal concrete structures may not be suitable for underground structures. This is due to the difference in fire scenarios, the different material properties at high temperatures, the spalling of concrete under a high temperature, and also the different restraint conditions for the members. So a user friendly simulation method which is also time effective for fire resistance design of structures both above ground and underground is needed.

(2) Most of the analyses methods for the fire behaviour of concrete members use implicit transient creep strain models of concrete under elevated temperatures while this may not be accurate enough if the strains of concrete are considered in detail. So the parametric study on the material models still need further researches.

(3) A literature review shows that there has been a limited research and fire test on concrete members considering the effect of various support conditions on the behaviour of reinforced concrete beams, while support conditions may have a great influence on the fire-resistance of concrete structures.

1.2 Objective and scope

In order to get a user friendly research method for both structures above ground and

underground structures, we need to study the important parameters like the explicit transient creep strain models for concrete and their influence on the fire behaviour of reinforced concrete beams, the effect of restraints on fire resistance of concrete members with various support conditions while considering the difference between members of structures above ground and underground structures. This thesis mainly treats the following aspects:

- (1) Existing research results are collected and summarized, including the calculation methods and conclusions regarding the high temperature properties of concrete and steel bars.
- (2) A simplified multi-iteration method on the fire performance of reinforced concrete members by taking the explicit transient creep strain model of concrete into account is proposed. The simplified method is validated by available experimental results of slab tests.
- (3) Parametric studies have been carried out with the proposed simplified method. The difference of fire behaviour of reinforced concrete beams simulated with transient creep strain considered implicitly and explicitly, and beams with various restraints are calculated and compared. Parameters including the size of the cross-section, the reinforcement ratio and different fire curves which influence the fire performances are also studied.
- (4) Fire performance of reinforced concrete members subjected to bending is concluded from the parametric studies. Finally, suggestions on performance based fire resistance design are formulated.

1.3 Outline of the thesis

To solve the problems outlined above, a multi-iteration method is proposed. Many computer simulations of RC beams subjected to bending are carried out. The thesis is subdivided into seven chapters. Chapter 1 is a general introduction to the problems and the objective of the research. Chapter 2 is a literature review on fire-resistance design methods. Chapter 7 summarizes the main conclusions and perspectives of the thesis. Besides Chapter 1, Chapter 2 and Chapter 7, the main scope of the other four chapters is the following.

- (1) Chapter 3 gives a summary of the research results on the high-temperature properties of concrete and reinforcing steel. The impact of each part of the strains of concrete are compared and discussed.
- (2) Chapter 4 gives an introduction and validation of the proposed multi-iteration method. A step by step introduction on the proposed simplified multi-iteration method, which is used for the calculation of the fire performance of reinforced concrete members, is carried out. The

proposed method can take the explicit transient creep strain model of concrete into account. Finally, fire tests on a one-way slabs executed previously are used to validate the model.

(3) Chapter 5 deals with a parametric study on the fire performance of RC beams simulated with transient creep strain of concrete considered implicitly and explicitly. The difference between fire behaviour of beams with the two material models are compared and analysed. Parameters including size of the cross-section, reinforcement ratio and fire curves are discussed in the comparisons.

(4) Chapter 6 discusses fire performances of beams with various axial and rotational restraints. The fire performance of reinforced concrete beams with varying support conditions which are subjected to the ISO-834 standard fire are compared and analysed.

Chapter 2

Review of Fire Resistance Research

This Chapter gives a literature review of fire-resistance research and design methods, from simplified calculation methods to sophisticated computer programs and experimental research. The important results about the influence of restraint conditions on fire behaviour of concrete beams and other members are presented. From the literature review, some problems that still need to be solved are listed and then based on these detected problems, the objective and main content of this thesis are given.

2.1 Design codes on fire resistance

Regarding fire resistance design, a structure can be evaluated at three levels in the light of increasing complexity and scale: (a) member analysis, (b) substructure analysis, and (c) global structural analysis.

(1) Member analysis





For member analysis, in order to simulate the forces that can develop as a result of thermal expansion, it's essential to apply boundary conditions that are similar to the ones expected for the structural element in the whole structure. However, as a consequence of simplification of the boundary conditions, there can be a huge difference between the actual fire behaviour and the one obtained from experiment or calculation. In a specific project, the elements could be a typical case with restraint from surrounding structures. The axial restraint can be modelled as a spring with different stiffnesses (Figure 2.01). In axially restrained beams, a compressive axial thrust is induced due to the inhibited expansion. The thrust combined with the deflection developed under fire conditions, will induce second-order effects.



Figure 2.01 Axially restrained beam ($K=0$, $EI/3L$, $EI/2L$, $EI/L \dots \infty$)

For a member in a continuous structure, which is rotationally restrained, various axial restraints can also be considered, assuming the fire affects only one span (Table 2.01). For these rotationally restrained elements, the thermal gradient will induce a bending moment at the clamped ends. The additional moment superposed to the one due to the regular service load will increase the moment at the supports and may lead to an unanticipated failure at the ends of the element.

Table 2.01 Rotationally restrained beams ($K=0$, $EI/3L$, EI/L , ∞) (Riva, P. 2008)

Element type	Restraint	Simplified model
One bay beam	$K=0$	
Two bay beam	$K=EA/L$	
Multi-bay beam	$K=EA/3L$	
One bay beam with fixed ends	$K=\infty$	

(2) Substructure analysis

In order to overcome the limitation of single elements, analysis should be performed at a level of a substructure. EC 2 states that the global structure may be divided into substructures, in a way that the interaction of thermal expansions and deformations during fire can be approximated by time-independent supports and boundary conditions. As dimensions of a substructure exceed the capabilities of standard fire furnaces, tests on substructures under fire are very rare.

(3) Global structural analysis

The most accurate method in predicting the structural response is the assessment of the complete structure by full-scale testing or modelling. Redistribution of forces and the effect of restraint thermal expansions can adequately be taken into account. Because of the computational effect, the use of this approach is limited.

2.1.1 Design methods in EC 2

There are two approaches for the assessment of fire resistance design in EC 2 (EN 1992-1-2, 2004): prescriptive design rules and performance based design. Tabulated data or simple and advanced models are provided at member level. Advanced models are suitable for the analysis both of partial and entire structure. Simple models are unavailable for complicated structures. For performance based design methods, the first step is the selection of fire models, and then, it follows more or less the same process as the prescriptive rules.

(1) Tabulated data

Minimum sizes of members and axis distance to reinforcement for achieving a specified fire resistance are given in sets of tables in Section 5 of EC 2, which include parameters related to fire resistance R, integrity E, and insulation I. The tabulated data approach is suitable for the vast majority of structures, and ideally, could be consulted before using the simplified or advanced calculation methods. The data give recognized design solutions for ISO-834 Standard Fire Exposure (ISO-834, 1975) periods up to 240 minutes.

(2) Simplified calculations based on limit state analysis

There are two simplified calculations introduced in EC 2: the 500 °C method and the zone method. Both of them are based on the analysis of an effective cross-section

(a) 500 °C method

The 500 °C method is based on the assumption that all the concrete with a temperature of 500 °C and more has lost all strength and that the concrete below 500 °C has the same strength as at 20°C. Then design is performed with the effective section. For the reinforcement bars, the strength is reduced according to the local temperature. The ultimate bearing capacity and deformation can be calculated. This method is simple and convenient for common cases. However, as it neglects all the strength of concrete within the 500°C zone, sometimes the cross-section is reduced too much and makes the calculation results too conservative.

(b) Zone method (Hertz's method)

The Zone method subdivides the cross-section into several equivalent thickness layers ($N \geq 3$) and evaluates the reduced strength of concrete by the mean temperature of each zone. Based on the value of each zone, a damaged zone and the residual strength of the reduced cross-section can be determined. Comparing to the 500°C isotherm method, this method is more accurate, but also more laborious. For standard fires, temperature contours of normal structure members can be found in FIP (FIP-78), ACI (ACI-81), Wade (Wad-91) and the Eurocode (EC2-95) (EC2-02). For fire conditions other than standard fires, the temperature profiles

should be determined using suitable computer programs.

(3) Advanced calculation methods

Advanced calculation methods are used for complex structures where the provisions of national regulations do not apply, such as sports stadia, exhibitions halls or airport terminals. General guidance is provided in EC 2. These methods link the phenomenon of heat transfer from a fire into structural members, and the combined effects of loads and heat on structural members. Where it is important to predict the whole building behaviour in a fire, allowance must also be made for other potential modes of failure such as anchorage failure or spalling of concrete.

In these analysis methods, spalling is also considered, but EC 2 only distinguishes between two types of concrete spalling, explosive spalling and falling off. Explosive spalling occurs in concrete members under compression, such as columns, during the early stages of exposure to fire, caused by a high water vapour pressure within the concrete mix. Falling off occurs in the tension zones of beams and slabs during the later stages of exposure to fire.

According to the guidelines in EC 2, explosive spalling is unlikely to occur if the moisture content of the concrete is less than 3% by weight, and as a result is also unlikely to occur in an internal environment for normal strength concrete. When the axis distance (concrete cover distance measured from structural member surface to centre of reinforcement) is not more than 70mm, the use of tabulated data is acceptable. If the axis distance is greater than 70mm, supplementary reinforcement should be included, where the surface mesh should have a spacing less than or equal to 100mm and a diameter greater than or equal to 4mm.

2.1.2 Design approaches in fib bulletins

Fire resistance calculation methods introduced in fib bulletins (fib bulletin 3, 1999; fib bulletin 38, 2007; fib bulletin 46, 2008) can be classified into four categories of increasing sophistication and complexity.

(1) Simplified calculations based on limit state analysis

Besides the 500°C isotherm effective cross-section method and the Zone method, also a more detailed effective cross-section method proposed by Hertz, are included.

(2) Thermal-mechanical finite element analysis

The model assumes that there is no interaction between thermal and mechanical processes, and moisture effects can also be neglected. Therefore both analysis programs (thermal and mechanical) are conducted separately. Results consistently show that the deformation of

simple elements can be reasonably predicted with the load induced thermal strains considered in the models. The decrease of load bearing capacity due to thermal cracks can be calculated, according to the types of finite element and the constitutive model adopted. However, the absence of the moisture migration analysis means that the evaporation plateau and explosive spalling can't be predicted.

(3) Thermal-hydro-mechanical finite element analysis

This method performs thermal, hydraulic and mechanical analyses in a fully integrated and interactive model capable of predicting explosive spalling and the moisture state of the concrete. As this model can simulate the phase change in concrete, the melting and evaporation of PP fibres can be modelled.

(4) Chemo- thermal-hydro-mechanical finite element analysis

A fundamental role in the chemical processes and in the heat and mass transfer is played by dehydration. For example, after a critical temperature of 374.15°C when water doesn't exist as a liquid, primary chemical reactions occur as calcium carbonate decomposition and silica components transformations.

The available *fib* bulletins give a systematic introduction on spalling of concrete and summarize many research results. In these design approaches, spalling is divided into six categories: (1) explosive spalling; (2) aggregate spalling; (3) surface spalling; (4) sloughing off spalling; (5) corner spalling and (6) post cooling spalling. In reality, there is no clear definition for spalling and there are no complete theoretical models for the different forms of spalling. Spalling is influenced by many factors: permeability, age of concrete, strength of concrete, compressive stress, restraint of the member, type of aggregate, aggregate size, cracking conditions, reinforcement, and cover of reinforcement, fibre addition and air-entrainment. Spalling in tunnels is more severe due to more severe temperature-time curves and the normally higher initial moisture content of the concrete (e.g. 75%) compared to buildings (55%). The rates of heating of the concrete surface in building fires are typically 20-30°C/min while in tunnel fires this can rise to about 250°C/min.

2.1.3 ACI Method

ACI 216.1 (2007) contains prescriptive requirements for building elements regarding the minimum section dimensions and the minimum thickness of concrete cover to the reinforcement, which vary with different concrete types and different fire resistance ratings. The fire resistance (based on the heat transmission end point) of a concrete member or assembly is found by calculating the equivalent thickness for the structure and then finding

the corresponding rating in the charts and tables provided.

An analytical method of calculating fire resistance for flexural members is also provided in ACI 216.1. This method involves estimating the actual temperatures of the concrete and reinforcing steel and using the properties of the materials at those temperatures in the analysis. Once it is established that the member has enough equivalent thickness to satisfy the heat transmission end point, it must also be determined whether there is enough cover on the reinforcing steel to prevent excessive heat from reducing the yield strength to the point where it can no longer carry the loads.

The International Building Code (IBC, 2006) contains prescriptive requirements for building elements in Section 720 based on ACI 216.1.

2.1.4 Limitations of current design methods

All the tabulated data and simplified methods proposed in fire-resistance codes (EC2, fib, or ACI) give good results for simply supported elements exposed to the Standard Fire Curves (ISO 834 and others). Since all these approaches are based on the sectional level, the results for simply supported elements under natural fires are generally conservative.

For restrained elements the limitations of current approaches, whether based on simplified or advanced models, may be listed as follows:

(1) Restraint conditions for elements in elevated temperatures can induce not only a high compressive stresses due to thermal expansion, the second order effect of elements accompanied with these high compressive forces would also increase their susceptibility to failure. Current simplified design methods will be either too conservative or unsafe for these members.

A review of the literature shows that there has been limited research on the influence of restraint on fire-resistance of RC structures, and no clearly-reported fire tests about RC beams under restraint conditions are available.

(2) Fire behaviour of normal concrete structures may be different from that for high-performance concrete structures and reinforced SCC structures due to the differences in material properties and in bonding performance between rebar and concrete at high temperatures.

(3) Spalling of SCC under a fire situation has to be accounted for as higher pore pressure will be built up at elevated temperatures than normal concrete. EC 2 has provided some design guidance on spalling of concrete, which states that it is unlikely to occur when the moisture

content of concrete is less than 3% by weight. Where spalling is considered possible, the Eurocode states that the member should be designed assuming local loss of cover to the reinforcement, although most of the fire disasters introduced in section 1.1 had a spalling depth of more than 10 cm, which is much thicker than the concrete cover. The *fib* bulletins give an introduction to six kinds of spalling, although it is concluded that in reality there is no clear dividing line between spalling and no spalling and there are no successful theoretical models for different types of spalling.

The advanced calculation methods like chemo-hydro-thermal-mechanical methods can analyse the phase change, inner stress-strain results of the concrete, allowing a more accurate simulation of spalling. These methods can also take more influence factors into account. However, these types of analysis are too complex for general structural design. Although a large amount of research has been conducted on spalling, the behaviour is difficult to predict and this is probably the reason why design codes provide no clear guidance.

(4) Most of the analysis methods neglect the fire induced transient strain and creep strain of concrete materials under high temperatures, while these strains respect an important part of the total strains. There are already some research results available on the transient strain and creep strain of concrete materials at high temperatures, but how these parameters influence structural behaviour and whether it is conservative or not to neglect them in the fire resistance design is still unclear.

2.2 Progress on fire-resistance research

Based on the basic fire resistance research and the mechanical models for normal reinforced concrete members and frames, fire resistance research on structures with special sections and support conditions are under development. Research about the influence of various support conditions on fire-resistance of concrete structures indicate that already a small amount of axial restraint will increase the fire resistance of reinforced concrete beams. However, as the support conditions are difficult to control in fire tests, there are limited fire tests focussing on these aspects, and until now, there are no well-reported test results about restrained concrete beams in fire.

2.2.1 Thermal analysis

Knowledge of the development of temperature distribution in concrete structures is the first key step in the understanding of the structure's behaviour in fire. As the heat transfer process in concrete structures is a nonlinear transient problem, its governing equation is a non-linear

parabolic type partial differential equation. For actual projects, it's impossible to get analytic solutions. So generally, numerical solutions like finite difference methods and finite element methods are adopted. The finite difference method can only consider regular cross-sections and can't consider the condition of joints. The finite element method can cover these problems and lead to more precise results, for which it is more popular used. However, the computing process for finite element method is more complex and the mathematical basis is not as clear as for the finite difference method. So many of the calculation programs use the finite element difference mixed method, in which the structures is divided into finite elements and then these are analysed by the difference method at each time step.

Wilson, E.L. et al. (1996) investigated a lot on the transient thermal field of structures. Bathe, K.J. (1982) elaborated a program ADINAT for the thermal field by a simplified non-linear variation functional. Church J.G. et al. (1988) performed research on the thermal field of reinforced concrete beams and its bearing capacity at high temperatures by a simplified method. Huang Z. et al. (1997; 1999; 2003) calculated the thermal field at different heating times by finite element simulations. Zha X.X. (2003; 2001) proposed two computing methods. One method solves the Fourier thermal conduction equations by a simplified method, which only applies to rectangular cross-sections. The other one solves the thermal conduction equation by non-linear finite element methods, which takes the high-temperature properties into account in a more accurate way. It is available for the calculation of steel structures, concrete structures and composite structures.

2.2.2 Sectional analysis

Based on the thermal field analysis results and the high temperature properties of concrete and steel bars, the non-linear stress-strain relationships at elevated temperatures on the section level can be introduced and the ultimate bearing capacity and the influence of different factors can be analysed.

Large commercial programs like ABAQUS and ANSYS are frequently used in the fire performance research area. They all have special modules for thermal calculations. Han, L.H. (2009; 2007) proposed a calculation model by ABAQUS for composite structures and beam-column junctions. However, these programs use simplified material properties and can't simulate the transient creep strain explicitly and can't consider spalling phenomenon of concrete at high temperatures.

SAFIR has been developed at Liège University, Belgium (Franssen, J.M. et al. 2005; 2000). It is a non-linear finite element program. The program is divided into a thermal and a structural

analysis part. It is possible to model 2D and 3D elements of steel, concrete and composite members. Xavier H.F. et al. (2010) compared the fire resistance results of beams and columns in a frame by the Zone method of EC 2 and SAFIR. The influence of thermal elongation of beams on the fire resistance of RC frames is analysed. However, according to the assumptions of the SAFIR program, transient strain and creep of the materials are not considered explicitly in the calculation.

Terro, M.J. (1998) has developed two programs for the 3D analysis of concrete structures in fire, TEMP and STRUCT. The TEMP program is used for the thermal analysis and the temperature distributions are then fed into the program STRUCT to perform the structural analysis. STRUCT was developed within the shell of a general purpose finite element program called LUSAS (London University Stress Analysis System). The program VULCAN has been developed in the University of Sheffield with the objective of enabling 3D modelling of the behaviour of composite buildings in fire (Huang, Z. et al. 1996; 1999; 2003; 2009). The program has been verified with several test results of the Cardington full-scale fire tests. Cai, J. (2003) states that the VULCAN program has been extended in such a way that steel, concrete and composite members like reinforced concrete beams and concrete filled columns can be modelled.

There are also many people who developed their own programs:

Lu, Z.D. et al. (1996; 1993; 1989) used a non-linear finite element method based on test results. Their reports mainly focus on the changes of inner forces, the thermal field and the deformation of the heated beam, and their analysis results are verified by tests.

Yang, J.P. et al.(2000) of Tsinghua University modified the reduced-section method and proposed a more accurate one. They simplified the concrete strength curve at high temperatures into three stage: (1) concrete with a temperature below 300°C, its strength being equal to normal temperature strength; (2) concrete with a temperature between 300°C and 800°C, its strength being 1/2 of normal temperature strength; and (3) concrete with a temperature above 800°C, its strength being zero. It is the same for steel bars. Because this method is easier than the zone method and more accurate, it's very convenient for fire-resistance design.

Bratina, S. et al. (2006) analysed the effects of different strain distributions of RC beams and columns in fire by a strain based finite element method. The research compared the deflections and the fire resistance time of beams with thermal strain and the transient strain separately. They conclude that the transient creep strain has little effect on the fire resistance time of simply supported beams but their effect on displacements is remarkable.

2.2.3 Structural analysis on restraints

Forsen, et al (1982) developed a non-linear finite element program, CONFIRE, to investigate the structural behaviour and fire resistance of concrete members exposed to fire. Their analyses relate to simply supported concrete beams with different amounts of allowable expansion. Their analyses showed that the fire resistance of the RC beams does not increase with increasing axial restraints.

Kodur, V.K.R. et al. (2013; 2011; 2010; 2008; 2007) and Dwaikat M.B. et al. (2009; 2008) did many computational researches on fire performance of concrete beams with the M-k (Moment-curvature relationship) method. They introduced the development of a computer model for tracing the flexural fire response of simply supported beams, considering the effect of fire scenarios, effect of load ratio, effect of concrete cover, effect of the aggregate type and failure criteria. They use the same method to analyse the restrained RC beams under realistic fire, loading and failure scenarios. Their research shows that fire induced rotational and axial restraint effects have a major influence on the fire resistance of RC beams. Generally, the fire resistance of RC beams increases when the beams are axially and/or rotationally restrained.

Riva, P. et al. (2008; 2008) have performed theoretical research and computational calculations by ABAQUS on the fire behaviour of a series of fixed-end rectangular beams with varying axial restraints (the translational stiffness of the axial restraints being in the range $0 \sim \infty$). The results are used to illustrate a simplified plastic verification procedure that allows determination of both the bearing capacity and the deflection during the fire. Their research shows that the developed axial force leads to good results for fire resistance of the RC beams. Neglecting the axial force provided by the support conditions may lead to a conservative design.

Bernhart, D. (2004) calculated the effect of support conditions in the fire resistance of reinforced concrete beams by the SAFIR program. The beams are modelled by 2D elements with varying support conditions and displacements. The axial force and reaction forces at the supports are compared after a four hours ISO-fire.

Lim. L. et al. (2004; 2003) present a computer model of axially restrained and rotationally restrained one-way RC slab in fire conditions. The analyses of the slabs were carried out with the SAFIR finite element program and the research results show that one-way slabs under fire conditions are very sensitive to the end support conditions and the axial restraint stiffness. Slabs with high axial restraint have good fire resistance. Slabs with rotationally restrained end supports have much better fire resistance than equivalent simply supported slabs and they are less sensitive to the axial restraint stiffness. The analyses have also shown that even if the

thrust line is located close to the soffit, the slab can still deform into a catenary if there is insufficient horizontal axial restraint.

2.2.4 Experiments

(1) ASTM E119 Standard Fire Test

The widely used and nationally accepted test procedure is that developed by the American Society of Testing and Materials (ASTM). It is designated as ASTM E119 (2000) Standard Methods of Fire Tests of Building Construction and Materials. A standard fire test is conducted by placing a full size assembly in a test furnace. Floor and roof specimens are exposed to a controlled fire from beneath, beams are exposed from the bottom and sides, walls from one side, and columns are exposed to fire from all sides. The temperature is raised in the furnace over a given period of time in accordance with ASTM E119 standard time-temperature curve. The end of the test is reached and the fire endurance of the specimen is established when any one of the following conditions first occurs.

- I. For walls, floors, and roof assemblies, the temperature of the unexposed surface raises an average of 150°F (65.5 °C) above its initial temperature of 325°F (165°C) at any location. In addition, walls achieving a rating classification of one hour or greater must withstand the impact, erosion and cooling effects of a hose steam test.
- II. Cotton waste placed on the unexposed side of a wall, floor, or roof system is ignited through cracks or fissures which develop in the specimen during the test.
- III. The test assembly fails to sustain the applied service load.
- IV. For certain restrained and all unrestrained floors, roofs and beams, the reinforcing steel temperature rises to 1100°F (593.3°C).

Experience shows that concrete floor/roof assemblies and walls usually fail by heat transmission (item a); and columns and beams by failure to sustain the applied loads (item c), or by beam reinforcement failing to meet the temperature criterion (item d).

(2) Fire Tests

The study on high temperature performance of concrete structures began early in the twentieth century, like the fire test on concrete column carried out by ANSI (American National Standards Institute) in 1925. But a large amount of research on this item began from the 1950's. During the 1960's, many large-scale fire test equipment have been built in many countries and lots of fire resistance research groups have been established: PCA (Portland

Cement Association) in U.S., BFRL (Building Fire Research Laboratory) in U.S., BRE (Building Research Establishment) in U.K., and National Academy of Canada, and they all achieved a lot in this area. However, most of these tests were conducted on unrestrained beams and thus there is limited information on the fire response of restrained RC beams in the literature.

Issen, L.A. et al. (1970) showed that almost any amount of restraint greatly enhanced the fire resistance of RC structures as they were able to support their loads considerably longer than simply supported elements. The tests have also shown that the maximum axial force is proportional to the cross-section of the specimen, which is exposed to fire, heating conditions and the elastic modulus of concrete.

Based on the tests conducted at the Portland Cement Association (PCA), a step-by-step method was developed to determine the amount of axial restraint required to prevent collapse of concrete structures. Gustafson, J.A. (1980) also provides recommendations for evaluating the position of the line of thrust at the slab supports. The thrust forces that occur can be quite large but are always considerably less than that calculated by use of elastic properties of concrete and steel together with appropriate coefficients of expansion as at high temperatures. Creep and stress relaxations play an important role.

Cooke, G.M.E. (1993) has conducted a series of fire tests on restrained concrete flat slabs. The tests showed that an axial load applied at mid-depth of the slab end supports resulted in a significantly lower chance to failure than a slab with no axial restraint.

2.3 Main Research

In order to solve the problems that were outlined it is necessary to develop a more accurate and convenient fire-resistance design method, which will take the explicit transient creep strain model at elevated temperatures into account, to improve the understanding of the influence of different support conditions, and to evaluate the effect of restraints on fire resistance. This thesis will mainly focus on the following:

(1) Literature study. Existing research results will be collected and summarized first, including the calculation methods and the conclusions related to high-temperature properties of concrete and steel bars. For concrete, the mechanical models with transient creep strain considered implicitly and explicitly at high temperatures for normal concrete and self-compacting concrete need special study and comparison, as they serve as input for the subsequent fire-resistance design method and calculations.

(2) A simplified but accurate fire-resistance design method. A multi-iteration method is proposed, which can analyse the influence of explicit transient creep strain model of concrete, the influence of various restraint conditions and the influence of various fire scenarios.

The design process should contain two parts: sectional analysis and structural analysis. The sectional analysis is based on the zone method introduced in EC 2, which divides the element section into small zones and determines an average property of each zone. For a standard fire, the average of each zone can be easily obtained by a numerical method, but for special fire condition, the temperatures of each zone are calculated by DIANA (de Witte, 2002). Nonlinear stress-strain relationships of concrete and steel bars at elevated temperatures are adapted and averaged data is used for each zone.

The structural analysis focusses on the deformation and deform rate by using the average stiffness method. The influence of various axial restraint and rotational restraint are considered as a boundary condition in this model, after which the elements with different restraint are analysed.

(3) Suggestions on fire-resistance design. After the analysis of calculation results on fire behaviour with and without transient strain and creep strain, with various restraint conditions and under different fire curves, suggestions on how to consider these parameters in fire-resistance design are proposed.

Material properties at elevated temperatures

The material properties at high temperatures will directly influence the behaviour of structures exposed to high temperatures. There are already a lot of research results both experimental and theoretical, on the properties of steel bars and concrete under elevated temperatures. This chapter gives a brief literature review on these material models.

3.1 Thermal properties of concrete under elevated temperatures

Concrete is considered as an isotropic material for high-temperature calculations. Its thermal material properties can be described by three characteristics which influence the temperature field of the cross-sections: thermal conductivity, specific heat and density. When subjected to high temperatures, these properties will change with the inner temperature field, and this will also influence the temperature field.

3.1.1 Thermal conductivity of concrete

The thermal conductivity of concrete is related to the ability of transferring heat through the concrete. It is calculated as the velocity of thermal energy transferred through a unit area of the cross-section under a unit temperature gradient, with unit W/mK . Normally, the conductivity of concrete will increase with increasing temperature. In general, the thermal conductivity of concrete with siliceous aggregates is larger than that of calcareous aggregates (Gustafson, J.A. 1980). The thermal conductivity of light weight concrete is the smallest. Some of the commonly used material models are listed below.

(1) Thermal conductivity model in EC 2

EC 2 takes the aggregate as the influencing factor for the thermal conductivity of concrete and it supplied upper and lower limit values, and all the various values should be between these two lines. The upper limit of thermal conductivity of normal weight concrete should be determined by Equation (3.01), and the lower limit of normal weight concrete is determined by Equation (3.02). The upper and lower limits are shown by Figure 3.01.

$$\lambda_c = 2 - 0.2451 \frac{\theta}{100} + 0.0107 \left(\frac{\theta}{100} \right)^2 \quad 20^\circ\text{C} \leq \theta \leq 1200^\circ\text{C} \quad (3.01)$$

$$\lambda_c = 1.36 - 0.136 \frac{\theta}{100} + 0.0057 \left(\frac{\theta}{100} \right)^2 \quad 20^\circ\text{C} \leq \theta \leq 1200^\circ\text{C} \quad (3.02)$$

where λ_c is the thermal conductivity of concrete.

θ is the temperature of concrete.

(2) Thermal conductivity model proposed by Lie, T.T. et al. (1992; 1991)

In the papers by Lie, T.T., one general model shown by Equation (3.03) is given for all types of aggregates since their research showed that the aggregate influence is not important.

$$\lambda_c = \begin{cases} 2.0 - 0.001775\theta & 0^\circ\text{C} \leq \theta \leq 500^\circ\text{C} \\ 1.402 - 0.000579\theta & 500^\circ\text{C} \leq \theta \leq 1000^\circ\text{C} \end{cases} \quad (3.03)$$

(3) Thermal conductivity model proposed by Lu, Z.D. et al. (1996; 1993)

Researchers at Tongji University have derived the following model for normal concrete by experimental analysis, shown by Equation (3.04)

$$\lambda_c = 1.6 - 7.1 \times 10^{-4} \theta \quad 20^\circ\text{C} \leq \theta \leq 1200^\circ\text{C} \quad (3.04)$$

(4) Thermal conductivity models for HPC

There are a few other thermal conductivity models which could be used for high performance concrete (HPC). Ren, H-M. (2006) of Tongji University modified the material model of Campbell-Allen and Thorne, and proposed separate equations, Equation (3.05) for the conductivity of siliceous aggregate concrete and Equation (3.06) for calcareous aggregate concrete.

$$\lambda_c = 2.44 - 0.24 \frac{\theta}{120} + 0.012 \left(\frac{\theta}{120} \right)^2 \quad 20^\circ\text{C} \leq \theta \leq 1200^\circ\text{C} \quad (3.05)$$

$$\lambda_c = 1.88 - 0.16 \frac{\theta}{120} + 0.008 \left(\frac{\theta}{120} \right)^2 \quad 20^\circ\text{C} \leq \theta \leq 1200^\circ\text{C} \quad (3.06)$$

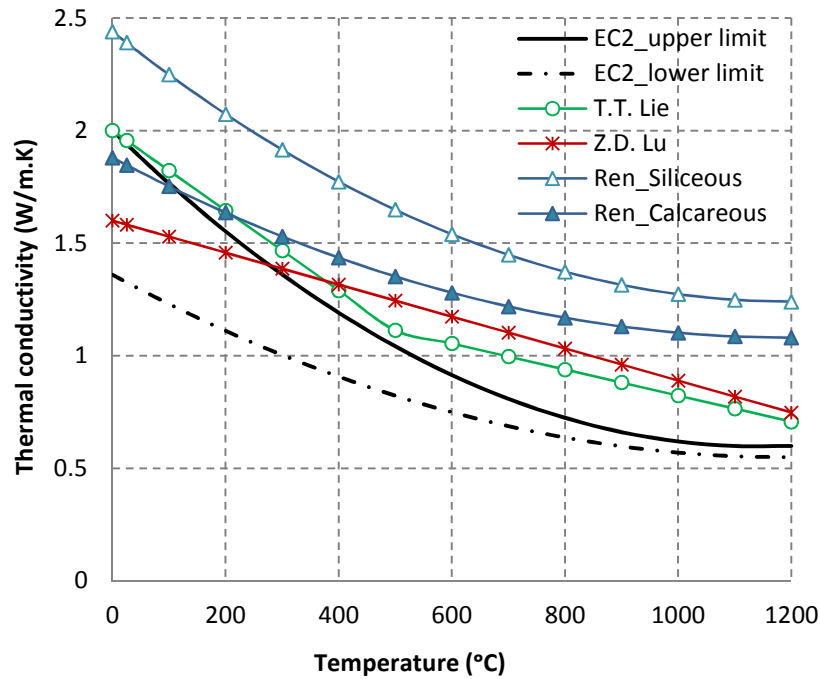


Figure 3.01 The thermal conductivity of concrete at elevated temperatures

3.1.2 Specific heat

The specific heat is the quantity of heat for one kilogram of concrete to increase (or decrease) one degree in temperature. It is designated by c_c , with unit $J/(kg \cdot ^\circ C)$. Experimental research shows that the various types of aggregate in the concrete mix have little influence on the specific heat of concrete.

(1) In EC 2 (2004), the specific heat of dry concrete ($u = 0\%$) model, shown by Equation (3.07), is valid both for siliceous and calcareous aggregates concrete.

$$c_c = \begin{cases} 900 & 20^\circ C \leq \theta \leq 100^\circ C \\ 900 + (\theta - 100) & 100^\circ C < \theta \leq 200^\circ C \\ 1000 + (\theta - 200)/2 & 200^\circ C < \theta \leq 400^\circ C \\ 1100 & 400^\circ C < \theta \leq 1200^\circ C \end{cases} \quad (3.07)$$

Since the water content has a significant influence on the specific heat of concrete, EC 2 suggest that the curve for concrete with given moisture content needs to be modified due to steam generation of water in heated concrete. According to EC 2, only the second part between $100^\circ C$ and $200^\circ C$ is different when the water content changes. A function for this part of the specific heat may be modelled by a constant value $c_{c,peak}$, situated between $100^\circ C$

and 115°C with linear decrease between 115°C and 200°C .

$c_{c,peak} = 900\text{J}/\text{kg}\cdot\text{K}$ is for moisture content of 0% of concrete weight;

$c_{c,peak} = 1470\text{J}/\text{kg}\cdot\text{K}$ is for moisture content of 1.5% of concrete weight;

$c_{c,peak} = 2020\text{J}/\text{kg}\cdot\text{K}$ is for moisture content of 3.0% of concrete weight;

The peaks of specific heat are illustrated in Figure 3.02.

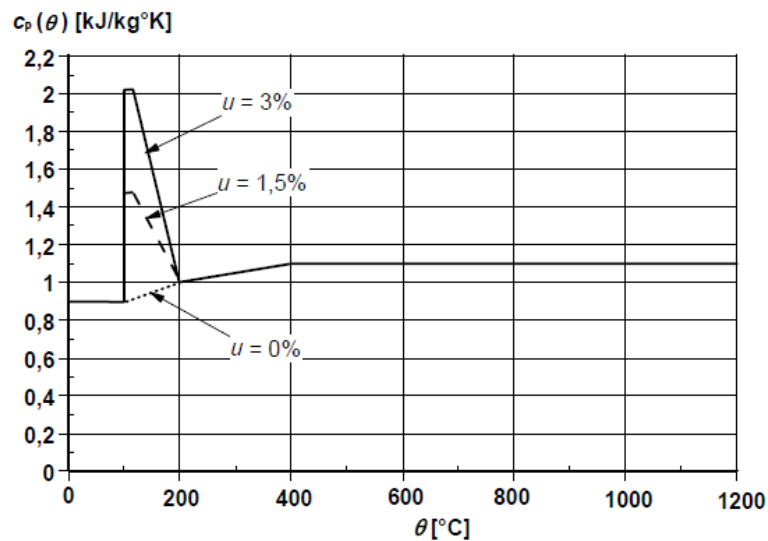


Figure 3.02 Specific heat as a function of temperature at 3 different moisture contents

($u = 0\%$ $u = 1.5\%$ and $u = 3\%$ by weight) (EC 2, 2004)

(2) The equation suggested by Lu, Z.D. et al. (1996; 1993) is shown by Equation (3.08).

$$c_c = 836 + 0.49\theta \quad 20^{\circ}\text{C} \leq \theta \leq 1200^{\circ}\text{C} \quad (3.08)$$

(3) Lie, T.T. et al. (1992; 1991) supplied an expression for the volumetric specific heat, which combines density and specific heat, expressed by Equation (3.09).

$$\rho_c c_c = \begin{cases} (1.70 + 0.005\theta) \times 10^6 & 0^\circ\text{C} \leq \theta \leq 200^\circ\text{C} \\ 2.70 \times 10^6 & 200^\circ\text{C} \leq \theta \leq 400^\circ\text{C} \\ (-2.5 + 0.013\theta) \times 10^6 & 400^\circ\text{C} \leq \theta \leq 500^\circ\text{C} \\ (10.5 - 0.013\theta) \times 10^6 & 500^\circ\text{C} \leq \theta \leq 600^\circ\text{C} \\ 2.70 \times 10^6 & \theta \geq 600^\circ\text{C} \end{cases} \quad (3.09)$$

where ρ_c is the density of the concrete.

(4) For high performance concrete, Ren, H.M. (2006) of Tongji University introduced Equation (3.10) based on the model given in EC 2.

$$c_c = 892 + 80 \frac{\theta}{120} - 4 \left(\frac{\theta}{120} \right)^2 \quad 20^\circ\text{C} \leq \theta \leq 1200^\circ\text{C} \quad (3.10)$$

3.1.3 Density of concrete

Experimental research shows that the density of concrete will decrease with temperature. At the early stage this is due to the evaporation of water in the concrete, and later on, it is caused by the thermal expansion of the concrete. However, this change on density is rather limited and the value is in between $2200 \text{ kg} / \text{m}^3 \sim 2400 \text{ kg} / \text{m}^3$ (Taerwe, L. et al. 2008).

EC 2 considers the influence of water loss, and gives a group of equations for the change of density, Equation (3.11).

$$\rho_c(\theta) = \begin{cases} \rho_c(20^\circ\text{C}) & 20^\circ\text{C} \leq \theta \leq 115^\circ\text{C} \\ \rho_c(20^\circ\text{C})[1 - 0.02(\theta - 115)/85] & 115^\circ\text{C} \leq \theta \leq 200^\circ\text{C} \\ \rho_c(20^\circ\text{C})[0.98 - 0.03(\theta - 200)/200] & 200^\circ\text{C} \leq \theta \leq 400^\circ\text{C} \\ \rho_c(20^\circ\text{C})[0.95 - 0.07(\theta - 400)/800] & 400^\circ\text{C} \leq \theta \leq 1200^\circ\text{C} \end{cases} \quad (3.11)$$

Since the small density change will lead to little influence on structural behaviour, a constant density in between $2200 \text{ kg} / \text{m}^3 \sim 2400 \text{ kg} / \text{m}^3$, which is a bit smaller than the one at normal temperature, is suggested to be used in fire behaviour research of RC structures.

3.2 Mechanical properties of concrete under elevated temperatures

A brief description of the behaviour of concrete when exposed to heating can be made as

follows. When concrete is heated, the free water in it evaporates, and above approximately 150°C the chemically bounded water in the hydrated calcium silicates starts being released. In some cases, the surface of the concrete is not able to resist the pressure of the water and steam, which leads to spalling. The release of water causes shrinkage of the hydrated cement paste, while the aggregate and reinforcement are subjected to a thermal expansion. This leads to stresses in the composite material and from approximately 300°C on, micro cracks will occur in the concrete. These cracks cause a reduction of the tensile strength and the modulus of the elasticity and unloaded specimens will be subjected to an irreversible expansion. The concrete starts weakening rapidly at about 400-535 °C , because the calcium hydroxide decomposes into calcium oxide and water. At about 700°C the rate of decomposition of the remaining calcium silicates reaches its maximum and at about 900°C the volume of quartz aggregates becomes unstable. Above 1150°C , concrete containing feldspar will melt (Hertz, K. 1999; 1998).

The temperature related mechanical properties of concrete mainly include the compressive strength, tensile strength, elastic modulus, temperature related strains (constitutive model), and spalling of concrete.

3.2.1 The compressive strength of concrete

The compressive strength is one of the most important mechanical properties of concrete. It is also one of the critical factors for the fire behaviour of RC structures exposed to fire. The compressive strength of concrete under elevated temperatures is dependent on parameters such as temperature, loading history, type of aggregate, and so on. However, it is clearly shown that for a specific concrete type, the strength is almost only dependent on the temperature, and the loading history may be neglected (Anderberg, Y. et al. 1982).

(1) EC 2 (2004) supplies the reduction factors of compressive strength of concrete at elevated temperatures in form of a table. They could be used for normal weight concrete with siliceous or calcareous aggregates. The curves for the compressive strength at elevated temperatures are shown in Figure 3.03.

(2) Lu, Z.D. et al. (1996; 1993) gives a function for compressive strength of concrete at high temperatures based on compression tests on cubic specimens of normal concrete, shown by Equation (3.12).

$$\frac{f_c(\theta)}{f_c(20^\circ C)} = \begin{cases} 1.0 & 20^\circ C \leq \theta \leq 400^\circ C \\ 1.75 - 1.9 \times 10^{-3} \theta & 400^\circ C \leq \theta \leq 800^\circ C \end{cases} \quad (3.12)$$

where $f_c(\theta)$ is the compressive strength of concrete at temperature θ ;

$f_c(20^\circ\text{C})$ is the compressive strength of concrete at 20°C .

(3) Kodur, V.K.R. et al. (2005; 2000) has suggested Equation (3.13) as the reduction function of the compressive strength of high performance concrete.

$$\frac{f_c(\theta)}{f_c(20^\circ\text{C})} = \begin{cases} 1.0 - 3.125 \times 10^{-3}(\theta - 20) & 20^\circ\text{C} \leq \theta \leq 100^\circ\text{C} \\ 0.75 & 100^\circ\text{C} < \theta \leq 400^\circ\text{C} \\ 1.33 - 1.45 \times 10^{-3}(\theta - 20) & \theta \geq 400^\circ\text{C} \end{cases} \quad (3.13)$$

(4) Tao, J. (2010) has proposed a compressive strength function under elevated temperatures for self-compacting concrete (SCC) by a series of stress-strain relationship experiments of SCC specimens exposed to high temperatures. Equation (3.14) is valid for normal strength SCC, and Equation (3.15) is for high strength SCC.

$$\frac{f_c(\theta)}{f_c(20^\circ\text{C})} = 2.08 \times 10^{-9} \theta^3 - 1.90 \times 10^{-6} \theta^2 - 7.87 \times 10^{-4} \theta + 1.023 \quad (3.14)$$

$$\frac{f_c(\theta)}{f_c(20^\circ\text{C})} = -9.86 \times 10^{-10} \theta^3 - 1.66 \times 10^{-7} \theta^2 + 2.08 \times 10^{-5} \theta + 0.989 \quad (3.15)$$

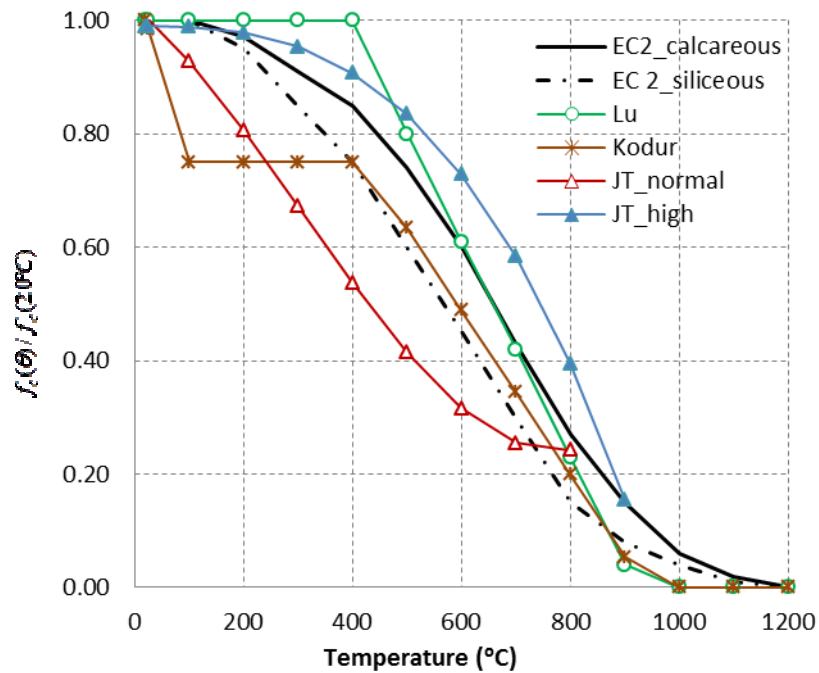


Figure 3.03 Reduction of compressive strength of concrete at elevated temperatures

3.2.2 The tensile strength of concrete

High temperatures will cause a much greater loss on the tensile strength of concrete than that on the compressive strength, which makes that the tensile strength of concrete has a very small influence on the structural behaviour of RC structures exposed to high temperatures. The tensile strength of concrete should normally be ignored in the design of RC members subjected to bending. However, for accurate calculations when using simplified or advanced models, it is necessary to take account of the tensile strength.

(1) The reduction of tensile strength at elevated temperatures given by EC 2 is shown by Equation (3.16).

$$\frac{f_{ck,t}(\theta)}{f_{ck,t}(20^{\circ}C)} = \begin{cases} 1.0 & 20^{\circ}C \leq \theta \leq 100^{\circ}C \\ 1.0 - (\theta - 100)/500 & 100^{\circ}C \leq \theta \leq 600^{\circ}C \end{cases} \quad (3.16)$$

where $f_{ck,t}(\theta)$ is the tensile strength of concrete at high temperature θ ;

$f_{ck,t}(20^{\circ}C)$ is the tensile strength of concrete at normal temperature.

(2) The simplified function derived from experiments on tensile strength under high temperature by Shi, X.D. et al. (2000) is given by Equation (3.17).

$$\frac{f_{ck,t}(\theta)}{f_{ck,t}(20^{\circ}C)} = 1 - \frac{\theta}{1000} \quad (3.17)$$

(3) Lu Z.D et al. (1996; 1993) suggests the following reduction factor, shown by Equation (3.18).

$$\frac{f_{ck,t}(\theta)}{f_{ck,t}(20^{\circ}C)} = \begin{cases} 1.0 - 1.6 \times 10^{-3} \theta & 20^{\circ}C \leq \theta \leq 500^{\circ}C \\ 0.2 & \theta > 500^{\circ}C \end{cases} \quad (3.18)$$

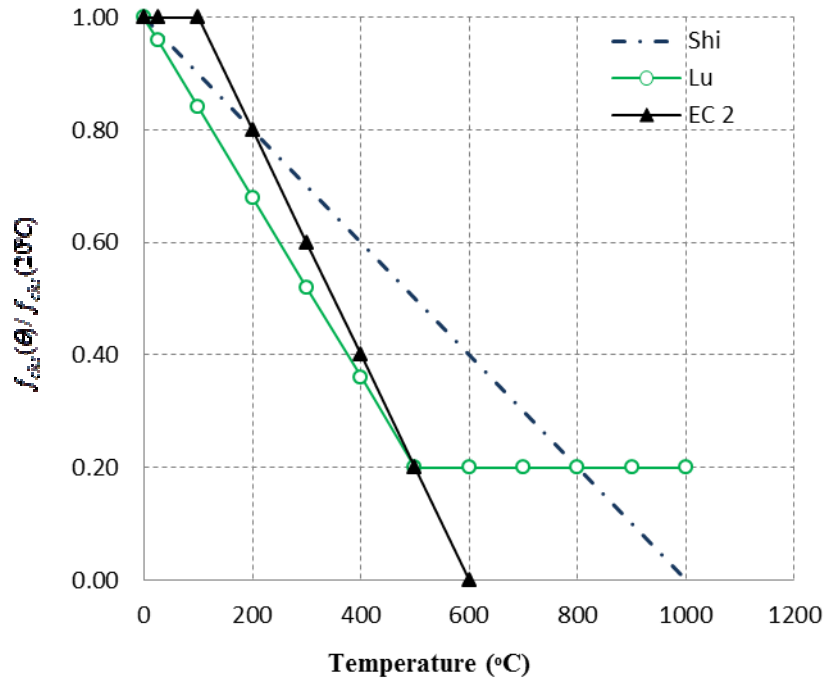


Figure 3.04 Tensile strength of concrete as a function of temperature

3.2.3 The elastic modulus of concrete

According to experiments, the elastic modulus of concrete will decrease with the increase of temperature. This is mainly influenced by the various types of aggregate, and the water/cement ratio. The decreasing factor for NSC is larger than that of HSC.

(1) EC 2 doesn't give separate functions for the elastic modulus of concrete under elevated temperatures since the complete stress-strain relationship is given by Equation (3.27).

(2) Shi, X.D. (1992) derived the reduction factors for elastic modulus of normal concrete, as shown by Equation (3.19).

$$\frac{E_c(\theta)}{E_c(20^\circ\text{C})} = \begin{cases} 1.0 & 20^\circ\text{C} \leq \theta \leq 60^\circ\text{C} \\ 0.83 - 0.0011\theta & 60^\circ\text{C} \leq \theta \leq 700^\circ\text{C} \end{cases} \quad (3.19)$$

where $E_c(\theta)$ is the elastic modulus of concrete at high temperature θ ;

$E_c(20^\circ\text{C})$ is the initial elastic modulus of concrete at 20°C .

(3) Lu, Z.D. (1996; 1993) took the tangent modulus at $0.4 f_c(\theta)$, and formulated the

descending curve of elastic modulus into three parts, as shown by Equation (3.20).

$$\frac{E_c(\theta)}{E_c(20^\circ C)} = \begin{cases} 1.0 - 0.0015\theta & 20^\circ C \leq \theta \leq 200^\circ C \\ 0.87 - 0.0084\theta & 200^\circ C \leq \theta \leq 700^\circ C \\ 0.28 & \theta > 700^\circ C \end{cases} \quad (3.20)$$

(4) Tao, J. (2012) has performed research on the elastic modulus of SCC at elevated temperatures. The derived model for normal strength SCC is shown by Equation (3.21) and for high-strength SCC by Equation (3.22).

$$\frac{E_c(\theta)}{E_c(20^\circ C)} = \begin{cases} 1.0 & 20^\circ C \leq \theta \leq 80^\circ C \\ 0.95 - 0.0013\theta & 80^\circ C \leq \theta \leq 800^\circ C \end{cases} \quad (3.21)$$

$$\frac{E_c(\theta)}{E_c(20^\circ C)} = \begin{cases} 1.0 & 20^\circ C \leq \theta \leq 80^\circ C \\ 1.01 - 0.0012\theta & 80^\circ C \leq \theta \leq 800^\circ C \end{cases} \quad (3.22)$$

3.2.4 Thermal strains of concrete

The expression of the total deformation, which is also called the constitutive model of concrete, describes the behaviour of heated and loaded concrete in mathematical terms. It is based on the stress-strain relationships of heated concrete. It is a sum of four parts: thermal elongation, stress dependent strain, transient strain and creep strain (Anderberg, Y. et al. 1976), as shown by Equation (3.23).

$$\varepsilon_{c,tot}(\theta) = \varepsilon_{c,th}(\theta) + \varepsilon_{c,\sigma}(\sigma, \theta) + \varepsilon_{c,tr}(\sigma, \theta) + \varepsilon_{c,cr}(\sigma, \theta, t) \quad (3.23)$$

where $\varepsilon_{c,tot}$ is the total strain of concrete under elevated temperature θ ;

$\varepsilon_{c,th}$ is the thermal elongation of concrete under elevated temperature θ ;

$\varepsilon_{c,\sigma}$ is the stress dependent strain of concrete under elevated temperature θ ;

$\varepsilon_{c,tr}$ is the transient strain of concrete under elevated temperature θ ;

$\varepsilon_{c,cr}$ is the creep strain of concrete under elevated temperature θ ;

σ is the stress in the concrete;

t is the time for concrete under creep;

In some literature, the last two items which are transient strain and creep strain, are merged into the transient creep strain. There are two kinds of models used for the transient creep strain: the implicit model and the explicit model.

I. Implicit material model

The most commonly used implicit transient creep strain material model is given by EC 2. It merges the transient creep strain into the stress-strain relationship, making the Equation (3.23) shorter into Equation (3.24).

$$\varepsilon_{c,tot}(\theta) = \varepsilon_{c,th}(\theta) + \varepsilon_{c,\sigma}(\sigma, \theta, t) \quad (3.24)$$

(1) The thermal elongation of concrete $\varepsilon_{c,th}$ is increasing with increasing temperature. The main influencing factors for this are the type of aggregates, the water content, the heating rate, etc. Since concrete is a kind of isotropic material, the variations in the thermal field yield different thermal strains in the concrete, so the thermal elongation in theory is actually the average strain.

EC 2 takes the aggregate as the main influencing factor and supplies two equations for the thermal elongation of concrete. Equation (3.25) holds for siliceous aggregate concrete and Equation (3.26) for calcareous aggregate concrete.

$$\varepsilon_{c,th} = \begin{cases} -1.8 \times 10^{-4} + 9 \times 10^{-6} \theta + 2.3 \times 10^{-11} \theta^3 & 20^\circ\text{C} \leq \theta \leq 700^\circ\text{C} \\ 14 \times 10^{-3} & 700^\circ\text{C} < \theta \leq 1200^\circ\text{C} \end{cases} \quad (3.25)$$

$$\varepsilon_{c,th} = \begin{cases} -1.2 \times 10^{-4} + 6 \times 10^{-6} \theta + 1.4 \times 10^{-11} \theta^3 & 20^\circ\text{C} \leq \theta \leq 805^\circ\text{C} \\ 12 \times 10^{-3} & 805^\circ\text{C} < \theta \leq 1200^\circ\text{C} \end{cases} \quad (3.26)$$

(2) The stress-strain relation curve for concrete (Figure 3.05) supplied in EC 2 can also be expressed by Equation (3.27), with a linear model for the decreasing branch.

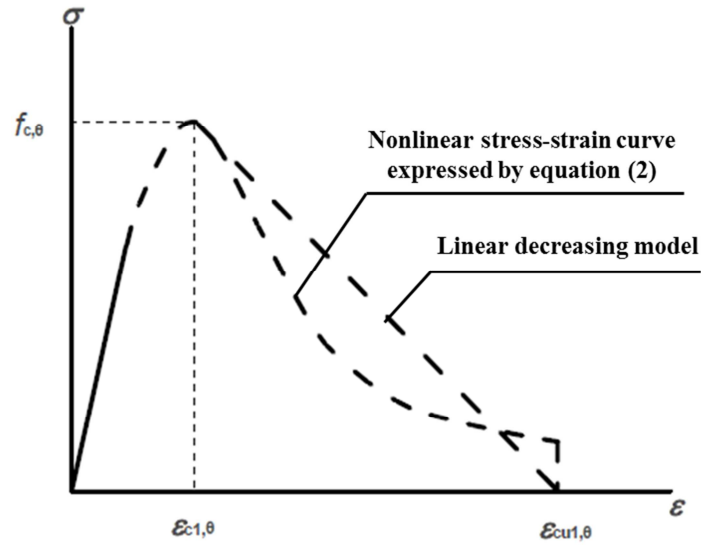


Fig.3.05. Stress-strain relation curve for concrete at elevated temperatures (EC 2, 2004)

$$\sigma_{c,\sigma} = \begin{cases} \frac{3\varepsilon_{c,\sigma} \cdot f_{c,\theta}}{\varepsilon_{c1,\theta} \left[2 + \left(\frac{\varepsilon}{\varepsilon_{c1,\theta}} \right)^3 \right]} & \varepsilon_{c,\sigma} \leq \varepsilon_{c1,\theta} \\ \frac{f_{c,\theta} (\varepsilon_{cu1,\theta} - \varepsilon)}{(\varepsilon_{cu1,\theta} - \varepsilon_{c1,\theta})} & \varepsilon_{c1,\theta} < \varepsilon_{c,\sigma} \leq \varepsilon_{cu1,\theta} \end{cases} \quad (3.27)$$

where $\sigma_{c,\sigma}$ represents the stress of concrete at temperature θ ;

$\varepsilon_{c,\sigma}$ represents the stress related strain of concrete at temperature θ ;

$f_{c,\theta}$ represents the compressive strength of concrete at temperature θ ;

$\varepsilon_{c1,\theta}$ represents the concrete strain corresponding to $f_{c,\theta}$ at temperature θ ;

$\varepsilon_{cu1,\theta}$ represents the ultimate strain of concrete at temperature θ .

The decreasing functions for compressive strength and ultimate strains under elevated temperatures can be obtained from Table 3.1 in EC 2. For intermediate values of the temperature, linear interpolation may be used.

II. Explicit material model

In explicit material models, the total strain is actually a sum of four parts: thermal strain $\varepsilon_{c,th}$, instantaneous stress-related strain $\varepsilon_{c,\sigma}$, transient strain $\varepsilon_{c,tr}$ and creep strain $\varepsilon_{c,cr}$, as expressed by Equation (3.23). The explicit material model of concrete adopted in this thesis was developed by Tao, J. (2008).

(1) Thermal elongation of SCC both for high strength or normal strength is the same as shown by Equation (3.28).

$$\varepsilon_{c,th} = 2.0 \times 10^{-8} (\theta - 20)^2 + 8.9 \times 10^{-7} (\theta - 20) \quad (3.28)$$

(2) Instantaneous stress related strain

With the transient strain and creep strain calculated separately, the stress is directly related to the instantaneous stress-related strain, which is given as Equation (3.29).

$$\sigma_{c,\theta} = \begin{cases} f_c(\theta) \left[a \left(\frac{\varepsilon_{c,\sigma}}{\varepsilon_{c1,\theta}} \right) + (3 - 2a) \left(\frac{\varepsilon_{c,\sigma}}{\varepsilon_{c1,\theta}} \right)^2 + (a - 2) \left(\frac{\varepsilon_{c,\sigma}}{\varepsilon_{c1,\theta}} \right)^3 \right] & \varepsilon_{c,\sigma} \leq \varepsilon_{c1,\theta} \\ \frac{\varepsilon_{c,\sigma} \cdot f_c(\theta)}{b(\varepsilon_{c,\sigma} - \varepsilon_{c1,\theta})^2 / \varepsilon_{c1,\theta} + \varepsilon_{c,\sigma}} & \varepsilon_{c1,\theta} < \varepsilon_{c,\sigma} \leq \varepsilon_{cu1,\theta} \end{cases} \quad (3.29)$$

where a and b are temperature related factors. For normal strength concrete, they can be calculated by Equation (3.30), and for high-strength concrete, they should be calculated by Equation (3.31).

$$\begin{cases} a = 0.00863e^{0.00313\theta} - 0.00983 \\ b = 345.33e^{-0.00005\theta} - 328.01488 \end{cases} \quad (3.30)$$

$$\begin{cases} a = -0.0784e^{\theta/313.06} + 1.180 \\ b = 0.20272e^{\theta/163.5371} + 0.05983 \end{cases} \quad (3.31)$$

The decreasing function for compressive strength under elevated temperatures is given by Equations (3.14) and (3.15) and the ultimate elastic strains under elevated temperatures are expressed by Equation (3.32).

$$\frac{\varepsilon_{c1}(\theta)}{\varepsilon_{c1}(20^\circ C)} = 0.17e^{\theta/287.36} + 0.79 \quad (3.32)$$

(3) Transient strain of concrete

When a loaded concrete structure is heated, an additional strain is introduced, called transient strain. This effect is absent for unloaded concrete and results in smaller concrete strength losses and smaller strains. The free thermal expansion is thus partly compensated by the external load. For high loading levels, the expansion can be zero or even negative. The transient strain is much larger than the creep strain and the stress-related strain under elevated temperatures, and can result in significant influence on the deformation of RC structures. In some literature, the transient strain is thought to be a kind of creep, so it's also called transient thermal creep or TTC.

The transient strain cannot directly be measured, but should be derived from the superposition of strains given in Equation (3.23). The model of Anderberg, Y. (1976) gives a linear relationship between the transient strain, the load factor and the free thermal strain till 500°C (Table 3.01). The parameter k_2 is a dimensionless constant that varies from 1.8 to 2.35 for quartzite aggregate concrete, based on published test results. Recently, more tests were performed by several authors to study the variation of the k_2 parameter for different concrete types (Schneider, U et al. 1985; 1988; Tokoyoda, M. et al. 2007; Hirashima, T. et al. 2007). A non-linear relationship is found between the transient strain and the temperature, which is also stated in the reports of Khoury, G.A. et al. (1986, 1985). Finally, for modelling the transient strain, the models by Tao, J. (2008) and Annerel, E. (2010, 2007) are chosen (Table 3.01).

Table 3.01 Transient strain formulations

Function	Reference
$\theta \leq 500^\circ\text{C}$ $\varepsilon_{c,cr} = -k_2 \frac{\sigma}{f_c(20^\circ\text{C})} \varepsilon_{c,th}$	Anderberg, Y. (1976)
Quartzite (OPC) NSC: $k_2 = 2.35$ (Anderberg) $k_2 = 2.0$ (Weiglerand Fischer) $k_2 = 1.8$ (Schneider)	Anderberg, Y. (1976)
Limestone (OPC) NSC: $k_2 = 1.3$	Tokoyoda, M. (2007)
Siliceous (OPC) HSC: $k_2 = 4.03$	Hirashima, T. (2007)

$\varepsilon_{c,cr} = c \cdot \frac{\sigma}{f_c(20^\circ C)} A_r$ $A_r = \begin{pmatrix} -2.6413 \times 10^{-13} \theta^4 + 2.9306 \times 10^{-10} \theta^3 - 9.4554 \times 10^{-8} \theta^2 \\ -5.7862 \times 10^{-6} \theta + 2.7 \times 10^{-4} \end{pmatrix}$ <p>Limestone (OPC) NS SCC: $c = 1.0$ Limestone (OPC) HS SCC: $c = 1.55$</p>	Tao, J. (2008)
$\theta \leq 400^\circ C \quad \varepsilon_{c,cr} = c \cdot \frac{\sigma}{f_c(20^\circ C)} A_r$ $A_r = \begin{pmatrix} -1.11 \times 10^{-10} \theta^4 - 1.82 \times 10^{-7} \theta^3 + 3.45 \times 10^{-5} \theta^2 \\ -1.3 \times 10^{-2} \theta + 0.202 \end{pmatrix}$ <p>TC (OPC, siliceous): $c = 1.06$ SCC (OPC, siliceous): $c = 0.94$</p>	Annerel, E. (2010)

Computer simulations that study the behaviour of heated concrete structures should include the transient strain, since otherwise the deformations will be overestimated. This remark is especially necessary for columns, because of their large compression area. For plates and beams this effect is less, since the compression zone is small and located further away from the heating zone, thus resulting in smaller temperature increases. Furthermore, the compression stresses are not uniform.

(4) Creep strain of concrete

The creep strain at normal temperature or under elevated temperature is the strain that increases with the time under load. The influencing factors for creep under elevated temperatures are the same as the ones at normal temperature: stress level, loading time, age of concrete and humidity. The experimental results of Tao, J. et al. (2012) show that for SCC, the increasing trend of creep strain with time under elevated temperature is similar to that of creep at normal temperature, but the corresponding creep strain is much larger.

The experimental results analysed by Tao, J. (2012) for the creep strain are given as follows. For normal strength SCC Equation (3.33) is valid and for high strength SCC Equation (3.34).

$$\varepsilon_{c,cr} = \frac{\sigma_c}{f_c} (123.21 + 43.11 e^{0.00477\theta}) \left(\frac{t}{10800} \right)^{0.3} \times 10^{-6} \quad (3.33)$$

$$\varepsilon_{c,cr} = \frac{\sigma_c}{f_c} \times 114.06(e^{0.00477\theta} - 1) \left(\frac{t}{10800}\right)^{0.5} \times 10^{-6} \quad (3.34)$$

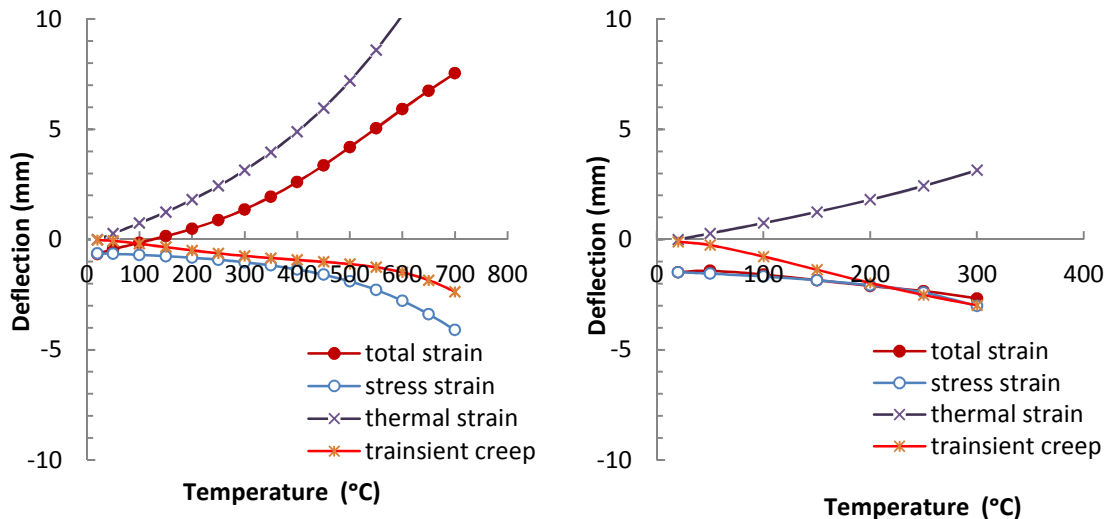
where σ_c represents the initial stress of concrete at normal temperature;

f_c represents the compressive strength of concrete at normal temperature;

t represents the time under load.

(5) The contribution of the strain components

The contribution of each strain component in the total concrete strain at elevated temperatures is shown by Figure 3.06, each time for a constant stress.



(a) Stress = 5 N/mm²

(b) Stress = 20 N/mm²

Fig.3.06 Component of strains of concrete at elevated temperatures

For the concrete subjected to a small stress (5 N/mm²), the transient creep strain is only a small part of the total strain. However, for the concrete submitted to a high stress (20 N/mm²), the transient creep strain is a large part and it nearly counteracts the complete thermal expansion, making the total strain close to the stress strain. During the cooling process, the thermal strain and the elastic part of the instantaneous stress strain are supposed to be recovered based on the temperature, but the plastic strain and the transient creep strain do not recover. From this we can conclude that the transient creep strain will affect the fire behaviour

of RC members submitted to strong compressive forces, as for example in case of columns. However, to find out whether it also has big influence on beams subjected to bending, still further research is needed.

The total strain for the concrete models with transient creep strain considered implicitly (EC 2 model) and explicitly (Tao, J. model) are not exactly the same, as shown by Figure 3.07. The applied stress is 5 N/mm^2 , 10 N/mm^2 , 15 N/mm^2 and 20 N/mm^2 , shown by “s=5, s=10, s=15, s=20” in the figure.

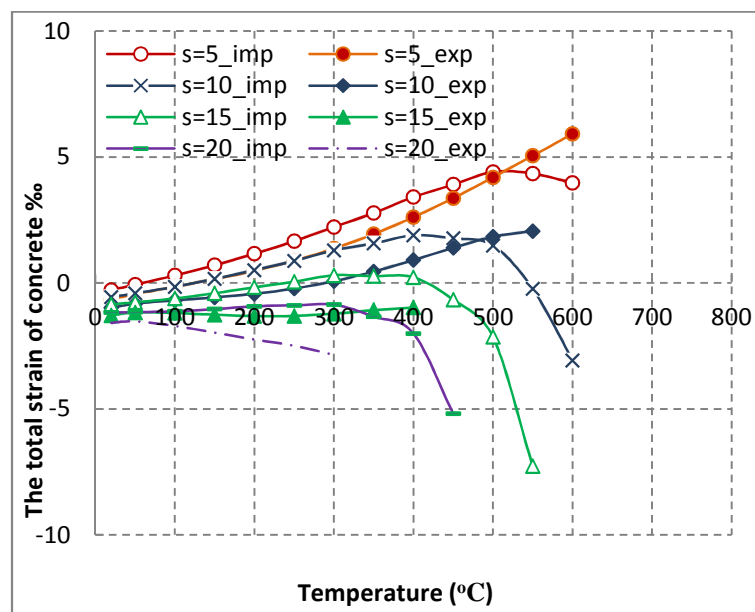


Fig.3.07 Total strains of concrete at elevated temperatures

The total strains of the explicit model are slightly lower than that of the EC2 model for the same stress level. The difference between the two total strains is increasing with the compressive stress and the main difference between them is the transient creep strains.

3.2.5 Spalling of concrete

Spalling is the violent or non-violent breaking off of layers or pieces of concrete from the surface of a structural element when it is heated rapidly to high temperatures. The heating rate influences the spalling type in the first 20-30 minutes of fire: aggregate spalling, explosive spalling and surface spalling can occur. A fourth type, corner sloughing-off spalling, is induced by the maximum temperature and occurs after 30-60 minutes of fire. Surface and explosive spalling is violent, while corner sloughing-off is non-violent. (Khoury, G.A. et al. 2000; 1999). These phenomena are most important during fire, but for post-fire assessments, the reduction in geometry and the existence of possible cracks in the surface region should be

incorporated (Schneider, U. 1988; 1985).

There are many influencing factors having been identified from experiments as summarized in Table 3.02 (Annerel, E. et al. 2010). From these results, several nomograms are produced, which identify spalling and non-spalling zones (e.g. Figure 3.08). However, the main factors are the heating rate (especially above 3°C/min), the permeability of the material (a denser concrete is more sensitive for pore pressure built up, for example HPC and SCC), pore saturation level (especially above 2-3% moisture content by weight of concrete), the presence of reinforcement and the level of externally applied load.

Table 3.02 Characteristics of the different forms of spalling (Annerel, E. et al. 2010)

Spalling	Time of occurrence [min]	Nature	Sound	Influence	Main influences
Aggregate	7-30	Splitting	Popping	Superficial	H, A, S, D, W
Surface	7-30	Violent	Cracking	Can be serious	H, W, P, f_t
Explosive	7-30	Violent	Loud bang	Serious	H, A, S, G, L, O, P, Q, R, S, W, Z, f_s
Corner	30-90	Non-violent	None	Can be serious	T, A, f_t , R

A = aggregate thermal expansion; D = aggregate thermal diffusivity; f_t = tensile strength of concrete; f_s = shear strength of concrete; G = age of concrete; H = heating rate L = loading/restraints; O = heating profile; P = permeability; Q = section shape; R = reinforcement; S = aggregate size; T = maximum temperature; W = moisture content; Z = section size

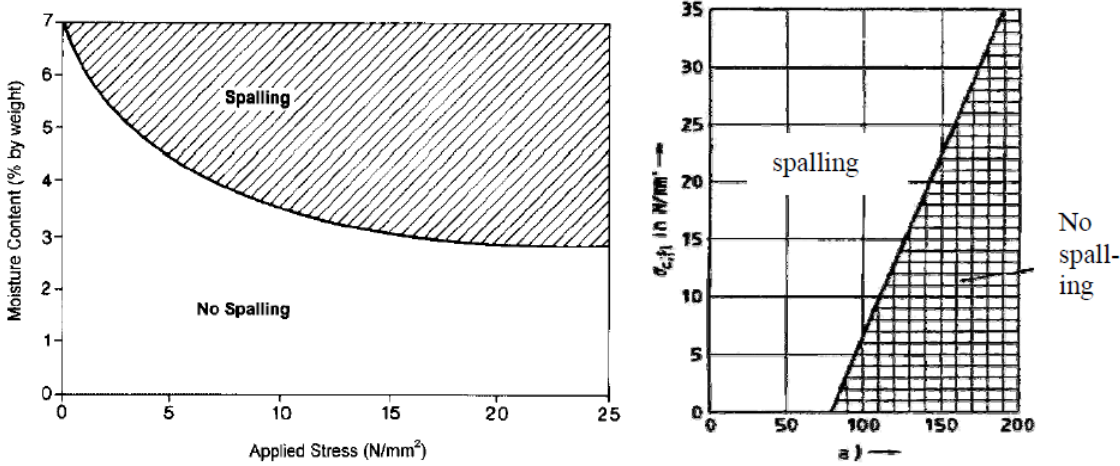


Figure 3.08 Nomograms for spalling: left: Khoury (2000), right: EC 2; (*a* is the smallest value of the width *b* and the height *h* of the elements [mm])

Several mechanisms can explain explosive spalling of concrete:

- (1) Pore pressure spalling: evaporation of the moisture inside the concrete results in a pore pressure increase which results in tensile stresses in the concrete exceeding its tensile strength. The main influencing factors are the permeability of the concrete, the initial water saturation level and the heating rate. However, most of the analytical models predict pore pressure levels which are substantially less than the tensile strength of concrete, as also confirmed by experiments. Notice that the generation of pore pressure in the heated concrete is difficult to predict reliably. Pore pressure spalling may occur for small unloaded specimens (Taerwe, L, et al. 2008).
- (2) Thermal stress spalling: due to rapid heating, a temperature gradient is introduced over the cross-section of a concrete element, which leads to thermal stresses. Compressive stresses are developed close to the heated surface due to restrained thermal expansion, whereas tensile stresses are found in the cooler interior regions. Surface compression may be augmented by load or prestress, which is superimposed upon the thermal stresses. However, very few concrete structures are loaded to levels where the necessary failure stress state is reached. This makes thermal stress spalling a relatively rare phenomenon (Liu, X. 2006).
- (3) Combined pore pressure and thermal stress spalling: explosive spalling generally occurs under the combined action of pore pressure, compression in the exposed surface region (induced by thermal stresses and external loading) and internal cracking. Cracks are developing parallel to the surface when the sum of the stresses exceeds the tensile strength of

the material. The action of relatively small pore pressures from within such planes of weakness could initiate spalling (Kalifa, P. et al. 2000).

HSC (high strength concrete) is believed to be more susceptible to this pressure build-up because of its low permeability compared to NSC (normal strength concrete) (Anderberg, Y. 1997). The extremely high water vapour pressure, generated during exposure to fire, cannot escape due to the high density of HSC and this pressure often reaches the saturation vapour pressure. At 300°C, the pressure may reach about 8 MPa. Such internal pressures are often too high to be resisted by the HSC mix having a tensile strength of about 5 MPa (Diederichs, U. 1995).

There is very limited guidance in current codes and standards for predicting fire induced spalling in concrete. Some codes and standards include broad guidelines for estimating and mitigating spalling. As an illustration, EC 2 specifications state that spalling is unlikely to occur when the moisture content of concrete is lower than 3%, without any consideration due to permeability and the tensile strength of concrete. Similarly, ACI 216.1 standard (2007) does not have any specifications for predicting when spalling might occur. However, this standard provides some guidelines for mitigating spalling in HSC through the use of polypropylene fibers in the concrete mix. It should be noted that the guidelines on spalling in current codes are mainly derived based on observations during fire tests on small specimens.

Dwaikat, M.B. et al. (2008) and Kodur, V.K.R. (2007; 2005) have suggested that during fire resistance calculations of RC structures, concrete of strength higher than 70 MPa is considered to be HSC. For HSC, it is supposed that spalling always occurs during fire.

3.3 Thermal properties of steel bars

Generally, the reinforcing ratio of steel bars in RC structures is less than 3%, which is not enough to influence the inner temperature field of a structure exposed to fire significantly. Hence, the effect of steel is neglected in the temperature field simulations. However, since the requirements of performance based fire resistance design become higher and higher, the temperature field and material properties need to be more and more precise. So it is necessary to study the thermal properties of steel bars, including its thermal conductivity, specific heat and density, which are all functions of temperature.

3.3.1 Thermal conductivity of steel bars

According to experimental research, the thermal conductivity of steel bars λ_s (W/m.K) will

decrease linearly with temperature, and when the temperature reaches a certain limit, it will maintain constant.

(1) Eurocode 3 (2002) gives the thermal conductivity of steel as Equation (3.35):

$$\lambda_s = \begin{cases} 54 - 3.33 \times 10^{-2} \theta & 200^\circ\text{C} \leq \theta \leq 800^\circ\text{C} \\ 27.3 & \theta > 800^\circ\text{C} \end{cases} \quad (3.35)$$

(2) Lie, T.T. (1992; 1991) has derived the following model for structural steels from experimental results, shown by Equation (3.36).

$$\lambda_s = \begin{cases} 48 - 2.20 \times 10^{-2} \theta & 0^\circ\text{C} \leq \theta \leq 900^\circ\text{C} \\ 28.2 & \theta > 900^\circ\text{C} \end{cases} \quad (3.36)$$

3.3.2 Specific heat of steel bars

According to experimental results, the specific heat of steel bars will increase with temperature, but this change is slight. Therefore, in most literature it is considered as a constant value under high temperatures, like in ECCS (1983) and British standard BSI (1990).

It is suggested to take the specific heat of steel c_s as given by Equation (3.37).

$$c_s = 520 \text{ J / (kg} \cdot ^\circ\text{C)} \quad (3.37)$$

In Eurocode 3 (2002), Equation (3.38) is proposed.

$$c_s = 3.8 \times 10^{-3} \theta^2 + 2.0 \times 10^{-3} \theta + 470 \quad \text{J / (kg} \cdot ^\circ\text{C)} \quad (3.38)$$

3.3.3 Density of steel bars

The density of the steel bars will decrease at elevated temperatures due to the thermal expansion of the material. However this difference is very small and could be neglected in design. So generally in the structural design standards, the density of steel is always assumed to be independent of temperature. The constant density of steel bars in this thesis is taken as

$$\rho_s = 7850 \text{ kg / m}^3.$$

3.4 Mechanical properties of steel bars at elevated temperatures

For reinforcing steel, the most important mechanical properties to be considered include the

yield stress, the tensile strength, the elastic modulus and the stress-strain relationship.

3.4.1 The strength of steel at high temperatures

The yield stress of steel bars is one of the most important characteristic for the bearing capacity of RC structures. Experimental research shows that the yielding plateau will decrease with temperature, and will disappear after 300°C. The strength of steel at high temperatures below 400°C will be higher than that at normal temperature, but after 400°C it will sharply decrease (BS, 1987; El-Rimawi, J.A.A. 1989). The commonly used functions of strength of steel with temperature are listed as follows:

(1) In EC 2, the reduction factors of reinforcing steel properties at elevated temperatures shall be obtained from Table 3.03 .The factors in Table 3.03 can also be applied for reinforcing steel in compression.

Table 3.03 Reduction factors for the parameters of the stress-strain relationship of hot rolled and cold worked reinforcing steel at elevated temperatures

Steel Temperature θ [°C]	$f_{sy,\theta} / f_{yk}$		$f_{sp,\theta} / f_{yk}$		$E_{s,\theta} / E_s$	
	hot rolled	cold worked	hot rolled	cold worked	hot rolled	cold worked
1	2	3	4	5	6	7
20	1,00	1,00	1,00	1,00	1,00	1,00
100	1,00	1,00	1,00	0,96	1,00	1,00
200	1,00	1,00	0,81	0,92	0,90	0,87
300	1,00	1,00	0,61	0,81	0,80	0,72
400	1,00	0,94	0,42	0,63	0,70	0,56
500	0,78	0,67	0,36	0,44	0,60	0,40
600	0,47	0,40	0,18	0,26	0,31	0,24
700	0,23	0,12	0,07	0,08	0,13	0,08
800	0,11	0,11	0,05	0,06	0,09	0,06
900	0,06	0,08	0,04	0,05	0,07	0,05
1000	0,04	0,05	0,02	0,03	0,04	0,03
1100	0,02	0,03	0,01	0,02	0,02	0,02
1200	0,00	0,00	0,00	0,00	0,00	0,00

(2) In the paper of Lu, Z.D. (1996), it has been suggested to model the yield stress of steel in function of temperature by Equation (3.39).

$$\frac{f_y(\theta)}{f_y(20^\circ C)} = \begin{cases} 1.0 & 0^\circ C \leq \theta \leq 200^\circ C \\ 1.33 - 1.64 \times 10^{-3} \theta & 200^\circ C < \theta \leq 700^\circ C \\ 0.182 & \theta > 700^\circ C \end{cases} \quad (3.39)$$

(3) In the paper of Shi, X.D. (1992) Equation (3.40) is given.

$$\frac{f_y(\theta)}{f_y(20^\circ\text{C})} = \frac{1}{1 + 24(\theta/1000)^{4.5}} \quad (\text{For steel grade I-IV})$$

$$\frac{f_y(\theta)}{f_y(20^\circ\text{C})} = \frac{1}{1 + 46(\theta/1000)^4} \quad (\text{For steel grade V})$$
(3.40)

(4) The reduction factor for yield stress of steel at high temperatures suggested by the ECCS (1983) is as Equation (3.41):

$$\frac{f_y(\theta)}{f_y(20^\circ\text{C})} = 1 + \frac{\theta}{767 \ln(\theta/1750)} \quad 0^\circ\text{C} \leq \theta \leq 600^\circ\text{C}$$
(3.41)

In all the above equations, $f_y(\theta)$ represents for the yield stress of steel under high temperature θ and $f_y(20^\circ\text{C})$ is the yield stress of steel at normal temperature.

3.4.2 The elastic modulus of steel at high temperatures

The elastic modulus of steel will also decrease with the increasing temperature, and the grade of steel has little influence on this change (European recommendations for the fire safety of steel structures, 1983). Some well-known research results are listed below:

(1) The reduction law for the elastic modulus of steel supplied in EC 2, which is generally used for RC structure design, is given in Table 3.03.

(2) In the paper of Lu, Z.D. (1996; 1993), a three stage function for the elastic modulus of steel based on experimental results is given.

$$\frac{E_s(\theta)}{E_s(20^\circ\text{C})} = \begin{cases} 1.0 - 4.86 \times 10^{-4} \theta & 20^\circ\text{C} \leq \theta \leq 370^\circ\text{C} \\ 1.515 - 1.978 \times 10^{-3} \theta & 370^\circ\text{C} \leq \theta \leq 700^\circ\text{C} \\ 0.13 & \theta > 700^\circ\text{C} \end{cases}$$
(3.42)

(3) The model given by Lie, T.T. (1992; 1991) is Equation (3.43).

$$\frac{E_s(\theta)}{E_s(20^\circ\text{C})} = \begin{cases} 1.0 + \frac{\theta}{2000 \ln(\theta/1000)} & 0^\circ\text{C} \leq \theta \leq 600^\circ\text{C} \\ \frac{690 - 0.69\theta}{\theta - 53.5} & 600^\circ\text{C} \leq \theta \leq 1000^\circ\text{C} \end{cases}$$
(3.43)

(4) The function suggested by ECCS (1983) is Equation (3.44).

$$\frac{E_s(\theta)}{E_s(20^\circ C)} = 1.0 - 17.2 \times 10^{-12} \theta^4 + 11.8 \times 10^{-9} \theta^3 - 34.5 \times 10^{-7} \theta^2 + 15.9 \times 10^{-5} \theta \quad (3.44)$$

In all the equations, $E_s(\theta)$ represents the elastic modulus of steel under high temperature θ ; and $E_s(20^\circ C)$ is the elastic modulus of steel at normal temperature.

3.4.3 Thermal strains of steel

The constitutive material model of steel describes the behaviour of heated and loaded steel in a mathematical model. Since the transient strain does not exist for steel, the model for steel is simpler than that of concrete described in Equation (3.23). The temperature related strain of steel $\varepsilon_{s,tot}$ contains three parts, as shown by Equation (3.45).

$$\varepsilon_{s,tot}(\theta) = \varepsilon_{s,th}(\theta) + \varepsilon_{s,\sigma}(\sigma_s, \theta) + \varepsilon_{s,cr}(\sigma_s, \theta, t) \quad (3.45)$$

where $\varepsilon_{s,tot}$ is the total strain of steel under elevated temperature θ ;

$\varepsilon_{s,th}$ is the thermal elongation of steel under elevated temperature θ ;

$\varepsilon_{s,\sigma}$ is the stress dependent strain of steel under elevated temperature θ ;

$\varepsilon_{s,cr}$ is the creep strain of steel under elevated temperature θ ;

I. Thermal elongation of steel

The thermal elongation of steel $\varepsilon_{s,th}$ is the free deformation of steel at high temperatures. It increases with temperature and is not influenced by the steel grade.

(1) EC 2 supplies a function for the variation of the thermal elongation of steel, as Equation (3.46).

$$\varepsilon_{s,th}(\theta) = \begin{cases} -2.416 \times 10^{-4} + 1.2 \times 10^{-5} \theta + 0.4 \times 10^{-8} \theta^2 & 20^\circ C \leq \theta \leq 750^\circ C \\ 11 \times 10^{-3} & 750^\circ C \leq \theta \leq 860^\circ C \\ -6.2 \times 10^{-3} + 2 \times 10^{-5} \theta & 860^\circ C \leq \theta \leq 1200^\circ C \end{cases} \quad (3.46)$$

(2) ECCS (1983) has suggested a constant value for the thermal elongation of steel by Equation (3.47).

$$\varepsilon_{s,th}(\theta) = 1.4 \times 10^{-3} \quad (3.47)$$

(3) Lie, T.T. (1992; 1991) proposed a function for the thermal elongation as Equation (3.48).

$$\varepsilon_{s,th}(\theta) = \begin{cases} (0.004\theta + 12) \times 10^{-6} & 20^\circ\text{C} \leq \theta < 1000^\circ\text{C} \\ 16 \times 10^{-6} & \theta \geq 1000^\circ\text{C} \end{cases} \quad (3.48)$$

(4) Lu, Z.D. (1996) proposed Equation (3.49).

$$\varepsilon_{s,th}(\theta) = (11 + 0.0036\theta) \times 10^{-6} \quad (3.49)$$

II. The stress related strain of steel

The stress related strain of steel can be directly found from the stress-strain relationship of steel at high temperatures. The stress-strain relationships may also be applied to reinforcing steel in compression. There are several well-known models found in the literature:

(1) The stress-strain relationship supplied by EC 2 is as follows, Equation (3.50).

$$\sigma_{s,\theta} = \begin{cases} \varepsilon_s E_{s,\theta} & 0 \leq \varepsilon_s \leq \varepsilon_{sp,\theta} \\ f_{sp,\theta} - c + (b/a)[a^2 - (\varepsilon_{sy,\theta} - \varepsilon_s)^2]^{0.5} & \varepsilon_{sp,\theta} < \varepsilon_s \leq \varepsilon_{sy,\theta} \\ f_{sy,\theta} & \varepsilon_{sy,\theta} < \varepsilon_s \leq \varepsilon_{st,\theta} \\ f_{sy,\theta} \left(1 - \frac{\varepsilon_s - \varepsilon_{st,\theta}}{\varepsilon_{su,\theta} - \varepsilon_{st,\theta}}\right) & \varepsilon_{st,\theta} < \varepsilon_s \leq \varepsilon_{su,\theta} \end{cases} \quad (3.50)$$

where $\sigma_{s,\theta}$ is the stress of steel at high temperature θ ;

$\varepsilon_{s,\sigma}$ is the stress related strain of steel at high temperature $\sigma_{s,\theta}$;

$E_{s,\theta}$ is the Young's modulus of steel at elevated temperature θ ;

$f_{sp,\theta}$ is the yield stress of steel at elevated temperature θ ;

$f_{sy,\theta}$ is the ultimate strength of steel at elevated temperature θ ;

$\varepsilon_{sp,\theta} = f_{sp,\theta} / E_{s,\theta}$; $\varepsilon_{sy,\theta} = 0.02$; $\varepsilon_{st,\theta} = 0.15$; $\varepsilon_{su,\theta} = 0.20$;

$a = (\varepsilon_{sy,\theta} - \varepsilon_{sp,\theta})(\varepsilon_{sy,\theta} - \varepsilon_{sp,\theta} + c / E_{s,\theta})$;

$$b = c(\varepsilon_{sy,\theta} - \varepsilon_{sp,\theta})E_{s,\theta} + c^2;$$

$$c = (f_{sy,\theta} - f_{sp,\theta})^2 / [(\varepsilon_{sy,\theta} - \varepsilon_{sp,\theta})E_{s,\theta} - 2(f_{sy,\theta} - f_{sp,\theta})].$$

(2) Researches at Qinghua University (Shi, X.D. 1992) show that, the yielding stage is not obvious for steel under elevated temperatures, and the steel deforms faster after yielding until it reaches the ultimate strength. So they set up a simplified model, which contains only an elastic part and a hardening part, shown by Equation (3.51).

$$\sigma_{s,\theta} = \begin{cases} \varepsilon_{s,\sigma} E_{s,\theta} & 0 \leq \varepsilon_{s,\sigma} \leq \varepsilon_{sy,\theta} \\ f_{sp,\theta} + (f_{sy,\theta} - f_{sp,\theta}) \left[1.5 \frac{\varepsilon_{s,\sigma} - \varepsilon_{sy,\theta}}{\varepsilon_{su,\theta} - \varepsilon_{sy,\theta}} - 0.5 \left(\frac{\varepsilon_{s,\sigma} - \varepsilon_{sy,\theta}}{\varepsilon_{su,\theta} - \varepsilon_{sy,\theta}} \right)^3 \right]^{0.62} & \varepsilon_{sy,\theta} < \varepsilon_{s,\sigma} \leq \varepsilon_{su,\theta} \end{cases} \quad (3.51)$$

(4) Lu, Z.D. (1996; 1993) gives a two stage elastic-plastic stress-strain relationship, Equation (3.52).

$$\sigma_{s,\theta} = \begin{cases} \varepsilon_{s,\sigma} E_{s,\theta} & 0 \leq \varepsilon_{s,\sigma} \leq \varepsilon_{sy,\theta} \\ f_{sy,\theta} & \varepsilon_{s,\sigma} > \varepsilon_{sy,\theta} \end{cases} \quad (3.52)$$

III. The creep strain of steel

The creep strain $\varepsilon_{s,cr}$ at high temperature is mainly influenced by temperature, fire exposing time, the steel stress and the heating rate. Generally, it is analysed based on Dorn's theory (Franssen, J.M. et al. 1994). Nowadays, the experimental research and theoretical analyses are not sufficient to give a reliable law for the creep model of steel under elevated temperature. Moreover, compared to the other two strain components, the creep strain of steel is rather small (Najjar, S.R. et al. 1995). Hence, it can be neglected as is also done in this thesis.

3.5 Bond strength between steel bars and concrete

The bond behaviour between steel bars and concrete is a fundamental property which allows the force transfer between the two materials. The bond strength can directly affect cracking, deformation and bearing capacity of RC structures (Sebastjan, B. et al. 2007, Chiang, C.H. et al. 2003). According to the literature review, the loss of bond strength between concrete and steel bars under elevated temperature is influenced by the cracking of concrete and the decreasing tensile strength of concrete (EI-Hawary, M.M. et al. 1996; Duederichs, V. et al.

1981).

In literature, it is concluded that the bond strength between concrete and steel bars will decrease with increasing temperature, and this trend is similar to that of the tensile strength of concrete (Abbasi, A. et al. 2005; Haddad, R.H. et al. 2004).

3.6 Summary

Based on the study and comparison of many available material models given in the literature, this chapter gives a review and analyses of the material properties of concrete and steel bars at elevated temperatures. These temperature-related physical and mechanical properties are the fundamental input parameters for fire behaviour research on reinforced concrete members and structures.

(1) With increasing temperature, the thermal conductivity and density of concrete will decrease, but the change is not important, and the density is normally taken as constant. The specific heat of concrete first tends to increase and then remains constant when the temperature reaches 600°C .

(2) The compressive strength and tensile strength of concrete both tend to decrease while exposed to high temperatures. The influence of temperature on tensile strength is much greater than that of compressive strength, so the tensile strength of concrete contributes very little to the structural behaviour of RC structures during fire. The elastic modulus of concrete will also decrease with temperature. There are two kinds of strain models for concrete, the implicit stress-strain model and the explicit model for the transient strain and creep strain considered separately.

(3) With increasing temperature, the thermal conductivity of steel will linearly decrease, and the specific heat will increase but to a small amount. The density of the steel shows little change, and is taken as a constant during fire calculations.

(4) The strength of all kinds of steel bars tends to decrease with increasing temperature, and the strength of the higher strength steel bars will decrease faster. The elastic modulus of steel bars tends to decrease with temperature.

(5) The bond strength between steel bars and concrete will decrease under elevated temperatures and this will be influenced by the profile of the steel bars and its corrosion conditions.

Chapter 4

Simplified multi-iteration method for fire resistance calculation of RC elements

Most calculations of the fire performance of reinforced concrete structures make use of various degrees of simplification. In most cases calculation methods are applied to simply supported beams and most of the analysis methods for the fire behaviour of concrete members don't consider detailed thermal and mechanical material models, realistic fire scenarios and restraint conditions and different load cases, while these items are very important for performance-based fire-resistance research, and still need further study.

Based on the mechanical properties of concrete and reinforcing steel at elevated temperatures, a multi-iteration analysis method is proposed, and an equivalent bending stiffness is defined in the multi-iteration method for the structural analysis. This chapter gives an introduction to the proposed numerical model and its validation process by simulating available experimental data coming from fire tests executed on simply supported slabs under the ISO 834 fire load. Next, the rotational restraints of the experimental slabs are changed and simulated in order to prove the approach is valid for various parameter combinations in fire performance simulations. By applying the proposed method, influencing factors for the fire performance of RC beams with transient creep strain considered implicitly and explicitly in the material model are investigated in Chapter 5. The influence of restraint conditions on fire performance of RC elements is studied in Chapter 6.

4.1 General Introduction

When a structure is subjected to fire, the thermal expansion of its members or components will lead to additional deformations and stresses. At the same time, the mechanical properties of the structural materials decrease at elevated temperatures. A sharp reduction in bearing capacity and excessive deflections are detrimental to structural safety. Models to predict the fire-behaviour of reinforced concrete (RC) elements are required in developing reliable and efficient design methods. The most applied design methods adopted in EC 2 (2004), fib

bulletins (2008; 2007) and ACI Guidelines (2007), are based on simplified calculations which provide minimum requirements for an unrestrained member exposed to Standard Fire Curves. The influence of specific concrete properties (such as transient strain and thermal creep) and restraint conditions under elevated temperatures on the performance of RC members are not considered in these guidelines. However, specific material aspects like transient creep strains may lead to significant differences in the fire performance of RC elements (Bratina, S. et al. 1998). User friendly numerical methods are really necessary for accurate fire performance simulations. Furthermore, in reality members of a RC structure always experience various axial and rotational restraints from other members. These restraints can have a significant influence on the flexural behaviour of RC members by generating longitudinal forces and additional bending moments at elevated temperatures due to the constraint of thermal expansions and rotations.

Advanced calculation methods could account for realistic fire conditions by combining the temperature-dependent material properties with thermal and mechanical models, but only a few published research results deal with the fire performance of restrained members. Effects of axial and rotational restraints on steel members during fire were mainly studied by Ali et al. (2001; 1998), Li et al. (2007) and many other researchers (Wang, Y.C. et al. 1997; Yin, Y.Z. 2004). The effects of restraints on steel–concrete composite structures were investigated by Huang, Z.F. et al. (2008; 2007; 2004). For RC members, some investigations on the effect of RC columns under fire were conducted by Benmarce, A et al. (2005), Lie, T.T. et al. (1986). These research projects lead to a sound evaluation of fire-resistance of RC structures. However, very little has been done on the effect of restraints on fire-performance of RC beams exposed to fire both from theoretical and experimental point of view. The most remarkable investigations on restrained RC members are from Wu, B. et al. (2011; 2009; 2006), Lu, J.Z. et al. (2008), Kodur V.K.R. et al. (2010; 2008) and Dwaikat, M.B. et al. (2009). Wu and Lu performed a numerical study based on the behaviour of restrained RC beams and ‘+’-shaped columns at elevated temperatures. However, their research program was limited to the linear behaviour of the axial and rotational restraints at the ends. Kodur and Dwaikat proposed a numerical model on the fire performance simulation of restrained beams and columns. They performed a series of calculations for various parameters and recently proposed a design equation for predicting the fire-resistance of restrained concrete beams. Riva, P. (2008) and Franssen computed the fire behaviour of a set of frames and restrained RC members with varying axial restraints with ABAQUS.

Although advanced calculation models with the help of finite element methods allow simulating sophisticated processes in RC structures under elevated temperatures, it is too

computationally demanding in practical design. A simplified research model is needed for fire safety design of RC beams for any given material model, beam size, load and restraint conditions. To solve the problem, a multi-iteration method is proposed and introduced in this chapter. The calculation procedure consists of a coupled thermo-mechanical analysis, including the development of temperature, the deflection and ultimate bending moment. The model is validated by previously obtained experimental data coming from fire tests executed on simply supported slabs and also rotationally restrained slabs under the ISO-834 fire load.

The thermal-mechanical analysis process of the proposed method is performed in three steps: 1) temperature field calculations (section 4.2); 2) sectional equilibrium analysis (section 4.3) and 3) structural analysis (section 4.4). Finally, the fire tests executed before will be used to validate the method in section 4.5.

4.2 Temperature field calculation

The increase of temperature in the member is the direct result of a member exposed to a fire. With increasing temperature inside the member, the strength of the concrete and steel bars will decrease and their deformation will also be influenced by temperature. Moreover, since the fire is a transient process, a non-uniform distribution of the temperature field will be obtained. This will lead to inner forces along the cross-section and an extra curvature. So for the fire-resistance research of RC members, the temperature field of the member should be analysed first.

The heat transfer between a fire and RC members is a transient problem which is described by a non-linear governing function. It can hardly be solved by an analytic method, so numerical methods are adopted instead, e.g. the finite difference method and the finite element method. The finite difference method is comparatively simple and time-effective, but it's only fit for members with regular shape. Moreover, it can't consider the behaviour of the connecting elements which makes finite element methods more efficient. The finite element method is an approach that first divides the structural volume into small elements, and then computes the values of the relevant variables at the nodes step by step in the time and temperature field. This method can solve all the complex shaped structures and can consider the contribution of all elements during the computing procedure, and thus covers the shortcomings of the finite difference method. The temperature calculations in this thesis are all carried out by means of the finite element package DIANA (De Witte, F.C., 2002), which has already proved to be accurate and practical.

4.2.1 General introduction

The temperature field of the flexural member is supposed to be uniform in the longitudinal direction, which means the heating conditions along the element are assumed to be identical. Hence, the temperature field of the element can be simplified into a 2D problem. The thermal conduction coefficient and the specific heat of concrete are considered to be temperature dependent, according to the models introduced in Chapter 3. Generally, beams are assumed to be heated from three sides and slabs only from the bottom.

The fire exposing process is a non-linear transient process. All the material properties and temperature field are changing with heating time. In order to simplify this process the following assumptions are adopted:

- (1) Concrete is assumed to be an isotropic material, the heat conduction factor in all directions is supposed to be the same;
- (2) The temperature field of the flexural member is supposed to be a 2D problem;
- (3) The heat energy only comes from the fire, there is no heat generated inside the concrete (Lie, T.T. 1983);
- (4) Steel bars are neglected as they only locally influence the temperature distribution in the cross-section and don't have a global significant influence (Buchanan, A.H. 2001).
- (5) The convection factor between concrete and air will increase with temperature. In order to make the simulation process simpler, it is supposed to be constant. Harmathy, T.Z. (1972) adopted $16W/(m^2 \cdot ^\circ C)$ in his researches, and Thelandersson (1987) suggests to take $25W/(m^2 \cdot ^\circ C)$ for the surfaces directly exposed to fire and $6.5W/(m^2 \cdot ^\circ C)$ for the surface further from the fire.

4.2.2 Fire curves

In order to investigate the fire behaviour of a RC structure, the kind of fire it is exposed to is one of the most fundamental items that needs to be studied first. For the temperature calculation, fire curves should be given as a boundary condition for the nonlinear heat transfer function. A parametric curve represents the description of a fire most accurately. However, there are many factors that contribute to the behaviour of the fire. The following curves are the most popular used fire curves (NFPA 502, 2001), which are shown by Figure 4.01:

- (1) ISO-834 standard fire curve: The fire curve suggested in EC2 for fire-resistance design of

RC structures is the ISO-834 fire curve. It presents the temperature property of fire with normal fuel, which is fit for fires in open space and on the ground. Its function is given by Equation (4.01).

$$\theta = 20 + 345 \times \lg(8t + 1) \quad (4.01)$$

(2) RABT fire curve: The RABT fire curve is proposed in Germany. It describes the temperature evolution of a fire in a closed space, and the temperature reaches 1200°C already after 5 minutes. For a car fire, this high temperature will last for 25 minutes, and for a train fire, it will last for 55 minutes until all the fuel has burned. It fits for underground structures and tunnels.

(3) HC fire curve (hydrocarbon curve): The HC fire curve is for a fire in an open space and with hydrocarbon as the resource. The hydrocarbon fuel makes the fire reaching the highest temperature 1100°C quickly and then keeps that temperature constant. The formulation for the HC curve is given by Equation (4.02).

$$\theta = 20 + 1080 \times (1 - 0.325 \times e^{-0.167t} - 0.675 \times e^{-25t}) \quad (4.02)$$

(4) HCM curve (Hydrocarbon Modified curve): The HCM curve was proposed by French researchers based on a modification of the HC curve. The highest temperature reached by the HCM curve is 1300°C . The formulation for the HCM curve is given as Equation (4.03).

$$\theta = 20 + 1280 \times (1 - 0.325 \times e^{-0.167t} - 0.675 \times e^{-25t}) \quad (4.03)$$

(5) RWS curve (Rijkswaterstaat curve; The Netherlands): The RWS curve is a fire curve for a fire in a closed space and with 50m^3 hydrocarbon fuel. The heating rate can reach 300MW , and the temperature reaches 1200°C in a short time.

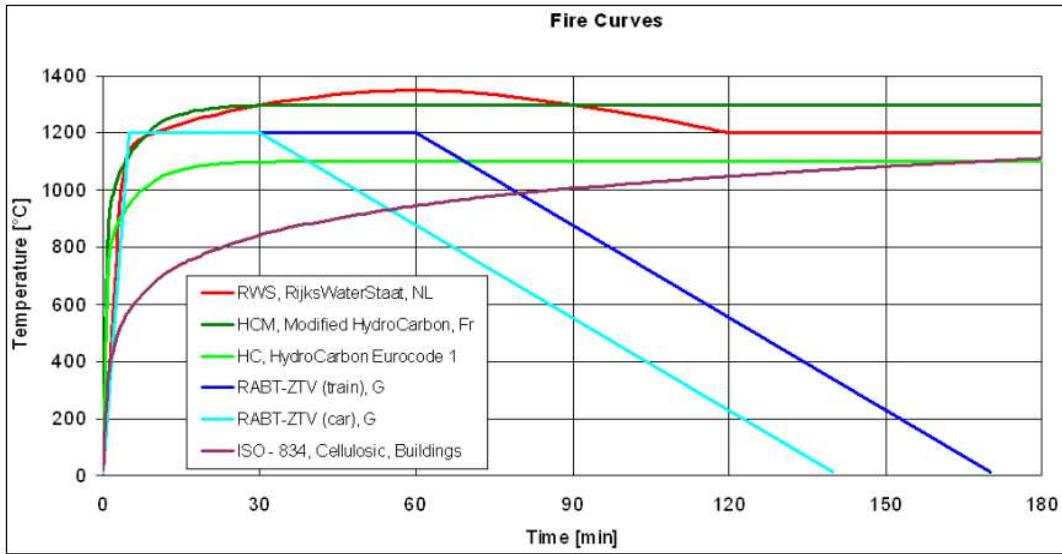


Figure 4.01 Frequently used fire curves (NFPA 502, 2001)

(6) To be able to create a model representative for a real fire, temperature-time curves considering a cooling part are needed. For this purpose, Eurocode 1 (2002) will be used. In the heating phase, it is assumed that the gas temperature will rise in time, independently of the fire load. The parametric fire curve is given by Equation (4.04):

$$\theta_g = 20 + 1325 \times \left(1 - 0.324 \times e^{-0.2t^*} - 0.204 \times e^{-1.7t^*} - 0.472 \times e^{-19t^*} \right) \quad (4.04)$$

where θ_g is the gas temperature in the fire compartment [$^{\circ}\text{C}$];

t^* is the parametric time to incorporate the ventilation conditions and compartment boundary conditions as given in Equation (4.05).

$$t^* = t \times \Gamma \quad (4.05)$$

where Γ is the time modification factor, which is based on the ventilation factor and the thermal properties of the boundaries of the enclosure.

When $\Gamma = 1$, Equation (4.04) approximates the standard fire curve as shown by Figure 4.02. The cooling parts for 30 min, 60 min, and 90 min are calculated separately. Depending on the value of the maximum heating time t_{\max}^* , three different linear curves for gas temperature are defined by Equation (4.06).

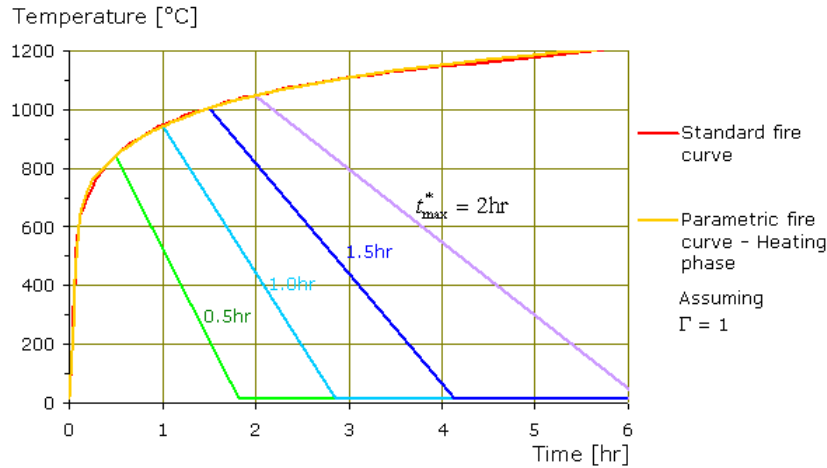


Figure 4.02 Parametric fire curves with $\Gamma = 1$ (Eurocode 1, 2002)

$$\theta_g = \begin{cases} \theta_{\max} - 625(t^* - t_{\max}^* x) & \text{for } t_{\max}^* \leq 0.5 \\ \theta_{\max} - 250(3 - t_{\max}^*) (t^* - t_{\max}^* x) & \text{for } 0.5 < t_{\max}^* < 2 \\ \theta_{\max} - 250(t^* - t_{\max}^* x) & \text{for } t_{\max}^* \geq 2 \end{cases} \quad (4.06)$$

When the fire is fuel controlled, $x = 1$, and the curves for the cooling part can be simplified into Equation (4.07).

$$\theta_g = \begin{cases} \theta_{\max} - 625(t^* - 0.5) & \text{for } t_{\max}^* = 0.5 \\ \theta_{\max} - 500(t^* - 1) & \text{for } t_{\max}^* = 1.0 \\ \theta_{\max} - 250 \times 1.5(t^* - 1.5) & \text{for } t_{\max}^* = 1.5 \\ \theta_{\max} - 250(t^* - t_{\max}^*) & \text{for } t_{\max}^* \geq 2.0 \end{cases} \quad (4.07)$$

(7) As required by performance-based fire resistance design, specific fire curves will be adopted for each fire condition considering different fire scenarios (Schleich, J.B. et al. 2001; SFPE, 2000; McGrattan, K. 2005).

4.2.3 Temperature field of members under various fire curves

Based on the assumptions introduced in section 4.2.1, with the finite element package DIANA, two typical RC cross-sections are simulated in this chapter. A slab which is supposed to be heated from only the bottom and a beam with rectangular cross-section, heated from three sides. The first group of members are heated with the frequently used fire curves: (1) ISO-834 standard curve; (2) RABT curve for trains; (3) HC curve, and (4) RWS curve. The second group of members are heated with parametric fire curves which consider the cooling part of

the fire (curves in Figure 4.02). For the program, a Newton-Raphson Laffer method is used to solve the non-linear differential equations and 30s is set as the calculation time-step and the total fire simulation time is 2 hours.

(1) Temperature field of a slab under different fire curves

The studied slab model is a one way slab with a cross-section of $1000\text{mm} \times 150\text{mm}$. A mesh size of $10\text{mm} \times 10\text{mm}$ is taken for the temperature simulations. Since the effect of steel bars is neglected based on the assumption (4), the steel bars are not modelled explicitly. The temperature field could be simplified to be a 1D problem over the height of the cross-section (shown by Figure 4.03).

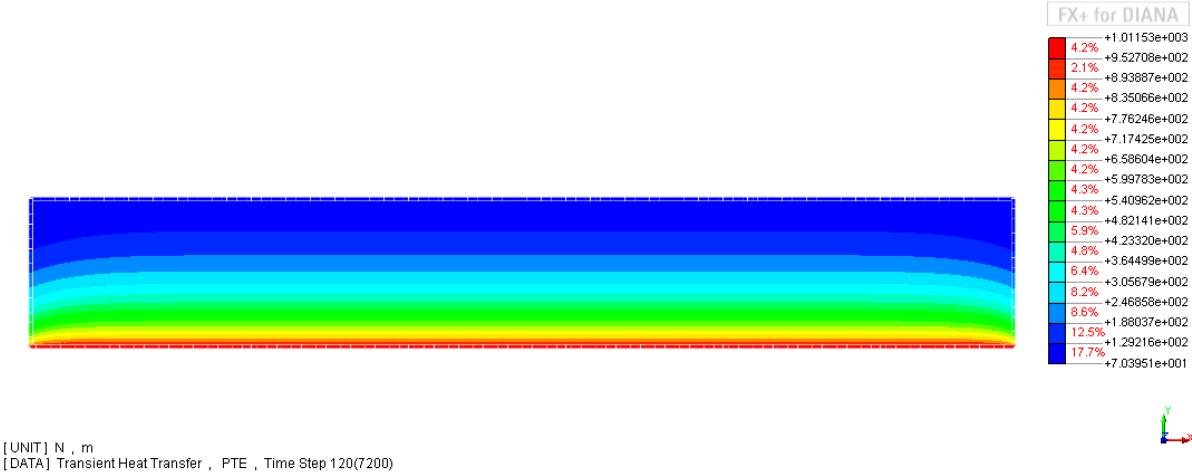


Figure 4.03 Temperature field of the slab (2hrs under ISO-834 fire curve)

The temperature of concrete at a certain height of the cross-section (point A is 20mm measured from the bottom which is important since it is also supposed to be the position of the steel bars, point B is 75mm measured from the bottom, which is at the centre of the slab) under the different fire curves are compared and analysed. Figure 4.04 shows the temperature of concrete at point A. Figure 4.05 shows the temperature of concrete at point B.

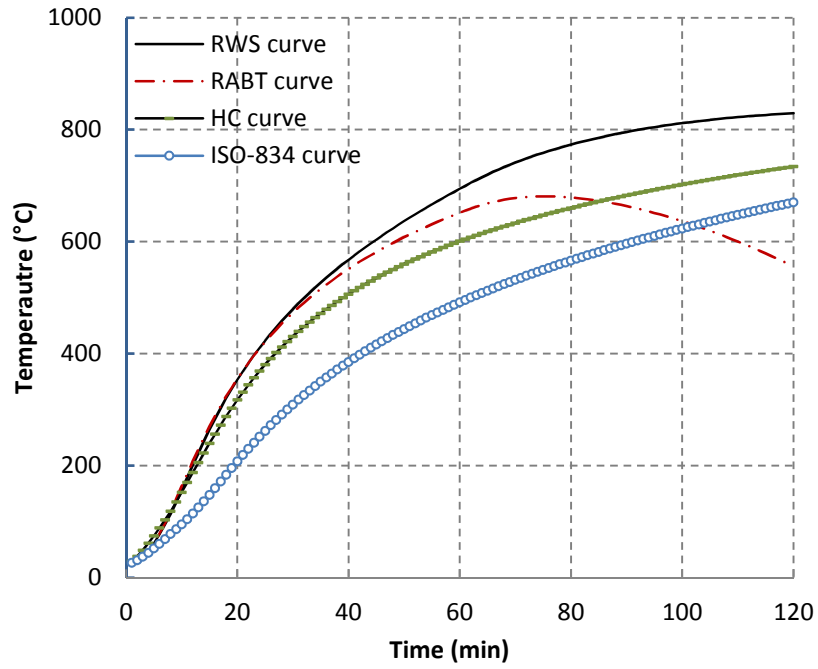


Figure 4.04 Temperature curves of concrete at point A (reinforcement level)

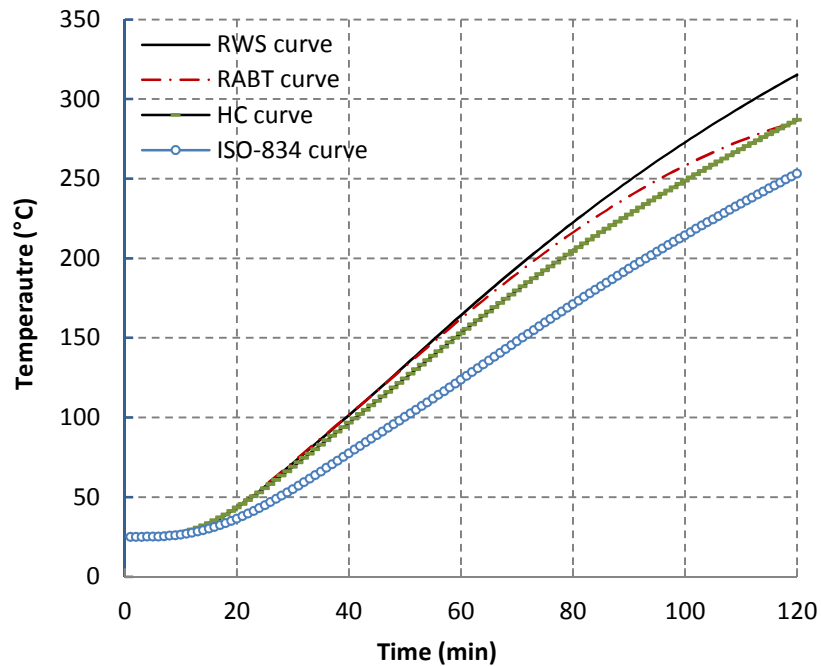


Figure 4.05 Temperature curves of concrete at point B (mid-height)

The temperature curves of point A have the same trend as the corresponding fire curves, and the fire curves with higher temperature lead to a higher temperature at point A which is

reasonable. This observed variation in temperature will make a huge difference on the strength of steel bars at this point. Comparing the temperatures of point A and point B, it can be seen that the difference of the four curves becomes smaller in the centre, especially for the RABT curve. Due to the low thermal conductivity of concrete, the temperature of point B is still increasing during the cooling part of the fire curve.

(2) Temperature field in a beam under parametric fire curves

The studied cross-section of a rectangular beam is $b \times h = 350\text{mm} \times 500\text{mm}$ with a mesh size of $10\text{mm} \times 10\text{mm}$. There are four steel bars in the tensile zone and two in the compressive zone, and the bars are designated as bar1, bar2 and bar3, as shown by Figure 4.06.

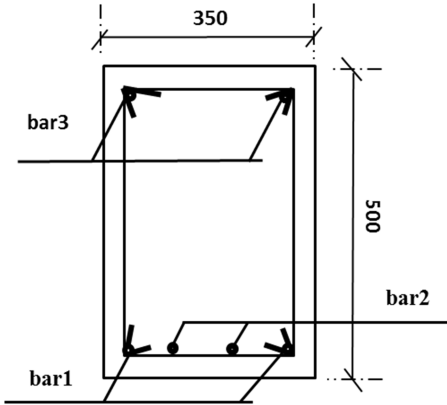


Figure 4.06 Name and arrangement of the steel bars on the cross-section

The temperature field of beams which are heated by three sides shows U-shaped layers, as shown by Figure 4.07. It is a 2D problem, which makes the sectional analysis become a more complex problem.

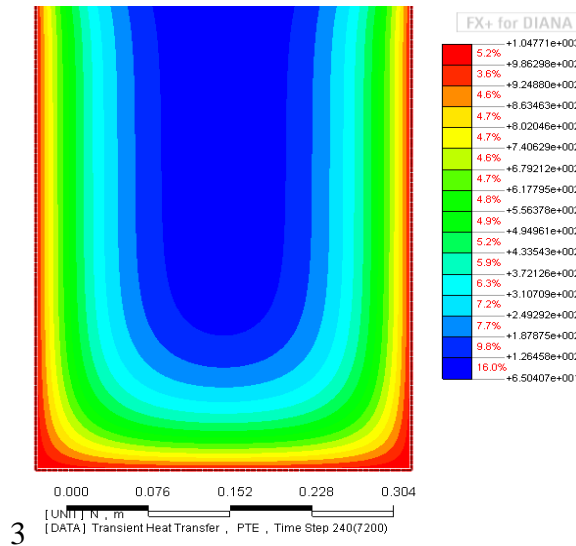
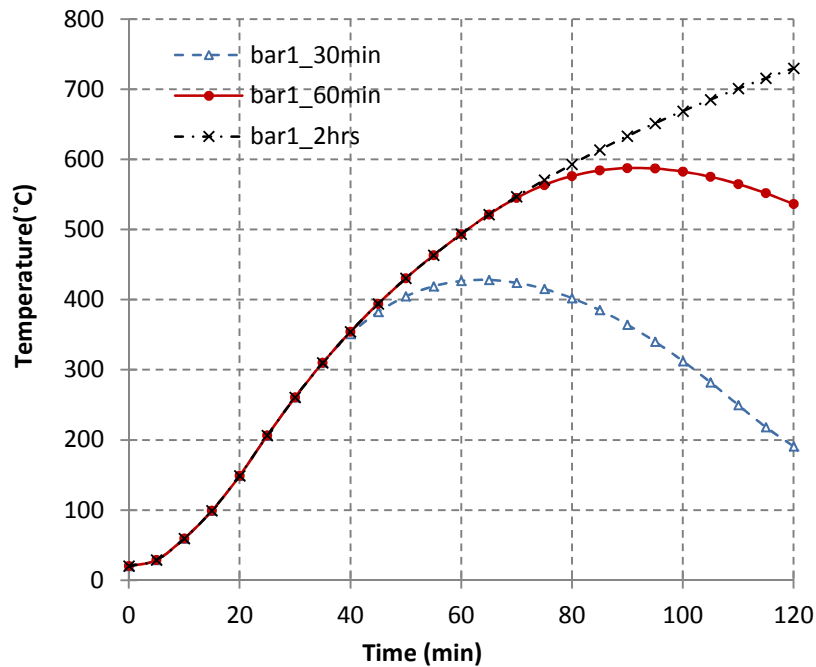
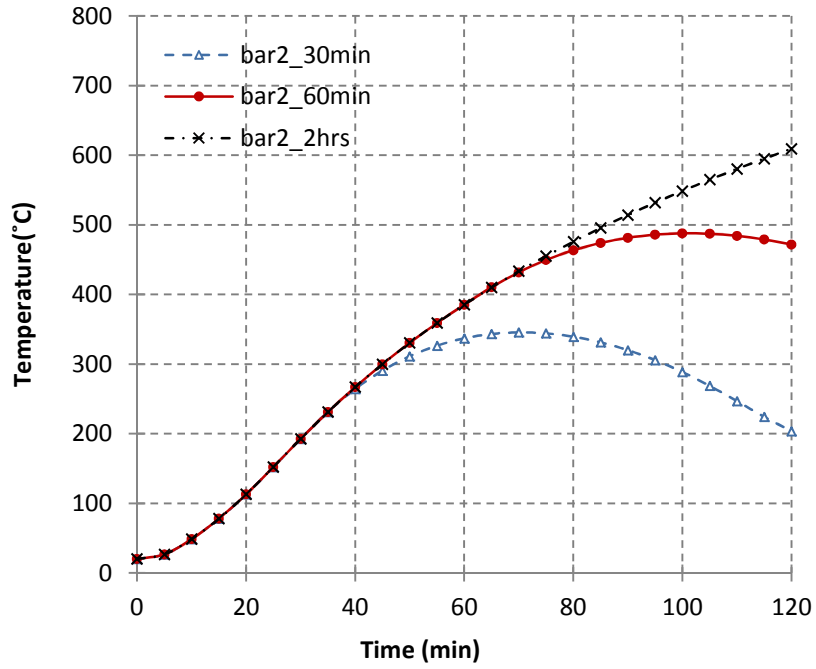


Figure 4.07 Temperature field of a beam cross-section heated from three sides (t=120 min)

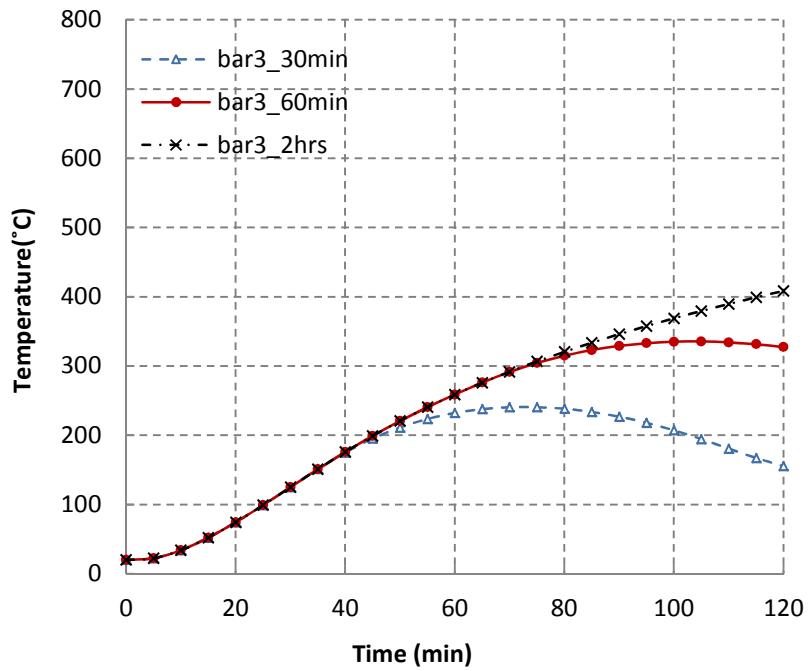
The temperatures of bar1, bar2, and bar3 under the three parametric fire curves (the time legend in the graph relates to the maximum heating time of the parametric fire curves) are compared in Figure 4.08(a), 4.08(b) and 4.08(c).



(a) Temperatures for bar1



(b)Temperatures for bar2



(c)Temperatures for bar3

Figure 4.08 Temperatures of steel bars under three fire curves

The temperatures of the steel bars are exactly the same for the heating part of the parametric curves as those of 2hrs standard heating curve. Their temperature will still increase for about 30 min while the fire curve began to decrease. This is because the concrete outside the steel bars still conducts heat from the outer layer to the cooler inner parts as long as the outer layers are still hotter. This delay of the temperature change depends on the thickness of the concrete cover: the thicker, the longer the delay time. So for bar3, the observed difference between the fire curves tends to appear later and is comparatively smaller than that of bar1 and bar2. For bar1 and bar2, which are steel bars in tension, their temperature under the fire curves with cooling is much smaller than that of the standard fire curve, which can reach 500 °C in 2hrs.

The difference in the temperature of the steel bars under different fire curves will significantly influence the fire behaviour and the bearing capacity of the RC members. Hence, the fire scenario is an important influencing factor for the fire-behaviour of RC members, which should be seriously considered in the performance based fire resistance research.

4.3 Analysis of sectional equilibrium

With the calculated temperature field of a member, the material properties under elevated temperatures can be determined. The stresses and strains can then be determined in function of temperature and fire exposure time. These temperature dependent material properties are critical to determine the stiffness of the whole member. They are computed by solving the equilibrium equations of forces and moments of the cross-sections.

4.3.1 Assumptions

The proposed method is suitable to analyse RC elements subject to bending. Since during the cross-section analysis, the average stiffness of the member is calculated and simplified in function of temperature and heating time, it is actually the most important step for the fire behaviour simulations. The thermal-mechanical analysis of a section is based on the following assumptions, mentioned by Lu Z.D. (1996) and Kodur V.K.R. (2011; 2008; 2006).

- (1) Plane sections will remain plane after bending;
- (2) Perfect bond between concrete and steel bars is assumed. Bond slip is neglected;
- (3) For RC members subjected to bending, shear deformations are not considered.
- (4) Spalling of concrete is incorporated into the model based on the following rules: (a) Spalling only occurs in RC members manufactured with HSC or HPC concrete. It is assumed that no spalling occurs in RC members with NSC concrete or in concrete with polypropylene

fibres. (b) Spalling occurs when the temperature in an element exceeds 350°C . (c) The spalling is considered in the calculation process by deleting the area of a surface layer outside the steel bars which is supposed to have exploded.

Thus, based on these assumptions, the proposed numerical model is capable of accounting for the nonlinear high-temperature material characteristics, the complete structural (beam) behaviour, various fire scenarios, the fire induced restraint effects, the concrete types (such as different aggregate types, fibre mixes and concrete strengths), and simple spalling mechanisms.

4.3.2 Strains of concrete and steel at elevated temperatures

I. Thermal strains of concrete

According to fib bulletin 46 (2008) and research by Anderberg, Y. (1982; 1976) and assumption (2) in section 4.3.1, the total concrete strain at elevated temperatures is a sum of four parts: instantaneous stress-related strain, thermal strain, transient strain and creep strain, as introduced in Chapter 3.

$$\varepsilon_{c,tot}(\theta) = \varepsilon_{c,\sigma}(\sigma_c, \theta) + \varepsilon_{c,th}(\theta) + \varepsilon_{c,tr}(\sigma_c, \theta) + \varepsilon_{c,cr}(\sigma_c, \theta, t) \quad (4.08)$$

where σ_c is the stress of concrete at temperature θ ;

θ is the temperature of the concrete;

t is the fire exposing time of the concrete;

$\varepsilon_{c,tot}$ is the total strain of concrete at temperature θ ;

$\varepsilon_{c,th}$ is the thermal elongation of concrete under elevated temperature θ ;

$\varepsilon_{c,\sigma}$ is the instantaneous stress dependent strain of concrete under elevated temperature θ ;

$\varepsilon_{c,cr}$ is the creep strain of concrete under elevated temperature θ ;

There are many models available for the deformation properties of concrete at elevated temperatures, and the most commonly used is the one from EC 2. For the concrete model with transient creep strain considered explicitly, the one presented by Tao, J. (2008) is adopted in this thesis. The proposed simplified method is convenient for the users to adopt any material

model for the strain equations, which makes it possible to investigate the difference of simulation results of RC members with implicit transient strain material model and the explicit transient strain material model. This is studied in Chapter 5.

II. Thermal strain of steel

Since transient strain is absent in the total strain of steel, the total strain of reinforcing bars contains only three parts as shown by Equation (4.09).

$$\varepsilon_{s,tot}(\theta) = \varepsilon_{s,th}(\theta) + \varepsilon_{s,\sigma}(\sigma_s, \theta) + \varepsilon_{s,cr}(\sigma_s, \theta, t) \quad (4.09)$$

where $\varepsilon_{s,tot}$ is the total strain of steel under temperature θ ;

$\varepsilon_{s,th}$ is the thermal elongation of steel under temperature θ ;

$\varepsilon_{s,\sigma}$ is the stress dependent strain of steel under temperature θ ;

$\varepsilon_{s,cr}$ is the creep strain of steel under temperature θ ;

Compared to the thermal strain and mechanical strain, the creep strain of steel is quite small, and can reasonably be neglected. The stress-strain relationship and thermal strain expressions suggested in EC 2 are adopted in this thesis, which have all been introduced in Chapter 3. The stress-strain relationship of steel was simplified into a three step curve, with the fourth decreasing part, occurring before the ultimate strain is reached, replaced by a constant value and combined into the third part, as shown in Figure 4.09.

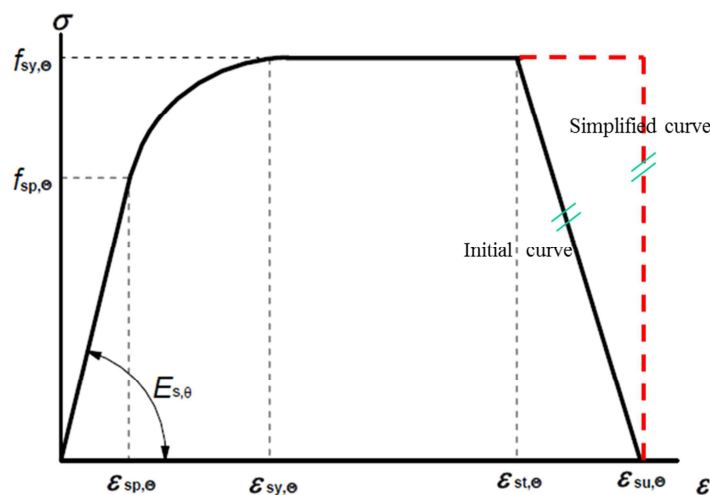


Figure 4.09 Simplified stress-strain relationship of reinforcing steel based on EC 2

4.3.3 Equilibrium state of a cross-section

From a given temperature field calculated by the method introduced in section 4.2, an equilibrium state for a cross-section in a flexural member can be calculated at each time step. Take the longitudinal direction of the beam as X coordinate, and the left point as the origin of the coordinate system (Figure 4.10). Then, the Y and Z coordinate are along the cross-section of the beam, as shown by Figure 4.11 (a). The stresses and internal forces on this cross-section are shown by Figure 4.11 (b) and (c).

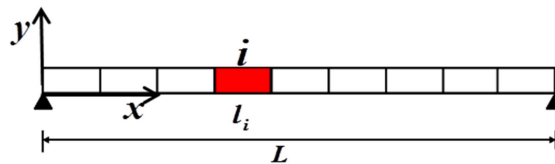
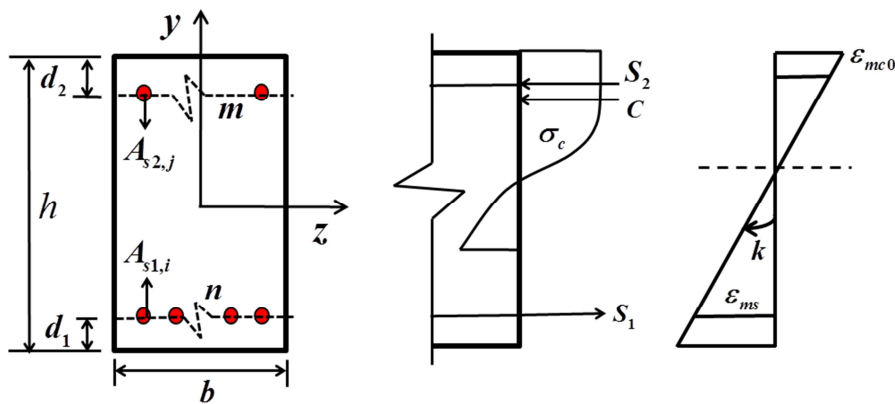


Figure 4.10 RC element and layout of coordinates



(a) Cross-section I-I (b) stress and forces (c) strain distribution

Figure 4.11 Cross-section of the beam

Based on the equilibrium criterion and assumption (3) in section 4.3.1, the final equilibrium state of the cross-section is governed by Equations (4.10) and (4.11).

$$N_{external} = N_{inner} \tag{4.10}$$

$$M_{external} = M_{inner} \quad (4.11)$$

where $N_{external}$ is the axial force applied to the cross-section;

N_{inner} is the total axial force resulting from the forces in the concrete and the steel bars of the cross-section;

$M_{external}$ is the moment applied on the given cross-section;

M_{inner} is the moment resulting from the forces in the concrete and the steel bars of the cross-section.

The internal axial force contains three parts (Figure 4.07(c)), as described in Equation (4.12):

$$C + S_1 + S_2 = N_{inner} \quad (4.12)$$

where C is the resultant force of the concrete stresses;

S_1 is the resulting force in the steel bars in tension;

S_2 is the resulting force in the steel bars in compression;

The resultant force of the concrete stresses can be determined by integrating the concrete stress over the cross-section, as expressed by Equation (4.13).

$$C = \iint \sigma_c(z, y, \theta, t) dydz \quad (4.13)$$

The resulting force of the steel bars in tension can be calculated by Equation (4.14) and that of the steel bars in compression by Equation (4.15).

$$S_1 = \sum_{i=1}^n A_{S_{1,i}} \sigma_{S_{1,i}}(\theta_{S_{1,i}}) \quad (4.14)$$

$$S_2 = \sum_{j=1}^m A_{S_{2,j}} \sigma_{S_{2,j}}(\theta_{S_{2,j}}) \quad (4.15)$$

where $A_{S_{1,i}}$ is the cross-section area of steel bar i in tension;

$A_{S_{2,j}}$ is the cross-section area of steel bar j in compression;

$\theta_{S_{1,i}}$ is the temperature at the centre of steel bar i in tension;

$\theta_{s_2,j}$ is the temperature at the centre of steel bar j in compression;

n and m are the number of steel bars in tension and in compression respectively.

After all the forces in tension and in compression are determined, the expression to get the internal moment can be derived, as shown by Equation (4.16), by taking the moment with respect to the steel bars in tension. It contains the effect of both the concrete and the steel bars in the compressive zone.

$$M_{inner} = \iint \sigma_c(z, y, \theta, t)(h/2 + y - d_1)dydz + \sum_{j=1}^m A_{s_2,i} \sigma_{s_2,i}(\theta_{s_2,i})(h - d_1 - d_2) \quad (4.16)$$

where M_{inner} is the internal moment of the given cross-section;

d_1 is the axial distance of the steel bars in tension to the bottom fibre of the cross-section;

d_2 is the axial distance of the steel bars in compression to the top fibre of the cross-section.

4.3.4 Multi- iteration method

To solve the equations for the inner forces, the cross-section is meshed into small elements. The total force on the cross-section can be obtained as a sum of the forces on the small elements. And then, a multi-iteration process for the critical parameters of the equations is carried out in order to solve the equilibrium equations. Mainly five steps are considered:

(1) Firstly, the cross-section is being meshed into small four-joints rectangular elements designated as (α, β) . The relevant position of the centre of the element in the coordinate system of the cross-section is (x_α, y_β) . The mesh size of the small elements will directly

influence the calculation results of the temperature gradient. The research results of Wen C.J. (2008) show that a 50 mm element size for the temperature calculation is accurate enough.

(2) Secondly, based on the temperature field results, from the temperature at the four corner points of the small elements, the average temperature at the centre of the element is calculated and used to represent the element. The temperature dependent properties of the small elements including thermal strains and the stress-strain relationships are then determined from this mean temperature.

(3) Thirdly, the forces on each of the small elements are calculated based on the stress-strain

expressions in function of the local temperature. Based on the assumption (1), the total strain distribution of the concrete and the steel bars has a linear relationship as shown by Figure 4.10(c), which can be expressed by the curvature k and a reference strain. The total strain at the upper most fibre is taken as the reference strain ε_{mc0} , Hence the total strain of the concrete elements can be expressed by Equation (4.17) and the total strains of the steel elements can be calculated by Equation (4.18) and Equation (4.19):

$$\varepsilon_{c,tot}(\alpha, \beta) = \varepsilon_{mc0} - k(h/2 - y_\beta) \quad (4.17)$$

$$\varepsilon_{s1,tot}(i) = \varepsilon_{mc0} - k(h - d_1) \quad (4.18)$$

$$\varepsilon_{s2,tot}(j) = \varepsilon_{mc0} - k \times d_2 \quad (4.19)$$

where $\varepsilon_{c,tot}(\alpha, \beta)$ is the total strain of the concrete element (α, β) ;

$\varepsilon_{s1,tot}(i)$ is the total strain of steel bar i in tension;

$\varepsilon_{s2,tot}(j)$ is the total strain of steel bar j in compression;

y_β is the Y-coordinate location of the centre of concrete element (α, β) ;

k is the curvature of the corresponding small segment of the RC member.

To obtain the stresses in each small element, the instantaneous stress dependent strain of concrete under elevated temperature $\varepsilon_{c,\sigma}$ and that of the steel bars $\varepsilon_{s1,\sigma}$ $\varepsilon_{s2,\sigma}$ should be calculated first. For concrete, $\varepsilon_{c,\sigma}$ could be generated by substituting the total strain $\varepsilon_{c,tot}(\alpha, \beta)$ into Equation (4.08), resulting in Equation (4.20). For the steel bars, $\varepsilon_{s1,\sigma}$ can be computed by substituting $\varepsilon_{s1,tot}(i)$ expressed by Equation (4.18) into Equation (4.09) resulting in Equation (4.21); $\varepsilon_{s2,\sigma}$ can be calculated by substituting $\varepsilon_{s2,tot}(i)$ expressed by Equation (4.19) into Equation (4.09) obtaining Equation (4.22);

$$\varepsilon_{c,\sigma}(\alpha, \beta) = \varepsilon_{mc0} - k(h/2 - y_\beta) - \varepsilon_{c,th}(\theta) - \varepsilon_{c,tr}(\sigma_c, \theta) - \varepsilon_{c,cr}(\sigma_c, \theta, t) \quad (4.20)$$

$$\varepsilon_{s1,\sigma}(\sigma_{s2,j}, \theta_{s1,i}) = \varepsilon_{mc0} - k(h - d_1) - \varepsilon_{s1,th}(\theta_{s1,i}) \quad (4.21)$$

$$\varepsilon_{s2,\sigma}(\sigma_{s2,j}, \theta_{s2,i}) = \varepsilon_{mc0} - k(h - d_2) - \varepsilon_{s2,th}(\theta_{s2,j}) \quad (4.22)$$

With the mechanical strain of concrete elements and steel bars, at each time step the mechanical stress of concrete $\sigma_c(z, y, \theta, t)$ can be calculated by iterating the stress-dependent strain of concrete $\varepsilon_{c,\sigma}(\alpha, \beta)$ into the stress-strain relationship equations, the implicit one suggested by EC 2 or the explicit one suggested by J. Tao as introduced in Chapter 3. In the same way, the stress of the steel bars $\sigma_{s1,i}$, $\sigma_{s2,j}$ can be determined by iterating the strain of steel $\varepsilon_{s1,\sigma}(\sigma_{s2,j}, \theta_{s1,i})$ and $\varepsilon_{s2,\sigma}(\sigma_{s2,j}, \theta_{s2,i})$ into the stress-strain relationships of the materials, adopted from standards or research reports.

(4) The fourth step, a summing up of the forces and moments in all the small elements is carried out for the force and moment of the whole cross-section, and a multi-iteration process is used to solve the equilibrium equations. At a given heating time t and temperature field, there are two critical equations. Equation (4.07) for the internal axial force and Equation (4.16) is for the internal moment. As a sum of the forces in all the small elements, these two equations will vary with the curvature k and the defined reference strain ε_{mc0} at the top fibre.

For a given axial force $N_{external}$, an iteration process for the curvature k can be carried out to fulfil the balance of axial force $N_{inner} = N_{external}$. The moment-curvature ($M - k$) relationship is then derived until k_{max} , where the ultimate strain of the steel (shown by Figure 4.09) at elevated temperatures is reached. The flowchart of the iteration process for the M-k relationship is shown by Figure 4.12.

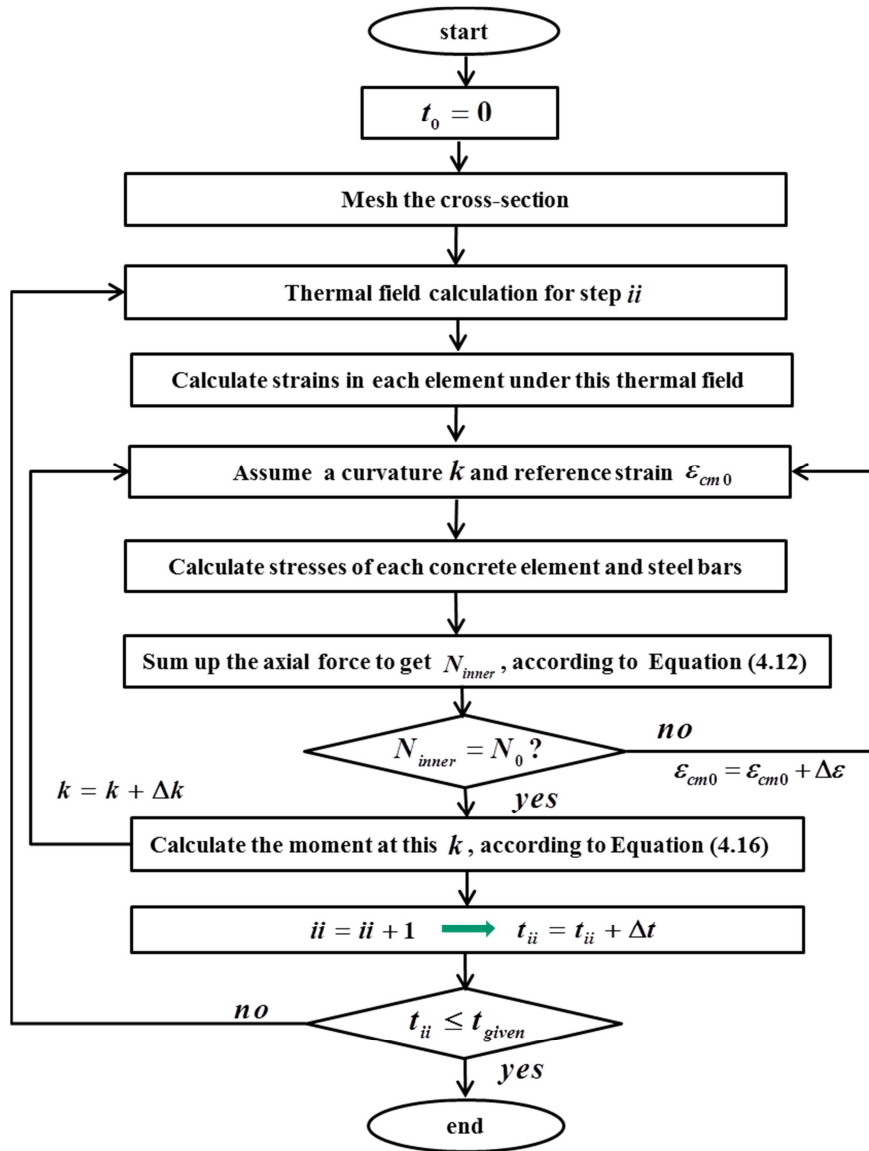


Figure 4.12 Flowchart for the calculation of the M-k relationship

(5) The fifth step: a concept of equivalent bending stiffness of the cross-section is proposed and calculated. The equivalent bending stiffness of each segment of the RC member is the critical parameter for the simulation of the structural deformation and the thermal forces. Each segment of the RC member can be presented by the cross-section in the middle, and based on the calculation results of the cross-sections, an effective stiffness of this segment can be defined by Equation (4.23), and could be calculated by Equation (4.24):

$$B(t, \tilde{\theta}) = (EI)_{eff}(t, \tilde{\theta}) \quad (4.23)$$

$$B(t, \tilde{\theta}) = \frac{M}{k - k_t} \quad (4.24)$$

where $\tilde{\theta}$ is the temperature field at a given time step t ;

$B(t, \tilde{\theta})$ is the effective bending stiffness of a segment at temperature field $\tilde{\theta}$;

EI is the bending stiffness of a member in which E is the elastic modulus of the material and I is the moment of inertia of the cross-section;

k_t is the curvature of the segment generated only by thermal deformation of the member at time step t ;

For the negative moment, like the moment at the supports of a member with rotational restraints, the equivalent stiffness is calculated with the same process. The compressive zone of the cross-section is subjected to higher temperatures in this condition.

4.3.5 An example of the cross-sectional analysis

The $M - k$ curves for a simply supported rectangular beam under ISO-834 fire, which is described in literature (Lu, Z.D. et al. 1996), are calculated with this numerical model. The basic parameters of the cross-section are shown by Table 4.01, and the $M - k$ curves are shown by Figure 4.13.

Table 4.01 Parameters of a cross-section of a simply supported beam (Lu, Z.D. et al. 1996)

b (mm)	h (mm)	d_1 (mm)	d_2 (mm)	f_c (MPa)	f_y (MPa)	A_{S1}, A_{S2} (mm ²)	m	n
250	400	25	25	30	500	314	2	3

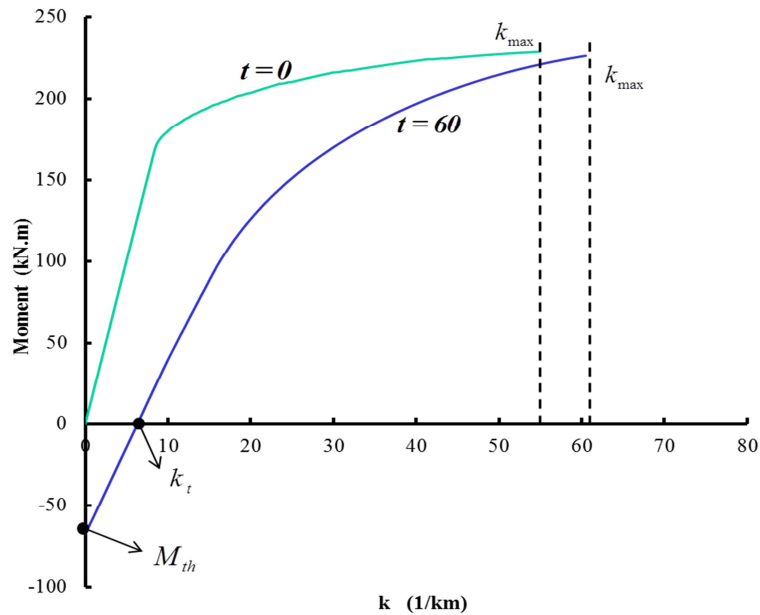


Figure 4.13 $M-k$ curves for a rectangular beam under ISO-curve heating

From this paragraph, the following conclusions could be made:

(1) When the axial force is fixed, in this case $N_{external} = 0$, a $M-k$ curve can be generated. The ultimate moment of the cross-section is determined by the ultimate strength of the steel bars at elevated temperatures, and can be found in the figure when k_{max} of that time step is arrived.

(2) At elevated temperatures, the thermal curvature when there is no internal moment is $k = k_t$. This curvature can be used to simulate the curvature of a load-free beam at elevated temperatures, which is only caused by the thermal deformation of the member.

(3) M_{th} is the moment needed to compensate the thermally-induced curvature k_t of the beam.

This moment is used to simulate the effect of a full rotational restraint which is a critical factor for the structural analysis.

4.4 Structural analysis

For a RC member in a complete structure, besides the loads transferred from the upper part of the structure, there can also be axial restraints and rotational restraints applied on both ends

from the surrounding members. These restraints could be exchanged by applying axial and rotational forces, and during the heating process, these forces may change with the variation of the temperature field. In order to simulate these forces and study the effect of these restraints, four springs are applied to the considered member, two for the axial restraints, and two for the rotational restraints, as shown by Figure 4.14.

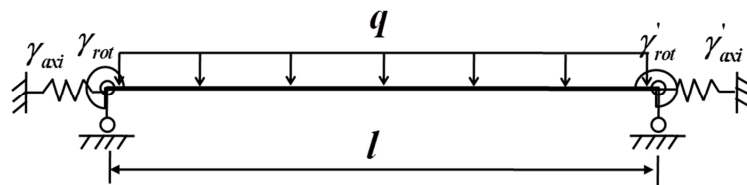


Figure 4.14 A beam under loading and restrains

With the simplified model shown by Figure 4.14, the structural analysis based on the proposed numerical method allows to study the following items at each investigated time step: the thermal restraint forces, the deflections of the member and the ultimate bearing capacity. Then the fire-resistance time (or fire-resistance) of a member can be determined, by applying the failure criteria on the deformation or on the bearing capacity. There are many failure criteria outlined by design codes and guidelines, the following ones are adopted in the proposed method. The first failure criterion is taken from ASTM 119 (1999) and the second and the third are taken from BS 476 (1987).

- (1) The applied service load exceeds the bearing capacity of the member at any fire exposing time t ;
- (2) The maximum deflection of the member exceeds $L/20$ at any fire exposure time t , where L is the span length of the member.
- (3) The rate of deflection exceeds the limit given by the following expression:

$\frac{L^2}{9000h_0}$ (mm/min), where L is the span length of the member (mm), and h_0 is the effective depth of the member (mm).

4.4.1 The equilibrium state of the member

In order to simulate the whole process of the fire-behaviour of a RC member, the structural problem is simplified into a sectional-analysis problem, and the member needs to be divided

into small segments as shown by Figure 4.15. For each segment j ($j = 1, 2, 3, \dots$), the internal forces and stiffness can be determined by a sectional analysis of its mid-section, which is calculated based on the assumption (5) in section 4.3.1.

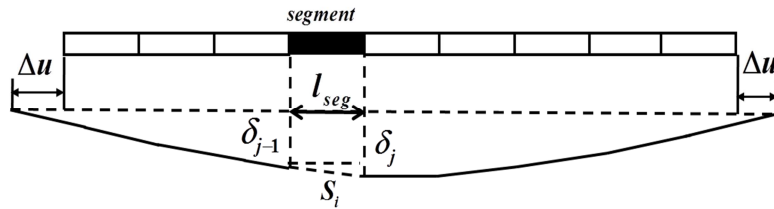


Figure 4.15 A diagram showing deflection and axial elongation of a member

For a RC member simplified as in Figure 4.15, two equilibrium equations of the load system can be derived: the equivalence between external axial load and internal axial load, and that between external moment and internal moment.

(1) Axial load equilibrium equations:

For the axial force calculation, it's assumed that the thermal induced axial restraint force is constant along the span of the member. The external axial force applied to the member under restraint conditions will develop with temperature as indicated in Equation (4.25).

$$N_{external} = N_{load} + N_{th} \quad (4.25)$$

where N_{load} is the initial axial load applied to the flexural member. N_{th} is a thermally-induced axial force, which is determined by the axial expansion of the member and the axial restraint stiffness, as shown by Equation (4.26).

$$N_{th} = \gamma_{axi} \frac{EA(\tilde{\theta})}{L} \Delta u = \gamma'_{axi} \frac{EA(\tilde{\theta})}{L} \Delta u' \quad (4.26)$$

where γ_{axi} and γ'_{axi} are the axial restraint ratios, the ratio between the axial restraint stiffness and that of the member;

Δu and $\Delta u'$ are the axial thermal elongations at the two ends of the member;

L is the span of the member at normal temperature;

A simplified method is adopted here to solve the axial elongations as shown by Figure 4.15 by assuming that each segment of the member will have an elongation along its axial geometric centre, as given by Equation (4.27). And the total length of the member after thermal elongation will be calculated as a sum of the lengths of all the segments at time step t .

$$l_j(t) = \sqrt{s_j^2 - (\delta_j - \delta_{j-1})^2} \quad (4.27)$$

$$L'(t) = \sum_j \sqrt{s_j^2 - (\delta_j - \delta_{j-1})^2} \quad (4.28)$$

where s_j is the total length of the segment after thermal elongation at time step t , which could be calculated based on the initial length of the segment l_{j0} and the total strain of the concrete element along the central line, as shown by Equation (4.29).

$$s_j = l_{j0} + l_{j0}(\varepsilon_{mc0} - k \times h/2) \quad (4.29)$$

l_{j0} is the initial length of each small segment along the x direction before heating;

$l_j(t)$ is the length of each small segment along the x direction at time step t ;

$L'(t)$ is the length of the member along the x direction at time step t ;

δ_j and δ_{j-1} are the vertical deflections at points j and $(j-1)$, as shown by Figure 4.15.

Since the deflection at time step t_{ii} is needed to determine the axial force, but it is actually unknown before the axial force is calculated first, the deflection of t_{ii-1} is used instead to solve the Equation (4.28). It was found that the deflection difference of $(\delta_j - \delta_{j-1})$ between time step t_{ii} and that of t_{ii-1} is quite small.

To conclude, the thermal elongation of the member along the axial direction could be determined by a function including the strain of the segments along the axial line of the cross-section and the deformation difference of the two ends of the segments, as shown by Equation (4.30).

$$\Delta u + \Delta u' = L'(t) - L = \sum_j \sqrt{[l_{j0} + l_{j0}(\varepsilon_{mc0} - k \times h/2)]^2 - (\delta_j - \delta_{j-1})^2} - L \quad (4.30)$$

Thus, for any time step, an iteration process to solve Equation (4.10), Equation (4.26) and Equation (4.30) is first carried out and the axial force is computed. Next, the M-k relationship of this time step will be calculated based on the sectional analysis procedure.

(2) Moment equilibrium equations:

The moment applied to the cross-section is a function of its position along the x -axis of the member. At elevated temperatures, due to the thermal restraints and second-order effects caused by the axial load and deflections, it mainly contains three parts, as shown by Equation (4.31):

$$M_{external}(x,t) = M_{load}(x) + M_{thermal}(x,t) + M_{sec-order}(x,t) \quad (4.31)$$

where M_{load} is the initial moment applied to the cross-section, which will not change with heating time; $M_{thermal}$ is the thermally induced restraint moment determined by temperature and the rotational restraint stiffness at both ends. $M_{sec-order}$ is the second order moment, which is the product of the axial force $N_{external}$ and the local deflection.

At any time step, the total thermal moment M_{th} is calculated first by the $M-k$ relationship as introduced in section 4.3.4. The thermally induced restraint moment could be calculated by encountering the total thermal moment depending on the rotational restraint ratios at the two ends γ_{rot} and γ'_{rot} . The thermal restraint moment at the left end where $x=0$ can be computed by Equation (4.32) and that at the right end where $x=L$ by Equation (4.33).

$$M_{thermal}(x=0,t) = \frac{c(1+b)}{1-(ab)^2} M_{th} \quad (4.32)$$

$$M_{thermal}(x=L,t) = \frac{d(1+a)}{1-(ab)^2} M_{th} \quad (4.33)$$

where the a , b , c and d are functions of the rotational restraint ratios, calculated by Equation (4.34).

$$\begin{cases} a = 2/(4 + \gamma_{tot}) \\ b = 2/(4 + \gamma'_{tot}) \\ c = \gamma_{tot}/(4 + \gamma_{tot}) \\ d = \gamma'_{tot}/(4 + \gamma'_{tot}) \end{cases} \quad (4.34)$$

4.4.2 Computation of deformations

After the forces are calculated and the equivalent stiffness of each segment is determined by the $M - k$ curves, the deflection of the member can then be computed by the load-stiffness matrix. At time step t , the stiffness matrix of each segment is computed by the sectional analysis results, and the displacement matrix of each segment $[u^e]$ is expressed as $[u^e] = [u_1, v_1, \theta_1, u_2, v_2, \theta_2]$. The global nodal displacement matrix $[U]$ consists of all the sub-matrices of the small segments. The complete structural behaviour can be expressed by Equation (4.35).

$$[K_g][U] = [P] \quad (4.35)$$

where $[K_g]$ is the global stiffness matrix, it is composed by the stiffness of the small segments based on the rules of structural mechanics;

$[U]$ is the nodal displacement matrix.

$[P]$ is the matrix of the nodal load vectors, containing both the equivalent nodal load vector due to the applied loading and the load due to the thermal restraints, including the axial load and second order effect.

Thus, the proposed numerical model is able to calculate the fire performance of a RC element under various fire curves, taking account non-linear thermal-dependent material properties the second-order effects and all components of the thermally-related strains. In this way, the effect of various restraints, the development of restraint forces and deflections under elevated temperatures can be simulated.

For simply supported members, this equation could be simplified by applying $N_{external} = 0$ and

$M_{external}(x) = M_{load}(x)$ into Equation (4.35), and the deflection could be simplified into Equation (4.36), which is quite normally used for the calculation of simply supported beams (Zha, X.X. 2003; 2001; Bratina, S. et al. 2005; 2003).

$$\delta(L/2) \approx \frac{L^2}{8} k(L/2) \quad (4.36)$$

$k(L/2)$ is the curvature of the segment in the middle of the member, which could be obtained by inserting $M_{load}(L/2)$ into the $M - k$ curve.

4.5 Verification by fire tests from literature

In this section, the proposed numerical model is validated by the fire test results presented by Minne R. et al. (1979) on one-way slabs both simply supported and with rotational restraints. A detailed discussion about the validation of the model is presented in the following sections, where 4.5.1 and 4.5.2 deal with the simply supported slabs and 4.5.3 and 4.5.4 with the rotational restrained slabs.

4.5.1 Set-up for simply supported slab tests

Three simply supported slabs, measuring $1900 \times 150 \times 4900$ mm, were positioned in a steel frame and loaded by means of two hydraulic jacks situated at $\frac{1}{4}$ and $\frac{3}{4}$ of the effective length of the span which measured 4.5 m (Figure 4.16). The slabs are one-way spanning, designed for a service live load of 3 kN/m^2 and an admissible steel stress of 240 N/mm^2 . The service loads considered in design are replaced by the forces applied by the hydraulic jacks, shown by Table 4.02. The three tested simply supported slabs, have a different thickness of the concrete cover on the longitudinal steel bars (as shown by Table 4.02) and different amounts of reinforcing steel (as given in Table 4.03). In order to have an equivalent maximum moment and forces at the supports, the applied forces of the two hydraulic jacks are calculated as 14.5 kN for G1, 15.7 kN for G2 and 14.6 kN for G3.

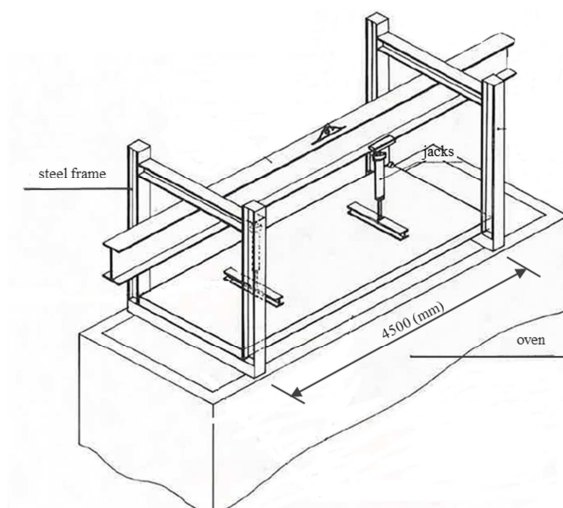


Figure 4.16 Lay-out of the tested simply supported slabs (Minne R et al. 1979)

Table 4.02 presents the total applied load during heating and the properties of the siliceous aggregates concrete before heating. Table 4.03 shows the reinforcement properties. For each group of slabs, differences can be found in the number of reinforcing bars and the concrete cover on the main reinforcement. During the fire tests, the temperature at the main reinforcement depth and the deflection at mid-span were measured.

Table 4.02 Applied force and concrete material properties

	Applied force [kN]	f_c [N/mm ²]	f_{ct} [N/mm ²]	E_c [N/mm ²]	ρ [kg/m ³]
G1	14.5	53.4	4.62	45200	2420
G2	15.7	54.6	4.63	38100	2400
G3	14.6	53.8	5.45	39800	2393

Table 4.03. Reinforcement properties before heating.

	Longitudinal reinforcement		Transversal reinforcement	Concrete cover [mm]
	f_y [N/mm ²]	$\epsilon_{failure}$ [%]		
G1	504	17.7	15 x Ø10 26 x Ø 6	15

G2	504	17.7	17 x Ø10	26 x Ø 6	25
G3	504	17.7	18 x Ø10	26 x Ø 6	35

4.5.2 Results and conclusions for the simply supported slab tests

Two types of measurements were performed during the experiments: the temperature at the level of the steel bars, and the mid-span deflection. So the main comparisons will be between the temperatures and the deflections.

(1) The slabs were submitted to an ISO-834 standard fire (introduced in section 4.2.2), with only the bottom surface exposed to the fire. So the temperature gradient along the slab could be simplified as a 1D problem. The test results and the simulation results of the temperature of the steel bars in tension are compared in Figure 4.17.

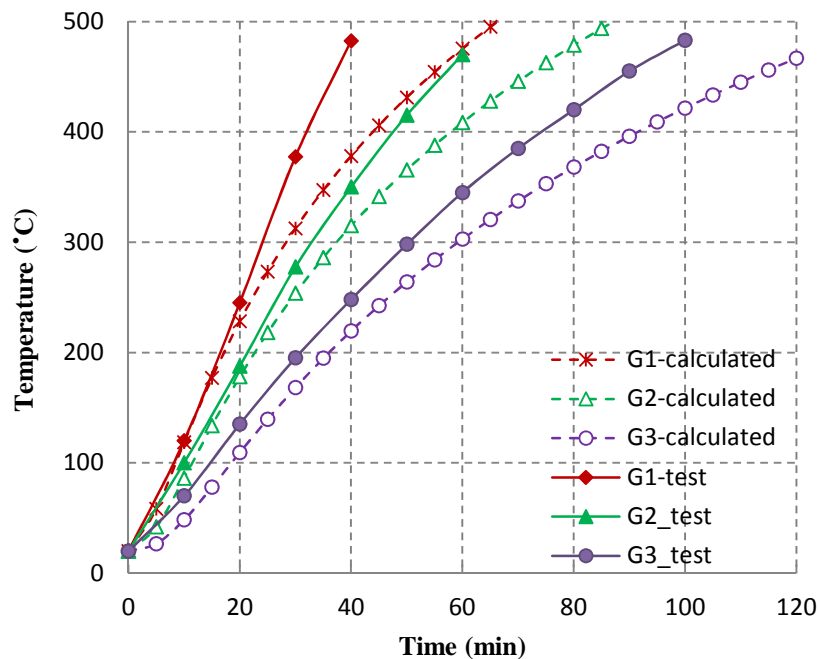
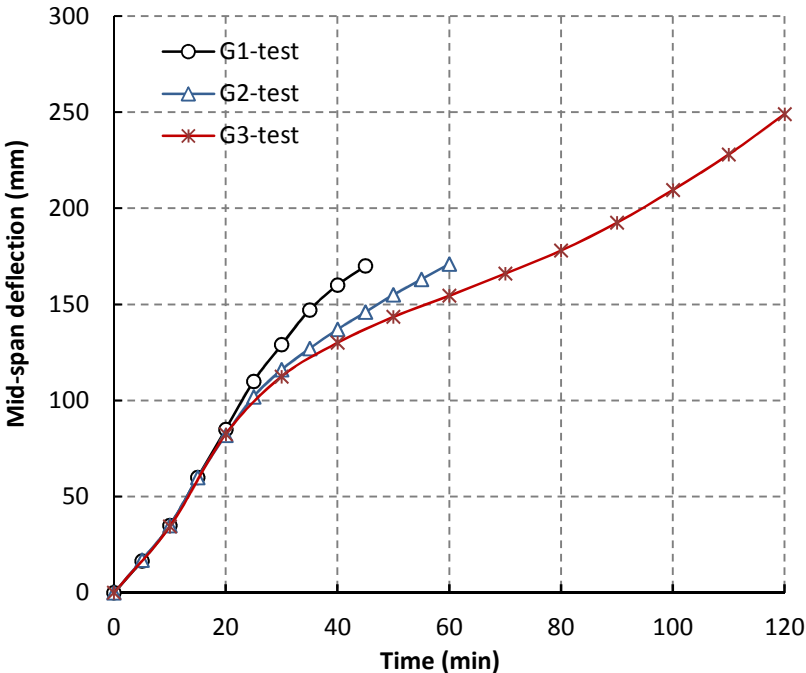


Figure 4.17 Comparison of temperatures of steel bars as measured and simulated

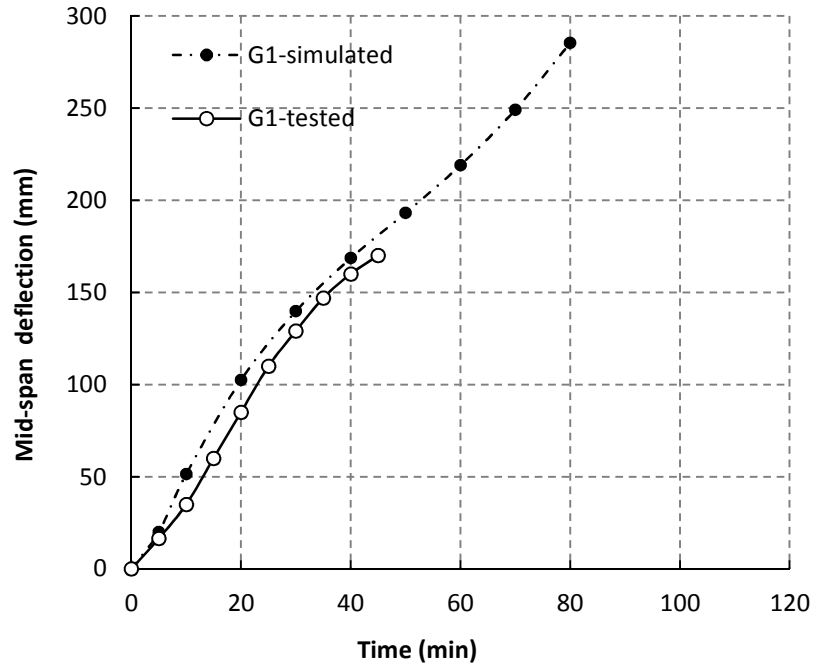
The calculated results are a little bit lower than the ones obtained in the experiments. This may be due to the experimental conditions and the spalling of concrete cover during experiments. Since it is normal concrete, spalling was not considered during the simulation but it was actually happening during the experiments. For the three series of reinforcing bars in the slabs,

the ones in G3 with the thickest concrete cover on the steel bars have the lowest temperature during heating, by which we can conclude that the concrete cover on the steel bars in tension significantly contributes to the fire-resistance of the RC members. Increasing the concrete cover on the steel bars is one of the effective ways of improving the fire-resistance of a RC structure, as is well known.

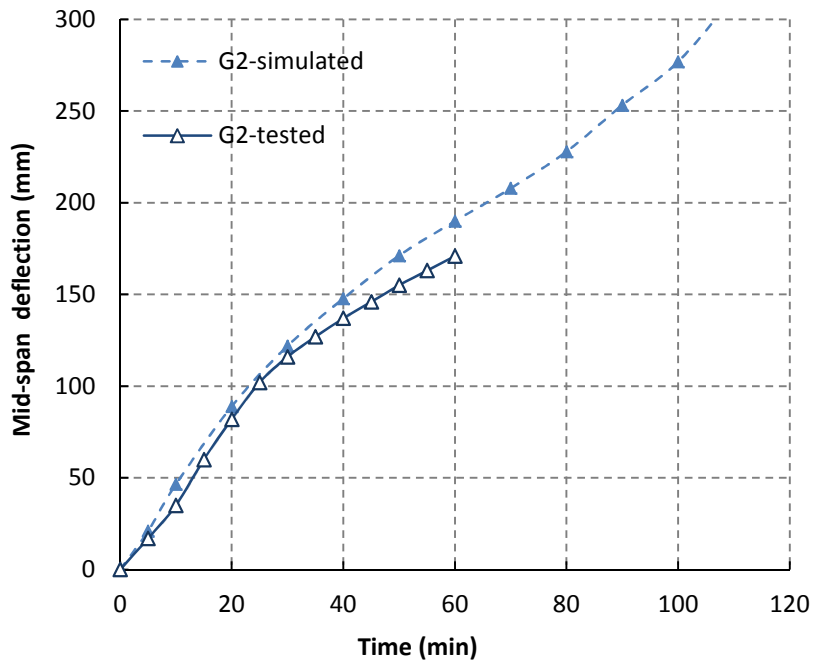
(2) The obtained mid-span deflection of slabs G1, G2 and G3 measured during tests as well as the results calculated with the implicit material model adopted from EC 2 are compared, as shown by Figure 4.18.



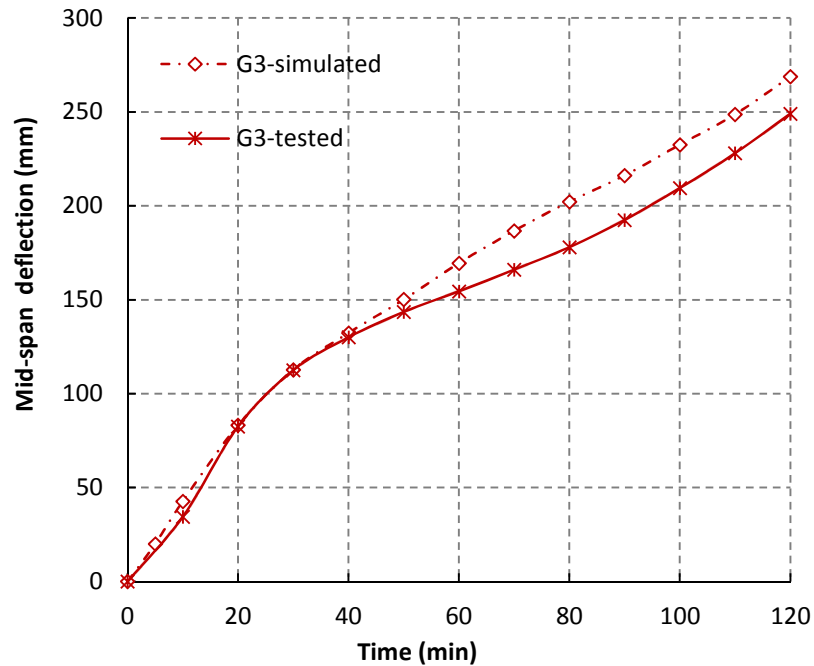
(a) Mid-span deflections of G1, G2 and G3 measured during tests



(b) Comparison of mid-span deflections of G1, tested and simulated



(c) Comparison of mid-span deflections of G2, tested and simulated



(d) Comparison of mid-span deflections of G3, tested and simulated

Figure 4.18 Mid-span deflections of G1, G2 and G3 as tested and simulated

From Figure 4.18, the following conclusions can be derived:

(1) G1 and G2 failed after 60 min of heating in the tests, and G3 lasted until 2 hours. As the slabs are heated from the tensile side, the ultimate bearing capacity of the elements was mainly determined by the steel bars. Hence, G3 with the thickest concrete cover on the steel bars has the highest fire resistance of the three slabs.

(2) With higher temperatures in the steel bars and less steel bars in tension, slab G1 has a faster increase in mid-span deflection than G2 and G3, from which we could see that the thickness of the concrete cover and reinforcement are essential for the fire-resistance of RC slabs.

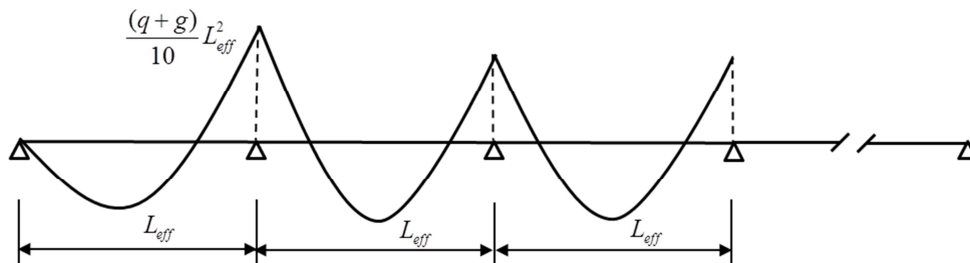
(3) Spalling is severely encountered during the experiments, which make the bearing capacity of the slabs decrease sharply and lead to an early failure. This was not considered accurately in the simulation, so the simulated G1 slab failed after 80 min of heating time, the simulated G2 failed after 100 min of heating time, which are all resisting longer than the tested ones.

(4) The numerical results and the test results are very close and show a similar trend with the heating time. After 30 min, the numerical results are higher than the tested ones, but the differences are acceptable. By comparison of the test results and the simulation results, we

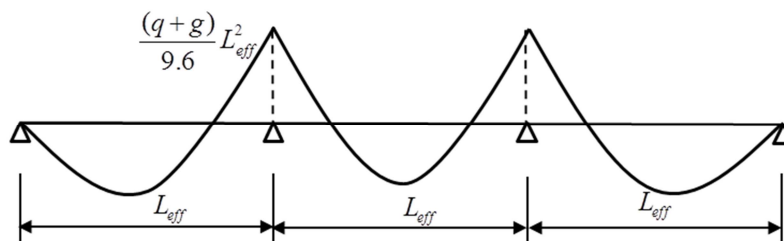
can conclude that the proposed numerical method is valid for the fire behaviour simulation of simply supported RC members, although it should be mentioned that the ultimate failure due to spalling cannot be predicted accurately.

4.5.3 Test set-up for rotationally restrained slabs

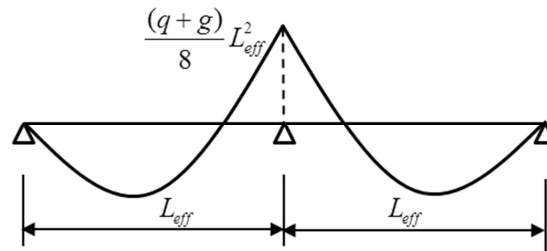
The structural calculation method for restrained members is validated by three one-sided rotationally restrained slabs (Minne R. et al. 1979). The three restrained slabs are considered to simulate the boundary span of three typical continuous slabs, with one-sided rotational restraint by the connected member and the other side simply vertically supported. (1) V5-a is the boundary span of a multi-span (more than three spans) slab, the first span from the left in Figure 4.19(a), with an initial restraint moment $M_0 = \frac{(q+g)}{10} L_{eff}^2$ from the connected members at one side; (2) V5-b is the boundary span of a three-span slab, the first span from the left in Figure 4.19(b), with an initial restraint moment $M_0 = \frac{(q+g)}{9.6} L_{eff}^2$ from the connected members at one side; (3) V5-c is the boundary span of a two-span slab, the left span in Figure 4.19(c), with an initial restraint moment $M_0 = \frac{(q+g)}{8} L_{eff}^2$.



(a) Layout of a multi-span continuous slab for slab V5-a



(b) Layout of a three-span continuous slab for slab V5-b



(c) Layout of a two-span continuous slab for slab V5-c

Figure 4.19 Layout of the continuous slabs for V5_a, V5_b and V5_c (Minne R. et al. 1979)

To simulate the three proposed slab configurations with a rotational restraint at one side, the tested slabs, measuring $1900 \times 150 \times 7500$ mm, were positioned in a steel frame with 4.5m effective heated span L_{eff} and a 1.5m cantilever each side (Figure 4.20). The live load adopted for the tested slabs was $q = 3kN/m^2$, and the self-weight equals $g = 3.6kN/m^2$. The live loads were replaced by twelve point loads $Q = 2.138kN$ distributed over the surface of the slabs as shown by Figure 4.20, and positioned at $1/8$, $3/8$, $5/8$ and $7/8$ of the slab length.

This value is equal to $3kN/m^2 \times 1.9m \times 4.5m/12$. An initial load was applied at one of the cantilevers by a hydraulic jack located 1.2m away from the support. The displacement of the piston of the jack was prevented and the jack's contact point remained at the same level throughout the fire test. This means that no vertical displacement of the slab was possible at that point. During the fire test, the force in the jack increased and the resulting increase in restraint moment can be calculated by multiplying the applied force increment by the distance of the jack from the support, being 1.2m.

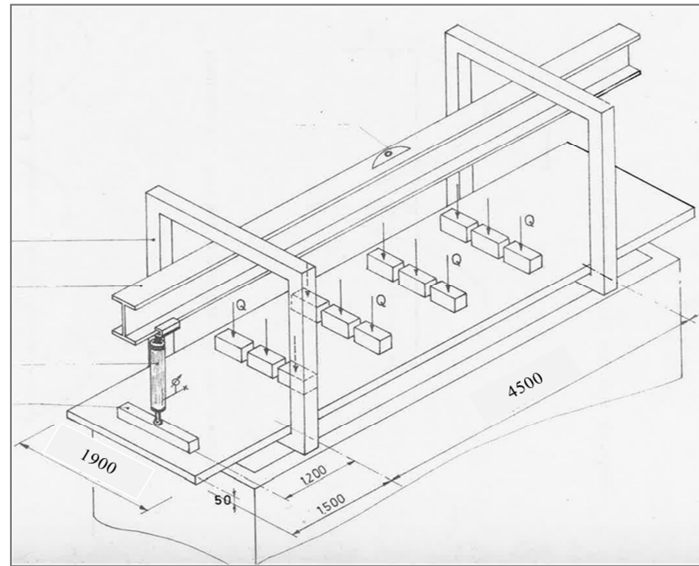


Figure 4.20 Test lay-out of the tested one-sided rotationally restrained slabs (Minne R et al. 1979)

The initial restraint moments of the slabs and the properties of the siliceous aggregates concrete at the age of the fire test (9 months) are shown by Table 4.04 and the properties of the reinforcement are listed in Table 4.05. During the fire tests, the temperature at the level of the main reinforcement and the deflection at mid-span were measured.

Table 4.04 Applied loads, initial restraint moment and concrete properties

	Applied load Q [kN]	Initial moment [kN.m/m]	f_c [N/mm ²]	f_t [N/mm ²]	E_c [N/mm ²]	ρ_c [kg/m ³]
V5_a	2.138	13.36	50.5	5.67	37300	2370
V5_b	2.138	14.22	51.0	5.48	37200	2380
V5_c	2.138	16.70	52.3	5.45	38100	2380

Table 4.05 Reinforcement properties of the slabs before heating

f_y [N/mm ²]	$\epsilon_{failure}$ [%]	top reinforcement	bottom reinforcement	d_1 . [mm]

V5_a	497	17.7	9 Ø10+6 Ø 8	13 Ø 8	19
V5_b	504	17.7	10 Ø10+6 Ø 8	11 Ø 10	19
V5_c	497	17.7	9 Ø12+6 Ø 8	16 Ø 8	19

4.5.4 Results and conclusions for the restrained slab tests

Similar to the simply supported slabs validation, as introduced in section 4.5.2, the comparison of the results for the rotationally restrained slabs also focus on two aspects: the reinforcement temperatures and the mid-span deflections. The tested rotationally restrained slabs were submitted to the ISO-834 standard fire with only the bottom surface exposed to the fire.

Time-dependent restraint moments developed at the restrained end of the slabs. The moments are calculated by multiplying the force of the hydraulic jack by the distance of it to the support. The increase of the moments with respect to the initial moments applied before heating, are measured during the tests, and the results are shown by Figure 4.21. The fire resistance time due to the critical deflection and during fire tests are shown by Table 4.06.

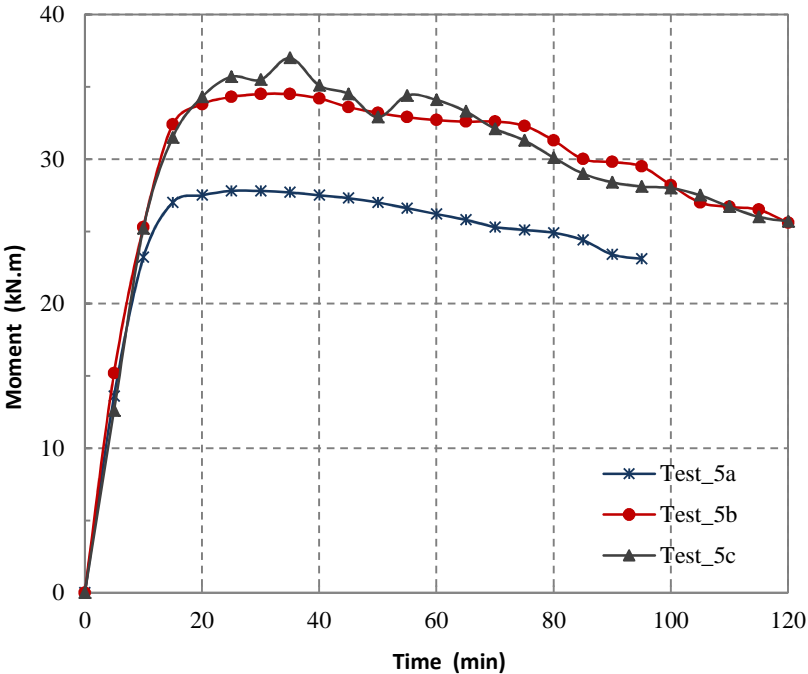
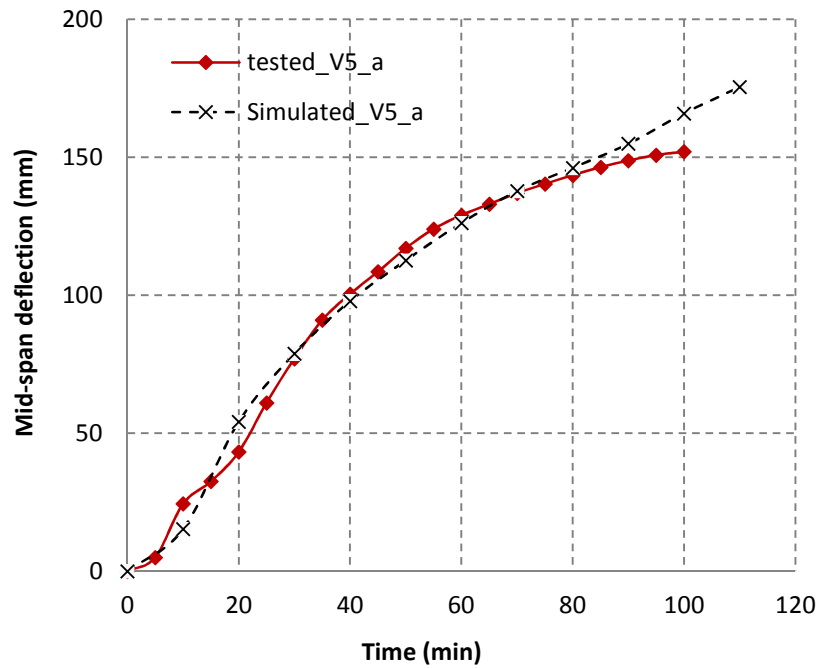


Figure 4.21 Increment of restraint moment of slabs V5_a, V5_b and V5_c during heating

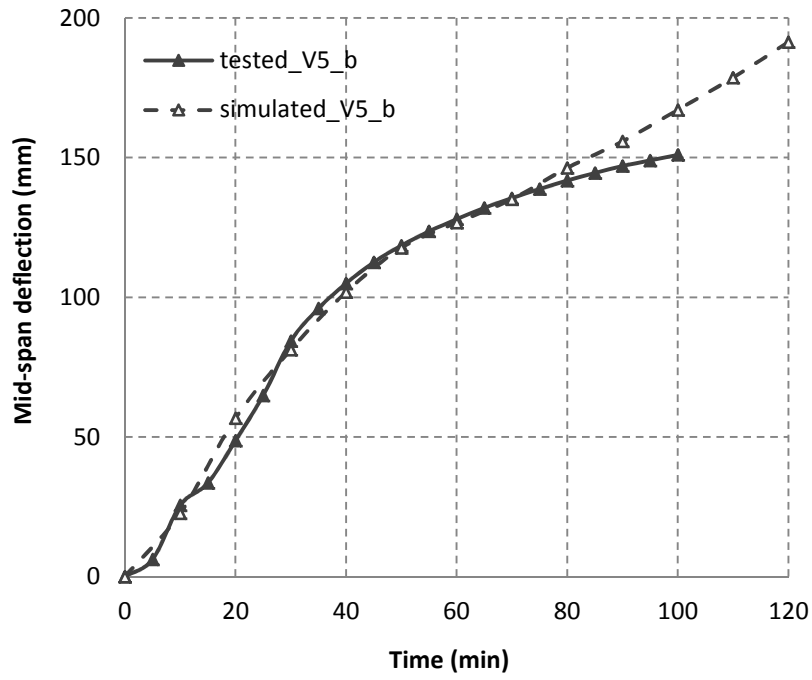
Table 4.06 Fire resistance time due to critical deflection and during tests

Slab	Time at which span deflection equals $L_{eff}/30$ [min]	Time at which the test was stopped [min]
V5A	93	97
V5B	96	120
V5C	123	135

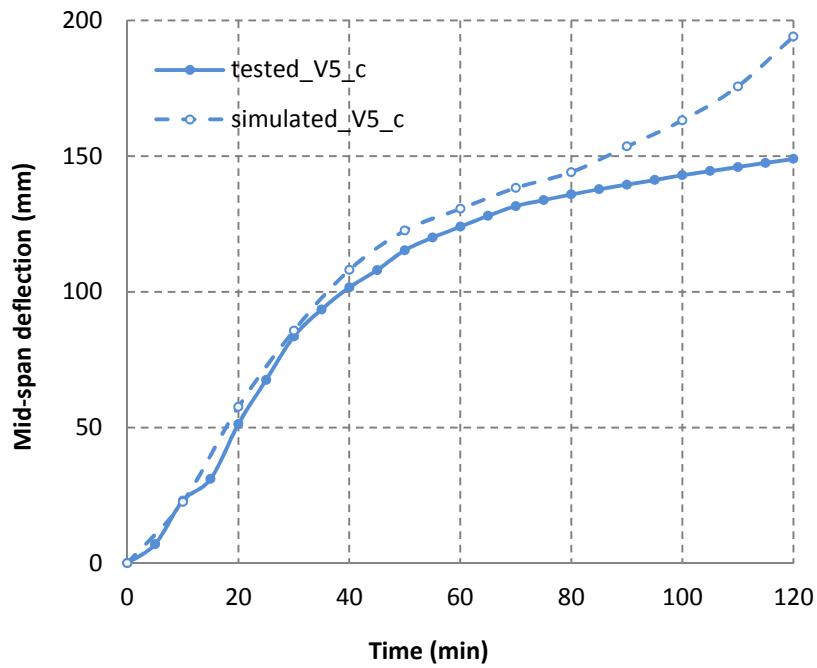
The deflections at mid-span of the slabs measured during the tests as well as the calculated results under the given rotational restraint moment are shown by Figure 4.22.



(a) Mid-span deflections of V5_a tested and calculated



(b) Mid-span deflections of V5_b tested and calculated



(c) Mid-span deflections of V5_c tested and calculated

Figure 4.22 Mid-span deflections of V5_a, V5_b and V5_c tested and calculated

From Figures 4.22, the following conclusions can be derived:

- (1) The calculated mid-span deflection of the slabs and the test results are quite close at the first stage. After about one hour of heating, the calculated results tend to be larger than the test results. Since spalling was observed during the fire tests, and this is not considered accurately in the simulations, the simulated slabs are always resisting longer than the tested ones. Anyhow, the numerical model is considered to be precise enough for the prediction of the fire performance of restrained concrete slabs and as a practical tool for fire-resistance design.
- (2) Since the induced restraint moment at the support increases sharply during the first 15 min of the fire, this phenomenon may also occur to the columns connected to beams and slabs. Hence, the influence of restraint on columns should be considered in the future research.

4.6 Conclusions

A simplified numerical model was developed to simulate the fire performance of reinforced RC members related to bending. A multi-iteration process is carried out in order to reach a force equilibrium based on the concept of equivalent bending stiffness at high temperatures. The proposed method was validated by fire tests executed on simply supported slabs and rotationally restrained slabs exposed to the ISO-834 standard fire. Slabs with various rotational restraints are simulated and analysed with the proposed approach. The following conclusions can be made:

- (1) The proposed numerical model is able to calculate the fire performance of a RC element under various fire curves, taking into account non-linear temperature-dependent material properties and all components of the temperature related strains. In this way the influence of various material models on the fire performance of RC members, the effect of restraints, the development of restraint forces and deflections under fire can be simulated and analysed.
- (2) A moment-curvature ($M-k$) relationship can be generated at the sectional analysis process for a given axial force. The curvature caused by thermal expansion of each of the segments of a member could be induced from the $M-k$ relationship. The ultimate moment of the RC member at elevated temperatures can be calculated when the maximum curvature of the member reached.
- (3) The proposed numerical model is verified to be practical and accurate by the fire test results of slabs executed with simple supports and with one side rotationally restrained.
- (4) Since the induced restraint moment at the support increases sharply during the fire heating

stage, this phenomenon may also occur to columns connected to beams and slabs. Hence, the influence of restraint on columns should be considered in future research.

Parametric study of the fire performance of RC beams with implicit and explicit transient creep strain models

Knowledge of the temperature dependent material properties of concrete and steel bars is important for understanding the fire-response of a reinforced concrete (RC) structure. At high temperatures, the total strain of concrete is largely influenced by load dependent strains, including transient strain and creep strain, which is called transient creep strain in literature (introduced in Chapter 3.2.4). The transient creep strain is much larger than the instantaneous stress-related strain under elevated temperature, and can influence significantly the deformation of RC structures subjected to compressive force. Computer simulations that study the behaviour of heated concrete structures should include this transient creep strain, otherwise the deformations will be slightly overestimated. This remark is especially valid for columns, because of their large compression area. Most of the fire resistance simulations use the implicit material models of concrete, as presented by EN 1992-1-2 (EC 2), which is a viable tool in current design practice, but cannot be used when transient creep effects have to be studied in detail. Therefore, it is necessary to compare the difference of fire performance of RC beams with implicit and explicit models and to study the influencing parameters to evaluate the difference between the two models.

To solve this problem, the simplified numerical model proposed in Chapter 4 is applied in this chapter. The difference between the fire performance of simply supported members with implicit and explicit models will be compared and validated by available experimental results. Three influencing factors are discussed by comparing the simulation results of the fire behaviour of RC rectangular beams. The three investigated parameters that may have an impact on the difference of the fire behaviour of members with the two models are heating curve, reinforcement, and size effect of the cross-section. The conclusions of the parametric study may lead to a better use of material models and more precise fire behaviour simulations, which are required by performance based fire resistance design.

5.1 General Introduction

Knowledge of the temperature dependent material properties of concrete and steel bars is important for understanding the fire behaviour of a RC structure. As introduced in Chapter 3.2.4, for concrete, a special phenomenon appears when subjected to high temperatures: transient strain, which is much bigger than the short time creep and instantaneous stress-related strain, becoming an important part of the total concrete deformation under elevated temperatures (fib bulletin 38, 2007; fib bulletin 46, 2008). Transient strain develops during the first time of heating and is irrecoverable (Tao, J. et al. 2010; Hasson, S. et al. 2006; Khoury, G.A. et al. 1985). This strain component depends on the temperature and on the stress applied during heating. Several uniaxial models of concrete integrating explicitly a term for transient creep strain have been proposed in the literature since the first works of Anderberg, Y. et al. (1976) and Schneider, U. (1985). Interesting state of the art reviews of the transient creep strain models can be found in recent literature, for example: Li, L. et al. (2005), Law, A. et al. (2008) and Youssef, M.A. (2007). Another complex phenomenon for concrete under elevated temperatures is creep. Creep under elevated temperatures exhibits the same trend as basic creep at normal temperature but typically has much bigger values (RILEM TC129-MHT, 1998). It is well established in literature that transient creep has to be considered in any fire analysis involving concrete in compression (Nielsen, C.V. et al. 2002; Terro, M. 1998; Riva, P. 2002). Hence, the total deformation of concrete at elevated temperatures is actually a sum of four parts: instantaneous stress-related strain, thermal strain, transient strain, and creep strain. However, the necessity of taking into account explicit terms in the strain decomposition has been questioned.

The most widely used deformation model of concrete at elevated temperature in EC 2 (2004), which is based on the standard ISO 834 fire curve, contains only two parts: the thermal strain and the stress related strain. The stress related strain obtained from experiments on uniaxial stressed concrete after heating, is an implicit term of the stress-strain relationship. The strain includes instantaneous stress dependent strain, transient strain, and creep. It follows that the EC 2 model is a viable tool in current design, but cannot be effective whenever transient creep may have a significant effect on the behaviour of the structural members. At the other hand, the EC 2 model is simpler in application and can be more easily implemented than the models based on the explicit introduction of transient creep strains. As transient creep strain is not explicitly considered, the material models in the Eurocode are applicable for heating rates between 2 K/min and 50 K/min. For heating rates outside the above range, the reliability of the properties needs to be checked. Law and Gillie (2008) have reported that considering

implicit transient strain can have implications on the Young's modulus of concrete, but the implications on the fire behaviour of RC members is still under research. Since performance based fire resistance design is more widely proposed, one of the important requirements is to use realistic fire curves based on real fire scenarios (Ellingwood, B. 1999). Therefore, for advanced and accurate simulations, which account for realistic fire scenarios and the non-linearity of the temperature field, the use of an explicit model for concrete strain is necessary.

Huang S.S. (2012) have presented the results of their parametric studies on CFT (concrete-filled tubular) columns, which show that the transient strain in the concrete constitutive relationship generally causes an increase of the deflection and a reduction of the buckling resistance. Gernay, T. (2012, 2011) reported that the use of an explicit model has an influence on the fire performance of axially loaded concrete columns, and this influence becomes significant when the cooling phase is taken into account. Sadaoui, A. (2009) has done research on the effect of transient creep stain on the compressive strength of columns, and found that transient creep results in additional compressive stresses in the column, which magnify the bending moments, and hence result in a sudden reduction in the stiffness of the column. This clearly explains the rapid failure of the columns at elevated temperatures where transient creep strain is important. A series of experimental fire tests on axially restrained concrete columns subjected to heating and cooling has been recently performed at South China University of Technology and described by Wu B. et al. (2011; 2009). It was shown that using the implicit model of Eurocode 2, the behaviour of the columns could not be simulated properly, especially during the cooling phase. There is limited research available considering explicit transient creep strain on the fire performance of RC columns, and even less on RC elements subjected to bending, like beams or one-way slabs (Bratina, S. et al. 2006). Moreover, how the other parameters could influence the difference of fire performance of RC beams with implicit and explicit material models is still under research.

To solve these problems, the Multi-iteration calculation method introduced in Chapter 4 is adopted in this chapter. The difference in fire simulation results with implicit and explicit transient creep strain models is validated with the results of fire tests. Then a set of beams with transient creep strain considered explicitly are simulated and the results are compared with the ones considered implicitly. With the proposed method, the parameters which may influence the difference in fire behaviour of RC members with implicit and explicit material models are discussed, i.e. heating curves, reinforcement ratios and size of the cross-section.

5.2 Analytical procedure and test validation

In order to compare the difference in fire performance of RC beams simulated with implicit and explicit transient creep strain, the implicit material model which is suggested in EC 2 (2004) and the explicit transient creep strain models of Tao, J. (2008) which are introduced in detail in Chapter 3, are adopted in this chapter. As introduced in Chapter 3, the total strains for the concrete models with transient creep strain considered implicitly (EC 2 model) and explicitly (J. Tao's model) are not exactly the same, and the strains for the explicit model are slightly lower than that of the EC2 model. The difference between the two total strains is increasing with the compressive stress, from which we could conclude that the main differences between them are the transient creep strains. During the cooling process, the thermal strain and the elastic part of the instantaneous stress strain are supposed to recover based on the temperature, but the plastic strain and the transient creep strain cannot recover.

The thermal and mechanical properties of steel bars used in this chapter are the ones suggested in EC 2 as described in sections 3.3 and 3.4 of Chapter 3. The upper limit of the thermal conductivity coefficient is adopted in this research. The tensile stress in the concrete is also considered and is assumed to be elastic. The reduction factors for the tensile strength of the concrete at elevated temperatures supplied by EC 2 are adopted in the simulations.

The proposed multi-iteration method is used in this chapter for the parametric studies. The fire experiment model used in Chapter 4.5.2 for the validation of the numerical method has been simulated again here with the two material models. The results are compared to see the difference in fire behaviour of RC members with implicitly and explicitly considered transient creep strain models.

5.2.1 General introduction of the simulation process

The proposed multi-iteration method (Lu, L.M. et al. 2015) is based on the material properties of concrete and reinforcing steel under elevated temperatures to analyse the structural performance of RC elements subject to bending. The numerical process is performed in three steps: 1) thermal calculation; 2) calculation of mechanical properties of the cross section and 3) structural analysis. During this process, the RC element is divided into a number of small segments along its length L (Figure 5.01). The mid-section of each segment presents the behaviour of the whole segment.

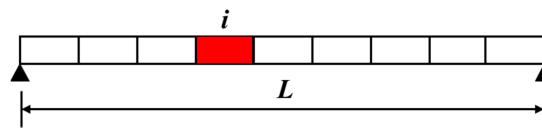


Figure 5.01 RC element and layout of segments

Firstly, the thermal field of the cross-sections is analysed at each time step and then material properties are adjusted according to the obtained temperatures. The temperature field at each time step within the element is calculated by a finite element method. As the heating conditions along the element are assumed identical, the temperature field of the element can be simplified into a 2D problem. Steel bars are neglected, as they do not significantly influence the temperature distribution in the cross-section. Generally, beams are assumed to be heated from three sides and slabs only from the bottom (Riva, P. 2004).

Secondly, the stiffness of each segment is generated by sectional stress strain analysis using the changing properties of concrete and steel bars. From a given temperature field according to the plane section assumption suggested in literature (Kudor, V.K.R. 2011; 2008; 2007), an equilibrium state for a cross-section in a flexural member can be calculated at each time step. After a multi-iteration calculation process, a moment-curvature relationship (M-k) can be generated by sectional analysis, and then the ultimate bearing capacity can be generated during this process.

Thirdly, the global stiffness matrix of the RC element will be assembled based on the results of the sectional analysis. A series of average bending stiffness of each segment, based on the results of the section analyses, is calculated and introduced into the function for the calculation of deflections.

5.2.2 Differences between the fire behaviour of members with transient creep strain considered implicitly and explicitly

In this section, the fire behaviour of the tested slabs executed with simple supports (Minne et al. 1979) is simulated with an explicit transient creep strain model. The simulated results are compared with the results obtained in the experiments and the ones simulated with the implicit material model. The test set-up and the material information can be found in Chapter 4.

The three slabs are of the same size $1900 \times 150 \times 4900$ (mm) and all are simply supported

under the heating of the ISO 834 standard fire curve. They differ by the amount of reinforcing steel (G1 had 15Ø10 steel bars, G2 had 17Ø10 steel bars and G3 had 18Ø10 in tensile zone) and also the concrete cover on the steel bars (15 mm for G1, 25 mm for G2 and 35mm for G3). The mid-span deflection curves for G1, G2 and G3, computed with the implicit and explicit transient creep strain models are compared, in Figure 5.02 for G1, Figure 5.03 for G2, and Figure 5.04 for G5.

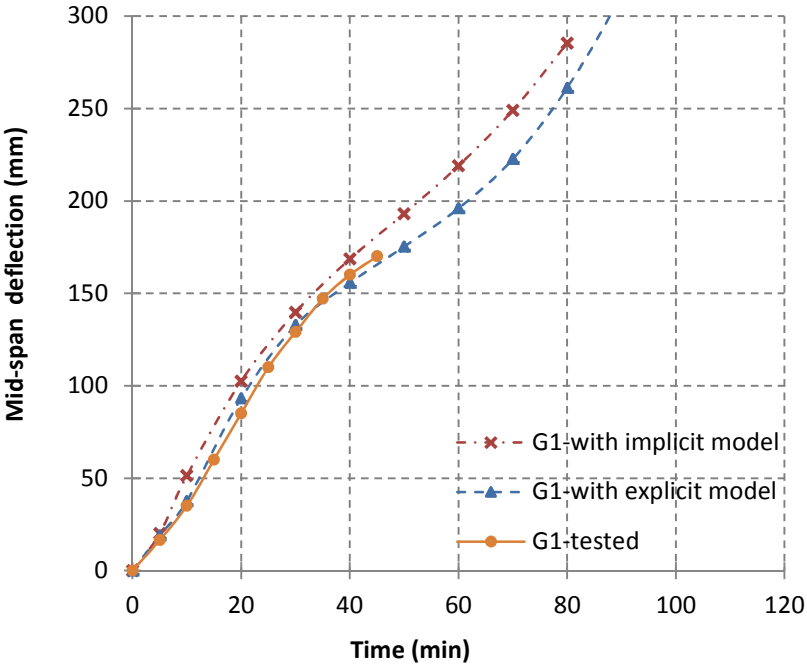


Figure 5.02 Mid-span deflections of G1 with transient strain considered implicitly and explicitly

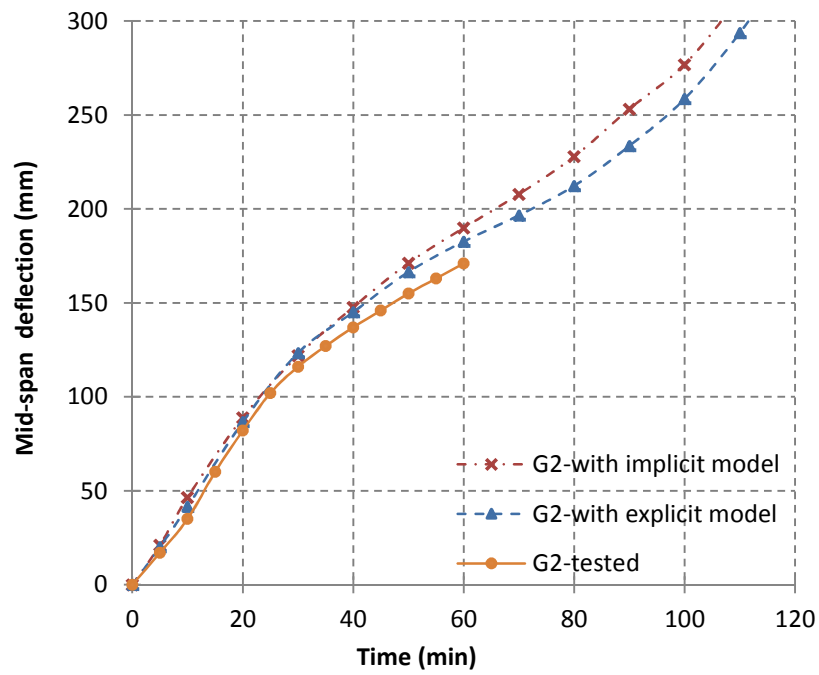


Figure 5.03 Mid-span deflections of G2 with transient strain considered implicitly and explicitly

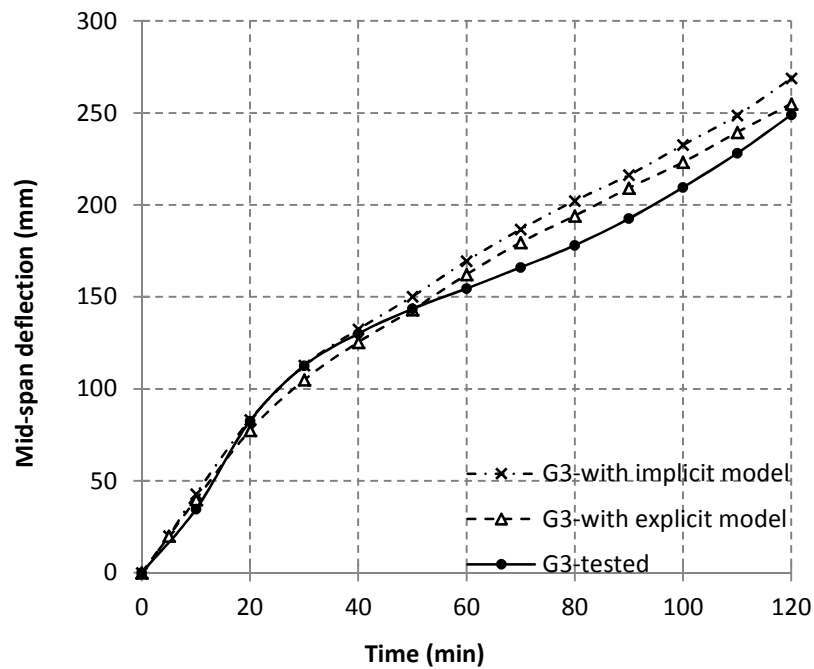


Figure 5.04 Mid-span deflections of G3 with transient strain considered implicitly and explicitly

From these three figures, the following conclusions can be drawn:

(1) The same trend can be observed when comparing the three slabs. The deflections simulated with the explicit transient creep strain model are a little bit smaller than those obtained with the implicit model. For RC elements subjected to bending, the compression area along the cross-section is decreasing due to the increasing of curvature while exposed to fire, but the transient creep strain is irrecoverable during the loading and reloading process. This actually reduced the mid-span deflections during heating. Therefore, the calculation results with the explicit model are closer to the test data. In this case, it is 5.6% closer after 2hrs of heating. This leads to the conclusion that the simulations with transient creep strain considered explicitly, are slightly lower than those obtained with the EC 2 model, and the deflections of RC elements will be overestimated with the material model in EC 2 although the differences are quite small.

(2) The difference between the mid-span deflections obtained with the implicit and explicit transient creep strain is comparatively bigger in the curves for slab G1 and smaller in G3. Based on the characteristics of the three slabs, this could be caused by the different number of steel bars and the difference in thickness of the concrete covers.

5.2.3 Differences between the fire behaviour of restrained members with transient creep strain considered implicitly and explicitly

Since continuous beams will experience negative bending moments at the ends, where the compressive area at the bottom is subject to significant heating, the transient creep strain is expected to have a larger impact on the members. In order to see whether restrained members will experience larger differences or not, slab model G3 with restraints is added to the comparison. Three cases are considered: (1) the simply supported slab; (2) the same slab with both the rotational restraint ratio and the axial restraint ratio equal to 0.5 and (3) rotationally fixed. Figure 5.05 shows the deflection curves for the three variants of slab G3.

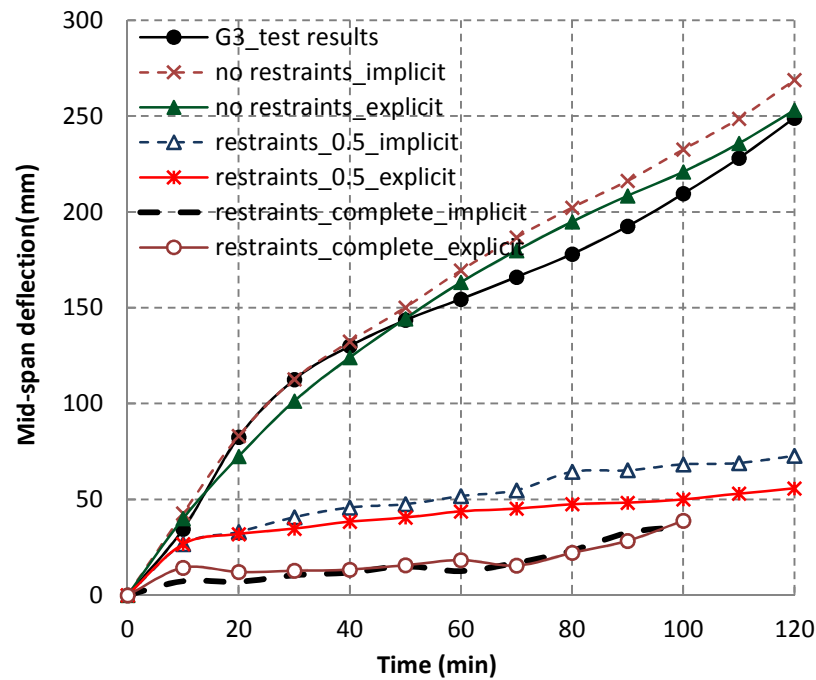


Figure 5.05 Mid-span deflections of rotationally restrained slab G3 with transient strain considered implicitly and explicitly

From the graphs, we can see that:

- (1) The simulated slabs without restraints are quite close to the tested curve, which was already mentioned in section 5.2.2. In the restrained cases, the deflections calculated with the explicit concrete model are smaller than the ones obtained with the implicit model.
- (2) The difference between the explicit model and the implicit model for the rotationally restrained members is not significantly larger than that of the simply supported member. This may be so because the rotational restraints reduced the mid-span deflection, which also make the difference between the two models smaller. The members with complete rotational restraints show little difference even up to failure of the member when the ultimate moment at the supports is reached.
- (3) The rotational restraints do not increase the difference between the members simulated with implicit and explicit transient creep strain, and even reduced the difference due to the reduced mid-span deflections. Therefore, the parametric study for the influencing factors of the transient creep strain models is carried out with simply supported RC members submitted to fire.

5.3 Influence of heating curves on the fire behaviour of RC beams simulated with the two material models

In this section, a series of beams having the same size and reinforcement ratios but submitted to fires according to different heating curves, which are the standard ISO-834 curve, and parametric curves introduced in EC 2, are simulated and the results are analysed.

5.3.1 Heating curves

In order to consider the difference of the two material models during the cooling process, a fire curve including a cooling stage as suggested in Eurocode 1: Actions on Structures Part 1-2, will be used (introduced in Chapter 4). The fire curves with $\Gamma = 1$ are adopted in this chapter. Three different fire curves are considered: (1) the ISO-834 fire curve, which is heating for 2 hrs. without cooling part; (2) a parametric fire curve with 30 min heating and a subsequent cooling part and (3) a parametric fire curve with 60 min heating and a subsequent cooling part. The fire curves are shown by Figure 5.06, where t_{\max}^* is the maximum heating time and Γ reflects the compartment boundary conditions for the fire. The beams are supposed to be heated from the bottom and two lateral sides. By considering both the fire heating time and time effectiveness of the simulations, three curves are used for the parametric study. They are the parametric curve with the heating part up to 30 min ($t_{\max}^* = 30$), the parametric curve with the heating part up to 60 min ($t_{\max}^* = 60$) and the ISO-834 standard heating curve ($t_{\max}^* = 120$). The comparisons are made up to a fire exposure time of 2 hrs.

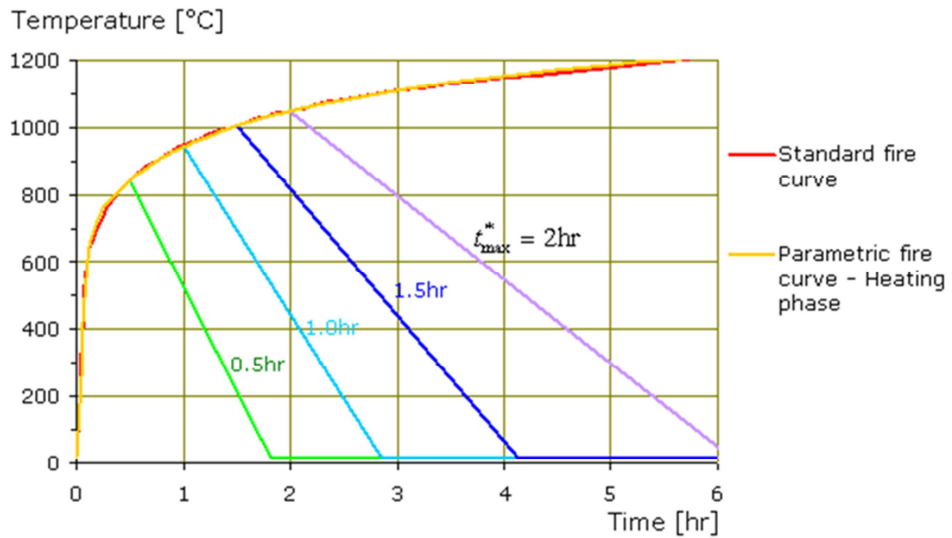
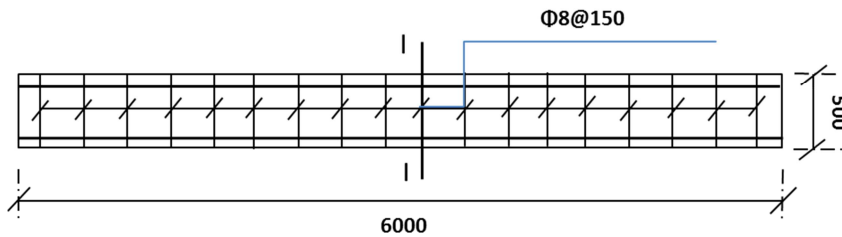


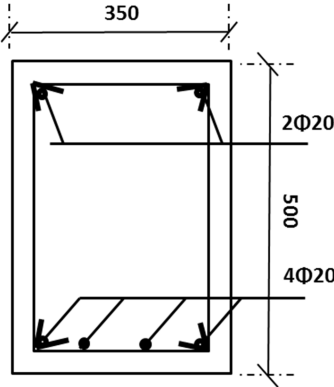
Figure 5.06 Parametric fire curves with $\Gamma=1$

5.3.2 Characteristics of the simulated beams

Since the fire curves are the main factor to study, the other parameters are the same, which means that only one beam model is simulated. The cross-section of the beam measures $b \times h = 350 \times 500$ (mm), and the effective span is $L = 6000$ (mm) as shown by Figure 5.07 (a) and (b), with 2 ϕ 20 mm steel bars in the compression zone and 4 ϕ 20 mm in the tensile zone.



(a) Longitudinal view



(b) Cross-section I-I

Figure 5.07 Beam geometry for the parametric study of fire curves (dimensions in mm)

The concrete adopted in the model is a normal strength siliceous aggregate concrete and the steel bars are made of cold worked steel. The detailed material information for the concrete and the steel bars before heating is listed in Table 5.01.

Table 5.01 Material properties of the concrete and the steel bars before heating

$f_c(N/mm^2)$	$f_t(N/mm^2)$	$E_c(N/mm^2)$	$f_y(N/mm^2)$	$f_u(N/mm^2)$	$E_s(N/mm^2)$
30	2.9	2.0×10^4	500	650	2.1×10^5

There are four steel bars in tension and two in compression, which can be designated as bar 1, bar 2, and bar 3, as shown in Figure 5.08. The distance between the axis of the reinforcing bars to the bottom surface is designated as d_1 , for the bottom bars. The distance between the axis of the reinforcing bars to the top surface is designated as d_2 , for the top bars. Both d_1 and d_2 are 35 mm. The distance between the axis of the reinforcing bars to the lateral surface of the beam is 45 mm.

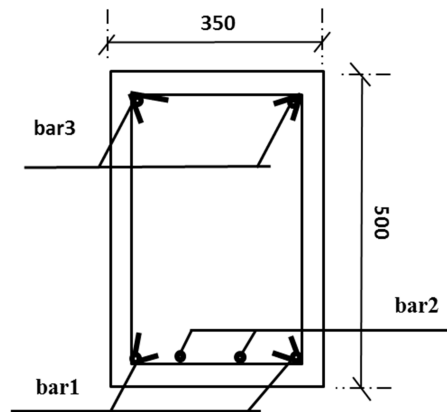


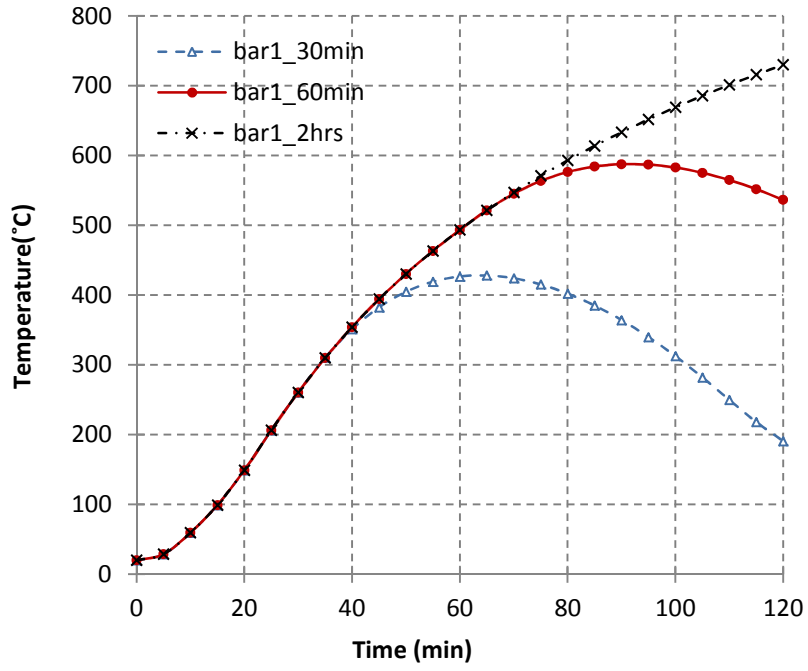
Figure 5.08 Arrangement of the steel bars in the cross-section

The load applied on the RC beams contains two parts: the gravity load and the live load, and both are considered uniformly distributed loads. In order to get a clear idea of the loading condition, the total applied load is supposed to be 30% of the bearing capacity of the RC beam at ambient temperature. According to the basic geometric and material information given here, the ultimate moment at ambient temperature of the studied beam is 2.73×10^2 $kN.m$, so the equivalent distributed load $q = 18.22$ kN/m is applied to the beam.

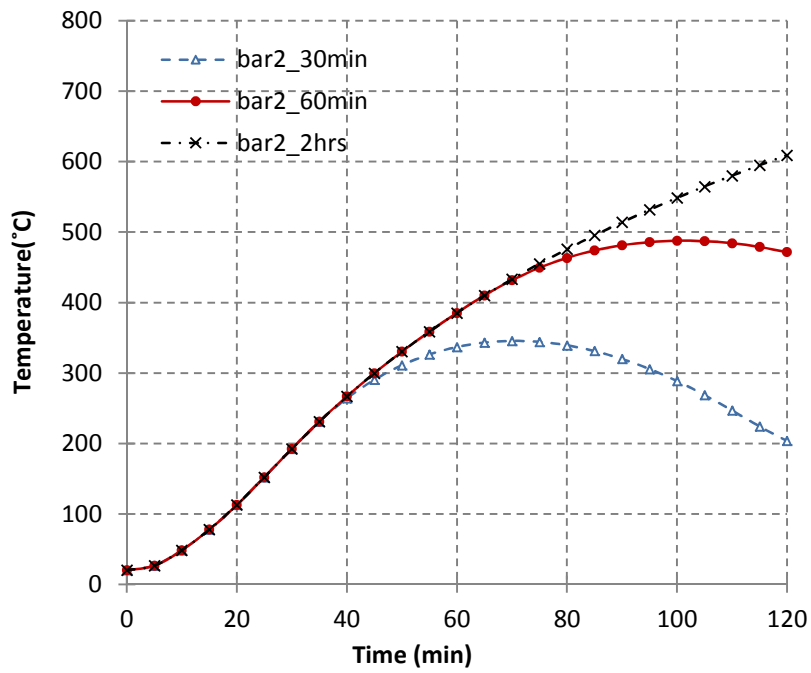
5.3.3 Simulation results and conclusions

Since the temperature field for this series of beam models is the main difference, the temperatures in the reinforcing bars are compared first.

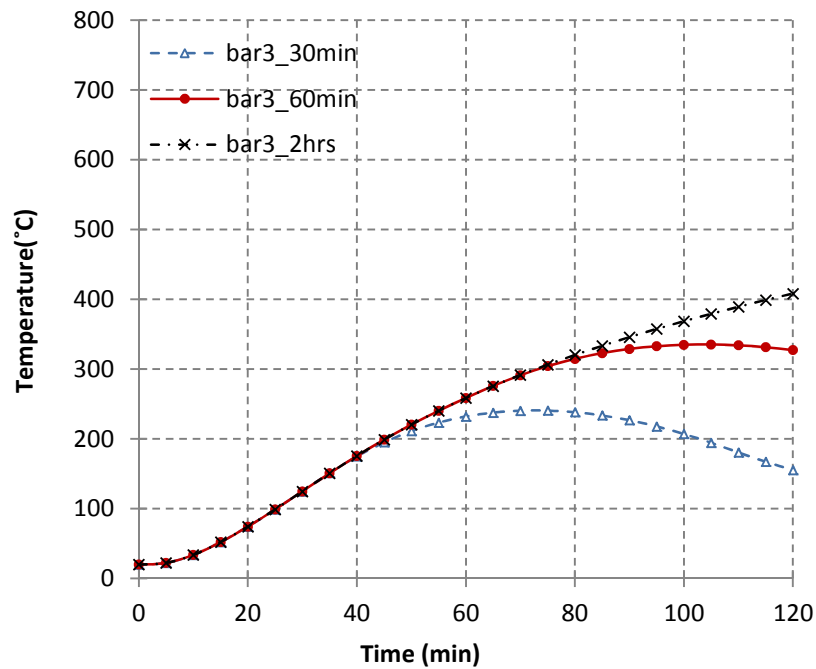
The temperatures of bar 1, bar 2, and bar 3 under the three different fire curves are compared in Figures 5.09 (a), 5.09 (b) and 5.09 (c). The time legend in the graph relates to the maximum heating time of the parametric fire curves.



(a) Temperatures for bar 1



(b) Temperatures for bar 2



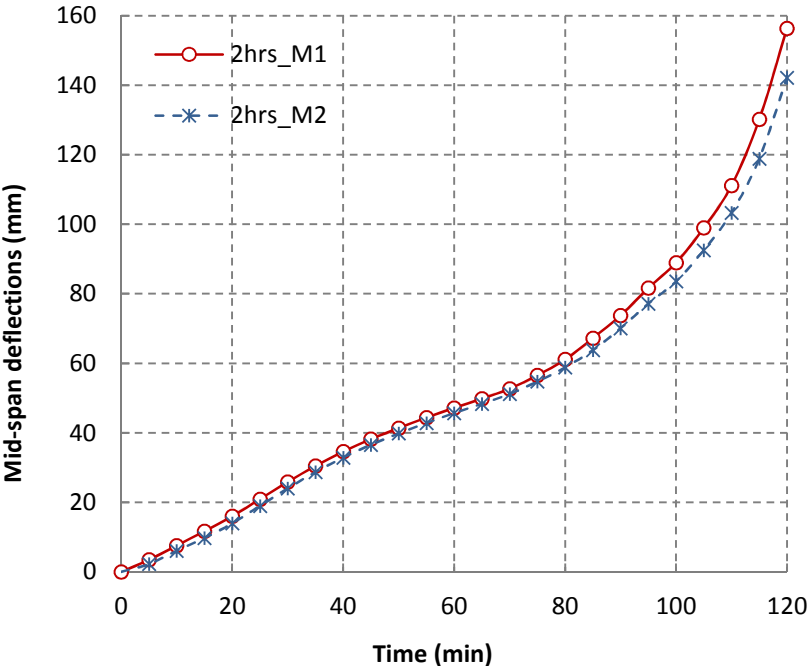
(c) Temperatures for bar 3

Figure 5.09 Temperatures of steel bars under three heating curves

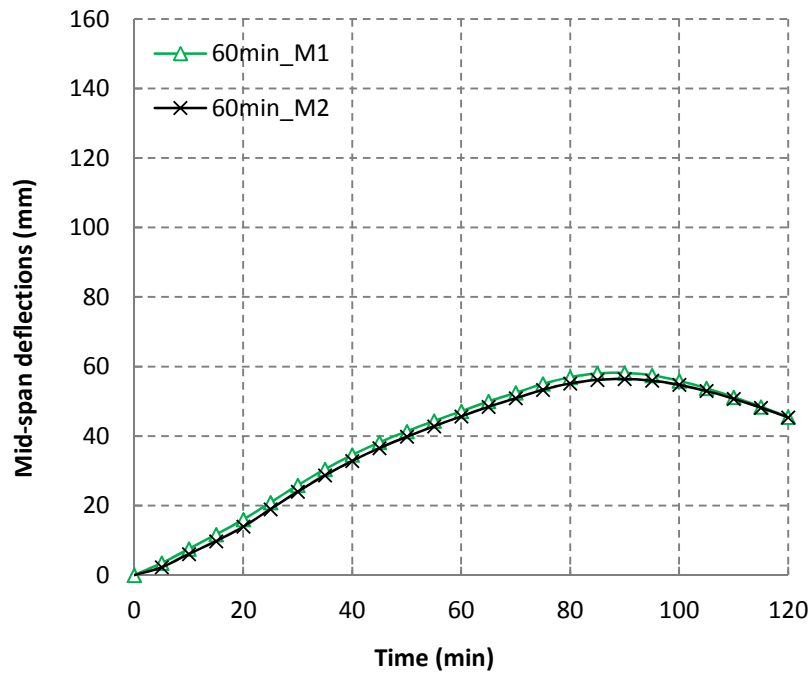
The temperature of each bar under the three fire curves is the same for the first 30 min as the heating curve is the same. So do the first 60 min of the $t_{max}^* = 60$ min fire curve with that of 2hrs standard heating curve. The temperature due to the parametric curves continues to increase for about another 30 min and then starts to decrease. This is because the concrete outside the steel bars still conducts heat from the outer layer to the cooler inner parts as long as the outer layers are still hotter. This delay of the temperature decrease is influenced by the thickness of the concrete cover: the thicker, the longer the delay time. Hence, for bar 3, the gaps between the three fire curves tend to appear later and are comparatively smaller than those of bar 1 and bar 2. The temperature of the corner steel bars is higher than that of the inner bars, which is logical. The temperature gap is increasing with the heating time and for the beam studied here, it is more than 100 °C after 2 hrs. of heating. The temperature of bar 3, which is in compression, is nearly 300 °C lower than bar 1 after 2hrs. of heating.

With the results of the temperature field, the structural behaviour of the beams under the three fire conditions are simulated and compared. Figure 5.10 shows the mid-span deflections of the beams under the three heating curves. The deflections are calculated respectively by two

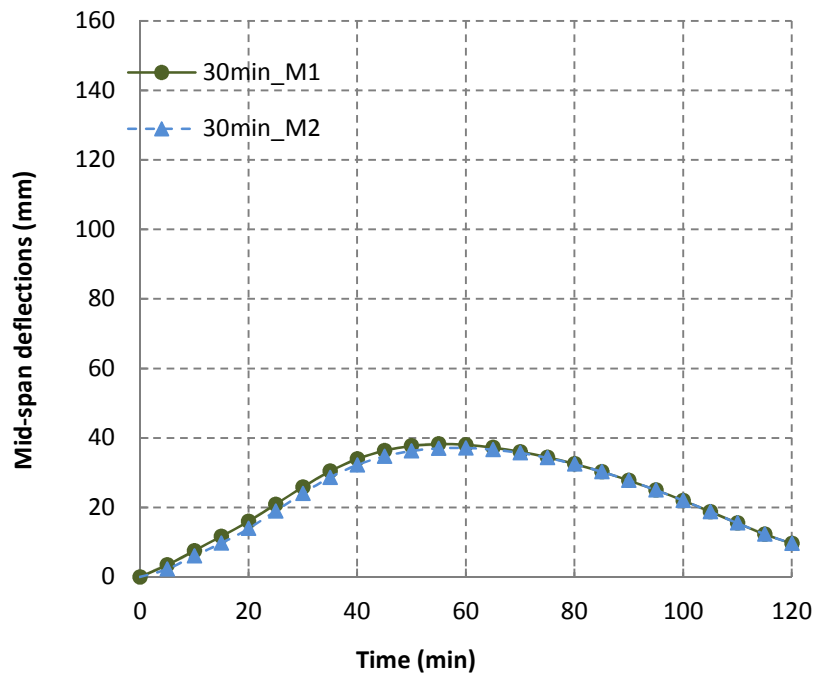
different transient creep strain models, the implicit transient creep strain model (M1), and the explicit material model (M2). In order to make a clear comparison of the differences of the deflections under the three fire curves, curves giving the difference in the mid-span deflections of the beams simulated with M1 and M2 are analysed and shown by Figure 5.11.



(a) Mid-span deflection of beam under ISO-834 standard curve



(b) Mid-span deflection of beam under $t_{\max}^* = 60$ min fire curve



(c) Mid-span deflection of beam under $t_{\max}^* = 30$ min fire curve

Figure 5.10 Mid-span deflections of beams under different heating curves

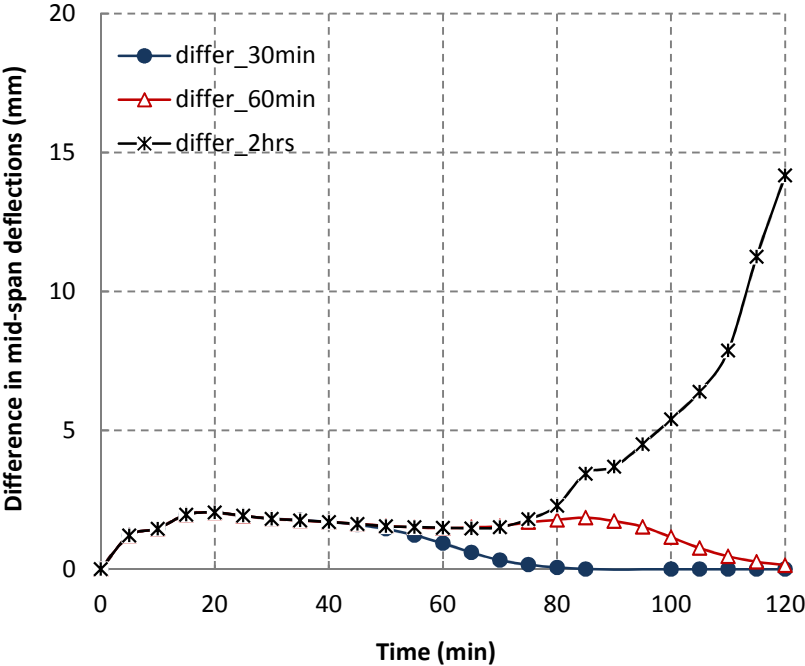


Figure 5.11 Difference in mid-span deflections of beams simulated with M1 and M2

From Figures 5.10 and 5.11 we can conclude the following:

- (1) Similar to the temperature trend, the mid-span deflections of the members increase with heating time and remain identical in the heating part. For $t_{max}^* = 30$ min fire curve, this holds for the first 30 min and for the $t_{max}^* = 60$ min fire curve, for the first 60 min. After this initial period and an additional increase during 30 min, the deflections start to recover. This trend is also observed in the differences of the mid-span deflections, which could be seen in Figure 5.11.
- (2) The differences in the mid-span deflections of beams simulated with M1 and M2 increase more in function of the heating time, because the redistribution of the inner stresses will change the transient creep strain of the concrete in the explicit model, while this does not happen in the implicit model. The mid-span deflections calculated under the explicit model are smaller than the ones calculated with the implicit model, and the ones related to the case exposed to fire for 2 hrs. has the biggest difference. After heating by standard fire curve for 2 hrs., the deflection calculated with the explicit material model will be nearly 20 mm smaller, which is 9.2% smaller than that of the implicit model for the beam studied.

(3) From the comparison of the difference in the mid-span deflection between beams simulated with M1 and M2, it can be seen that the differences become smaller and even disappear under the parametric fire curves. This is because that the deflections simulated with the implicit model (EC 2 model) recover faster than the explicit model as it recovers the transient creep strain during the cooling process. The less difference between the two models contributes to the conclusion that in case of the parametric fires with cooling parts considered, it makes less sense to consider the transient creep strain explicitly.

5.4 Influence of the reinforcement ratio on the fire behaviour

In this part, beams of the same cross-section size but with different reinforcement ratios are simulated and compared. The beams are under the ISO-834 standard fire curve and are supposed to be heated from the bottom and the two lateral sides. The reinforcing bars in the compression zone are the same while the tensile steel bars are taken respectively as 4 \varnothing 20, 4 \varnothing 25, 4 \varnothing 28 and 6 \varnothing 28, with geometric reinforcement ratios calculated as 0.72%, 1.12%, 1.41% and 2.11% respectively.

5.4.1 Characteristics of the simulated beams

For beams subjected to bending, the steel bars in tension are critical for the determination of their bearing capacity and deformation. The simulated beams in this section measure 350 \times 500 \times 6000 (mm), as shown by Figure 5.12(a) and 5.12(b), with 2 \varnothing 20 steel bars in the compression zone. The tensile reinforcing bars are taken respectively as 4 \varnothing 20 in the beam designated as 4R20, 4 \varnothing 25 in beam 4R25, 4 \varnothing 28 in beam 4R28 and 6 \varnothing 28 in beam 6R28.

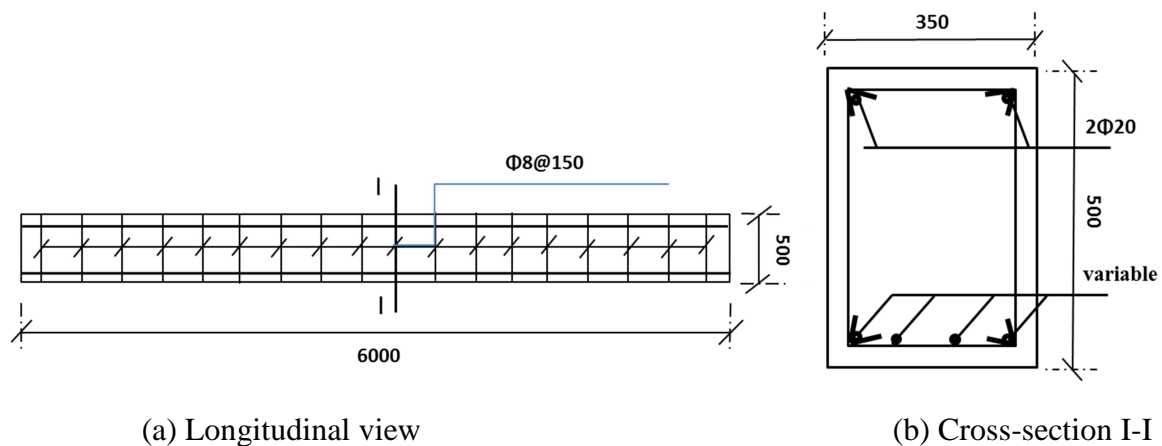


Figure 5.12 Beam geometry for the influence of reinforcement area (diameter in mm)

The concrete adopted in the model is a normal strength siliceous aggregate concrete and the steel bars are made from cold worked steel. The detailed material information for the concrete and the steel bars before heating are the same as in section 5.3 and listed in Table 5.01. The loads applied on the RC beam are considered uniformly distributed loads, which correspond to 30% of the bearing capacity of the RC beam at ambient temperature. For the beams studied here, the ultimate moments and the applied loads are listed in Table 5.02.

Table 5.02 Loads applied on the simulated beams with different reinforcing bars

Beam	tensile bars	$M_u(20^\circ C)$ ($kN.m$)	$30\%M_u(20^\circ C)$ $\dots(kN.m)$	q (kN/m)
4R20	4Ø20	2.73×10^2	0.82×10^2	18.22
4R25	4Ø25	3.89×10^2	1.17×10^2	26.00
4R28	4Ø28	5.18×10^2	1.56×10^2	34.56
6R28	6Ø28	7.33×10^2	2.20×10^2	48.86

5.4.2 Simulation results and conclusions

Under the assumption that the steel bars are not considered in the temperature field simulation, the temperature field of the cross-sections of all the beam models considered in this section are the same and equal to the one under the ISO 834 fire curve in section 5.3. The temperatures of the corresponding steel bars bar 1, bar 2 and bar 3 are also the same except for beam 6R28, since it has 2 more tensile steel bars and the position of these tensile steel bars in beam 6R28 is different from the other ones. With the temperature fields, sectional analyses are carried out and the structural behaviour of the four cases is simulated and compared. Figure 5.13 shows the difference in mid-span deflection of the beams calculated with two different transient creep strain models, being the implicit transient creep strain model (M1), and the explicit material model (M2). The differences are calculated as the mid-span deflections of beams simulated with M1 minus that simulated with M2.

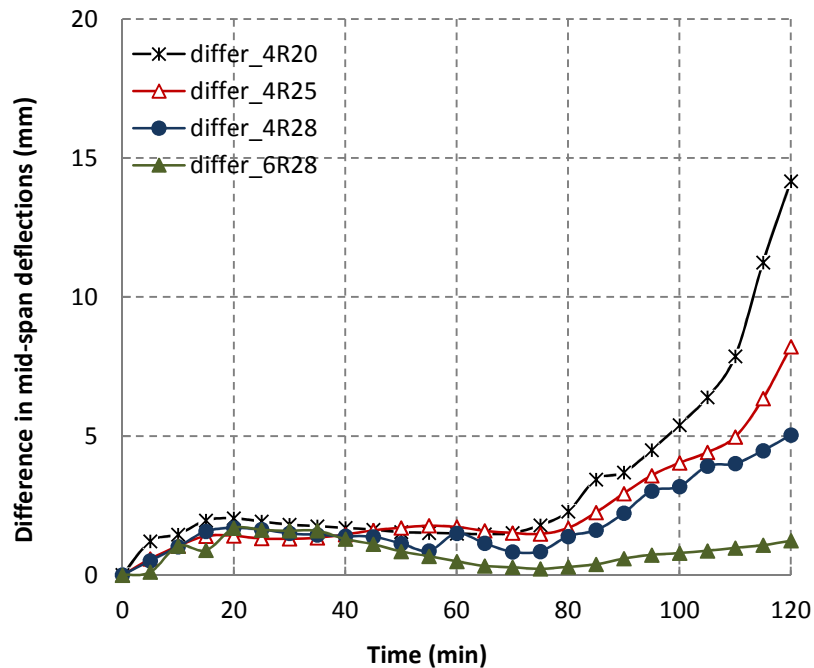


Figure 5.13 Differences in mid-span deflections of beams simulated with M1 and M2

(For beams with different reinforcement ratios)

From Figure 5.13, the following conclusion can be drawn:

- (1) The differences in mid-span deflection between beams simulated with the two described material models are not obvious. During the early stage of heating, since the stress redistribution along the cross-section is not important, the difference of the two results shows a plateau for a certain period.
- (2) Beams with more reinforcement yield a smaller difference in deflections between the simulation results based on M1 and M2. The beam with 4Ø20 reinforcing bars shows the largest difference, the deflection calculated with M2 is 9.2% smaller than that with M1. The one with 6Ø28 has the smallest difference, with the deflection calculated with M2 being 1.1% smaller than that with M1. Hence, it could be concluded that the increase of reinforcement ratio decreases the influence of transient creep strain models on the fire behaviour of RC beams.

5.5 Influence of the size of the cross-section on the fire behaviour

The beams discussed in this section are intended to compare the influence of the size effect of

the cross-section. Beams of a same width but different heights and beams with a same height but different widths are simulated and compared. Since the influence of the reinforcement ratios was already analysed, the same amount of reinforcing steel bars is placed in all the beams of two out of the three series considered, with $2\text{Ø}20$ steel bars in the compression zone and $4\text{Ø}20$ in the tensile zone. The beams are submitted to the ISO-834 standard fire and supposed to be heated from the bottom and the two lateral sides.

5.5.1 Characteristics of the simulated beams

The beam models considered here are of the same effective span (6000 mm), with various heights and widths of the rectangular cross-sections, as shown by Figure 5.14(a). There are three series of beam models for the comparison of height and width. (1) One series of beams have the same width of 200 mm . The heights of them are ranging from 350 mm to 500 mm . They are denoted by their size: B200x350, B200x400, B200x450, B200x500. (2) One series of beams are of the same height of 500 mm . The width of them are ranging from 200 mm to 350 mm . They are denoted by their size: B200x500, B250x500, B300x500, B350x500. (3) One series of beams have the same reinforcement ratio. They are denoted by their size: B3_200x350, B3_200x500, and B3_350x500. All the beams of series (1) and series (2) are reinforced by the same amount of steel bars, with $2\text{Ø}20$ steel bars in compression and $4\text{Ø}20$ in tension, as shown by Figure 5.14 (b). The reinforcement of B3_200x500 is the same as B200x500, which is $4\text{Ø}20$ in tension. The geometric reinforcement ratio in series (3) is $\rho = 0.0135$, and the reinforcing bars in tension are $4\text{Ø}16.4$ in B3_200x350 and $4\text{Ø}26.4$ in B3_350x500. These bar diameters are purely theoretical in order to obtain exactly the same reinforcement ratio for the beams.

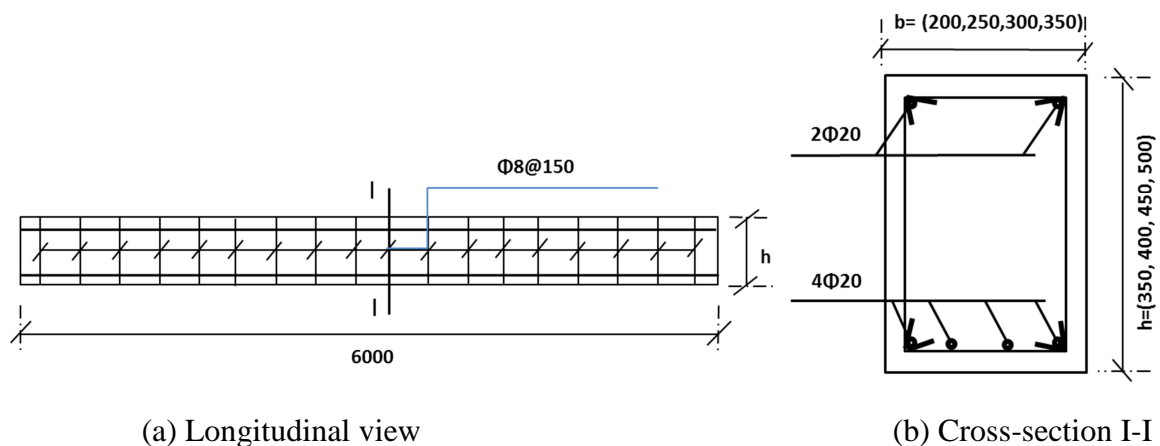


Figure 5.14 Beam geometry for size effect simulation (dimensions in mm)

The concrete adopted in the model is again a normal strength siliceous aggregate concrete and the steel bars are made from cold worked steel. The detailed material information for the concrete and the steel bars before heating are the same as in section 5.3 and are listed in Table 5.01. The loads applied on the RC beam are considered uniformly distributed loads, which correspond to 30% of the bearing capacity of the RC beam at ambient temperature.

For the beams of different sizes in series (1) and series (2), the ultimate moments and the applied loads are listed in Table 5.03.

Table 5.03 Loads applied on the simulated beams of different size

Beam	$b \times h$ (mm)	$M_u(20^\circ C)$ (kN.m)	30% $M_u(20^\circ C)$ (kN.m)	q (kN/m)
B200x350	200x350	176	52.7	11.70
B200x400	200x400	207	62.1	13.80
B200x450	200x450	238	71.5	15.89
B200x500	200x500	270	80.9	17.99
B250x500	250x500	271	81.4	18.09
B300x500	300x500	272	81.7	18.16
B350x500	350x500	273	82.0	18.22

For the beams with the same reinforcement ratio in series (3), the ultimate moments and the applied loads are listed in Table 5.04.

Table 5.04 Loads applied on the simulated beams with same reinforcement ratio

Beam	$b \times h$ (mm)	$M_u(20^\circ C)$ (kN.m)	30% $M_u(20^\circ C)$ (kN.m)	q (kN/m)
B3_200x350	200x350	124	37.2	8.28
B3_200x500	200x500	270	80.9	17.99

B3_350x500	350x500	466	140	31.06
------------	---------	-----	-----	-------

5.5.2 Simulation results for beams with the same width

As in section 5.3 (Figure 5.08), we divide the steel bars into three groups: bar 1, bar 2 and bar 3. For the beams with the same width (B200x350, B200x400, B200x450, B200x500), the temperatures in all bar 1 of the four beams are the same, so that for the four bar 2. The temperatures of bar 3 in the four beams are nearly the same because of the beams are heated also by lateral sides, and the temperatures of the steel bars in compression are determined by the distance of the steel bars to the fire-exposed lateral surface. In the series of beams with the same width, these distances are the same. Therefore, the temperatures of bar 1, bar 2 and bar 3 are the same for the four conditions, as shown by Figure 5.15.

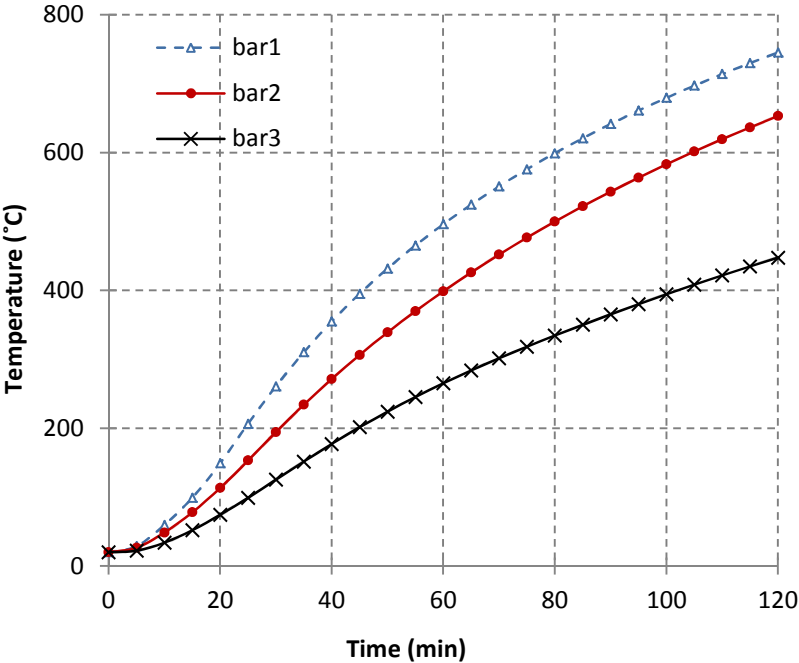


Figure 5.15 Temperatures of steel bars with the same width (b=200 mm)

With the results of the temperature field, the structural behaviour of the four cases are simulated and compared. Figure 5.16 shows the differences in mid-span deflections of the beams simulated with M1 and M2, the different curves being for beams of different width.

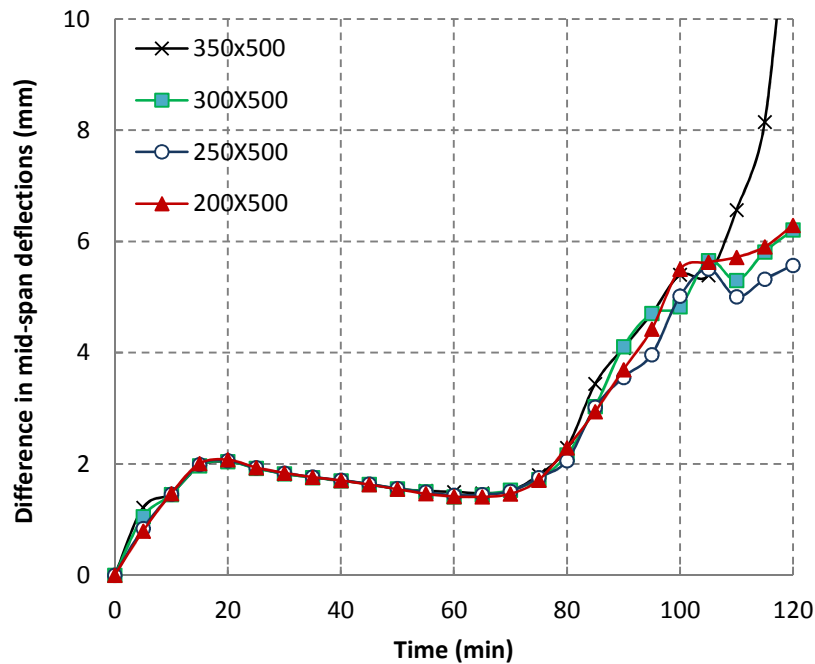


Figure 5.16 Differences in mid-span deflections of beams simulated with M1 and M2
(For beams with different width)

From the comparison of the differences in mid-span deflections of beams with the two material models, the following comments can be made:

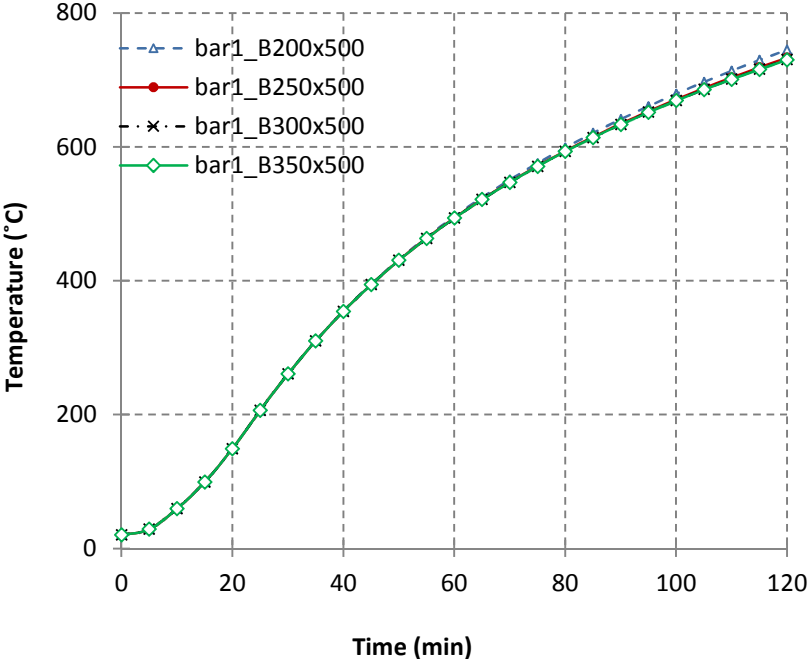
(1) All the curves show the same trend with heating time: first increasing with temperature, and then followed by a slightly decreasing plateau, and after that, the curves increase significantly with heating time. Hence, the explicit consideration of transient creep strain makes the simulation results more precise, and the difference can reach 5% to 9.2% after 2 hrs. of heating.

(2) As shown by Table 5.03, with the same amount of reinforcement ratio and same beam height, the ultimate moment of this series of beams are quite close to each other, and the load applied to the beams are also more or less the same. Therefore, the beams yield the same curves as shown by Figure 5.16. No significant differences were observed. It can be concluded that the difference of fire performance simulated with implicit and explicit transient creep models is not sensitive to the beam width.

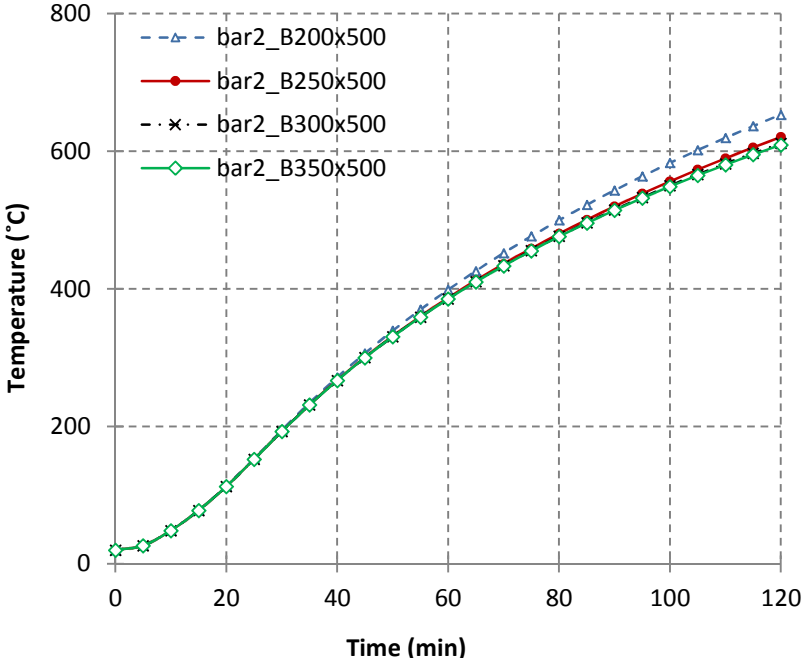
5.5.3 Simulation results for beams with the same height

For the steel bars in the beams with the same height (B200x500, B250x500, B300x500,

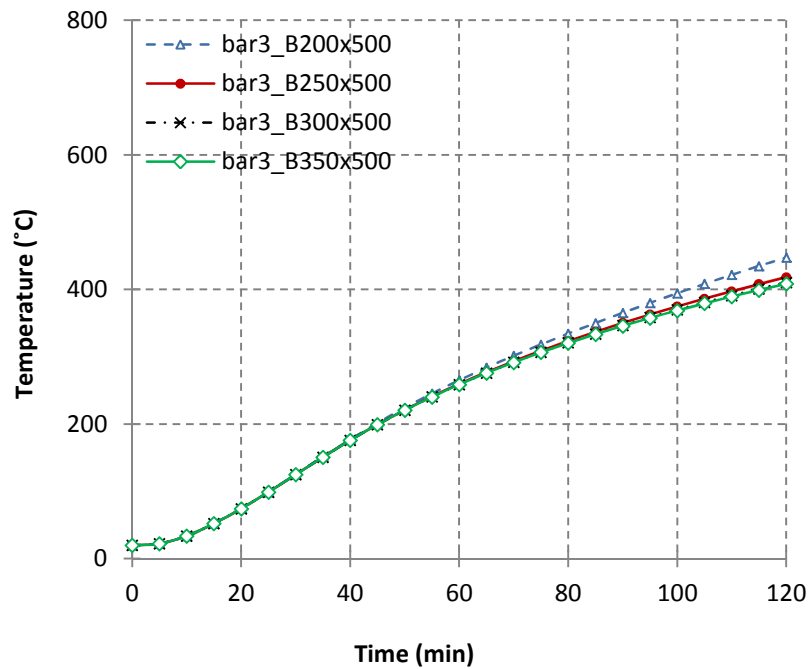
B350x500), the temperature curves as a function of the heating time are shown by Figures 5.17 (a), 5.17 (b) and 5.17 (c).



(a) Temperatures in bar 1



(b) Temperatures in bar 2



(c) Temperatures in bar 3

Figure 5.17 Temperatures of steel bars for beams with the same height ($h=500$ mm)

From Figure 5.17 it can be seen that:

- (1) The temperatures for bar 1, bar 2 and bar 3 are all different. However, because of the same distance of bar 1 both to the bottom fire-exposed surface and to the lateral fire-exposed surface, the temperatures in bar1 are nearly the same and are not much influenced by the size of the cross-section.
- (2) The temperatures for bar 2 are nearly the same during the first hour of heating, where after the differences are increasing with heating time. So do the temperatures for bar 3. The temperature differences between bar 2 and bar 3 of the four beams are nearly 50°C after 2 hrs. of heating.
- (3) The temperatures of bar 2 and bar 3 in the wider beams are comparatively lower and the highest temperatures of bar 2 and bar 3 both occur in beam B200x500.

Figure 5.18 shows the differences in mid-span deflections between beams simulated with M1 and M2, for beams with different height.

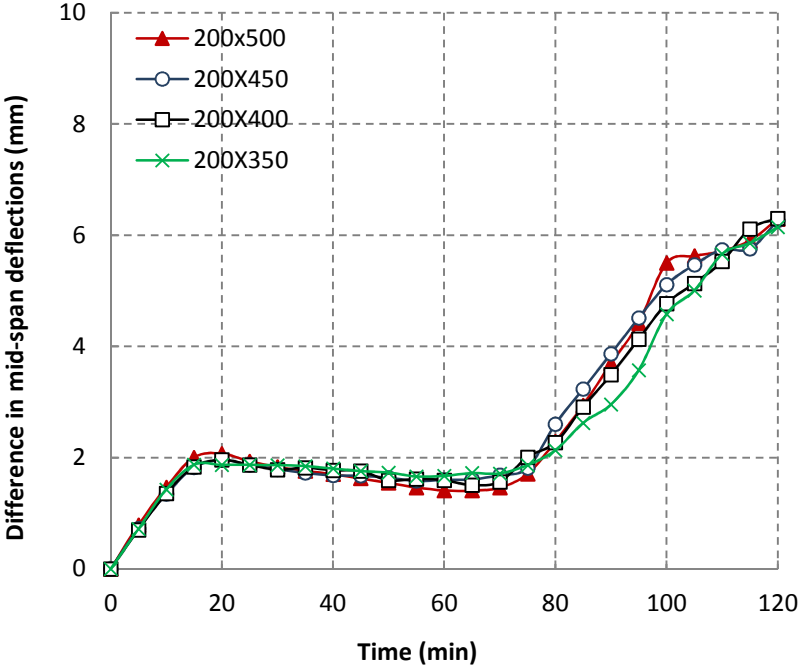


Figure 5.18 Difference in mid-span deflections of beams simulated with M1 and M2
(For beams with different height)

From Figure 5.18 it can be seen that the curves of beams with different height show little difference, but the difference increases with heating time. After 1 hour of heating, the curves of beams with larger height tend to be bigger than the ones with smaller height.

5.5.4 Simulation results for beams with the same reinforcement ratio

Since the reinforcement is assumed not to influence the temperature distribution of the cross-section, the temperature curves for the steel bars in B3_200x350 are the same as the ones in B200x350, and so those for B3_200x500 and B3_350x500 are the same as B200x500 and B350x500. The difference between mid-span deflections of the beams simulated based on M1 and M2 are compared in Figure 5.19.

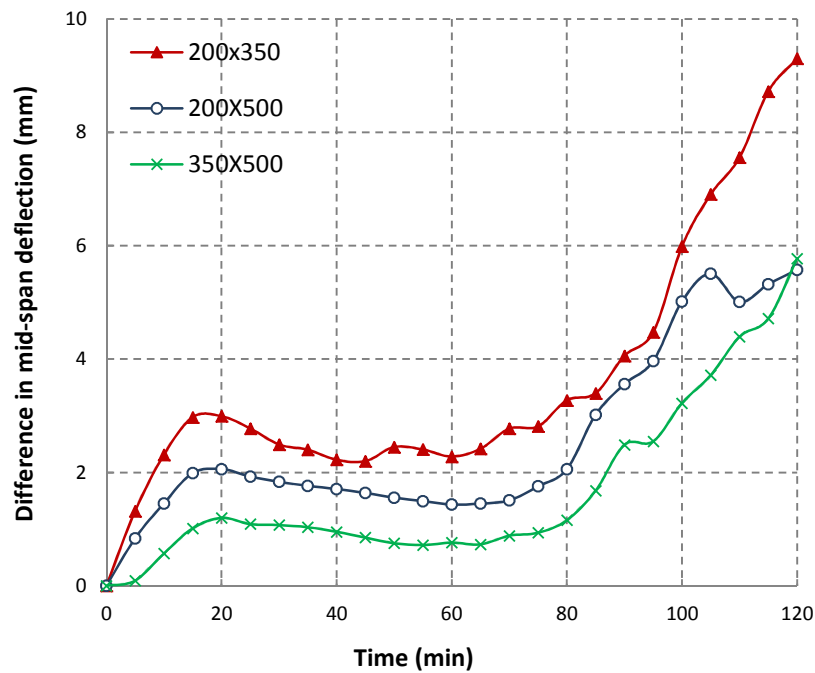


Figure 5.19 Differences in mid-span deflections of beams simulated with M1 and M2
(For beams of different size)

In contrast to the results shown by Figures 5.16 and 5.18, the obtained deflection differences show a clear scatter depending on the geometric reinforcement ratio. However, the differences shown by Figure 5.19 remain small.

5.6 Conclusions

The effect of transient creep on the behaviour of RC elements subjected to bending is investigated using two different material models: one with the transient creep strain considered implicitly in the total strain and one with the transient creep strain considered explicitly. The multi-iteration method is adopted in this chapter and the fire tests of simply supported slabs are simulated to see the difference of fire simulation results with implicit and explicit transient creep strain models. Parameters that may influence the simulation results with these two material models are discussed. The following conclusions can be made:

(1) The parametric study of the fire performance of RC members with an implicit and an explicit transient creep strain model shows that: the calculations become slightly more accurate when transient creep strain is considered explicitly. The deflections of RC elements

during fire submitted to bending like beams and one-way slabs will be slightly overestimated with the material model in EC 2. In the simulated cases in this thesis, this overestimation is in the range of 5% to 9.2% after 2hrs of heating, from which it can be concluded that the influence of different transient creep strain models can be neglected in most of the cases for beams and slabs subjected to bending.

(2) The differences in deflections with implicit and explicit transient creep models increase with heating time, the one under 2hrs heating by the standard fire is the biggest at the end. The difference becomes smaller and even disappears during the cooling process of the fire under the parametric fire curves. This means that the deflections simulated with implicit material models recover faster when the temperature decreases due to the implicit recover of the transient creep strain.

(3) Beams with more reinforcement show smaller differences in deflections calculated with the two material models, from which it can be concluded that due to the increase of the reinforcement ratio, the influence of transient creep strain on the fire behaviour of RC beams decreases.

(4) The comparison of the difference in mid-span deflections calculated based on the two material models shows that the fire performance simulated with implicit and explicit transient creep models is not be influenced by the width of beams. The curves for beams of different height show little difference, but the difference increases with heating time.

(5) The comparisons in the parametric studies mainly focussed on simply supported RC members subjected to bending. The restraint effects including the axial and rotational restraints are not considered in detail. Further research is suggested to study the influence of transient creep strain for restrained members.

Influence of restraints on fire behaviour of RC elements

Although the effects of high temperature on the response of beams and slabs that are subjected to bending have been widely studied in recent years, a literature review indicates that the fire behaviour of a single member has been the main focus of most of the research projects. Especially for experimental research, due to the limitations of fire test set-up, few fire tests include restrained beams and slabs. However, separate members in an actual reinforced concrete (RC) structure are always experiencing various types of axial and rotational restraints from the adjacent members. These restraints may have a significant influence on the flexural behaviour of RC members at elevated temperatures.

In order to have a clear idea of the fire performance of RC beams in real conditions, i.e. considering various restraints from surrounding members, and to get a deep insight on the influence of these restraints on the fire behaviour of RC members, beams with different restraint conditions are simulated and analysed in this chapter. Since the fire simulation of restrained members is always very complex, finite element packages have to be applied. However, finite element methods are always time consuming, and the process is not clear since all the computing is performed by the computer “in the back”. Moreover, some of the programs are not so user friendly to define material models freely, so the simplified multi-iteration analysis method proposed in Chapter 4 is adopted in this chapter too. Fire performance of RC beams with various axial and rotational restraints are simulated and compared with each other. Based on the analysis and comparison of the simulation results, a parametric study on the effect of restraints on the fire performance of RC members is carried out. Finally, some suggestions on how to consider the influence of restraint conditions in fire conditions are proposed.

6.1 General Introduction

Beams in a frame experience both axial and rotational restraints from the connected beams and columns. Under elevated temperatures, the restraint conditions for beams can induce both

compressive forces and thermal bending moments by restrained thermal expansions and second-order moments induced by these high compressive forces. The axial restraints and the rotational restraints can have important influences on the fire behaviour of the RC members (Riva, P. 2002; 2004).

6.1.1 Influence of axial restraints

Axial restraints can have a significant influence on the fire performance of RC beams. When a heated member is restrained from thermal expansion by a more rigid surrounding structure, it results that compressive axial forces will develop in the beam. Figure 6.01 shows the effect of axial restraint on a simply supported RC beam in case of rigid supports as stated by Buchanan, A. (2001).

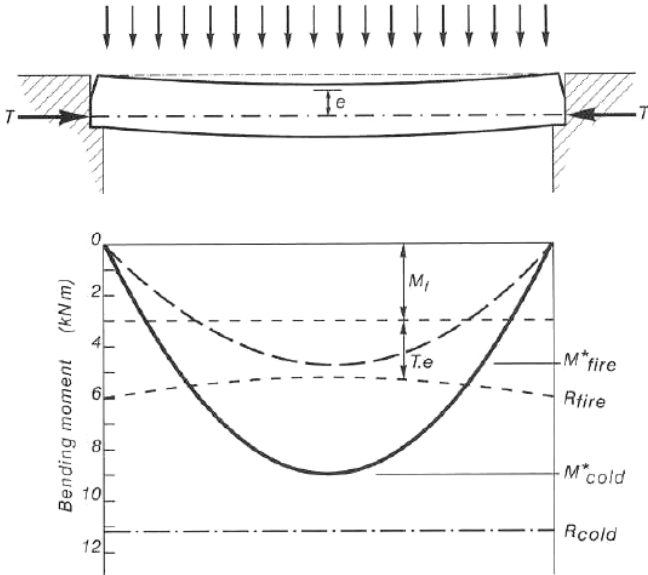


Figure 6.01 Effect of axial restraint force on bending moment diagram (Buc-01)

Due to the heating of the beam an axial force T develops, which can be considered as an external prestressing. It can be seen that the total resistance R_{fire} of the member can be calculated as:

$$R_{fire} = M_f + T \times e \tag{6.01}$$

where M_f is the ultimate moment under fire, T is the axial force developed during fire and e

is the eccentricity between the line of action of the thermal axial force and the centroid of the compression block near the top of the beam. It can be seen from Equation (6.01) that the positive effect of the thermal thrust is strongly dependent on the position of the axial force. The additional moment may become negative if large deflections occur or the axial force acts at the top of the beam. Consequently, the resulting moment will tend to deflect the beam downwards. Unless T is large enough to induce sufficient compressive stress to counteract the tensile stresses caused by $T \times e$ and the applied moment, the failure of the structure will occur earlier (Carlson, C.C. 1965; 1962).

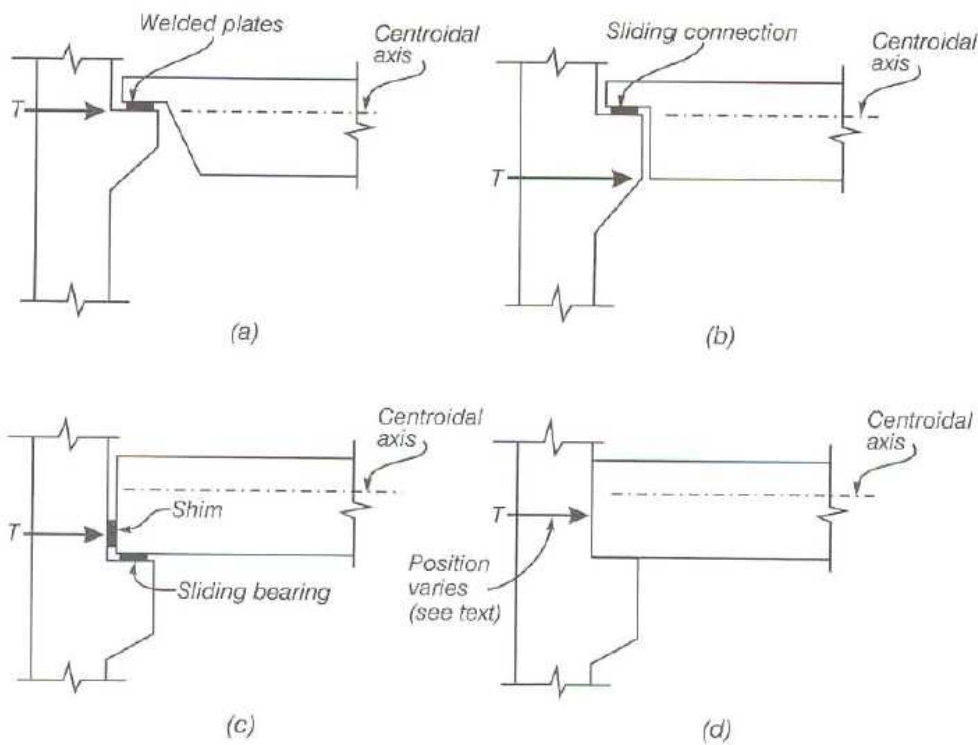


Figure 6.02 Location of axial thrust for several support conditions (Gus 1977)

The position of the axial thrust can only be located accurately for specific support conditions where the thrust line is well defined due to the method of construction. Figure 6.02 (a) to (c) show such determinate support conditions which mainly exist in precast concrete constructions. Figure 6.02 (d) represents a situation, such as cast-in-place concrete, where the position of the thrust line is not clearly defined. Fire tests have shown that when only minimal thrust occurs, the thrust line is near the bottom of the member throughout the fire exposure. For highly restrained members the thrust line will be at the bottom of the member at the start

of the fire, with the position rising slowly during the fire (Gustaferro, A.H. et al. 1977). In order to develop the beneficial effects of axial restraint, the surrounding structures have to provide sufficient strength and stiffness to restrain the thermal elongation. According to Gustaferro, A.H. et al. (1986; 1977; 1971) the thrust forces that occur can be quite large but are always considerably less than that calculated using elastic properties of concrete and steels together with appropriate coefficients of expansion, as at high temperatures, creep and stress relaxation plays an important role.

There are many experimental results available on fire behaviour of restrained steel members (Ali, F.A., et al. 2001; 1998; Huang, Z.F., 2007; 2004; Tan K.H. et al. 2006; Wang Y.C. 1997), and there is also research on RC columns (Benmarce, A. et al. 2005; David, E.A. et al. 1977; Lie, T.T. 1986; Tan, Q.H. et al. 2012). However, for restrained beams and slabs, the test investigations are limited. The Portland Cement Association (Selvaggio, S.L. et al. 1963) has first executed experimental investigations of the effects of axial restraint on fire exposed concrete members. A series of double-T shaped specimens were exposed to the American standard fire ASTM E119 (2000). Each specimen was permitted to expand a given amount and then further expansion was prevented. Issen, L.A. (1970) reported that all tested beams supported their load longer than would have anticipated for simply supported beam analyses. The tests have also shown that the maximum thrust for a given allowed expansion is proportional to the “heated perimeter” and the concrete’s elastic modulus, where the heated perimeter is defined as the perimeter of the cross-section of the specimen, perpendicular to the direction of the thrust, which is exposed to fire. Based on the test results, a step-by-step method incorporating several nomograms was developed to estimate the thrust requirements for a given fire endurance for simply supported beams (Gustaferro, A.H. et al. 1971). The applicability of this approach to slabs and beams other than those tested has not been demonstrated.

Forsen, N.E. et al (1982) developed a non-linear finite element program, CONFIRE, to investigate the structural behaviour and fire resistance of concrete members exposed to fire. Their analyses were on simply supported concrete beams with different amounts of allowable expansion. Their analyses showed that the fire resistance of the RC beams does not increase with increasing axial restraint. Wade, C. (1991) recommends that the positive effects of thermal restraint should be disregarded when the location of the thrust is difficult to determine. Lim, L. et al. (2004; 2003) present a computer model of axially restrained and rotationally restrained one-way RC slabs in fire conditions. The analyses of the slabs were carried out with the SAFIR finite element program and the research results show that one-way slabs under fire conditions are very sensitive to the end support conditions and the axial restraint

stiffness. If the position of the thrust line is located much above the soffit of the slabs, the slabs will rapidly undergo large deformations and sag into a catenary, imposing axial tensile forces at the supports. Slabs with rotationally restrained end supports have much better fire resistance than equivalent simple supported slabs and they are less sensitive to the axial restraint stiffness. The analyses have also shown that even if the line of thrust is located close to the soffit, the slab can still deform into a catenary if there is insufficient horizontal axial restraint.

6.1.2 Influence of rotational restraints

The rotational restraints of a beam mainly result from the restraint provided by the connected columns and beams. It depends on which layer and span it belongs to. All the beams and columns that connected to the beam at the joints will contribute to the rotational restraint. The rotationally restrained elements have a considerably greater resistance than simply supported elements. Their superior performance is due to the beneficial changes in the moment redistribution in response to fire exposure, and their high level of redundancy against failure (Harmathy, T.Z. 1993; Ellingwood, B. et al. 1980).

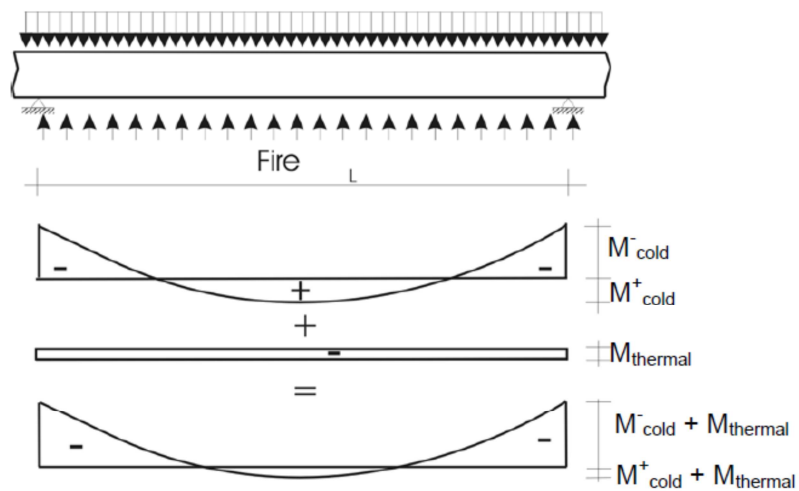


Figure 6.03 Components of moments in a continuous beam (Gus-1977)

Figure 6.03 shows the centre beam of a member that is continuous over several supports with the effect that the studied member is rotationally restrained. When it is heated, the beam wants to deflect downwards due to the temperature gradient, which arises from the different thermal elongations at the top and the bottom of the beam. This thermally induced curvature results in

a uniform negative bending moment $M_{thermal}$ along the length of the beam. Consequently, the support moments of the beam increase and the bending moment at the span decreases. This is beneficial to the beam's fire endurance, as the moment is reduced at the mid-span where the beam's flexural capacity is reduced faster due to higher temperatures in the steel bars. The change in bending moment line will always be limited by the reduced positive and negative flexural capacity of the beam. Gustafarro, A.H. (1977) state that the amount of redistribution that occurs is sufficient to cause yielding of the negative reinforcement. By increasing the amount of negative moment reinforcement, a greater negative moment will be attracted. To avoid a compression failure in the negative moment region, the amount of negative moment reinforcement should not be too high.

Experimental tests on the behaviour of continuous beams carried out by Ehm, H. et al. (1986) show that the negative flexural capacity at the supports can be reached quite early during the fire exposure. The reduction in flexural stiffness due to cracks forming at the support reduced the induced moment. As the temperatures increased and the flexural stiffness of the span dropped, the support moment increases again.

Tests carried out by the Portland Cement Association (Lin, T.D. et al. 1988; 1981) report beneficial effects of the continuity over the supports. The tests were also simulated with mathematical models, which showed sufficient accuracy (Ellingwood, B. et al. 1991).

However, Malhotra, H.L. (1982) reports that the continuity over supports without any horizontal restraint showed only marginal effects on the overall performance of beams compared to simply supported ones. The beams failed through the formation of three plastic hinges, but those formed more or less simultaneously.

Kodur V.K.R. et al. (2011; 2010; 2009; 2008) and Dwaikat M.B. et al. (2009; 2008) did many computational investigations on the fire performance of concrete beams with the M-k (Moment and curvature relationships) method. They introduced the development of a computer model for tracing the flexural fire response of simple supported beams, considering the effect of fire scenarios, effect of load ratio, effect of concrete cover, effect of the aggregates and failure criteria. They use the same method to analyse the restrained RC beams under realistic fire, loading and failure scenarios. Their research shows that fire induced rotational and axial restraint effects have a major influence on the fire resistance of the RC beams. Generally, the fire resistance of the RC beams increases when the beam is axially or rotationally restrained.

Riva, P. (2008; 2002) have done theoretical research and computer calculations with the

ABAQUS software on the fire behaviour of a set of fixed-end rectangular beams with varying axial restraints. The results are used to illustrate a simplified plastic verification procedure that allows the determination of both the bearing capacity and the deflections during a fire. Their research shows that an axial force leads to better results for fire resistance of the RC beams. Neglecting the axial force generated by the support conditions may lead to a conservative design. Their research on the rotational restraints has shown that the fire resistance of the RC beams increases when the beam is rotationally restrained.

Bernhart, D. (2004) calculated the effect of support conditions on the fire resistance of reinforced concrete beams by the SAFIR program. The beams are modelled by 2D elements with varying support conditions and the displacements, axial forces and reaction forces at the supports are compared after a four hours ISO-834 fire. The analyses show that for the pin-supported beams, the horizontal restraint is usually beneficial to the structural behaviour of beams compared to an unrestrained beam. The highly restrained beams appeared to fail in compression while less highly restrained beams appeared to fail in tension. The rotational restraint at the supports resulted in a large increase in the fire resistance rating compared to the pin-supported beams. The deflections occurring during the fire exposure were very small for the rotationally restrained beams. Besides, it has also concluded that the SAFIR program was not able to predict the final failure of the restrained beams because of convergence problems.

6.1.3 Objective of the research

The literature review reveals that the location of the fire induced axial restraint has a great influence on the fire performance of a member, and the effect of varying the location of the axial restraint on the fire response of restrained beams has been investigated both theoretically and experimentally on single members. The location of the axial restraint force can vary depending on the type and configuration of the connections between the beam and the column. For a simply supported beam, assuming the restraint location to be at the geometric centroid results in a fire induced axial force not generating any moment around the beam centre. If the location of the axial restraint is not at the centroid of the section, then a significant bending moment might develop at supports due to the eccentricity of the fire induced restraint force. In many situations, the location of the axial restraint can vary depending on the connection configuration. However, for a member in a realistic RC structure, the connections between beams and between beams and columns are fixed and the thrust is normally assumed to be in the centre of the member. This could lead to a negative effect on the fire resistance of the member because of the second-order effect caused by the combination of the axial force and

the bending deflections.

It has been shown in recent studies that the magnitude of restraint forces is dependent on many factors, including fire scenario and restraint stiffness. However, most of the researchers assume that the axial force or the restraint moment remains constant during the fire exposure. In real fire conditions, the restraint stiffness will comparatively increase with heating time and temperature due to the decrease of the stiffness of the member exposed to fire. This will lead to an increase in axial restraint force and a redistribution of the bending moment along the member and between the restraints. Hence, the present study also focusses on investigating the temperature-dependent fire restraint stiffness and restraint forces.

The main objective of this chapter is to present a time effective and practical study on the effect of the restraints on the fire behaviour of RC beams. Beams in a frame structure under realistic fire conditions are simulated, not only with restraints that are more accurate but also with temperature-dependent restraint forces. In order to get more realistic restraint conditions, the investigation considers the following: (1) the temperature-dependence of the axial force and the second-order effect caused by the axial force are considered and discussed. The axial force is however supposed to be at the axis of the beam, so the influence of the thrust line is not considered. (2) The redistribution of moments along the member at each time step due to the decreasing bending stiffness of the member is considered. The simplified multi-iteration analysis method (Lu, L.M. et al. 2015) proposed in Chapter 4 is adopted in this chapter too and the following stages are carried out: (1) The beam models that are used to do the parametric study are illustrated in section 6.2; (2) Influence of various axial restraints are compared and analysed in section 6.3 and (3) Influence of various rotational restraints are compared and analysed in section 6.4.

Based on the analysis and comparison of the simulation results, conclusions on the effects of restraints on fire behaviour of RC members subjected to bending are made. In the end, some suggestions on how to consider the influence of restraint conditions in fire conditions are proposed.

6.2 The beam model as part of a frame and the corresponding restraints

In order to perform a more accurate study on a RC beam in an actual frame, a multi-layered frame is firstly analysed and simplified as shown by Figure 6.03. A standard fire (ISO-834) is assumed to happen in one of the compartments of the frame, and the beam exposed to fire in

this compartment is studied. The deformation of the beam is restrained by the surrounding beams and columns, both axially and rotationally. Therefore, the studied beams can be simulated separately from the whole structure by adding restraint springs to the ends instead, as shown by Figure 6.04.

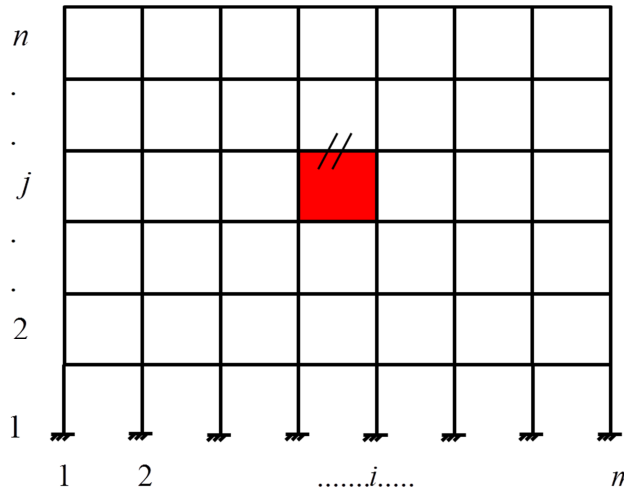


Figure 6.03 A multi-storey frame structure subjected to fire

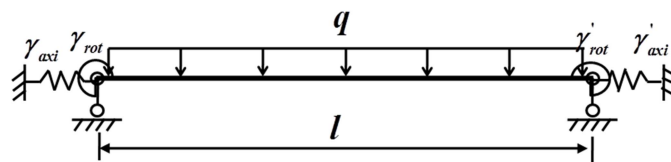


Figure 6.04 Restrained beams with various axial and rotational restraints

The axial and rotational restraints for the studied beams are modelled with axial and rotational springs as shown by Figure 6.04. The thrust line of the axial forces is supposed to be the axis of the beam. The strength of the restraints is expressed by the restraint ratios: γ_{rot} and γ'_{rot} present for the rotational restraint ratios at the two ends while γ_{axi} and γ'_{axi} present for the axial restraint ratios of the two ends. They are determined by the restraint conditions provided by the beams and columns connected to the beams in the frame structure. The restraint ratios of the springs are measured relative to the stiffness of the beam, such that 100% restraint is equivalent to an identical additional beam at the one support as shown by Equation (6.02) and

Equation (6.03).

$$\gamma_{axi} = \frac{\text{stiffness of the spring}}{\text{stiffness of the beam}} = \frac{(EA/L)_{spring}}{(EA/L)_{beam}} \times 100 \% \quad (6.02)$$

$$\gamma_{rot} = \frac{\text{stiffness of the spring}}{\text{stiffness of the beam}} = \frac{(EI/L)_{spring}}{(EI/L)_{beam}} \times 100 \% \quad (6.03)$$

The beams exposed to fire are supposed to be heated from three sides and the columns exposed to fire are supposed to be heated from four sides except the ones on the boundary, which are supposed to be heated on one side only. The effective bending stiffness of the members exposed to fire will be calculated based on the multi-iteration method proposed in Chapter 4. The moment-curvature ($M-k$) relation curves are calculated at each time step, and then the effective bending stiffness is defined for that time step. The time dependency of the restraint factors is calculated based on the following simplifications (Wang, K.Q. et al. 2011).

(1) The axial restraint rigidity mainly results from the lateral resistance of all the columns of this layer and the upper layer. These columns are restrained by connected beams and columns and the supporting condition at the opposite side of these restraining beams and columns are assumed to be hinges. The lateral deformations of the columns in the same layer are assumed the same.

(2) The rotational restraint rigidity mainly results from the bending stiffness of the connected columns and beams. The opposing side of these restraining beams and columns are assumed to be hinges except for the bottom columns, where the bottom of these columns is assumed to be clamped.

6.2.1 Axial restraint stiffness for beams in a multi-layered frame

According to the assumption (1), the axial restraint stiffness is mainly determined by the flexural stiffness and rotational restraint rigidity at the opposite side of the related columns. These columns are restrained by the connected beams and columns and the opposite end connections of these restraining beams and columns are assumed to be hinges. The lateral deformations of the columns in the same layer are assumed the same. For the columns that provide axial restraint to beams, there are two conditions, restraint from upper-side, and from bottom side. Based on the layer and the support condition at the opposite side, the lateral resistance rigidity can be classified into four cases, as shown by Figure 6.05.

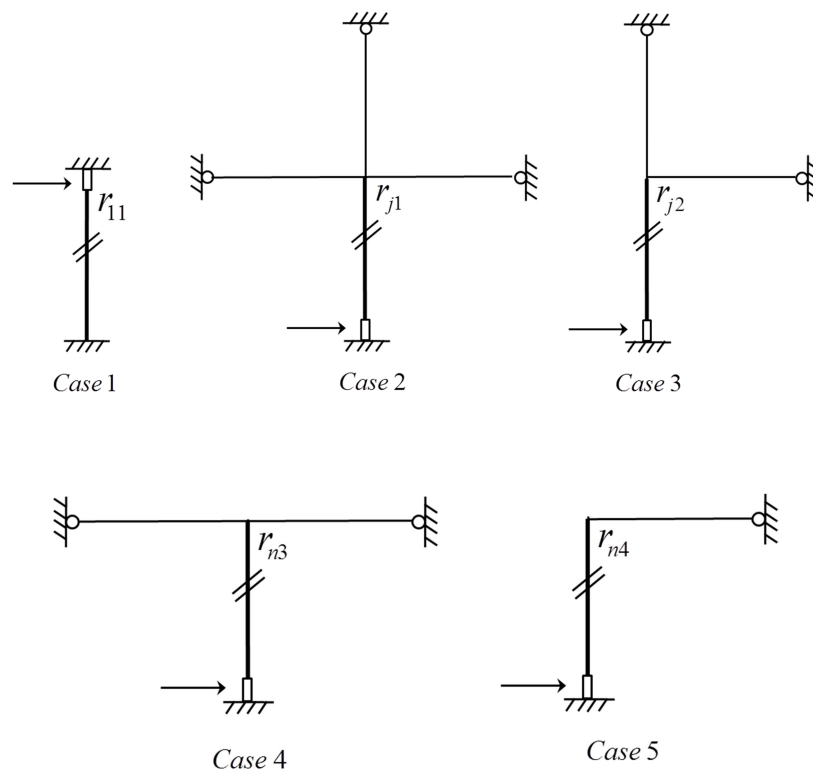


Figure 6.05 Lateral restraint stiffness of columns in a frame

(1) Case 1, the supporting condition at the opposite side of the bottom layer columns are assumed to be fixed. Which means their lateral restraint rigidity is $r_{11} = \infty$.

(2) For the columns in a layer j ($j = 2, 3, \dots, n-1$), the lateral stiffness of the top side is determined by the rotational restraints at the bottom side, which is restrained by two beams (one beam) and one column from the lower layer, shown as Case 2 and Case 3. The Equation (6.04) is valid for Case 2. Equation (6.05) is valid for Case 3 when the column is at the edge and only one beam connected to it.

$$r_{j1} = 6EI_{beam}(j-1)/L_b + 3EI_{column}(j-1)/L_c \quad (6.04)$$

$$r_{j1} = 3EI_{beam}(j-1)/L_b + 3EI_{column}(j-1)/L_c \quad (6.05)$$

(3) For the columns in a layer j ($j = 2, 3, \dots, n-1$), the lateral stiffness of the bottom side is determined by the rotational restraints at the other side of the columns, which can also be

expressed by Case 2 and Case 3 in Figure 6.05. Equation (6.06) is valid for Case 2 and Equation (6.07) is valid for Case 3.

$$r_{j1} = 6EI_{beam}(j)/L_b + 3EI_{column}(j+1)/L_c \quad (6.06)$$

$$r_{j1} = 3EI_{beam}(j)/L_b + 3EI_{column}(j+1)/L_c \quad (6.07)$$

(4) For the columns in the layer n , when restrained from the top side, the lateral stiffness of it is the same as layer j , which is restrained by two beams (one beam if at the edge) and one column. So the Equations (6.04) and (6.05) are valid for r_{n1} and r_{n2} . The lateral stiffness of the column when restrained from the bottom side is determined by only two beams as shown by Case 4 in Figure 6.05, or one beam as shown by Case 5 in Figure 6.05. The restraint rigidity of Case 4 can be expressed by Equation (6.08) and that for Case 5 by Equation (6.09).

$$r_{n3} = 6EI_{beam}(n)/L \quad (6.08)$$

$$r_{n4} = 3EI_{beam}(n)/L \quad (6.09)$$

The restraint rigidity for the cases could be simplified as Equations (6.10) (a), and (6.10) (b); the effective stiffness of the columns in the same compartment of the beam will change with temperature while the other ones remain constant as the effective stiffness at normal temperatures.

$$\begin{cases} k_r = \frac{12(r_1 + 1) B}{(r_1 + 4) l^3} & \text{-----(a)} \\ k_r = \frac{3r_1 r_2 (r_1 + 4) + 12(r_1 + 3)(r_1 + 1) B}{36r_1 (r_1 + 1)(r_2 + 1) l^3} & \text{-----(b)} \end{cases} \quad (6.10)$$

These two equations could be simplified as $k_r = N \frac{B}{l^3}$ and that for columns exposed to fire

$k_r^T = N \frac{B^T}{l^3}$, where B reflects the bending stiffness EI of the RC member, B^T is the effective

bending stiffness of the member under elevated temperatures (introduced in Chapter 4) and N is a factor that related to the rotational restraint of the opposite side of the column.

According to the restraint conditions of the columns, we could obtain the factors N_{11}, N_{j1} for

the normal columns; for the ones that are at the edge, the factor is defined as N_{j2} ; for the columns of the top layer, when they are restrained from the bottom side, the factors N_{n3} , N_{n4} are used. The final restraint formulas for the beams could be substituted into these conditions:

For beams in layer 1, the restraint stiffness is expressed by Equation (6.11):

$$\begin{cases} k_{1L} = (m_L - 1)(N_{11} \frac{B_1}{l_1^3} + N_{21} \frac{B_2}{l_2^3}) + (N_{12} \frac{B_1}{l_1^3} + N_{22} \frac{B_2}{l_2^3}) \\ k_{1R} = (m_R - 1)(N_{11} \frac{B_1}{l_1^3} + N_{21} \frac{B_2}{l_2^3}) + (N_{12} \frac{B_1}{l_1^3} + N_{22} \frac{B_2}{l_2^3}) \\ k_1 = 1/(\frac{1}{k_{1L}} + \frac{1}{k_{1R}}) \end{cases} \quad (6.11)$$

For beams in layer j ($j = 2 : n - 1$), the restraint stiffness is expressed by Equation (6.12):

$$\begin{cases} k_{jL} = (m_L - 1)(N_{j1} \frac{B_j}{l_j^3} + N_{(j+1)1} \frac{B_{(j+1)}}{l_{(j+1)}^3}) + (N_{j2} \frac{B_j}{l_j^3} + N_{(j+1)2} \frac{B_{(j+1)}}{l_{(j+1)}^3}) \\ k_{jR} = (m_R - 1)(N_{j1} \frac{B_j}{l_j^3} + N_{(j+1)1} \frac{B_{(j+1)}}{l_{(j+1)}^3}) + (N_{j2} \frac{B_j}{l_j^3} + N_{(j+1)2} \frac{B_{(j+1)}}{l_{(j+1)}^3}) \\ k_j = 1/(\frac{1}{k_{jL}} + \frac{1}{k_{jR}}) \end{cases} \quad (6.12)$$

For beams in layer n , the restraint stiffness is expressed by Equation (6.13):

$$\begin{cases} k_{nL} = (m_L - 1)N_{n3} \frac{B_n}{l_n^3} + N_{n4} \frac{B_n}{l_n^3} \\ k_{nR} = (m_R - 1)N_{n3} \frac{B_n}{l_n^3} + N_{n4} \frac{B_n}{l_n^3} \\ k_n = 1/(\frac{1}{k_{nL}} + \frac{1}{k_{nR}}) \end{cases} \quad (6.13)$$

According to the equations of axial restraint stiffness, the following typical conditions could be listed:

(1) For simply supported beams, with no connected beams or columns, as shown in Figure 6.02, the rotational restraints are zero ($\gamma_{rot} = \gamma_{rot}' = 0$). The axial restraint results from the boundary supports. Therefore, the axial restraint ratio could vary from zero to axially fixed.

(2) For a beam in a frame, both axial restraints and rotational restraints exist. The axial restraint according to Equation (6.11) to Equation (6.13) can vary from zero to fixed.

6.2.2 Rotational restraint stiffness for beams in a multi-storey frame

According to Fig. 6.03, the rotational restraint rigidity of beams in the frame depends on which layer and span it belongs to. All the beams and columns that are connected to the beam at the connection will contribute to the rotational restraint.

(1) Except for the bottom-layer columns, the supporting condition at the opposite side of the members that contribute to the rotational restraint rigidity are assumed hinge connections, the rotational restraint rigidity of them is calculated by Equation (6.14):

$$r_{c,i} = 3B_{c,i} / l_c \quad (6.14)$$

(2) Equation (6.15) is for the rotational restraint rigidity of bottom-layer columns.

$$r_{c,1} = 4B_{c,1} / l_c \quad (6.15)$$

The total rotational restraint rigidity of one end of the beam can be calculated as a combination of the rotational restraint rigidity of the connected members, in which the restraining columns from the same layer as the beam are supposed to be exposed to the fire.

For beams in layer 1, which are restrained by columns from the bottom layer, the rotational restraint rigidity can be expressed by Equation (6.16):

$$K_{1,j} = 4B_{c,1}^T / l_c + 3B_{c,2} / l_c + 3B_{b,1} / l_b \quad (6.16)$$

For beams in layer j ($j = 2 : n - 1$), the rotational restraint rigidity can be expressed by Equation (6.17):

$$K_{i,j} = 3B_{c,i}^T / l_c + 3B_{c,i+1} / l_c + 3B_{b,i} / l_b \quad (6.17)$$

The beams on the top layer n only have columns connected below it. Therefore, the rotational restraint rigidity can be expressed by Equation (6.18):

$$K_{n,j} = 3B_{c,n}^T / l_c + 3B_{b,n} / l_b \quad (6.18)$$

For the three cases, if the connection is at the edge, which means the left connection of the beams of first span and the beams of last span, the left part should be zero.

According to the equations for rotational restraint stiffness, the following typical conditions could be listed:

(1) For continuous beams, when there is no column cast together with the beams, it is supposed that there is no axial restraint ($\gamma_{axi} = \gamma_{axi}' = 0$). The rotational restraint results from the connected beams, so the rotational restraint ratio could vary from zero to rotationally fixed, which is dependent on the material and the size of the connected beams.

(2) For a beam being part of a frame, when the axial restraint factor ranges from zero to fixed, the maximum rotational restraint factor is the condition shown by Equation (6.16), and the minimal restraint factor is the condition shown by Equation (6.18). For limited conditions, the restraint factors can also change from zero to be fixed.

6.2.3 Characteristics of the beam model

To study the effects that the end restraints have on typical beams subjected to the ISO-834 fire, a parametric study was carried out on the beam model that is described in the following. Since the restraints are the main factors to study, the other parameters are left the same. The beam measure $b \times h \times L = 350 \times 500 \times 6000$ (mm), as shown by Figure 6.06 (a), with 4 ϕ 20 steel bars in the compression zone and 4 ϕ 20 in the tensile zone for the cross-section I-I, as shown by Figure 6.06 (b).

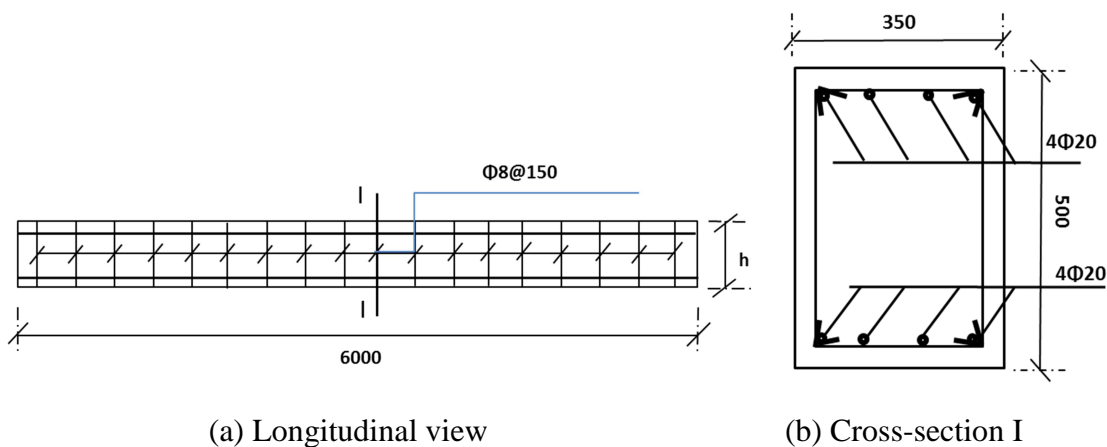


Figure 6.06 Beam geometry for the simulation of the influence of restraints
(Diameter in mm)

The concrete adopted in the model is a normal strength siliceous aggregate concrete and the steel bars are made of cold worked steel. The detailed material information on the concrete and the steel bars before heating are listed in Table 6.01.

Table 6.01 Material properties of the concrete and steel bars before heating

$f_c(N/mm^2)$	$f_t(N/mm^2)$	$E_c(N/mm^2)$	$f_y(N/mm^2)$	$f_u(N/mm^2)$	$E_s(N/mm^2)$
30	2.9	2.0×10^4	500	650	2.1×10^5

There are four steel bars in tension and four in compression, which can be designated as bar 1, bar 2, bar 3 and bar 4, as shown by Figure 6.07. The distance between the axis of the bottom reinforcing bars to the bottom surface is designated as d_1 . The distance between the axis of the top reinforcing bars to the top surface is designated as d_2 . Both d_1 and d_2 are 35 mm. The distance between the axis of the reinforcing bars to the lateral surface of the beam is 45 mm.

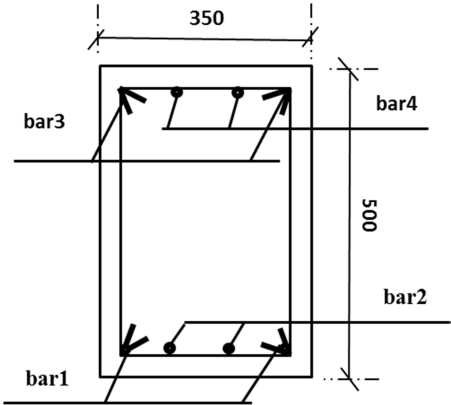


Figure 6.07 Designation and arrangement of the steel bars in the cross-section

The beams are assumed to be heated on three sides: the bottom side and two lateral sides. The temperature field calculation for this series of beams is the same as that introduced in Chapter 5, so it will not be illustrated in detail here again.

The fire-resistance behaviour of the member is checked according to the failure criteria mentioned in section 4.4:

(1) The applied service load exceeds the bearing capacity of the member at any fire exposing time t ;

(2) The maximum deflection of the member exceeds $L/20$ at any fire exposure time t , where L is the span length of the member.

(3) The rate of deflection exceeds the limit given by the following expression: $\frac{L^2}{9000h_0}$

(mm/min), where L is the span length of the member (mm), and h_0 is the effective depth of the member (mm).

The load applied on the RC beam contains two parts: the gravity load and the live load, both are considered uniformly distributed loads. In order to get a clear idea of the loading condition, the total applied load is supposed to be 30% of the bearing capacity of the RC beam at ambient temperature. The ultimate moment of the studied beam for both mid-span and the supports is $2.73 \times 10^2 kN/m$ at ambient temperature. Therefore, the equivalent uniform load $q=18 kN/m$ is applied to the beam, which is based on the ultimate condition of the simple supported beam. In order to keep the models being different only on the restrained conditions, the same load of $q=18 kN/m$ is applied for all the models. Based on the criterion (2), the critical deflection is $d_{critical} = 300 mm$, and the rate of deflection for failure criterion (3) is $\Delta d = 8.6 mm/min$.

6.3 Fire behaviour of beams with various axial restraints

This section describes the numerical analyses of single RC beams with various axial restraints subjected to the ISO-834 standard fire, including the simulation of a series of rotationally free beams with various axial restraints and a series of rotationally restrained beams with various axial restraints. The purpose of the analysis is to investigate the effect of axial restraints on the structural behaviour and fire resistance of RC beams.

6.3.1 Survey of the simulations

According to the introduction on the effect of axially restrained beams and the objective of

this section, two general models are analysed:

(1) Rotationally free beams with varying axial restraints. The rotational restraint ratio as shown by Figure 6.04 is $\gamma_{rot} = \gamma_{rot}' = 0$, thus only thermally induced axial loads are considered during this process. The bending moment will change due to the second-order effect caused by the axial loads and the deflection. This is a rather hypothetical case as in reality, both types of restraint will occur simultaneously.

(2) Rotationally restrained beams with varying axial restraints. These beams are partly or completely rotationally restrained at the ends $\gamma_{rot} = \gamma_{rot}' > 0$. The rotational restraints for this part are set to be 0.05, 0.1, 0.5, 1.0 and fixed. These conditions are suitable for beams in a frame, which will have both axial restraints and rotational restraints from the connected beams and columns.

The beams in these two cases are modelled with several different levels of axial restraint, ranging from no restraint to be axially fixed. The axial spring stiffness adopted in this chapter includes 0, 0.05, 0.1, 0.5, 1.0 and fixed.

6.3.2 Rotationally free beams with varying axial restraints

This section discusses the behaviour of the simply supported beams with varying levels of axial restraint exposed to the 2-hours ISO-834 standard fire. Three factors of the RC beams are studied during the fire exposure simulations: the axial force, the mid-span moment, and the mid-span deflections. The legend “Ro” in the following figures designates the rotational restraint ratio γ_{rot} and “Ra” designates the axial restraint ratio γ_{axi} .

I. Comparison of the axial forces

The axial force is calculated by two methods in this part, the proposed multi-iteration method and the simplified method introduced in Structural Mechanics books. The simplified method is based on the average temperature of the cross-section of the members. According to the structural mechanics method, the thermal thrust axial force can be calculated by Equation (6.19).

$$N_{th} = \varepsilon_{th}(\theta) \times EA(\theta) \quad (6.19)$$

where N_{th} is the thermal thrust axial force.

θ is the average temperature of the cross-section.

$\varepsilon_{th}(\theta)$ is the thermal elongation of the material.

$EA(\theta)$ is the axial stiffness of the cross-section of the member.

The axial stiffness is simplified by combining the stiffness of concrete and stiffness of steel bars, as shown by Equation (6.20):

$$EA(\theta) = E_c(\theta) \times (b \times h - A_{s1} - A_{s2}) + E_s(\theta) \times (A_{s1} + A_{s2}) \quad (6.20)$$

where $E_c(\theta)$ is the elastic modulus of concrete at temperature θ .

$E_s(\theta)$ is the elastic modulus of steel bars at temperature θ .

b is the width of the cross-section and h is the height of the cross-section.

A_{s1} is the area of the steel bars in tension.

A_{s2} is the area of the steel bars in compression.

The elastic modulus of concrete and steel bars introduced in EC 2 is adopted. The average temperature of the cross-section is calculated each time step for the simplified calculation of axial force, given by Figure 6.08.

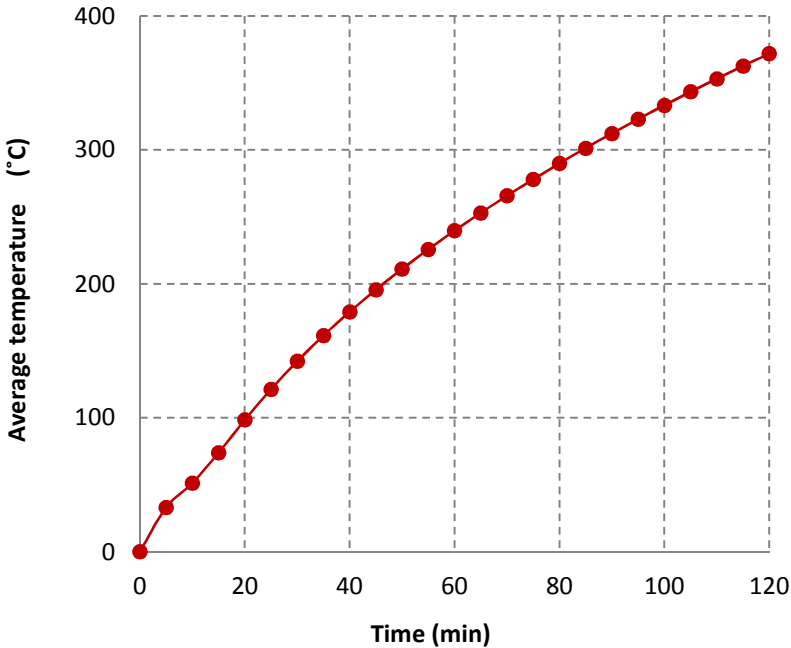


Figure 6.08: Average temperature of the cross-section

Due to the decrease of material properties at elevated temperatures, the axial stiffness of the member itself is also reduced. Figure 6.09 shows the reduction factor of the axial stiffness at elevated temperatures. Figure 6.10 shows the temperature-dependent axial restraint factor decided by Equation (6.01) according to the average temperature. Figure 6.11 shows the thermal restraint axial force calculated by the simplified average temperature method, with the temperature-dependent axial restraint factors applied.

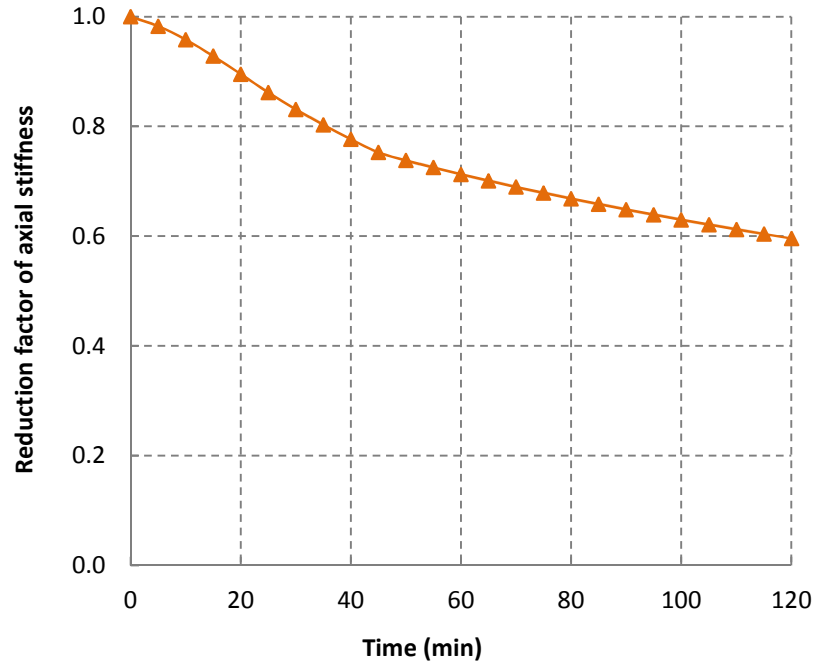


Figure 6.09: The reduction factor of axial stiffness based on average temperature

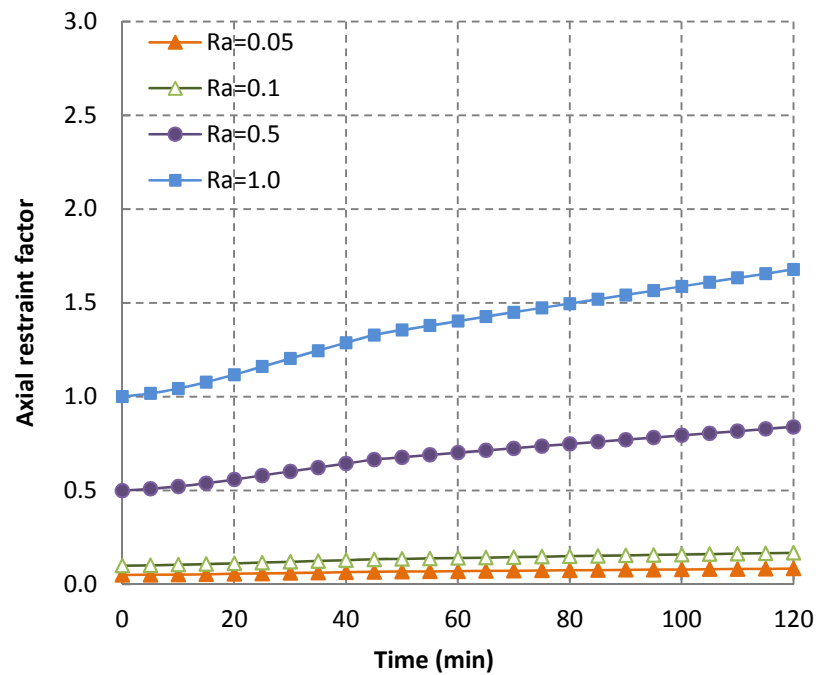


Figure 6.10: Time-dependent axial restraint factors based on average temperature

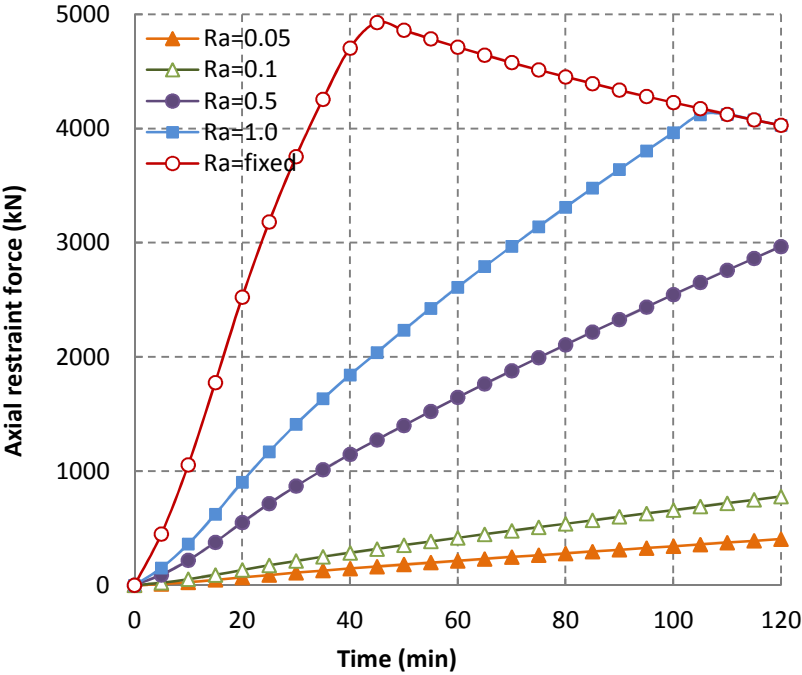


Figure 6.11: The axial force for beams with various axial restraint ratios
(Computed by the average temperature)

The axial stiffness of the RC beams is decreasing with the fire exposing time, and decreased to be 0.6 of the initial after 2hrs. The axial restraint factor is comparatively increasing with heating time due to the decrease of the axial stiffness of the member at elevated temperatures. However, the increase of the ones calculated by the average temperature is not serious. The thermal restraint forces are increasing with heating time. For the axially fixed members, the ultimate axial force, which is decreasing during heating, can be reached in a short time. However, from this method, it is difficult to decide about the failure time of the RC member.

The reduction factor of the axial stiffness calculated by the multi-iteration method is larger than the average temperature method, and the increasing of the restraint factors are also faster. It is increased to be 2.7 times of that at ambient temperature, as shown by Figure 6.12 and Figure 6.13. Figure 6.14 shows the axial forces computed by the multi-iteration method.

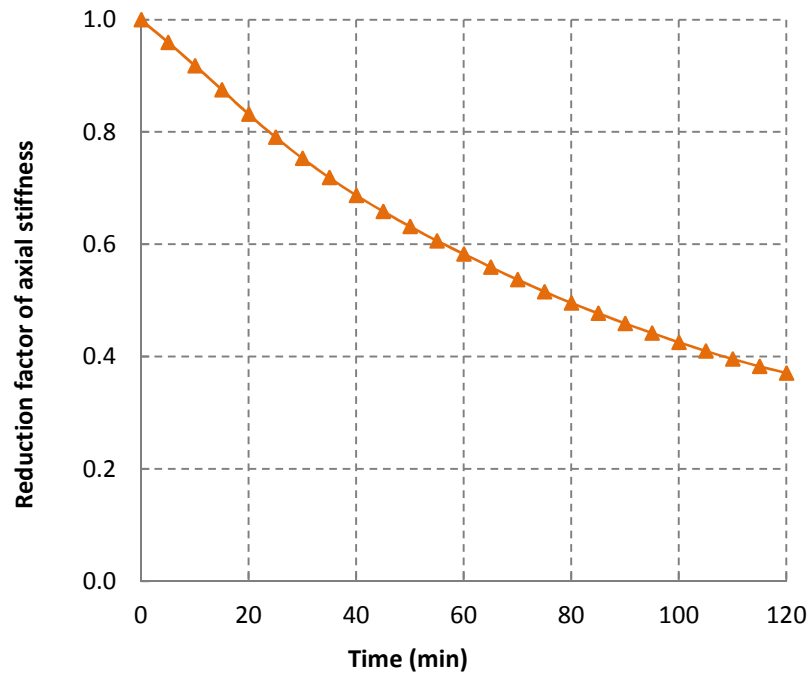


Figure 6.12 The reduction factor of axial stiffness (Multi-iteration method)

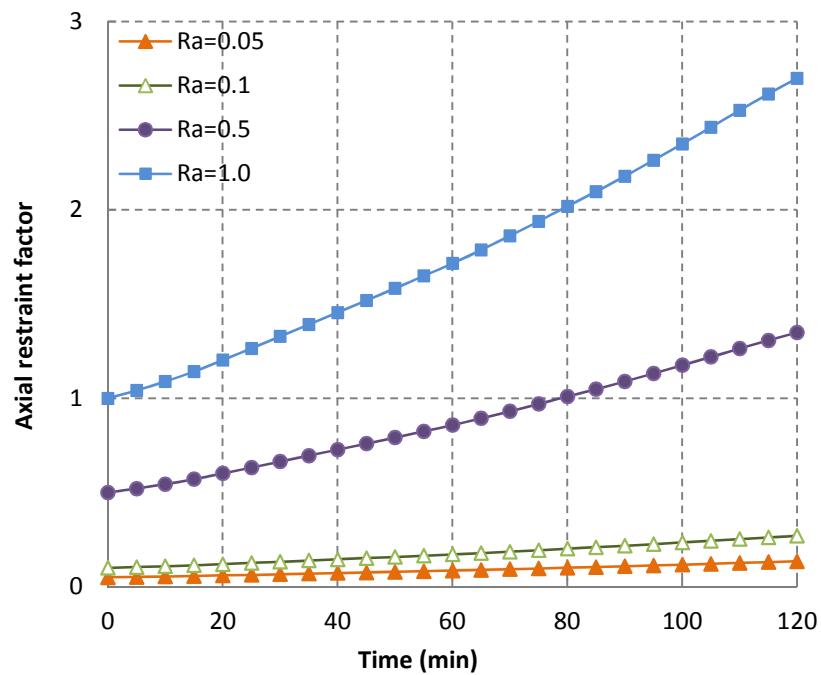


Figure 6.13 The axial restraint factors during heating (Multi-iteration method)

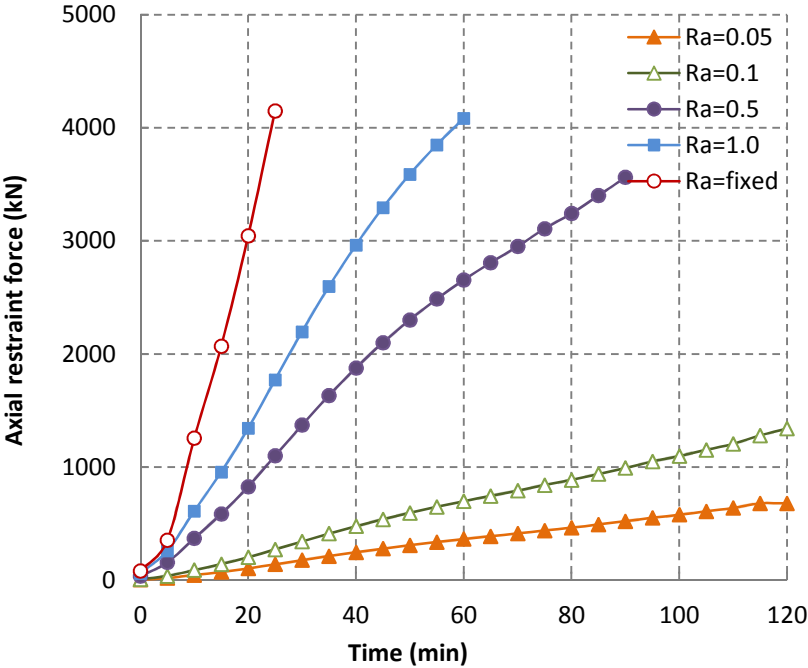


Figure 6.14 The axial force for beams with various axial restraint ratios (kN)
(Multi-iteration method)

The axial forces shown by Figure 6.14 increase with heating time. The members with weak axial restraint, the ones with $\gamma_{axi} = 0.05$ and $\gamma_{axi} = 0.1$ can well resist 2 hrs. of fire, and the ones with strong axial restraint are failed earlier during heating. The one with $\gamma_{axi} = 0.5$ failed after 90 min of heating, the one with $\gamma_{axi} = 1.0$ failed after 55 min of heating, and that with $\gamma_{axi} = fixed$ failed after 25 min of heating. The failure of these members is because of the bearing capacity of the mid-span is reached due to the second-order effect. It can be concluded that for axially restrained members subjected to bending, the stronger axial restraint lead to a shorter fire-resistance time.

From the comparison of Figure 6.11 and Figure 6.14, we can conclude that:

- (1) For all the axial restraint ratios, the axial forces calculated by the average temperature method are slightly smaller than the ones calculated by the iteration method. From one side, it validates that the multi-iteration method is reliable, and from another side, it shows that the simplified average temperature method will supply a smaller prediction of the thermal forces, which is unsafe for fire-resistance design of RC structures.

(2) The simplified method cannot show the failure time of the member while the multi-iteration method can. This makes the multi-iteration method more practical and helpful to use for the fire-resistance design of RC structures.

II. Comparison of the mid-span moments

Figure 6.15 shows the developments of the mid-span bending moments for the beams with various axial restraint ratios.

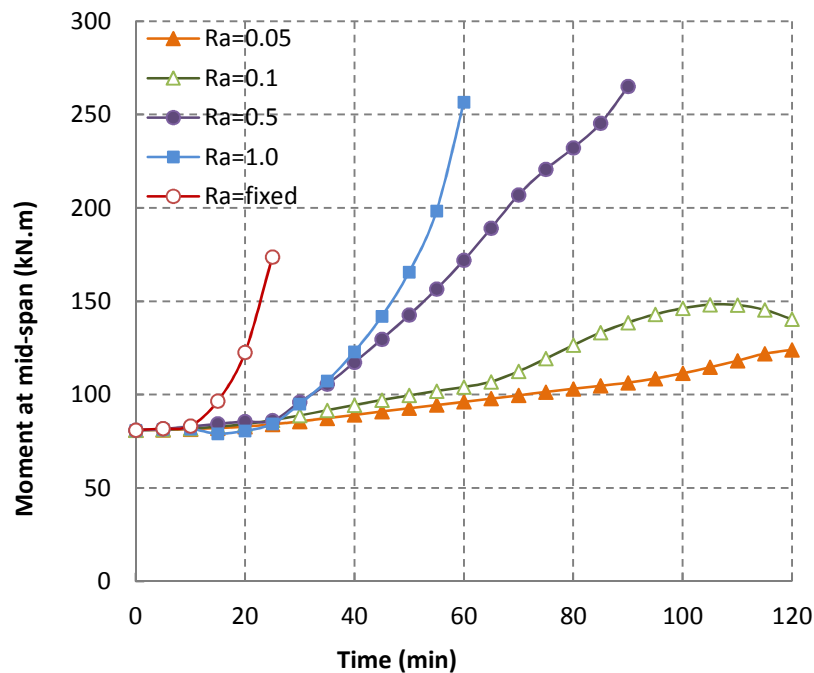


Figure 6.15: Mid-span moments for beams with various axial restraint ratios

From the comparison of the mid-span moments of beams with increasing spring stiffness, the following can be concluded.

(1) Compared to the simply supported beams, the axially restrained beams will experience an increasing restraint axial force and an increasing mid-span moment. The increasing of the moment is due to the second-order effect caused by the multiply of the axial force and the deflections. This could make the member reach its bearing capacity in a short time and fail early during fire: the stronger axial restraint the earlier.

(2) The weak springs have a slight increase in the mid-span moment and can well resist 2hrs of fire. For the members with strong axial restraints, the mid-span moment is the critical index

for their failure. Therefore, the effective ways of increasing their fire-resistance time are decreasing their service load, increasing their mid-span reinforcement or applying proper rotational restraints.

III. Comparison of the mid-span deflections

Figure 6.16 shows the developments of the mid-span deflections for the beams with various axial restraint ratios.

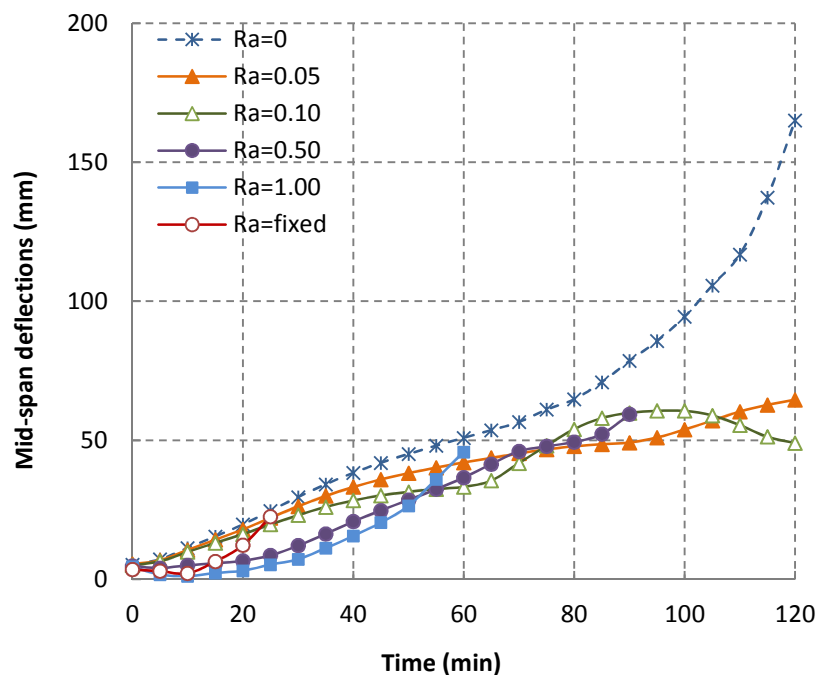


Figure 6.16 Mid-span deflections for beams with various axial restraint ratios

The analysis of the mid-span deflections for beams with various axial restraint ratios has shown the following:

(1) All beams with some amount of restraint have smaller mid-span deflections than the simply supported beam, which is the curve of $\gamma_{axi}=0$ in Figure 6.14. The mid-span deflections are restrained by the springs, their developing process during the fire depends on the axial stiffness of the springs. Generally, the mid-span deflections of RC beams will increase with heating time, and the stronger spring leads to a slower increase on mid-span deflections of the beam.

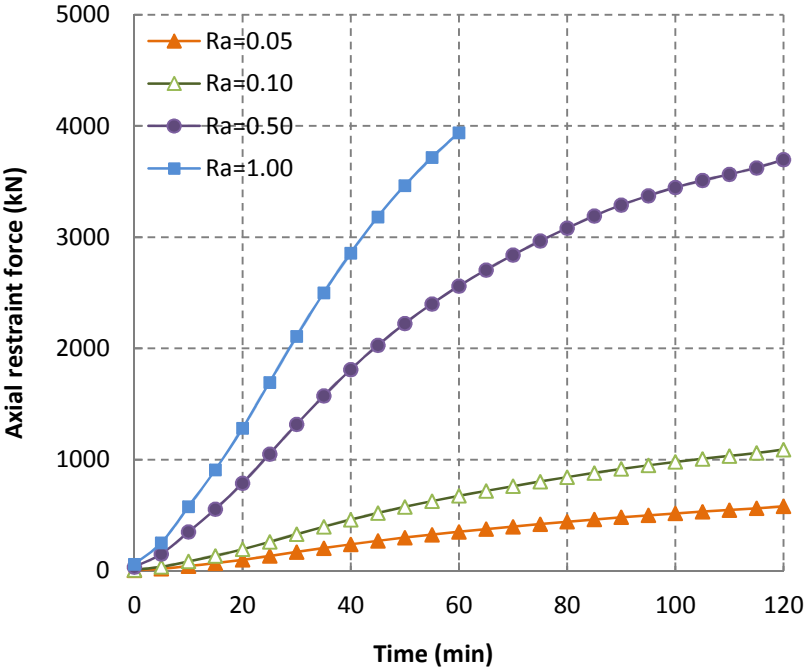
(2) For beams with weaker springs, the restraint effect on the mid-span deflection compared to the simply supported beam is obvious, and for the comparison between beams with strong restraint springs, like beams with $\gamma_{axi}=0.5$, $\gamma_{axi}=1.0$ and even $\gamma_{axi} = fixed$, they are nearly the same. Therefore, for the members subjected to bending, a proper amount of axial force is useful for the controlling of thermal deflections.

6.3.3 Rotationally restrained beams with varying axial restraint

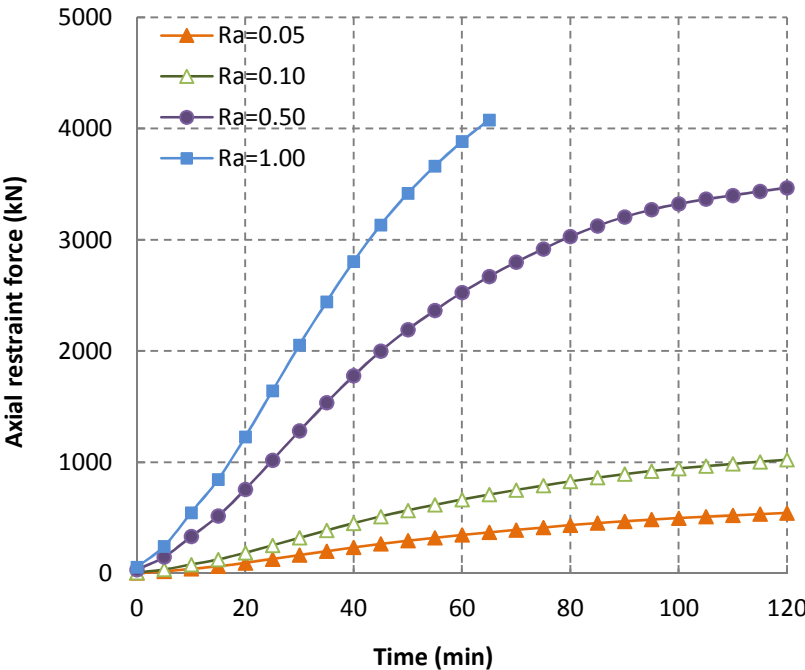
The beams analysed in this section are rotationally restrained at both end supports and are submitted to the 2hrs ISO-834 standard fire. The axial spring, allowing for varying axial restraint, at the supports are connected to the centre of the cross-section of the beam. The spring stiffness adopted in this chapter is varied from 0% to 100% including: 0, 0.05, 0.1, 0.5, 1.0 and fixed as well. However, all the axially fixed members simulated with various rotational restraint fails quite early, in 30 min of heating. So the forces and the deflections curves for them are not shown in the following figures. The legend “Ro” in the following figures respect for the rotational restraint ratio γ_{rot} .and “Ra” respect for the axial restraint ratio γ_{axi} .

I. Comparison of the axial forces

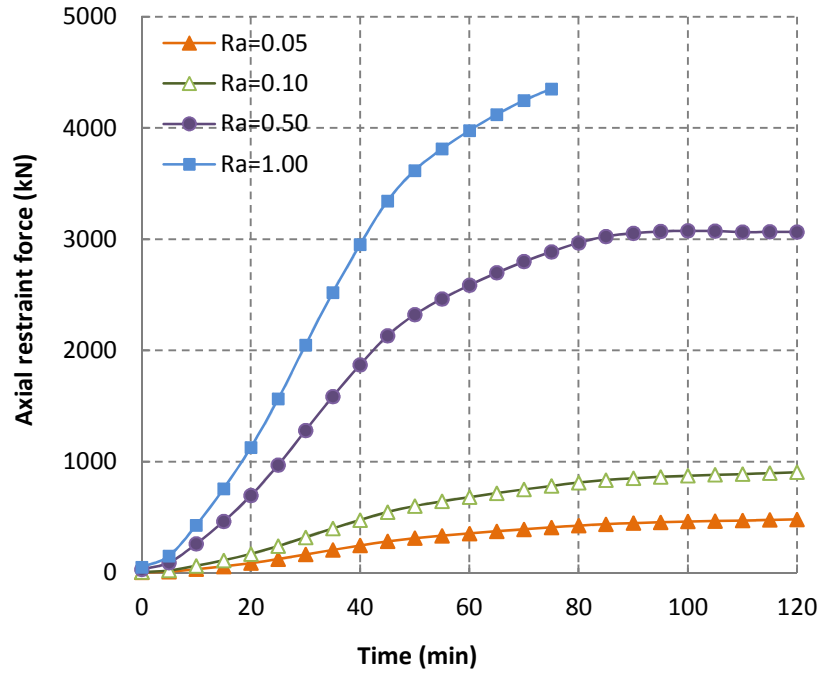
The development of the axial forces during the fire exposure for the beams with different levels of axial restraint ratio are shown by Figure 6.17, with (a) $\gamma_{rot}=0.05$, (b) $\gamma_{rot}=0.10$, (c) $\gamma_{rot}=0.5$, (d) $\gamma_{rot}=1.0$, and (e) $\gamma_{rot} = fixed$.



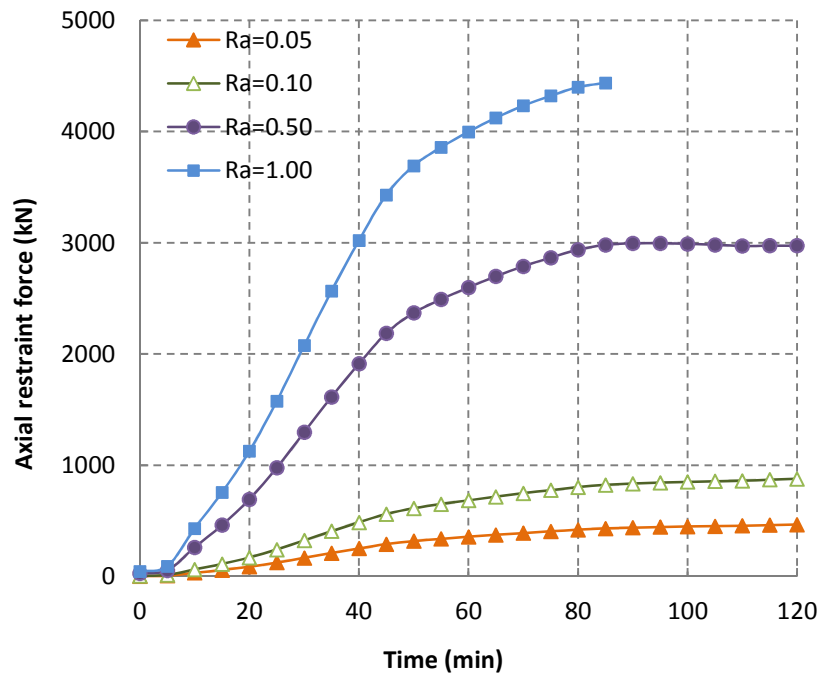
(a) Axial forces for beams with various axial restraints ($\gamma_{rot} = 0.05$)



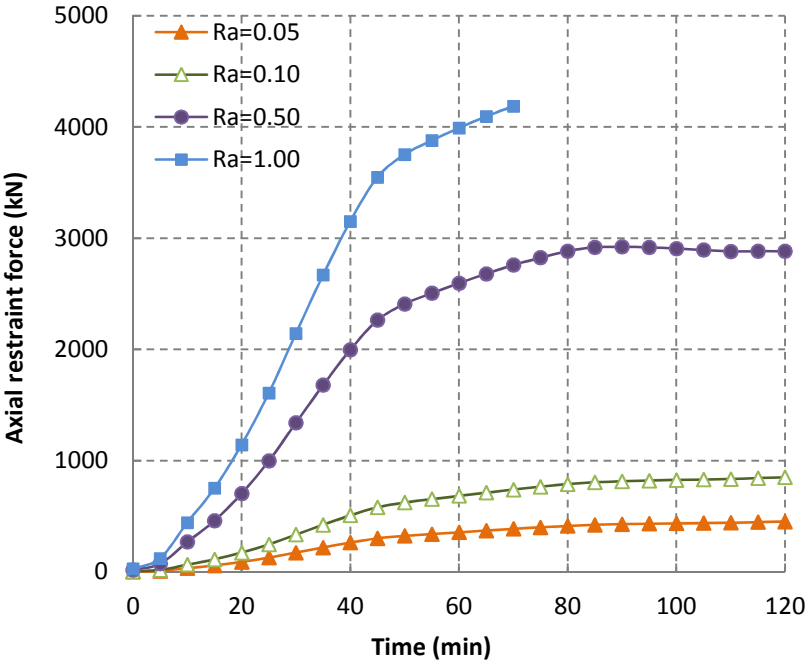
(b) Axial forces for beams with various axial restraints ($\gamma_{rot} = 0.10$)



(c) Axial forces for beams with various axial restraints ($\gamma_{rot} = 0.50$)



(d) Axial forces for beams with various axial restraints ($\gamma_{rot} = 1.0$)



(e) Axial forces for beams with various axial restraints ($\gamma_{rot} = fixed$)

Figure 6.17 Axial forces for beams of different levels of axial and rotational restraints

From the comparison of axial forces of rotationally restrained beams with various axial restraints shown by Figure 6.17 from (a) to (e), these conclusions can be made.

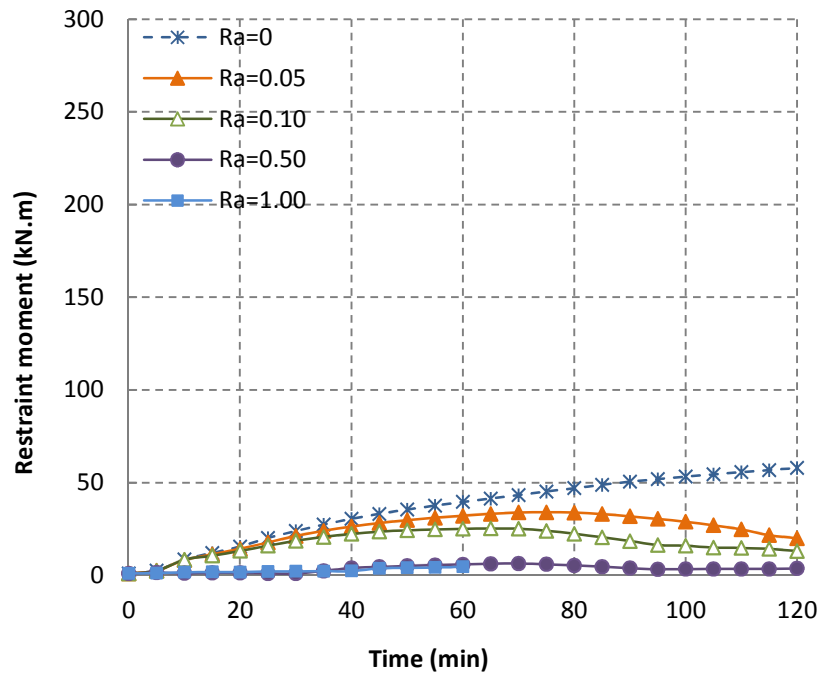
(1) For all the rotationally restrained beams, the axial force increases with heating time and with increasing axial restraint ratios. For weak axial restraint springs, the axial forces continuous rise during the 2hrs of heating, which means they will reach their maximum at a later stage, as the weaker springs allow for more thermal elongation. For the one with $r_{axi}=0.5$, the axial forces increase sharply at first, then the increase slows down with heating time or even keeps constant at the later stage. The axial force of the one with $r_{axi}=1.0$ increases until its failure.

(2) Compared to the simply supported beams with various axial springs, the axial force curves of rotationally restrained beams have the same trend of increasing with time. However, the maximum forces are comparatively smaller, and the fire-resistant time for the members with $r_{axi}=0.5$ and $r_{axi}=1.0$ is well increased. The rotational restraint is benefit for improving the fire-resistance time of the members subjected to bending.

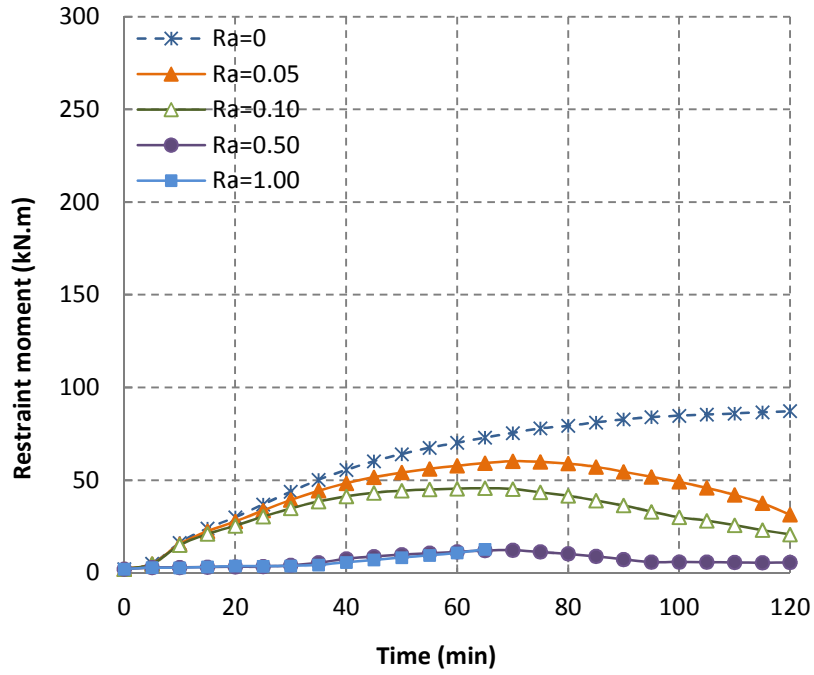
(3) The comparison between the figures shows that the stronger rotational restraint leads to a smaller axial force in the beam. The fire-resistance time of the member with $r_{axi}=1.0$ is increasing with the rotational restraints. This means that the effect of axial restraints is reduced by the rotational restraints.

II. Comparison of the restraint moments

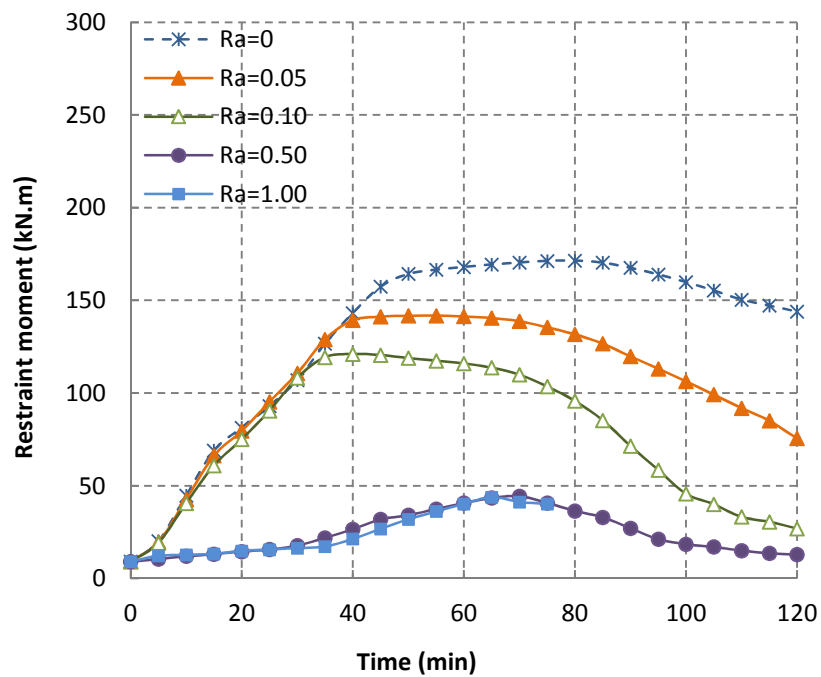
The development of the restraint moments for the beams of different levels of axial restraint are shown by Figure 6.18, with (a) $\gamma_{rot}=0.05$, (b) $\gamma_{rot}=0.10$, (c) $\gamma_{rot}=0.5$, (d) $\gamma_{rot}=1.0$, and (e) $\gamma_{rot} = fixed$.



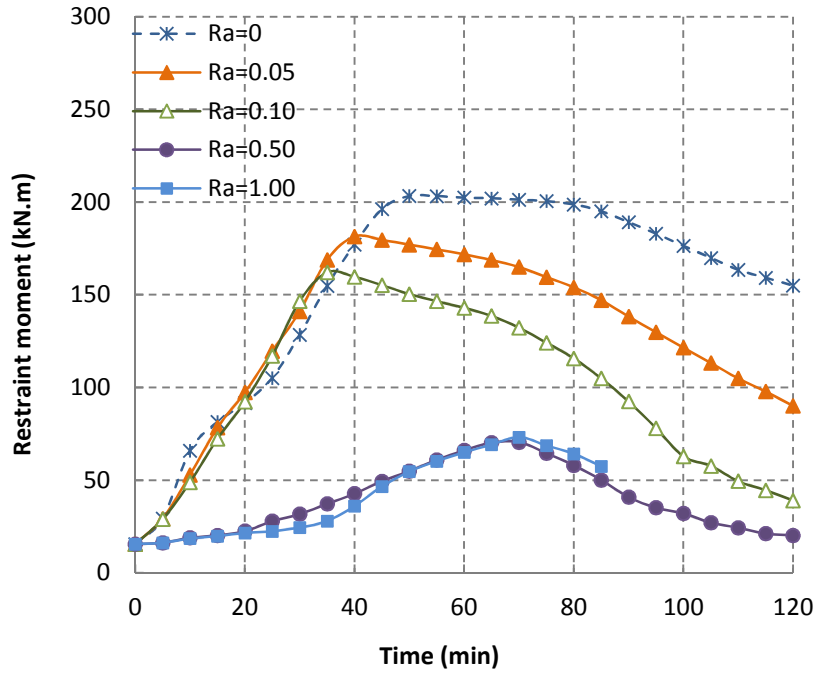
(a) Restraint moments for beams with various axial restraints ($\gamma_{rot}=0.05$)



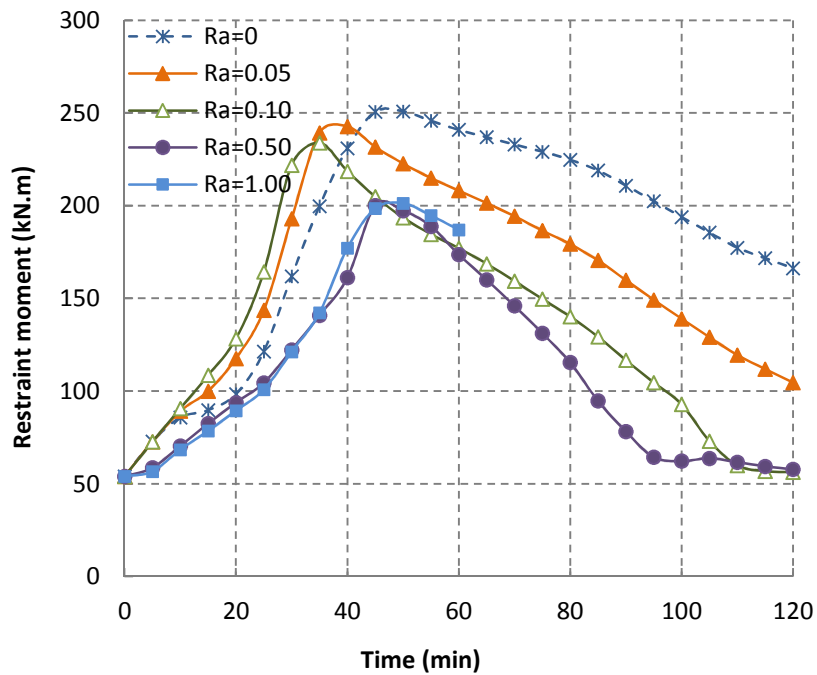
(b) Restraint moments for beams with various axial restraints ($\gamma_{rot} = 0.10$)



(c) Restraint moments for beams with various axial restraints ($\gamma_{rot} = 0.50$)



(d) Restraint moments for beams with various axial restraints ($\gamma_{rot} = 1.0$)



(e) Restraint moments for beams with various axial restraints ($\gamma_{rot} = fixed$)

Figure 6.18 Restraint moments for beams with various axial and rotational restraints

From the comparison of the restraint moments of the beams with various axial and rotational restraints, it can be concluded that:

(1) The restraint moment is generally increasing with heating time at the early stage, and then tend to decrease during the later stage, which is due to the soften of the member under elevated temperatures. It is obvious that for rotationally restrained beams, the restraint moments are increasing with rotational restraint factors, a large restraint factor lead to a large restraint moment. Therefore, from Figure 6.18 (a) to (e), the restraint moments are comparatively larger.

(2) From the comparison of the figures for the same rotational restraint factor but with various axial restraints, it can be conclude that the restraint moment is also influenced by the axial restraint ratios. Their increases are greatly restrained by the axial force. A larger axial restraint factor leads to a comparatively smaller end moment, and smaller maximum moment. The axially free beam has the largest restraint moment and the axially fixed beam experience the smallest restraint moment although they fail earlier.

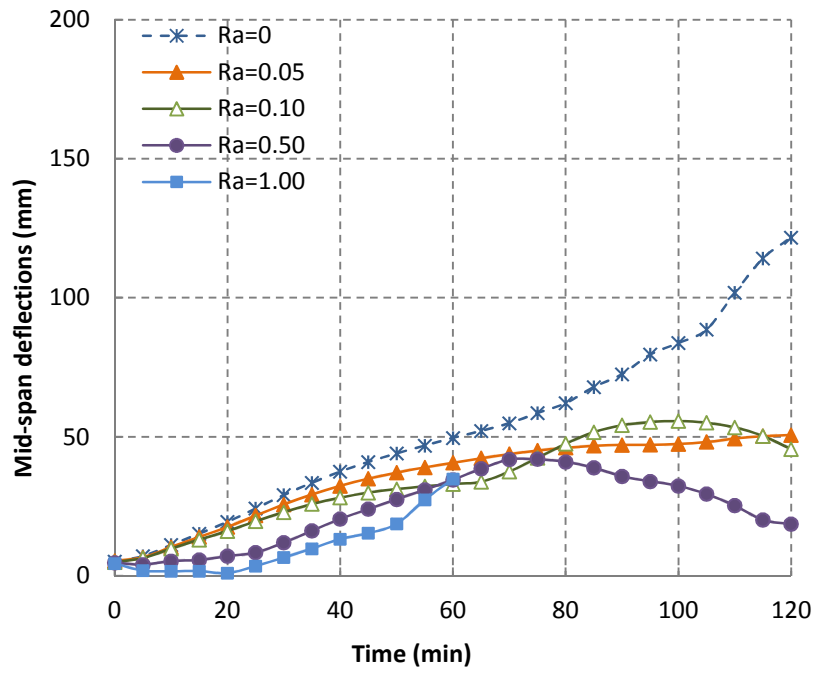
(3) For all the eight series of rotationally restrained beams, the restraint moments could significantly reduce the mid-span moment. This shows that the rotational restraints can improve the fire-resistance behaviour of axially restrained RC members subjected to bending. While this beneficial influence is obvious for weakly axially restrained members, it is not so effective for strongly axially restrained members.

(4) The bearing capacity of the supports, which is heated from the compressive side of the cross-section, is decreasing sharply with the increasing axial force. So the members with fixed axial restraints fail in a short heating time because of the bearing capacity of the supports is reached, so that for the members with $\gamma_{axi} = 1.0$.

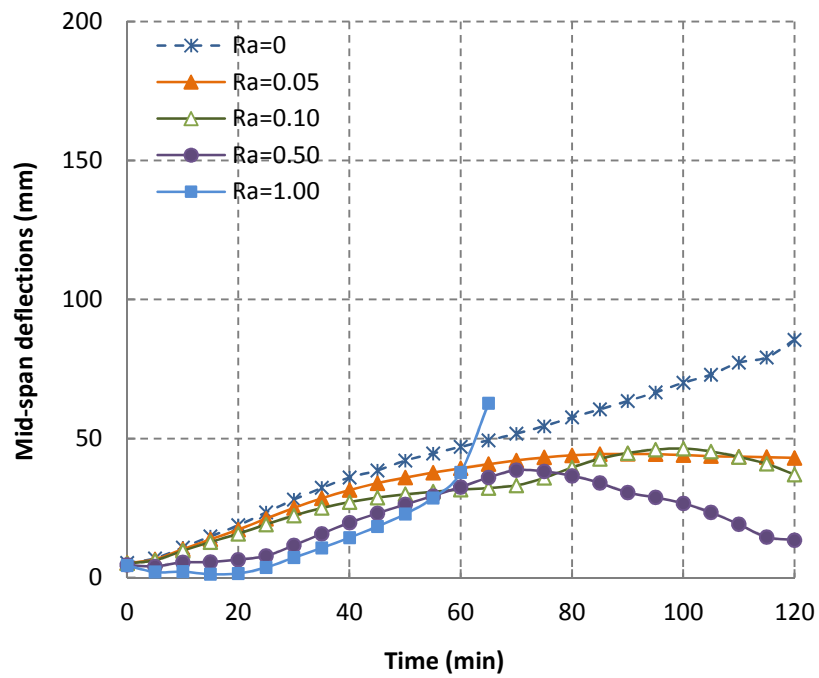
III. Comparison of the mid-span deflections

The development of the mid-span deflections for the different levels of axial restraints are shown by Figure 6.19, with (a) $\gamma_{rot} = 0.05$, (b) $\gamma_{rot} = 0.10$, (c) $\gamma_{rot} = 0.5$, (d) $\gamma_{rot} = 1.0$, and (e)

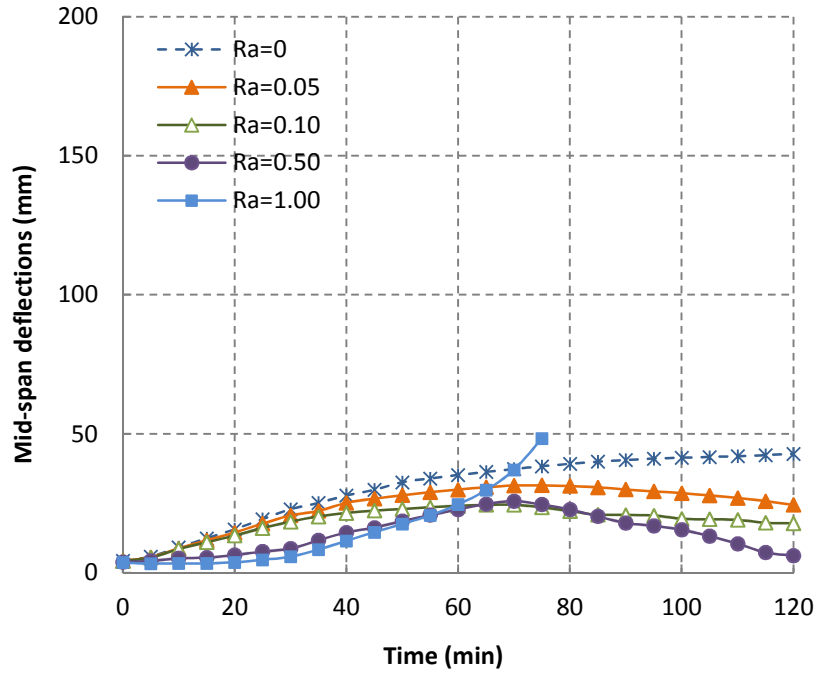
$\gamma_{rot} = fixed$.



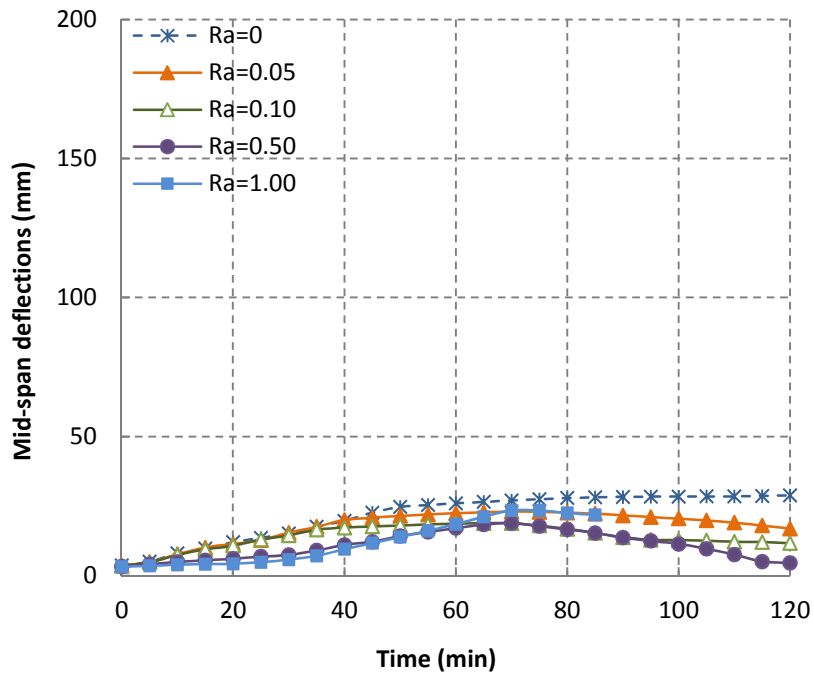
(a) Mid-span deflections of beams with various axial restraints (Ro=0.05)



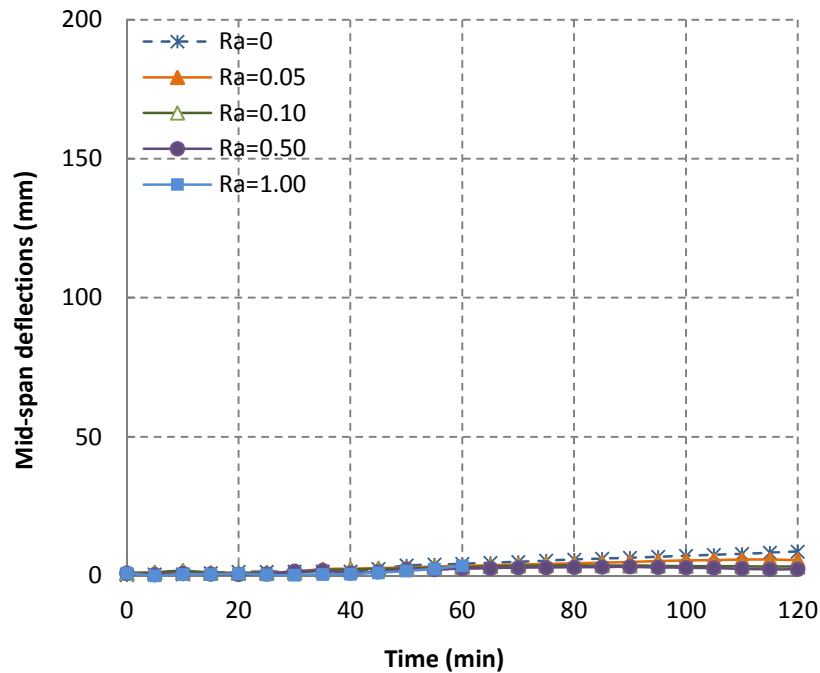
(b) Mid-span deflections of beams with various axial restraints (Ro=0.10)



(c) Mid-span deflections of beams with various axial restraints ($R_o=0.50$)



(d) Mid-span deflections of beams with various axial restraints ($R_o=1.0$)



(e) Mid-span deflections of beams with various axial restraints (R_o =fixed)

Figure 6.19 Mid-span deflections for beams with various axial and rotational restraints

The analysis of the mid-span deflections for rotationally restrained beams with different levels of axial restraint has shown the following:

(1) Similar to the rotationally free members, for all the rotational restrained conditions, it can be seen that the stronger axial restraints lead to smaller mid-span deflections. In these conditions, the mid-span deflection curves will first increase with heating time, and tend to decrease after that. It is again contribute to the conclusion that the axial restraints are beneficial for the controlling of deflections.

(2) The effect of axial restraint ratios on the mid-span deflections of RC beams are influenced by rotational restraints. The increase of rotational restraint ratios leads to a gradually decreasing of the maximum deflections, from the maximum deflection 135 mm in the condition of $R_o=0.05$, Figure 6.19 (a), to less than 10 mm in the rotationally fixed beams, Figure 6.19 (e). Moreover, rotational restraints also lead to smaller difference between mid-span deflections of members with different axial restraints. This means that the rotational restraints can decrease the influence of axial restraints on the fire-behaviour of RC members subjected to bending.

6.3.4 Summary

The analysis of the simplified beams and rotationally restrained beams with varying axial restraints showed that:

(1) Due to the weakening of the material properties during heating, the axial stiffness of the member is actually decreasing with heating time, which makes the axial restraint ratio comparatively increasing. The increasing rate for all the axially restraint factors is the same and can reach 2.7 times of the initial one after 2hrs fire exposure of ISO-834 fire.

(2) For all the axially restrained beams, from simply supported beams with various axial restraints to the rotationally restrained beams with various axial restraints, the axial force increases with heating time and with increasing axial restraint ratios. For weak axial restraint springs, the axial forces continuous rise during the 2hrs of heating, which means they will reach their maximum at a later stage, as the weaker springs allow for more thermal elongation. For strong axial restraints, the axial forces increase sharply at first, and then the increase slows down with heating time or even keeps constant at the later stage until its fail.

(3) Due to the second-order effect, in the simply supported members with axial restraints, an increase in bending moment occurs during fire exposure. The stronger axial restraints lead to larger mid-span moments. This could make the member reach its bearing capacity and fail earlier during fire. Therefore, the effective ways of increasing their fire-resistance time are decreasing their service load, increasing their mid-span reinforcement or applying proper rotational restraints.

(4) All beams with some amount of axial restraint have smaller mid-span deflections than the simply supported beam and the stronger the restraints, the smaller mid-span deflections. It can be conclude that the axial restraints contribute to the controlling of thermal deflections of RC members. However, strong axial restraint will decrease the fire-resistance time of the RC members. For rotationally free members, the failure is due to the bearing capacity (ultimate moment) of the mid-span is reached. For rotationally restrained members it is due to the bearing capacity of the supports is reached.

(5) The effect of axial restraints on the mid-span deflections of RC beams is influenced by rotational restraints. The increase of rotational restraint ratios leads to a gradually decreasing of the maximum deflections, and a smaller difference between mid-span deflections of members with different axial restraints. This means that the rotational restraints can decrease the influence of axial restraints on the fire-behaviour of RC members subjected to bending.

6.4 Fire behaviour of beams with various rotational restraints

This section describes the numerical analysis of single RC beams with various rotational restraints subjected to the standard fire, including the simulation of a set of axially free beams with various rotational restraints and a set of axially restrained beams with various rotational restraints. The purpose of the analysis is to investigate the effect of rotational restraints on the structural behaviour and fire resistance of RC beams.

6.4.1 Survey of the simulations

According to the introduction on the effect of rotationally restrained beams and the objective of this chapter, two general models are analysed:

(1) Axially free beams with varying rotational restraints. Under this condition, the axial deformations are not restrained, which means $\gamma_{axi} = \gamma_{axi}' = 0$ and the axial force $N_{thermal} = 0$.

Therefore, the bending moment only contains two parts, the moment applied by the loading system and the thermal moment caused by the rotational restraints. This condition is typical for the spans of continuous beams, or one-way slabs as introduced in section 4.5.3. So there are actually two groups of models simulated and compared in this section: 1) Firstly, the slabs introduced in chapter 4.5.3 are simulated with designed rotational restraint springs, with the spring stiffness varying from 0 to fixed, including: 0.1, 0.3, 0.5, 1.0, 2.0, 4.0 and fixed. 2) Secondly, the beam model introduced in section 6.2 is simulated and compared with no axial restraint but various rotational restraints.

(2) Axially restrained beams with varying axial restraints. These beams are partly or completely axially restrained at the ends $\gamma_{axi} = \gamma_{axi}' > 0$. The axial restraint for this part are set to be 0.05, 0.1, 0.5, 1.0 and fixed. These conditions fit for the beams in a frame, which may have both axial and rotational restraints transferred from the connected beams and columns.

The beams in these two conditions are modelled with several different levels of rotational restraints, ranging from no restraint to complete rotational restraint. The spring stiffness adopted in this chapter is including 0, 0.05, 0.1, 0.5, 1.0 and fixed.

6.4.2 Axially free but rotationally restrained slabs

In order to have a general idea of the influence of rotational restraints on fire-resistance of RC elements subjected to bending, the typical rotationally restrained member, which is the mid-span of a continuous slab, with both ends rotationally restrained with a same restrained ratio is

simulated. The slab model is the same with the slab V5_a that was introduced in Chapter 4 (section 4.5.3), and is simulated with various rotational restraints. The rotational restraint factors for the restrained ends are considered as 0.1, 0.3, 0.5, 1.0, 2.0, 4.0 and fixed. (1) For the first simulation model V5_a: the restraint moment at the end of the member and the mid-span deflections of the slabs under different restraint ratios are compared. Figure 6.20 shows the restraint moments at the ends, and Figure 6.21 shows the mid-span deflections under these restraint moments. The legend “Ro” in the figures respect for the rotational restraint ratio γ_{rot} .

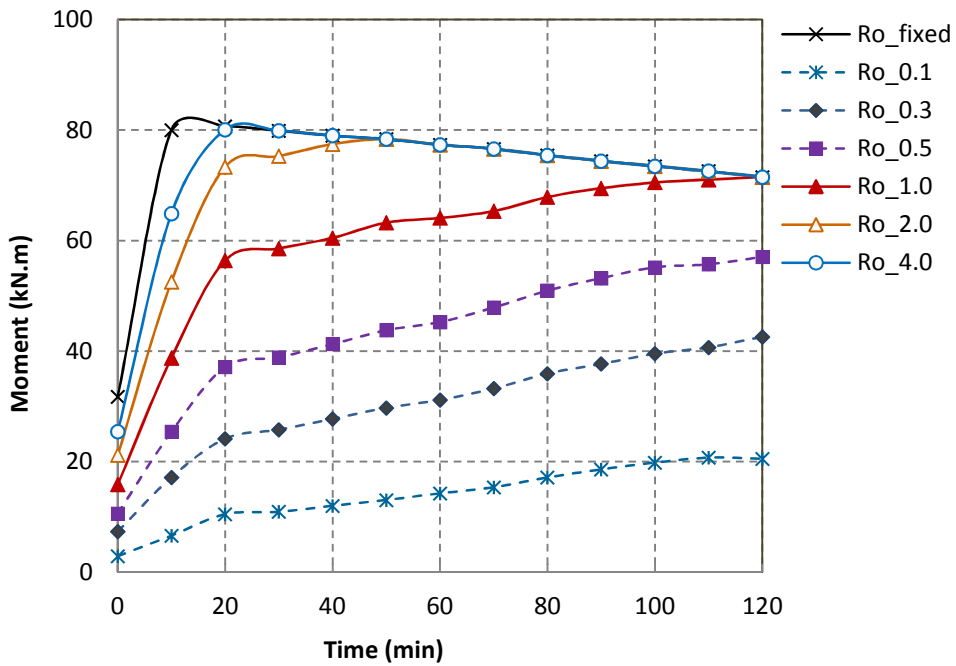


Figure 6.20 Restraint moments of V5_a with various rotational restraint ratios

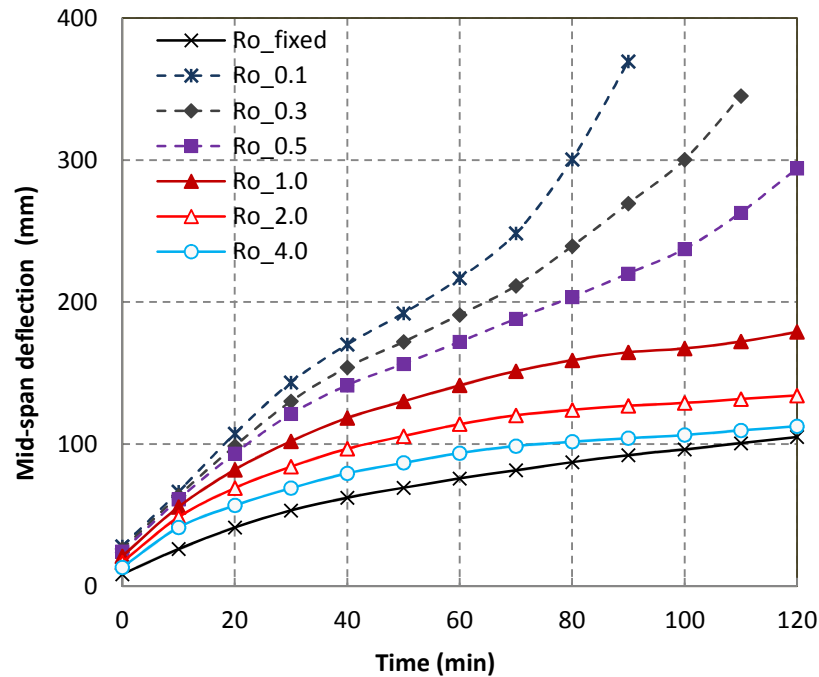


Figure 6.21 Mid-span deflections of V5_a with various rotational restraint ratios

From Figure 6.20 it can be seen that the rotational restraint moments at the ends increases with heating time, and the bigger restraint ratios lead to a larger thermal restraint moment. Since the restraint ratio will increase with heating time due to the decrease of the bending stiffness of the member exposed to fire, when the rotational restraint is big enough, which is larger than 1.0 in this case, the ultimate thermal restraint moment will approach the same value of the one with fixed rotational restraints. Due to the sharp increase of the restraint moment, the negative moment at the two restraint supports should be considered for fire resistance design. Extra reinforcement should be placed for resisting the negative moment.

Based on the failure criterion introduced before, 225 mm is the critical mid-span deflection. We can observe failure of the ones with smaller rotational restraint ratios: the slab with $\gamma_{rot} = 0.1$ fails at 65 min of heating time, the slab with $\gamma_{rot} = 0.3$ fails at 75 min of heating time and the one with $\gamma_{rot} = 0.5$ fails at 95 min of heating time. The comparison of the mid-span deflection curves of a same slab with different rotational restraints shows that members with stronger rotational restraints will have lower mid-span deflections during fire exposure. It can be concluded that the rotational restraints are beneficial for increasing the fire-resistance time of RC elements subjected to bending. The same holds for the restraint moment as shown by Figure 6.20. The effect of increasing the rotational restraint ratio on the increase

of the fire resistance of RC members is obvious when the initial restraint ratio is small, and becomes not sensitive anymore once the restraint stiffness is large enough which in this case appears to be 1.0.

6.4.3 Axially free but rotationally restrained beams

The beam model introduced in this chapter is also simulated and studied for the effect of various rotational restraints. The beams are axially free but with various rotational restraint factors including 0.05, 0.1, 0.5, 1.0, and fixed. Since the axial force are remains zero, only two items are discussed, the restraint moments and the mid-span deflections. The legend “Ro” in the following figures respect for the rotational restraint ratio γ_{rot} .and “Ra” respect for the axial restraint ratio γ_{axi} .

I. Comparison of the restraint moments

The rotational stiffness of the members is decreasing during the fire exposure process (shown by Figure 6.22), and the restraint factors are comparatively increasing with temperature, as shown by Figure 6.23.

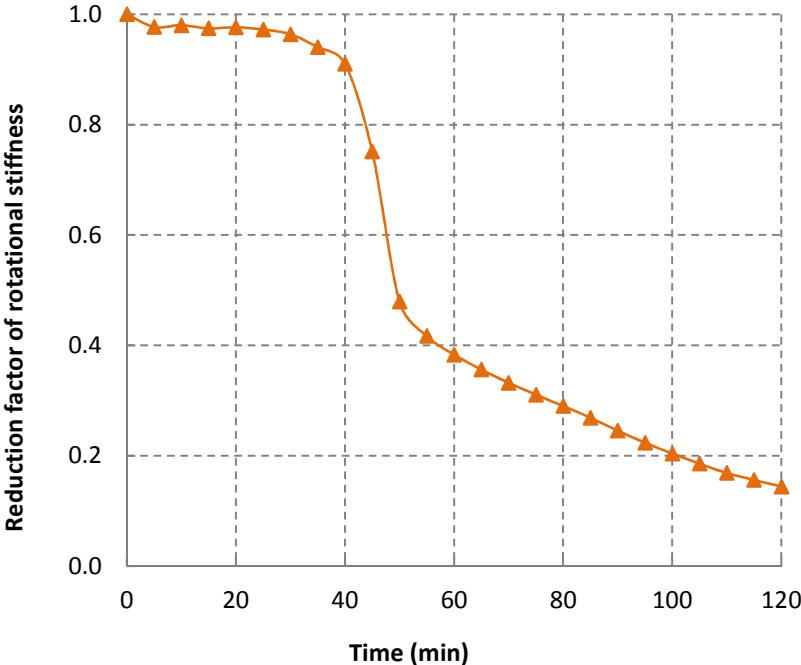


Figure 6.22: The reduction factor of the rotational stiffness with fire exposure time

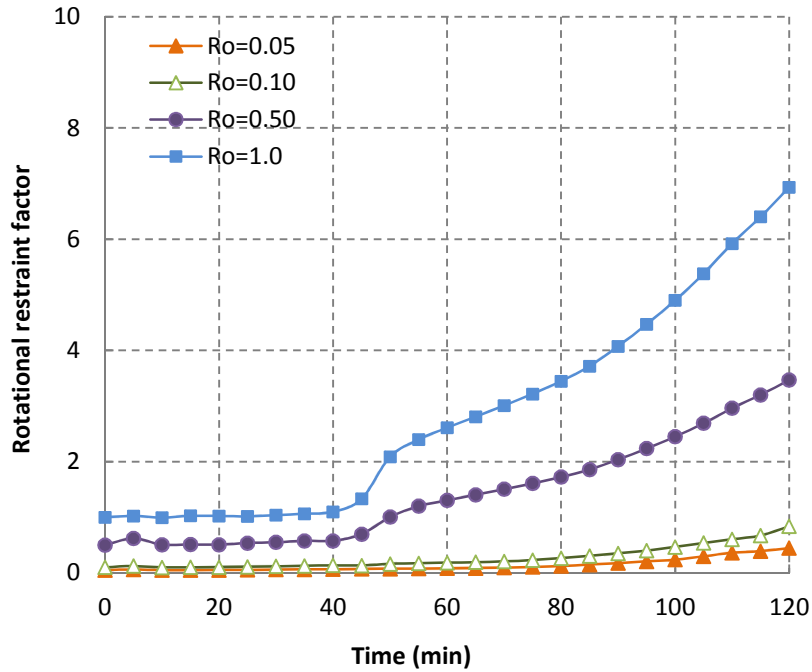


Figure 6.23: The increasing factor of rotational restraint factors with fire exposure time

As we already introduced, the bending stiffness of the beams is also decreasing with fire exposing time. It is going to decrease sharply after a period of heating, 40 min in this case. After 2 hrs. of exposing to ISO-834 standard fire, it can decrease to be 0.14 of the initial. Due to the decrease of the stiffness of the member, the restraint factor is comparatively increasing with temperature.

Figure 6.24 shows the restraint moments at the supports of the beams.

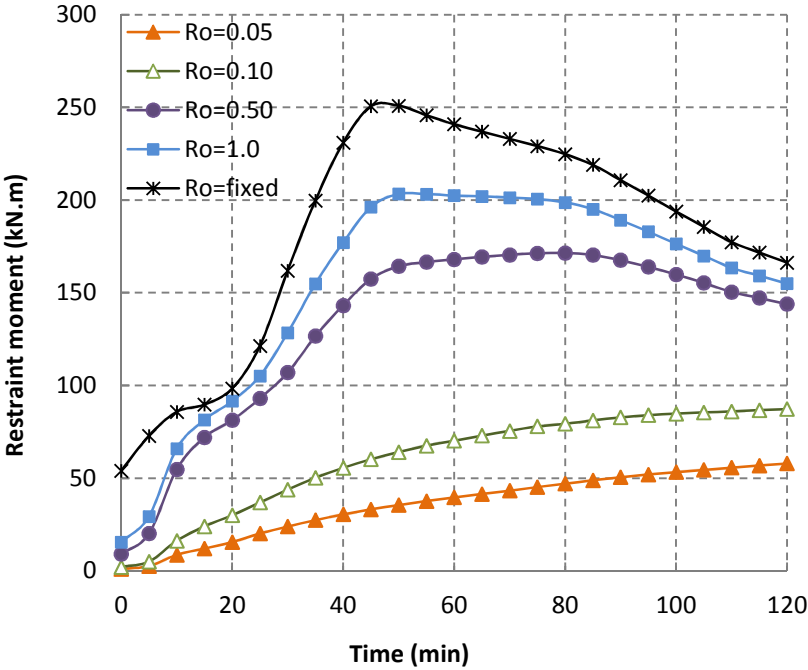


Figure 6.24 Restraint moments of the axially free beam with various rotational restraints

From Figure 6.24 it can be concluded that, for small restraint ratios, the restraint moments are increasing with heating time. However, for stronger restraints in this case when $r_{rot} \geq 0.5$, the restraint moment first increases with heating time but later on, even if the thermal curvature is still increasing with heating time, due to the severe decrease of the bending stiffness of the member, the restraint moment tends to decrease. The comparison of different restraint ratios, the restraint moment of the beams shows a similar trend as that of the slabs. For strong rotational restrained members, due to the sharp increase of the restraint ratio, the final restraint moments are close to the fixed one.

II. Comparison of the mid-span deflections

Figure 6.25 shows the mid-span deflections under these restraint moments.

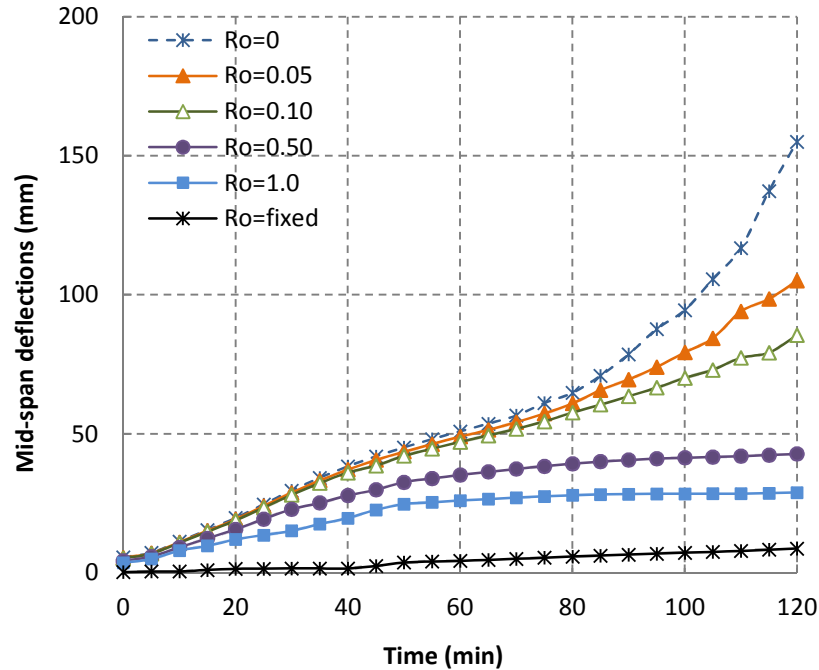


Figure 6.25 Mid-span deflections of the axially free beam with various rotational restraints

All the rotationally restrained members simulated stay well after 2 hrs. of fire. The mid-span deflections of the beams are greatly reduced by the rotational restraints, the bigger rotational restraint ratio leads to a smaller mid-span deflection. This gives a great support on the conclusion that the rotational restraints are beneficial for the fire resistance behaviour of RC members subjected to fire.

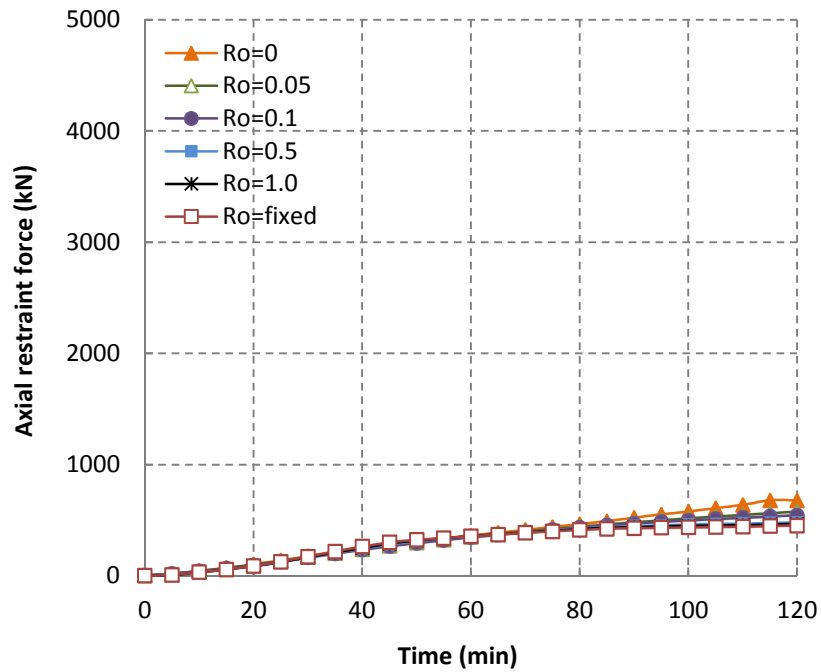
6.4.4 Axially restrained beams with various rotational restraints

This section discusses the behaviour of the axially restrained beams with varying levels of rotational restraint exposed to the 2-hours ISO-834 standard fire. The axial spring stiffness are designed to be 0.05, 0.1, 0.5, 1.0, and fixed. The rotational spring stiffness for each axially restrained condition ranges from no restraint to rotationally fixed, including 0, 0.05, 0.1, 0.5, 1.0, and fixed. The legend “Ro” in the following figures respect for the rotational restraint ratio γ_{rot} .and “Ra” respect for the axial restraint ratio γ_{axi} .

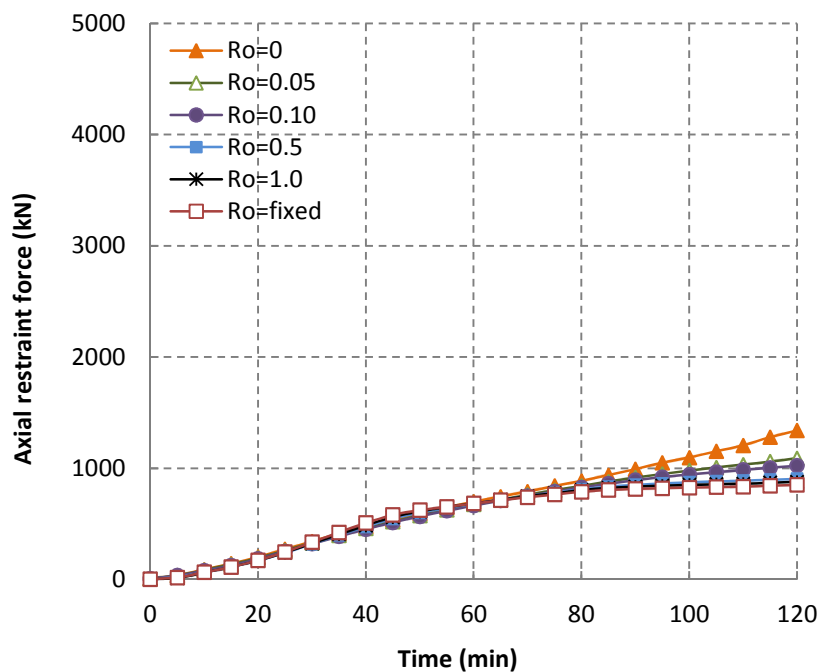
I. Comparison of the axial forces

The development of the axial forces during the fire exposure for the beams of different levels of rotational restraints are shown by Figure 6.26, with (a) $\gamma_{axi} = 0.05$, (b) $\gamma_{axi} = 0.1$, (c)

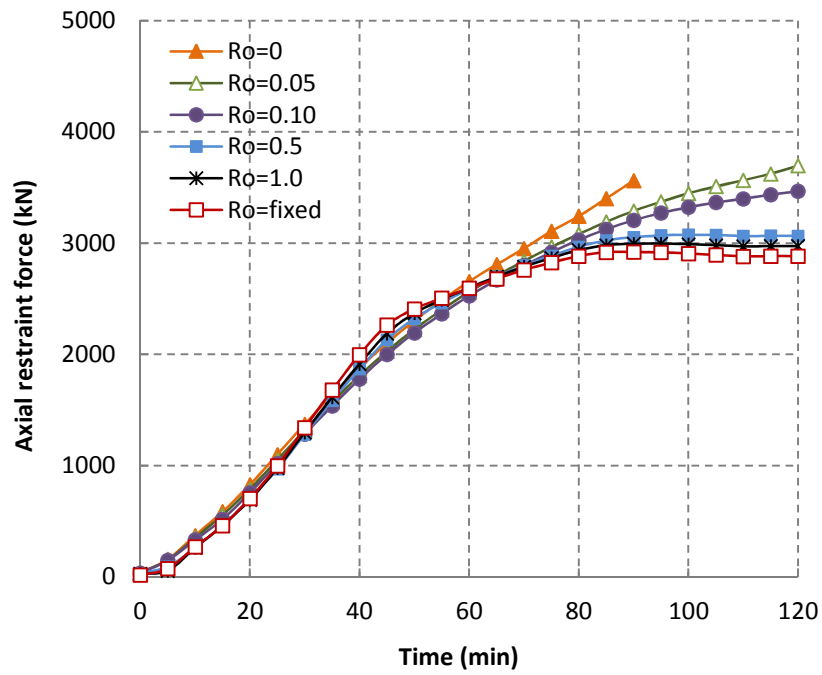
$\gamma_{axi} = 0.5$, (d) $\gamma_{axi} = 1.0$. As all the members with $\gamma_{axi} = fixed$ were failed quite early due to the failure of the supports, the curves for the axial force of them are not shown.



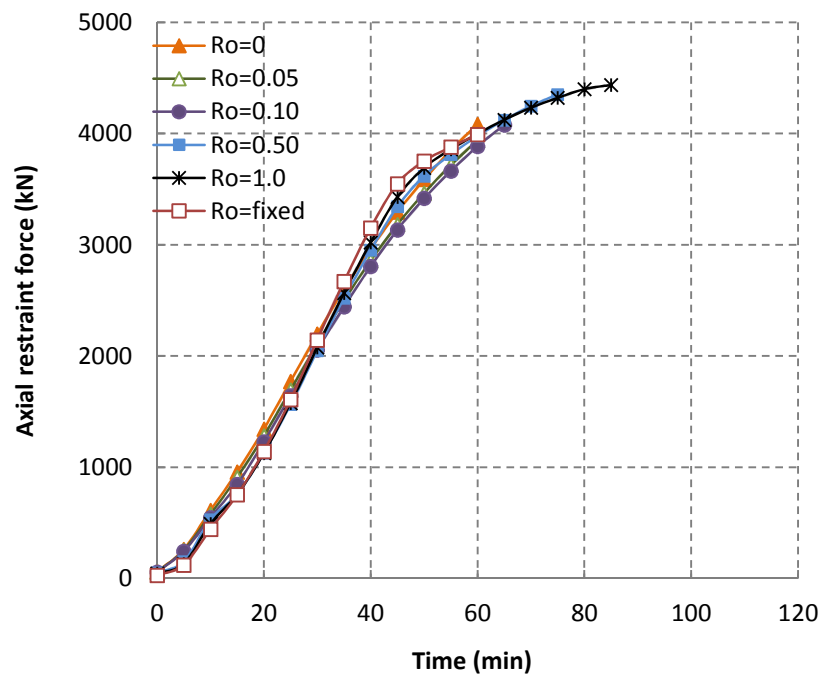
(a) Axial forces for beams with various rotational restraints ($\gamma_{axi} = 0.05$)



(b) Axial forces for beams with various rotational restraints ($\gamma_{axi} = 0.10$)



(c) Axial forces for beams with various rotational restraints ($\gamma_{axi} = 0.50$)



(d) Axial forces for beams with various rotational restraints ($\gamma_{axi} = 1.0$)

Figure 6.26 Axial forces of the beam with various axial and rotational restraint ratios

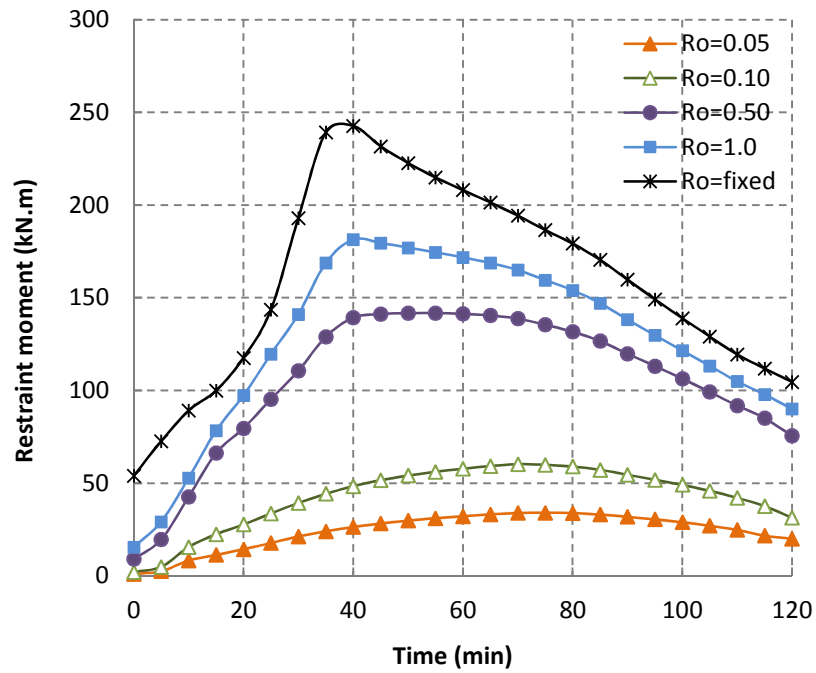
From the comparison of axial forces of axially restrained beams with various rotational restraints shown by Figure 6.26, we can make the following conclusions:

(1) The axial forces of all the beams with various rotational restraints are increasing with heating time. They have little difference at the early stage, and the increase of the ones for larger rotational restraints slows down or even keeps constant at the later stage. The rotational fixed beams have the smallest thermal restraint axial forces, which strongly reduced the mid-span bending moments caused by the second-order effects. From Figure 6.26 (a) to 6.26 (d), the difference between axial forces of various rotational restraints is decreasing, and for the members with $\gamma_{axi} \geq 1.0$ they are nearly the same. From this, it can be conclude that the effect of rotational restraints on the axial force is limited for strong axial restrained members.

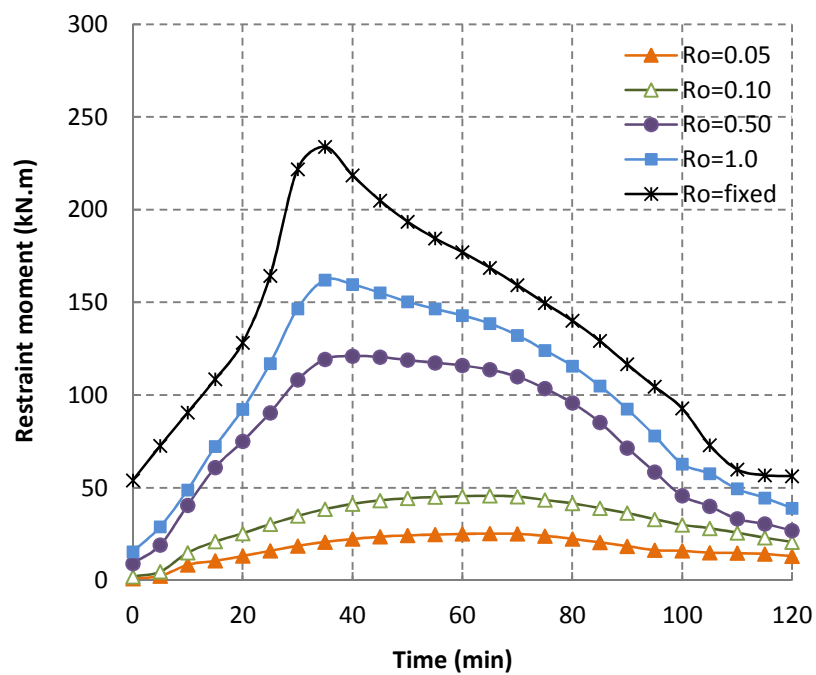
(2) As introduced before, section 6.3.3, the axial forces of beams with stronger axial restraints are larger, and strong axial restraints lead to shorter fire-resistance time. According to the comparisons from Figure 6.26(c) and 6.26(d), for members with a same axial restraint, stronger rotational restraints lead to longer fire-resistance time besides the rotationally fixed one. This contributes to the conclusion that rotational restraints are benefit to improve the fire-resistance of the RC members.

II. Comparison of the restraint moments

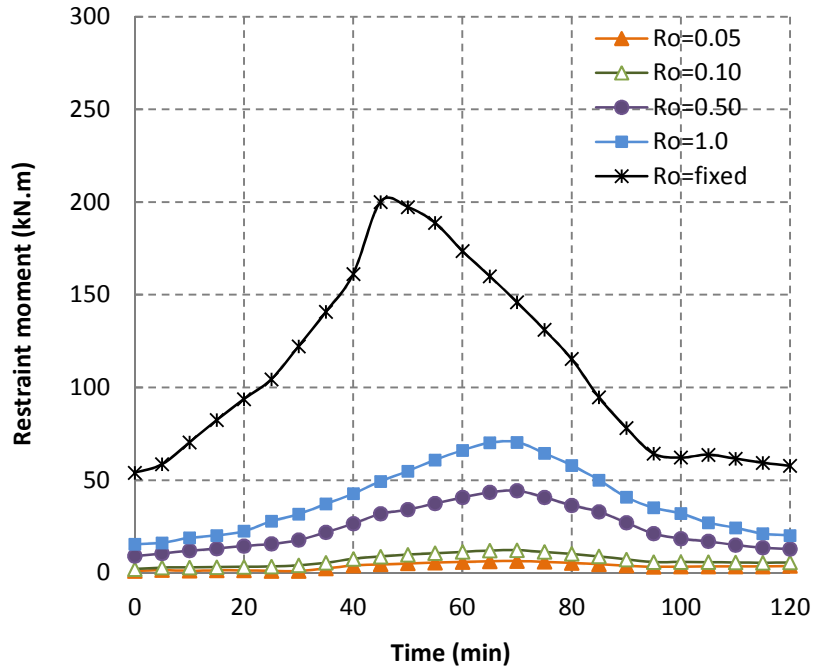
The development of the restraint moments at the supports during the fire exposure for the beams of different levels of rotational restraint are shown by Figure 6.27, with (a) $\gamma_{axi} = 0.05$, (b) $\gamma_{axi} = 0.1$, (c) $\gamma_{axi} = 0.5$, (d) $\gamma_{axi} = 1.0$. The curves for the restraint moments of members with $\gamma_{axi} = fixed$ are not shown.



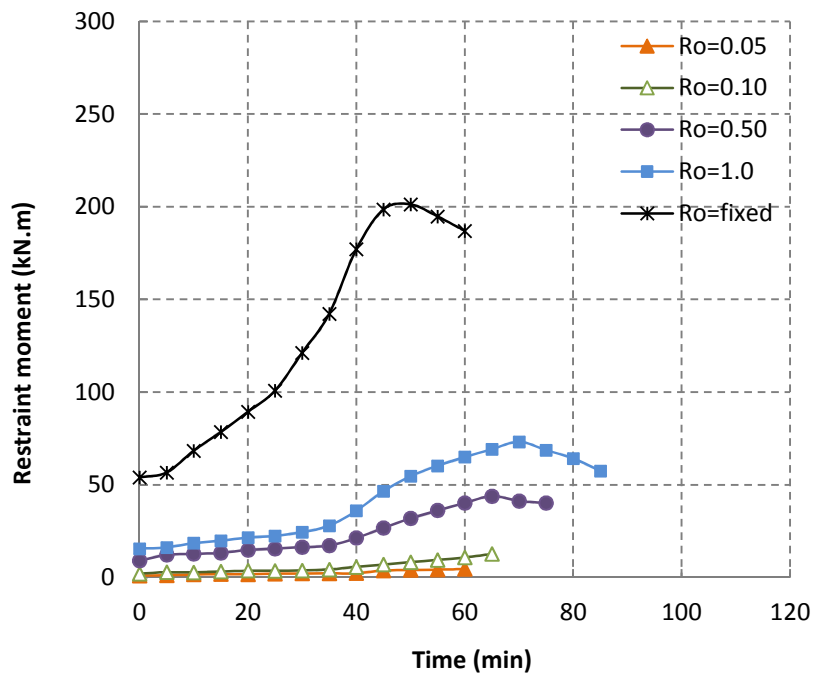
(a) Restraint moments for beams with various rotational restraints ($\gamma_{axi} = 0.05$)



(b) Restraint moments for beams with various rotational restraints ($\gamma_{axi} = 0.1$)



(c) Restraint moments for beams with various rotational restraints ($\gamma_{axi} = 0.5$)



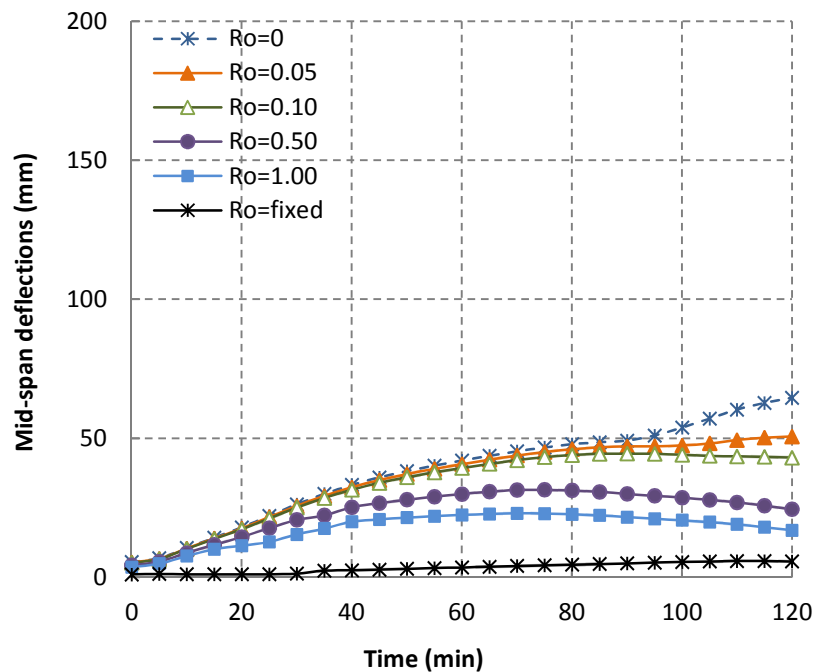
(d) Restraint moments for beams with various rotational restraints ($\gamma_{axi} = 1.0$)

Figure 6.27 Restraint moments for the beams with various axial and rotational restraints

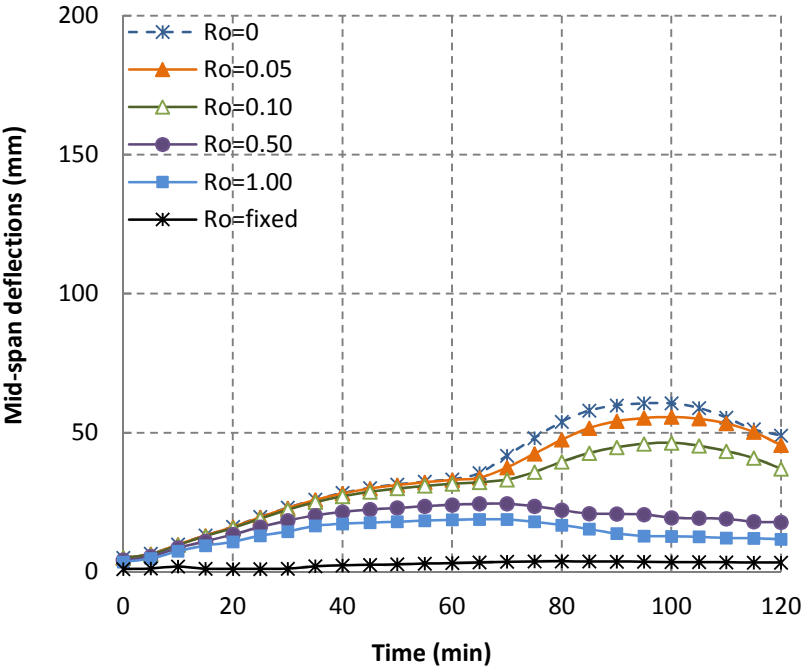
The figures for the restraint moments of axially restrained beams with various rotational restraints show that the restraint moment increases with heating time at the early stage, and after they reach their maximum, they tend to decrease during the later heating stage. The stronger rotational restraints lead to larger restraint moments at the same heating time, and the restraint moments grow faster to their maximum point. The comparison of restraint moments from Figures 6.27(a) to 6.27 (d) shows that with the increase of the axial restraint ratios, the maximum restraint moments are gradually decreasing, and the gaps between the curves of various rotational restraints getting smaller. This means that the difference of rotational restraints have great influence on the fire resistance behaviour of members with weak axial restraints, but this difference turns to be not so obvious in beams with strong axial restraints. Therefore, it can be conclude that the effect of the rotational restraints can be reduced by the axial restraints.

III. Comparison of the mid-span deflections

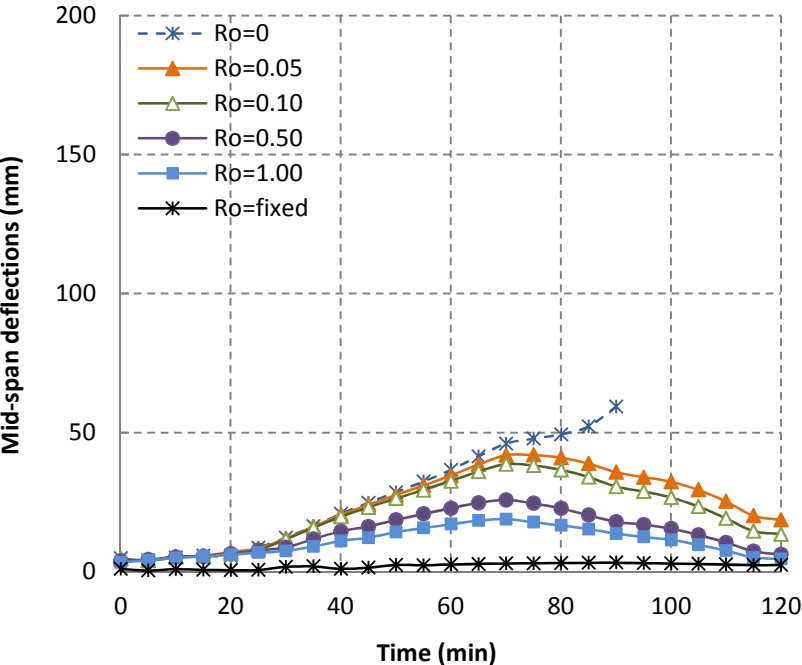
The development of the mid-span deflections for the beams of different levels of rotational restraint are shown by Figure 6.28, with (a) $\gamma_{axi} = 0.05$, (b) $\gamma_{axi} = 0.1$, (c) $\gamma_{axi} = 0.5$, (d) $\gamma_{axi} = 1.0$. The curves for the restraint moments of members with $\gamma_{axi} = fixed$ are not shown.



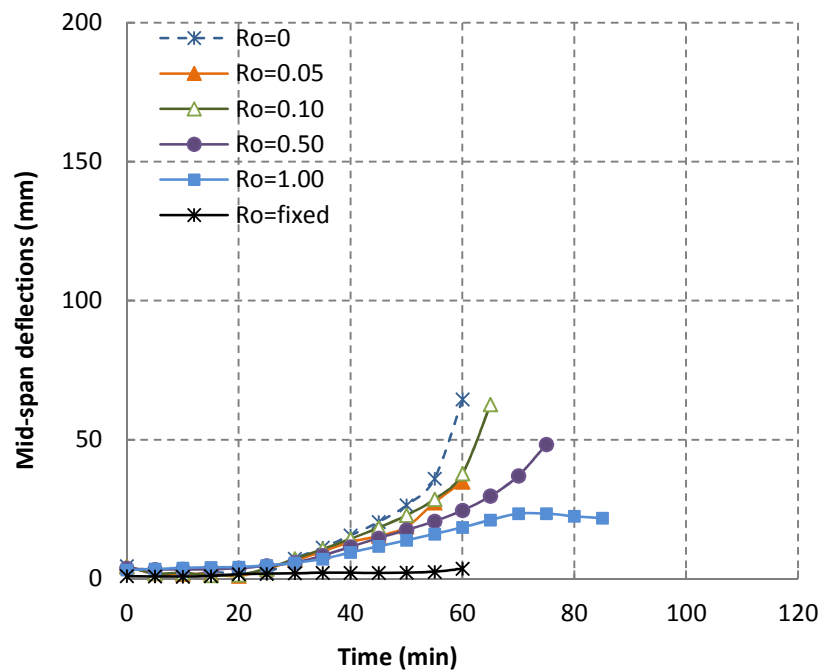
(a) Mid-span deflections for beams with various rotational restraints ($\gamma_{axi} = 0.05$)



(b) Mid-span deflections for beams with various rotational restraints ($\gamma_{axi} = 0.1$)



(c) Mid-span deflections for beams with various rotational restraints ($\gamma_{axi} = 0.5$)



(d) Mid-span deflections for beams with various rotational restraints ($\gamma_{axi} = 1.0$)

Figure 6.28 Mid-span deflections for the beams with various axial and rotational restraints

It can be seen from Figure 6.28 that the mid-span deflections are greatly influenced by the rotational restraints. The strong rotational restraints will severely limit the mid-span deflection and for rotationally fixed beams, the mid-span deflections are smaller than 5mm during the complete heating process. This also contributes to the conclusion that the rotational restraints are beneficial for the fire-resistance behaviour of RC members that subjected to bending, and the stronger rotational restraints have a greater effect.

Based on the comparisons from Figure 6.28 (a) to (d), the maximum mid-span deflections of the rotational restraints are smaller with the increase of axial restraints, from which we could see that the effect of rotational restraints are influenced by the axial restraint ratios besides the rotationally fixed condition. The stronger axial restraints lead to smaller difference between the deflections of members with various rotational restraints. This contributes to the conclusion that the effect of rotational restraints is reduced by the axial restraints.

For the strong axially restrained beams, the effect of rotational restraints is still important although the members break earlier. The rotational restraints in a certain range can increase

the fire-resistance time of the axially restrained members until they are strong enough and cause the failure of the supports.

6.4.5 Summary

The analysis of the axially free and axially restrained beams with varying rotational restraints has shown that:

(1) The thermal moment caused by the rotational restraints are increasing with heating time. For the members with stronger rotational restraints, the restraint moments at the supports reach their maximum earlier than the weaker ones. Therefore, for the supports of the rotationally restrained members, extra reinforcement should be placed for resisting the negative moment.

(2) The axial forces of all the beams with various rotational restraints are increasing with heating time. The beams with strong rotational restraints experience smaller axial forces, and the rotationally fixed beams have the smallest thermal restraint axial force, which greatly reduces the mid-span bending moments caused by the second-order effects.

(3) The restraint moments of axially restrained beams with various rotational restraints increase with heating time and rotational restraint ratios. The restraint moments of beams with stronger rotational restraints grow faster with heating time and lead to a larger restraint moment at the same heating time. The difference of rotational restraints have great influence on the fire resistance behaviour of members with weak axial restraints, but this difference turns to be not so obvious in beams with strong axial restraints. Therefore, it can be seen that the effect of the rotational restraints can be reduced by the axial restraints.

(4) The mid-span deflections are greatly influenced by the rotational restraints. The strong rotational restraints will severely limit the mid-span deflection and for rotationally fixed beams, the mid-span deflections are not influenced by the axial restraint stiffness. This means that the rotational restraints are beneficial for the fire-resistance of RC members that subjected to bending, and the greater rotational restraints have a larger effect. The maximum mid-span deflections of the rotational restraints are smaller with the increase of axial restraint, from which we can see that the effect of rotational restraints are influenced by the axial restraint ratios.

6.5 General Conclusions

In order to have a profound understanding of RC members in real structures, which are

restrained axially and rotationally by the surrounding members when exposed to fire, the simplified multi-iteration analysis method proposed in Chapter 4 is applied in this chapter. Series of beam models are simulated under ISO-834 standard fire: (1) simply supported beams with various axial restraints; (2) rotationally restrained RC beams with various axial restraints; (3) axially free RC beams with various rotational restraints, and (4) axially restrained RC beams with various rotational restraints. The comparison of the simulation results are used to analyse the effect of restraints on the fire-resistance behaviour of RC beams. Based on the information presented in this chapter, the following conclusions can be drawn.

(1) Due to the weakening of the material properties during heating, the stiffness of the member is actually decreasing with heating time, which makes the axial and rotational restraint ratios comparatively increasing. The increasing rate for all the axially restraint ratios is the same while that for rotational restraint ratio is different.

(2) Due to the second-order effect, an increase in bending moment occurs in the simply supported members with axial restraints during fire exposure. The stronger axial restraints lead to larger mid-span moments. This could make the member reach its bearing capacity and fail earlier during fire. Therefore, the effective ways of increasing their fire-resistance time are decreasing their service load, increasing their mid-span reinforcement or applying proper rotational restraints.

(3) All beams with some amount of axial restraint have smaller mid-span deflections than the simply supported beam and the stronger the restraints, the smaller mid-span deflections. It can be conclude that the axial restraints contribute to the controlling of thermal deflections of RC members. However, strong axial restraint will decrease the fire-resistance time of the RC members. For rotationally free members, the failure is due to the bearing capacity (ultimate moment) of the mid-span is reached. For rotationally restrained members it is due to the bearing capacity of the supports is reached.

(4) The effect of axial restraints on the mid-span deflections of RC beams is influenced by rotational restraints. The increase of rotational restraint ratios leads to a gradually decreasing of the maximum deflections, and a smaller difference between mid-span deflections of members with different axial restraints. This means that the rotational restraints can decrease the influence of axial restraints on the fire-behaviour of RC members subjected to bending.

(5) The beams with stronger rotational restraints experience smaller axial forces and larger rotational restraint moments. The mid-span deflections are greatly influenced by the rotational restraints. The strong rotational restraints will severely reduce the mid-span deflection and for rotationally fixed beams, the mid-span deflections are not influenced by the axial restraint

stiffness. This means that the rotational restraints are beneficial for the fire-resistance of RC members subjected to bending, and the greater rotational restraints have larger effect.

(6) The rotational restraints are beneficial for the fire-resistance behaviour of RC members subjected to bending, and this beneficial effect is influenced by the axial restraints. The difference between members with various rotational restraints becomes smaller with the increase of axial restraint, from which we can see that the effect of rotational restraints will be reduced by the axial restraint ratios

Conclusions and suggestions

This final chapter summarizes the main conclusions of the research project and the main contributions to the research field. Also some suggestions recommendations for future research are given.

7.1 Summary of the research project and conclusions

This research project was conducted to study the effect of various support conditions on the fire behaviour of reinforced concrete members subjected to bending. A simplified multi-iteration method is first proposed and is validated by available experimental results. Next, parametric studies have been carried out with this approach and the influence of various restraint conditions on the fire behaviour of reinforced concrete beams are compared and analysed. The main conclusions and the contributions of this research are given below:

(1) A simplified multi-iteration method is proposed and validated to be practical and accurate.

A simplified numerical model was developed to simulate the fire performance of reinforced RC members related to bending. The numerical model is based on the temperature field of the cross-section and the mechanical properties of concrete and reinforcing steel at elevated temperatures. A multi-iteration process is carried out in order to reach force equilibrium, and an equivalent bending stiffness is defined for the structural analysis. A moment-curvature (M-k) relationship can be generated at the sectional analysis process for a given axial force. The curvature caused by thermal expansion as well as the ultimate moment of the RC member at elevated temperatures can be calculated according to the M-k relationship. The proposed model is user friendly and allows inputting user defined material models, fire curves, and restraint stiffness. The proposed method was validated by fire tests executed on simply supported slabs and rotationally restrained slabs exposed to the ISO-834 standard fire. It is proved to be practical and time effective for fire performance simulations.

(2) Parametric analysis on the difference of fire behaviour of RC members simulated with transient creep strain considered implicitly and explicitly.

The parametric study of the fire performance of RC members with an implicit and an explicit transient creep strain model shows that the calculations become slightly more accurate when transient creep strain is considered explicitly. The deflections for RC elements during fire related to bending like beams and one-way slabs will be slightly overestimated with the material model in EC 2. From this it can be concluded that the influence of different transient creep strain models can be neglected in most of the cases for beams and slabs subjected to bending. The sensitivity analysis on the differences in deflections with implicit and explicit transient creep models shows that: 1) the difference increases with heating time; 2) it can be reduced by increasing the reinforcement area; and 3) it is not sensitive to the size of the cross-section.

(3) Influence of restraints on the fire resistance of RC members subjected to bending.

Four series of beam models are simulated under the ISO-834 standard fire: 1) simply supported beams with various axial restraints; 2) rotationally restrained RC beams with various axial restraints; 3) axially free RC beams with various rotational restraints and 4) axially restrained RC beams with various rotational restraints. The comparison of the simulation results are used to analyse the effect of restraints and to present some guidelines regarding the fire resistance design of RC beams.

According to the analysis of axial restraints: (1) Due to the second-order effects, the simply supported members with axial restraints experience an increasing bending moment during fire exposure, which has a detrimental effect on the fire resistance of RC members. Therefore, the effective ways of increasing their fire-resistance time are decreasing their service load, increasing their mid-span reinforcement or applying proper rotational restraints. (2) All rotationally restrained beams with some amount of axial restraint have smaller mid-span deflections than the simply supported beam, from which we can conclude that the axial restraints yield a beneficial contribution to the controlling of thermal deflections of RC members. However, strong axial restraint will severely decrease the fire-resistance time of the RC members. (3) The increase of rotational restraint ratios leads to a gradually decreasing of the maximum deflections, and a smaller difference between mid-span deflections of members with different axial restraints. This means that the rotational restraints can decrease the influence of axial restraints on the fire-behaviour of RC members subjected to bending.

According to the analysis of rotational restraints: (1) the thermal moment caused by the rotational restraints are increasing with heating time. For the members with stronger rotational restraints, the restraint moments at the supports reach their maximum earlier than the weaker ones. So for the support of the rotationally restrained members, extra reinforcement should be

provided for resisting the additional negative moment. (2) The mid-span deflection curves of the RC members are reduced by the rotational restraints, the larger rotational restraint ratios lead to smaller mid-span deflections. This supports the conclusion that the rotational restraints are beneficial for the fire-resistance behaviour of RC members subjected to bending. (3) The beneficial effect of rotational restraint on the fire resistance of RC members can be reduced by the axial restraints.

7.2 Suggestions for future research

In this thesis a multi-iteration numerical method for the fire performance simulation has been proposed. Several series of flexural members were simulated in a parametric analysis of different transient creep strain models and various restraint conditions. Additionally, the following topics need further research:

(1) Members of other shapes. Although all the simulations in this thesis are on the rectangular beam and slab cross-sections, the proposed multi-iteration method can also be used for parametric studies and fire resistance research on beams with cross-sections of different shape, e.g. T-beams. So, further research for other shaped RC members can be carried out with the proposed method, not only for members subjected to bending, but also for columns.

(2) Sensitivity analysis of the restraints on the difference of fire performance with implicit and explicit transient creep strain model. Since the comparisons in the parametric studies on the difference of fire performance with implicit and explicit transient creep strain models mainly focused on simply supported RC members subjected to bending, the restraint effect was only studied for a series of members which are not considered in detail. Further research on axially restrained members is suggested.

(3) Fire performance of the complete frame. A single member in a frame with the axial and rotational restraints from the surrounded members simplified into springs is investigated; the results are validated and used for the parametric study of the influence of restraints. However, how these restraint forces affect the other members in the frame is not analysed. The performance of the complete frame still needs to be investigated.

(4) Experimental investigations. The model proposed in the thesis is validated by the fire tests of slabs which were executed in 1979, and the slabs were only rotationally restrained, the axial restraints were not considered. The research on the influence of both axial and rotational restraints is based on numerical simulations. Hence, further experimental research on restrained RC members is necessary.

References

- Abbasi, A., Hogg, P.J. Temperature and environmental effects on glass fiber rebar: modulus, strength and interfacial bond strength with concrete, *Composites: Part B*, 2005, 36: 394-404.
- ACI Committee 216.1, Standard Method for Determining Fire Resistance of Concrete and Masonry Construction Assemblies, American Concrete Institute, Detroit, 2007.
- ACI Committee 216R, Guide for Determining the Fire Endurance of Concrete Elements, American Concrete Institute, Farmington Hills, MI, 2001, 48 pp.
- Ali, F.A., O'Connor, D.J. Structural performance of rotationally restrained steel columns in fire, *Fire Safety Journal*, 2001, 36: 679-691.
- Ali, F.A., Shepherd, P., Randall, M., Simms, I.W., O'Connor, D.J., Burgess, I. The effect of axial restraint on the fire resistance of steel columns, *J Constructional Steel Res*, 1998, 98: 305-306.
- Anderberg, Y. Spalling phenomenon of HPC and OC, in: *Proceedings of the International Workshop on Fire Performance of High Strength Concrete*, Gaithersburg, MD, 1997, NIST SP 919, pp. 69-75.
- Anderberg Y, Forsen N.E. *Fire Resistance of Concrete Structures*. Division of Structural Mechanics and Concrete Construction, Lund Institute of Technology: Lund, Sweden, 1982.
- Anderberg, Y, Thelandersson, S. Stress and deformation characteristics of concrete at high temperatures: experimental investigation and material behaviour model. *Bulletin 54*. Sweden (Lund): Lund Institute of Technology. 1976.
- Annerel, E. Assessment of the residual strength of concrete structures after fire exposure. PhD thesis, Gent University. 2010.
- Annerel, E., Taerwe, L. Approaches for the assessment of the residual strength of concrete exposed to fire. *Proceedings of the international workshop: fire design of concrete structures, from materials modeling to structural performance*, J.P.C., Rodrigues, G.A., Khoury, N.P., Høj, eds. Coimbra: University of Coimbra, 2007. pp. 489-500.
- Annerel, E., De Schutter, G., Microstructure and aesthetic appearance of SCC, De Schutter, G., Boel, V., *Self-Compacting Concrete SCC2007*, *Proceedings of the Fifth International RILEM Symposium Volume 1,3-5, September, 2007*, Ghent, RILEM Publications S.A.R.L., pp:381-386.
- Antonio, J.P., Correia, M., Paulo J., Rodrigues, C. Fire resistance of partially encased steel columns with restrained thermal elongation, *Journal of Constructional Steel Research*,

- 2011, 67: 593-601.
- ASTM E 119-00a, Standard Test Methods for Fire Tests of Building Construction and Materials, ASTM International, West Conshohocken, PA, 2000, 21 pp.
- Bathe K.J. Finite Element Procedures in Engineering Analysis. 1982.
- Beard, A., Carvel, R. The hand book of tunnel fire safety. Press: Thomas Telford London, British, 2005.
- Benmarce, A. Guenfoud, M. Behaviour of axially restrained high strength concrete columns under fire. Construction and Building Materials, 2005, 01(58), pp: 1-6.
- Benmarce, A., Guenfoud, M. Experimental behavior of high-strength concrete columns in fire, Concrete Research, 2005, Vol. 57 (5), pp: 283–287.
- Bernhart, D. The Effect of Supporting Conditions on the Fire Resistance of a Reinforced Concrete Beam. University of Canterbury: Christchurch, New Zealand, 2004, 147p.
- Bratina, S., Saje, M., Planinc, I. The effects of different strain contributions on the response of RC beams in fire. Engineering Structures, 2006, 29:418–430.
- Bratina S, Čas B, Saje M, Planinc I. Numerical modelling of behaviour of reinforced concrete columns in fire and comparison with Eurocode 2. International Journal of Solids and Structures 2005, 42(21-22):5715–33.
- Bratina, S., Planinc, I., Saje M. et al. Non-linear fire-resistance analysis of reinforced concrete beams. Structural Engineering and Mechanics, 2003, 16(6):695-712.
- BSI, Structural use of steel work in building. Part 8, Code of Practice for Fire Resistance Design, 1990.
- BS. Fire tests on building materials and structures-Part 20: Method from determination of the fire resistance of elements of construction. BS476-3: 1987, BSI, UK; 1987
- Buchanan, A.H. Structural Design for Fire Safety, John Wiley & Sons, West Sussex, 2001.
- Cai, J., Burgess, I., Plank, R. A generalized steel/reinforced concrete beam-column element model for fire conditions. Engineering Structures, 2003, 25 pp: 817–833.
- Carlson, C.C.; Selvaggio, S.L.; Gustafarro, A.H. A Review of Studies of the Effect of Restraint on the Fire Resistance of Prestressed Concrete, Portland Cement Association Research and Development Laboratories, Bulletin 206, Skokie, Illinois, 1965.
- Carlson, C.C. Fire resistance of prestressed concrete beams study A-Influence of thickness of concrete covering over prestressing steel strand, Research Development Laboratories of the Portland Cement Association, Research Department, Bulletin 147, 1962.
- Cheng, J.L., Zou, S.H. Simulation of Underground fire. Safety and Environment Engineering, 2006, 13(1): pp 96-99.

References

- Chiang, C.H., Tsai, C.L. Time-temperature analysis of bond strength of a rebar after fire exposure, *Cement and Concrete Research*, 2003, 33:1651-1654.
- Chinese Academy of Engineering, Study on Development and Utilization of Underground Space in Chinese Cities. 2001. Press, China Architecture & Building Press, Beijing, China.
- Church, J.G., Clark, L A. The effect of combined thermal and force loads on the behavior of reinforced concrete beams. *Journal of Structural Engineering*, 1988, 66(16):262-267.
- Cooke, G.M.E. Results of Tests on End-restrained Reinforced Concrete Floor Strips Exposed to Standard Fires. Report prepared for the Construction Directorate of the Department of the Environment. Fire Research Station: Hertfordshire, UK, 1993.
- David E., Tiam, A., Lie, T.T. Fire analysis of reinforced concrete columns and walls. Proceedings of the Canadian Structural concrete conference, Ottawa, Canada, June 1977.
- De Witte, F.C., DIANA finite element analysis, user's manual release 8.1, TNO Building and Construction Research, Department of Computational Mechanics, Delft, 2002.
- Diederichs, U., Jumppanen, U.M., Schneider, U. High temperature properties and spalling behavior of HSC, Proceedings of the Fourth Weimar Workshop on HPC, HAB Weimar, Germany, 1995, pp: 219–235.
- Duederichs. V., Schneider. V. Bond Strength at High Temperature. *Magazine of Concrete Research*, 1981, 33(115): 75-84
- Dwaikat M.B., Kodur V.K.R. Response of restrained concrete beams under design fire exposure. *ASCE J Structural Engineering*, 2009, 135(11):1408–1417.
- Dwaikat, M.B. and Kodur, V.K.R. Hydrothermal model for predicting fire induced spalling in concrete structural systems. *Fire Safety Journal*, 2008, 44(3): 425-434.
- Dwaikat, MB, Kodur, V.K.R. A numerical approach for modeling the fire induced restraint effects in reinforced concrete beams. *Fire Safety Journal*, 2008, 43(4): 291–307.
- ECCS, European Recommendations for the Fire Safety of Steel Structures, 1983.
- Ehm, H., Postel, R., Versuche an Stahlbetonkonstruktionen mit Durchlaufwirkung unter Feuerangriff, Fire resistance of prestressed concrete, proceedings of a symposium held at Braunschweig, Germany, 1965, pp:24-31.
- Ellingwood, B., Lin, T.D. Flexure and Shear Behaviour of Concrete Beams during Fires, *Journal of Structural Engineering*, American Society of Civil Engineers, New York, 1991, 117(2), pp: 440-458.
- Ellingwood, B., Shaver, J.R. Effects of Fire on Reinforced Concrete Members, *Journal of the Structural Division*, Proceedings of the American Society of Civil Engineers, 1980, 106(11), pp: 2151-2166.
- Ellingwood, B., Structural Design Paradigm and Analogy, Second Conference on fire safety

- design in the 21th Century, WPI. 1999.
- EI-Hawary, M.M., Hamoush, S.A. Bond Shear Modulus of Reinforced Concrete at High Temperatures. *Engineering Fracture Mechanics*. 1996, 55(6):991-999.
- EI-Rimawi, J.A.A. The behaviour of flexural members under fire conditions. PhD thesis, University of Sheffield, Sheffield, U.K. 1989.
- EN 1992-1-1: 2004-Eurocode 2: Design of concrete structures–Part 1-1: General rules and rules for buildings, CEN, Brussels, 2004
- EN 1992-1-2: 2004-Eurocode 2: Design of Concrete Structures–Part 1-2: General Rules-Structural Fire Design, CEN, Brussels, 2004
- EN 1991-1-2: Eurocode 1: Actions on structures – Part 1-2: General actions –Actions on structures exposed to fire, CEN, Brussels, 2002.
- EN 1993-1-2 part 1.2: Eurocode 3: General rules-Structural fire design, European Committee for Standardization, Brussels, 2002.
- European recommendations for the fire safety of steel structures. Elsevier Science, Amsterdam, 1983.
- fib Bulletin 38, Fire Design of Concrete Structures-Materials, Structures, and Modeling, 2007, 106p.
- fib bulletin 3, Durability - Design for fire resistance - Member design – Maintenance - Assessment of repair - Practical aspect, Dec., 1999, 292p.
- Franssen, J.M., SAFIR, A thermal/Structural Program for Modeling Structures under Fire, *Engineering Journal*, A.I.S.C. 42, No. 3, 2005, pp. 143-158.
- Franssen J.M., Kodur VKR and Mason J. User's manual for SAFIR2001: A computer program for analysis of structures at Elevated temperature conditions. University of Liege, Belgium, 2000.
- Franssen, J.M., Schleich, J.B., Talamona, D., Twilt, L. A comparison between five structural fire codes applied to steel elements. *Proc., 4th Int. Symp. Fire Safety Sci.*, T. Kashiwagi, ed., IAFSS, Gaithersburg, 1994, 1125-1136.
- GB50157-2003: Code for design of metro, Beijing: China Planning Press, 2003 (in Chinese).
- GB50098-1998: Code for fire protection design of civil air defense works, Beijing: China Planning Press, 1998 (in Chinese).
- GB T9978-1999: Ministry of Public Security (MPS) of P.R. of China, Fire-Resistance Tests-Elements of Building Construction, China Standard Press, Beijing, 1999 (in Chinese).
- Gernay, T., Franssen, J.M. A formulation of the Eurocode2 concrete model at elevated temperature that includes an explicit term for transient creep, *Fire Safety Journal*, 2012, 51:1-9.

References

- Gernay, T., Franssen, J.M. A comparison between explicit and implicit modelling of transient creep strain in concrete uniaxial constitutive relationships. Proceedings of the Fire and Materials Conference, San Francisco, USA, 2011.
- Gustaferro, A.H., Martin, L.D. Design for Fire Resistance of Precast Prestressed Concrete, Prestressed Concrete Institute: Illinois, USA, 1988.
- Gustaferro, A.H. Design implementations- Concrete Structures, Design of Structure against Fire, ed. Anchor, R.D., Elsevier, Essex, 1986, pp.189-211.
- Gustaferro, A.H.; Martin, L.D. PCI Design for fire resistance of precast prestressed concrete, Prestressed Concrete Institute, USA, 1977.
- Gustaferro, A.H.; Abrams, M.S.; Salse, E.A.B. Fire resistance of prestressed concrete beams study C: structural behaviour during fire test, Research and Development Bulletin, Portland Cement Association, 1971.
- Gustafson, J.A. Reinforced Concrete Fire Resistance. Concrete Reinforcing Steel Institute: Chicago, IL, 1980.
- Haddad, R.H., Shannis, L.G. Post-fire behavior of bond between high strength pozzolanic concrete and reinforcing steel, Construction and Building Materials, 2004,18 (4): 425-435.
- Han, L.H., Zheng, Y.Q. and Tao Z. Fire Performance of Steel-reinforced Concrete Beam-column Joints, Magazine of Concrete Research, 2009. 61(7): 499-518.
- Han, L.H. Concrete filled steel tubular columns. Peking: Science Press, 2007 (in Chinese).
- Harmathy, T.Z. Fire Safety Design of Concrete, Longman Scientific & Technical, Essex, England, 1993.
- Harmathy T.Z, Alto L.W. Thermal properties of concrete subject to elevated temperature. Concrete for Nuclear Reactors. Detroit. ACISP34, 1972, 376-406.
- Hassen, S., Colina, H. Transient thermal creep of concrete in accidental conditions at temperatures up to 400°C. Magazine of Concrete Research, 2006, 58(4): 201-208.
- Hirashima, T., Toyoda, K., Yamashita, H., Tokoyoda, M., Uesugi, H., Compression of high-strength concrete cylinders at elevated temperature, in Rodrigues, J.P.C., Proceedings of the international workshop: fire design of concrete structures, from materials modelling to structural performance, University of Coimbra, Portugal, 2007, pp:47-58.
- Huang, S.S, Burgess, I.W. Effect of transient strain on strength of concrete and CFT columns in fire-part II: Simplified and numerical modelling. Engineering Structure, 2012, 44:389-399.
- Huang, Z., Burgess, I.W., Plank, R.J. Three-dimensional analysis of reinforced concrete beam-column structures in fire. Journal of Structural Engineering, ASCE 2009, 135 (10): 1201–1212.

-
- Huang, Z., Burgess, I.W., Plank, R.J. A non-linear beam-column element for 3D modelling of general cross-sections in fire, Research Report DCSE/03/F/1, Department of Civil & Structural Engineering, University of Sheffield, 2003.
- Huang, Z., Burgess, I.W., Plank, R.J. Nonlinear analysis of reinforced concrete slabs subjected to fire, *ACI Structural Journal*, 1999, 96 (1) pp: 127–135.
- Huang, Z, Platten, A. Non-linear finite element analysis of planar reinforced concrete members subjected to fires. *ACI Structural Journal*, 1997; 94(3):272–282.
- Huang, Z., Platten, A., Roberts, J. Non-linear finite element model to predict temperature histories within reinforced concrete in fires, *Building and Environment*, 1996, 31(2) pp: 109–118.
- Huang, Z.F., Tan, K.H., Toh, W.S., Phng, G.H. Fire resistance of composite columns with embedded I-section steel—Effect of section size and load level. *Journal of Constructional Steel Research*. 2008, 64:312-325.
- Huang, Z.F., Tan, K.H., Phng, G.H. Axial restraint effects on the fire resistance of composite columns encasing I-section steel, *Journal of Constructional Steel Research*, 2007, 63(4):437–447.
- Huang, Z.F., Tan, K.H. Effects of external bending moments and heating schemes on the responses of thermally restrained steel columns, *Engineering Structure*. 2004, 26 (6):769-780.
- Hertz, K. Analysis of concrete structures exposed to fire, Technical university of Denmark, Lyngby.1999.
- Hertz, K. Additional documentation for simplified design of fire exposed concrete columns. Department of building and energy, Technical university of Denmark, Lyngby.1998.
- IBC 2006: International Building Code, International Code Council, Inc., Falls Church, VA, 2006, pp: 109-155.
- International Tunneling Association. Guidelines for Structural Fire-resistance for Road Tunnels. 2004, May.
- ISO 834-1975: Fire resistance tests-elements of building construction. International Organization for Standardization, 1975.
- Issen, L.A., Gustaferro, A.H. and Carlson, C.C. Fire tests of concrete members: An improved method for estimating thermal restraint forces. *Fire Test Performance*, ASTM, STP 464, American Society for Testing and Materials, Philadelphia, 1970, 153–185.
- Johan Rigberth. Simplified Design of Fire Exposed Concrete Beams and Columns. Lund University: Lund, Sweden, 2000.
- Joint ACI-TMS Committee 216, Standard Method for Determining Fire Resistance of Concrete and Masonry Construction Assemblies (ACI 216.1-07/TMS 0216.1-07),

References

- American Concrete Institute, Farmington Hills, MI, 2007, 28 pp.
- Jurij Modic. Fire simulation in road tunnels. *Tunneling and Underground Space Technology* 18 (2003), P525-530.
- Kalifa, P., Menneteau, F.D., Quenard, D. Spalling and pore pressure in HPC at high temperature. *Cement Concrete Res* 2000, 30 (12): 1915-1927.
- Khoury, G.A., Anderberg, Y. *Concrete Spalling Review*, Fire Safety Design, 2000
- Khoury, G.A., et al. Mechanical behavior of HPC and UHPC concretes at high temperature in compression and tension, *ACI International Conference on State-of-Art In High Performance Concrete*, Chicago, 1999.
- Khoury, G.A. Strain of concrete during first cooling from 600°C under load. *Magazine of Concrete Research*, 1986, 38(134):3-12.
- Khoury, G.A., Grainger, B.N. and Sullivan, P.J.E. Transient Thermal Strain of Concrete: Literature review, Conditions within Specimen and Behavior of Individual Constituents, *Magazine of Concrete Research*, 1985, 37 (132):131-144.
- Khoury, G.A., Grainger, B.N., Sullivan, P.J.E. Strain of concrete during first heating to 600°C under load, *Magazine of Concrete Research*, Cement and Concrete Association, 1985, 37(133), pp:195-215.
- Kirkland, C.J. The fire in the Channel Tunnel, *Tunneling and Underground Space Technology*, 2002, 17, pp: 129-132.
- Kodur, V.K.R., Yu, B.L. and Dwaikat M.M.S. A simplified approach for predicting temperature in reinforced concrete members exposed to standard fir, *Fire Safety Journal* 2013, Vol.56, pp: 39-51.
- Kodur, V.K.R., Dwaikat, M.B. Design equation for predicting fire resistance of reinforced concrete beams, *Engineering Structure*, 2011, 33: 602-614.
- Kodur V.K.R., Dwaikat M.B. Effect of fire induced restraint on fire resistance of reinforced concrete beams. *Structural Fire Engineering*, 2010; 1(2):73–88.
- Kodur, V.K.R, Dwaikat, M.B. Performance-based fire safety design of reinforced concrete beams. *J. Fire Protection Engineering*, 2008, 17(3): 293–320.
- Kodur, V.K.R. and Dwaikat, M.B. Flexural response of reinforced concrete beams exposed to fire. *Structural Concrete*, 2008, 1(9):45-54.
- Kodur, V.K.R. and Dwaikat, M.B. A numerical model for predicting the fire resistance of reinforced concrete beams, *Cement and Concrete Composites*, 2007; 8(4):1-13.
- Kodur, V.K.R. and Dwaikat, M.B. Performance-based Fire Safety Design of Reinforced Concrete Beams, *Journal of Fire Protection Engineering*, 2007, 17: 293-320.
- Kodur, V.K.R., Phan, L. Critical factors governing the fire performance of high strength

- concrete systems, *Fire Safety Journal*, 2007, 42: 482-488.
- Kodur, V.K.R. Guidelines for fire resistance design of high strength concrete columns, *J. Fire Prot. Eng.* 2005, 15 (2): 93-106.
- Kodur, V.K.R. Spalling in high strength concrete exposed to fire-concerns, causes, critical parameters and cures, in: *ASCE Structures Congress Proceedings*, Philadelphia, USA, 2000, pp: 1-8.
- Law, A., Gillie, M., Load induced thermal strain: implications for structural behaviour, *Proceedings of the Fifth International Conference-Structures in Fire, SIF2008*, Singapore, pp: 488-496.
- Li, G.Q., Wang, P.J., Jiang, S.C. Non-linear finite element analysis of axially restrained steel beams at elevated temperatures in a fire, *Journal of Constructional Steel Research*, 2007, 63(9): 1175-1183.
- Li, L., Purkiss, J. Stress-strain constitutive equations of concrete material at elevated temperatures, *Fire Safety Journal*, 2005, 40, pp: 669-686.
- Lie, T.T. *Structural Fire Protection. ASCE Manuals and Reports of Engineering Practice*, No. 78, American Society of Civil Engineers, New York, 1992.
- Lie, T.T., Celikkol B. Method to Calculate the Fire Resistance of Circular Reinforced Concrete Columns. *ACI Material Journal*, 1991, 81(1), pp: 84-91.
- Lie T.T., Lin T.D. Influence of restraint on the fire performance of reinforced concrete columns. *Fire safety science-proceedings of the first international symposium*, Gaithersburg, 1985.
- Lie T.T., A procedure to calculate fire resistance of structural members, *International Seminar on Three Decades of Structural Fire Safety*. Feb, 1983.139-153.
- Lim, L., Buchanan, A., Moss, P. and Franssen, J.M. Computer Modeling of Reinforced Concrete Slab in Fire Condition. *Journal of structural engineering*, 2004, 130(12):1964-1971.
- Lim, L., Buchanan, A., Moss, P. Restraint of fire-exposed concrete floor systems. *Fire and materials*, 2004, 28:95-125.
- Lim, L., *Membrane Action in Fire Exposed Concrete Floor Systems*, research Report No. 03/2, University of Canterbury, Christchurch, New Zealand, 2003.
- Lin, T.D.; Ellingwood, B.; Piet, O. Flexural and Shear Behaviour of Reinforced Concrete Beams During Fire Test, *Research and Development Bulletin RD091T*, Portland Cement Association, Illinois, USA, 1988.
- Lin, T.D.; Gustafarro, A.H.; Abrams, M.S. Fire Endurance of Continuous Reinforced Concrete Beams, *Research and Development Bulletin RD072.01B*, Portland Cement Association, Illinois, USA, 1981.

References

- Liu, T.C.H., Fahad, M.K., Davies, J.M. Experimental investigation of behavior of axially restrained steel beams in fire, *Journal of Constructional Steel Research*. 2002, 58 (9) p:1211-1230.
- Liu, X., Microstructural investigation of self-compacting concrete and high-performance concrete during hydration and after exposure to high temperatures, PhD thesis, Tongji University, Gent University, 2006.
- Lu, J.Z., Huang, X.J. Effect of Restraint Stiffness on the Fire Resistance of Reinforced Concrete Beam, *Journal of Huaqiao University (Natural Science)*, 2008, Vol.29(4), pp:593-599 (in Chinese).
- Lu, L.M., Yuan Y., Annerel, E., Taerwe L. A simplified multi-iteration method for restrained beams under fire. *Material and Structures*, 2015, 48(1), pp: 9-19.
- Lu Z.D, Zhu B.L. Response analysis of reinforced concrete beam exposed to fire loads. *Fire Safety Science*, 1996, 5 (2) pp: 36-45.
- Lu Z.D., Zhu B.L. and Zhou Y.H. Experimental study on fire response of simple supported reinforced concrete beams. *China Civil Engineering Journal*, 1993, 26(3) pp: 47-54.
- Lu Z.D. A Research on fire response of reinforced concrete beams. PhD thesis, Tongji University, 1989 (in Chinese).
- Malholtra, H.L. Design of fire-resisting structures, Surrey University Press, London, 1982.
- McGrattan, K., Forney, G. Fire Dynamics Simulator (Version 4) User's Guide. 2005.
- Minne R, Vandamme M., Fire Resistance of Reinforced Concrete Slabs, Laboratory for Fuel Technology and Heat Transfer, Ghent University, 1979.
- Najjar, S.R., Burgess, I.W. A nonlinear analysis for three dimensional steel frames in fire conditions. *Engineering Structure*, 1995, 18(1), pp: 77-89.
- NFPA 502, Standard for Road tunnels, bridges and limited access highway's. USA, 2001.
- Nielsen, C.V., Pearce, C.J., Bicanic, N. Theoretical model of high temperature effects on uniaxial concrete member under elastic restraint, *Magazine of Concrete Research*. 2002, 54 (4), pp: 239–249.
- Ren H.M. Theoretical analysis and fire-resistance design of HPC shear walls. Master thesis, Tongji University, Shanghai, China, 2006 (in Chinese).
- RILEM TC 129-MHT Part 7, Transient creep for service and accident conditions. *Materials and Structures*, 1998, 31 (209): 290-295.
- Riva, P. Structural behavior of continuous beams and frames. *fib bulletin 46: Fire design of concrete structures-structural behavior and assessment*, 2008.
- Riva, P. and Franssen, J.M. Non-linear and plastic analysis of RC beams subjected to fire. *Structural Concrete*, 2008, 1(9), pp: 32-43.

- Riva, P. Nonlinear and plastic analysis of reinforced-concrete beams. Proceedings of the workshop Fire Design of Concrete Structures: What now? What next? Milan, Italy, 2004 December 2-3. 147-158.
- Riva, P. Parametric study on the behavior of RC beams and frames under fire conditions. FIB Guidelines for the structural design of concrete buildings exposed to fire. 2002, 9.
- Ron, A. Special report: Channel Tunnel fire, Fire Safety Engineering, 2008, Vol.15 (8), pp: 13
- Sadaoui, A., Khennane, A. Effect of transient creep on the behaviour of reinforced concrete columns in fire, Engineering Structures, 2009, 31, pp: 2203-2208.
- Schleich, J.B., Cajot, L.G., Natural fire safety for buildings, INTERFLAM, conference proceedings, Interscience communications Ltd, London, 359-368, 2001.
- Schneider, U.; Morita, T.; Franssen, J.M. A concrete model considering the load history applied to centrally loaded columns under fire attack. Fourth International Symposium on Fire Safety Science, 1994, Ottawa, pp. 1101-1112.
- Schneider, U. Concrete at high temperatures-a general review. Fire Safety Journal, 1988, 13(1):55-68.
- Schneider, U., Properties of Materials at High Temperatures-Concrete. RILEM-Committee 44-PHT, Department of Civil Engineering, University of Kassel, June, 1985.
- Selvaggio, S.L. and Carlson, C.C. Effect of restraint on fire resistance of prestressed concrete. American Society for Testing and Materials, STP 344, ASTM, Philadelphia, 1963, 1-25. (Reprinted as PCA Research Dept. Bull. 164).
- SFPE Engineering guide to performance-based fire protection analysis and design of buildings, Society of fire protection engineers, Bethesda, MD, 2000.
- Shi, X.D. Experimental study and nonlinear finite element analysis on strength and deformation of concrete planar frame structure at elevated temperature. PhD thesis, Tsinghua University, 1992 (in Chinese).
- Song, T.Y., Han, L.H. and Brian Uy. Performance of CFST column to steel beam joints subjected to simulated fire including the cooling phase. Journal of Constructional Steel Research, 2010, 66(4): 591-604.
- Taerwe, L., Bamonte, P., Both, K., Denoël, et al, fib bulletin 46, Fire Design of Concrete Structures-Structural Behavior and Assessment, State-of-the art Report, International Federation for Structural Concrete (fib TG 4.3.2), Lausanne, 2008.
- Tan, Q.H., Han, L.H. and Yu, H.X. Fire performance of concrete filled steel tubular (CFST) column to RC beam joints. Fire Safety Journal, 2012, Vol.51, pp: 68-84.
- Tan K.H., Huang Z.F. Structural responses of axially restrained steel beams with semi-rigid moment connection in fire. Journal of Structural Engineering, 2006, 131(4): 541-550.

References

- Tao, J., Liu, X., Yuan, Y., Taerwe, L. Transient strain of self-compacting concrete loaded in compression heated to 700 °C, *Mater. Struct.*, 2012, vol. 46, nr. 1–2, pp. 191–201.
- Tao, J., Yuan, Y., Taerwe, L. Thermal stress-strain of self-compacting concrete in compression, *Fire Mater.*, 2012, vol. 37, nr. 3, pp. 187–199.
- Tao, J., Yuan, Y., Taerwe, L. Compressive Strength of Self-Compacting Concrete during High-Temperature Exposure, *J. Mater. Civ. Eng.*, 2010, vol. 22, nr. 10, pp. 1005–1011.
- Tao, J. Mechanical performance and thermal-mechanical constitutive model of self-compacting concrete at high temperature. PhD thesis, Tongji University, Gent University. 2008.
- Terro, M. J. Numerical modeling of the behavior of concrete structures in fire, *ACI Structural Journal*, 1998, 02.
- Thelandersson, S. Modeling of combined thermal and mechanical action in concrete. *Journal of Engineering Mechanics*, 113(6), pp: 893-906, 1987.
- Tokoyoda, M., Yamashita, H., Toyoda, K., Hirashima, T., Uesugi, H., An experimental study of transient strain for a concrete with limestone aggregate, in: Rodrigues, J.P.C., Khoury, G.A., Høj, N.P., Proceedings of the international workshop: fire design of concrete structures, from materials modelling to structural performance, University of Coimbra, Portugal, 2007, pp:105-114.
- Valente, J.C., Cabrita Neves I. Fire resistance of steel columns with elastically restrained axial elongation and bending, *Journal of Constructional Steel Research*, 1999, 52(3): 319-331.
- Wade, C., Method for Fire Engineering Design of Structural Concrete Beams and Floor Systems, Building Research Association of New Zealand, Technical Recommendation No: 8, 1991.
- Wang, K.Q., Li, G.Q., Tang, W.K. Research on restraint rigidity on beams in frame structure, *Building Structure*, Vol. 41(1), pp: 91-94, 2011.
- Wang Y.C. The effects of frame continuity on the behavior of steel columns under fire conditions and fire resistant design proposals. *Journal of Constructional Steel Research* 1997, 41(1):93-111.
- Wen-Chen Jau, Kuo-Li Huang, A study of reinforced concrete corner columns after fire. *Cement and Concrete Composites*, 2008, 30:622-638.
- Wilson, E.L., Nicked, R.E. Application of the Finite Element Method to Heat Conduction Analysis. *Journal of Nuclear Engineering and Design*, 1996, Vol. 4(10), pp: 276-286.
- Wu, B. Qiao, C.J. Experimental study on fire behavior of RC restrained beams during heating and cooling phases, *Engineering Mechanics*, 2011, 28(6), pp:88-95 (in Chinese).
- Wu B., Lu J.Z. A numerical study of the behaviour of restrained RC beams at elevated temperatures. *Fire Safety Journal*, 2009, 44(4): 522-531.

- Wu B, Xu Y.Y. Behavior of axially and rotationally restrained concrete columns with '+'-shaped cross section and subjected to fire. *Fire Safety Journal*, 2009, 44(2):212-218.
- Wu, B., He X.Y. A study on the redistribution of internal forces in reinforced concrete frames under high temperature. *China Civil Engineering Journal*, 2006, 39(9): 54-61(in Chinese).
- Xavier, H.F., Faria, R. and Real, P.V. Influence of thermal elongation of beams on the fire resistance of RC Frames. Structures in fire-proceedings of the sixth international conference. East Lansing, America, 2010.
- Yang G. Computer Simulation of Fire Smoke Flow in Underground Building with Large Space. Paper for master's degree, Shenyang Institute of Aeronautical Engineering, 2006.
- Yang, J.P., Shi X.D., Guo Z.H. Comparison of the mechanical behavior between RC eccentrically compression members heated on two and three surfaces. *Industrial Construction*, 2000, 30(6):27-34.
- Youssef, M.A, Mofteh, M. General stress-strain relationship for concrete at elevated temperatures. *Engineering Structure*, 2007, 29:2618–2634.
- Yin, Y.Z., Wang, Y.C. A numerical study of large deflection behavior of restrained steel beams at elevated temperatures, *Journal of Constructional Steel Research*, 2004, 60(7): 1029-1047.
- Zha, X.X. Three-dimensional non-linear analysis of reinforced concrete members in fire. *Building and Environment*, 2003, Vol.38: 297-307.
- Zha, X.X, Li, L.Y., Purkiss, J.A. FE analysis of fire resistance of RC columns. Proceedings of the Eighth International Conference on Civil and Structural Engineering Computing, Vienna, Austria, 2001.
- Zhang Y. H. Research on Performance of Resistance to Fire for Steel Frame Based on FDS. Paper for master's degree, Wuhan University of Technology, 2007 (in Chinese).
- Zhou Y., Tang T.B., Liao H.W. Review and Prospect of Disaster Prevention of Urban Underground Space. *Chinese Journal of Underground Space and Engineering*, 2006, 2(3): pp: 467-474.

Curriculum vitae

Personal Data

First name	Li-Min
Last name	Lu
Date of birth	12/10/1982
Place of birth	Jilin, China
Email	dami21th@hotmail.com

Education

2009-2014	PhD: Civil Engineering The Magnel Laboratory for Concrete Research, Department of Structural Engineering, Faculty of Architecture and Engineering, Ghent University, Belgium
2006-2009	Master: Structural Engineering School of Civil Engineering Tongji University, China
2002-2006	Bachelor: Civil Engineering School of Civil Engineering, Tongji University, China

Publications

AI

L.M. Lu, Y. Yuan, E. Annerel, L. Taerwe, A simplified multi-iteration method for restrained beams under fire. *Material and structures*, 2015, Vol. 48 (1), pp: 9-19.

L.M. Lu, Y. Yuan, R. Caspeele, L. Taerwe, Influencing factors for fire performance of RC beams with implicit and explicit transient creep strain material models, *Fire Safety Engineering* (Accepted).

E. Annerel, L.M. Lu, L. Taerwe, Punching shear tests on flat concrete slabs exposed to fire. *Fire Safety Journal*, April 2013, Volume 57, Pages 83–95.

L.M. Lu, Y. Yuan, R. Caspeele, L. Taerwe, Influence of rotational restraints on fire performance of RC beams subjected to bending. (In preparation).

Conference and oral presentations

L.M. Lu, Y. Yuan, L. Taerwe, Influence of rotational restraints on fire behaviour of RC elements, Proceedings for 6th International Conference on Protection of Structures against Hazards (PSH14), 15-17 Oct. 2014, Tianjin, China.

L.M. Lu, E. Annerel, L. Taerwe, Y. Yuan, Influence of transient strain on fire resistance of concrete elements, Proceedings for Application of Structural Fire Engineering Conference (ASFEC), 29 April 2011, Prague, Czech Republic, 2011, pp. 109-114.

L.M. Lu, Y. Yuan, L. Taerwe, A plastic analysis method for restrained RC beams at elevated temperature, proceedings for Third International Symposium on Computational Mechanics (ISCM III) and Second Symposium on Computational Structural Engineering (CSE II), December 5-7, 2011, Taipei, TAIWAN. pp. 22-23.

E. Annerel, L.M. Lu, L. Taerwe, Punching shear tests on flat concrete slabs at high temperatures, Proceedings for 2nd international RILEM workshop on concrete spalling due to fire exposure, Delft, The Netherlands, 2011, pp. 125-131.